UNIVERSITÀ
DEGLI STUDI
FIRENZE

DOTTORATO DI RICERCA IN
Area del Farmaco e Trattamenti Innovativi

(Curriculum Scienze Farmaceutiche)

CICLO XXXI

COORDINATORE
Prof.ssa Elisabetta Teodori

"Synthesis, characterization, biological assays and development of new enzyme modulators for the treatment of human pathologies"

Settore Scientifico Disciplinare CHIM/08

Dottorando
Dott. Andrea Angeli

Tutore Scientifico
Prof. Claudiu T. Supuran

Tutore Teorico
Prof.ssa Silvia Selleri

Coordinatore
Prof.ssa Elisabetta Teodori

Anni 2015/2018

Table of contents

Table of contents

Table of contents

Table of contents

Table of contents

Table of contents

Summary

Carbonic anhydrases (CAs, EC 4.2.1.1) are a family of metalloenzymes widespread in all life kingdoms genetically classified in 7 unrelated classes (i.e. α-, β-, γ-, δ-, ζ-, η- and θ). These enzymes catalyse a very simple and essential physiological reaction, which is the carbon dioxide hydration to afford bicarbonate and protons. So far, 16 different α-CA isoforms were isolated and characterized in mammals. In many tissues CAs are concomitantly present in a variety of isoforms, which differ for their kinetics, structural properties as well as cellular and tissutal abundancy.

To date, human (h) CAs are well established therapeutic targets to treat a hypertension, glaucoma. New *proof-of-concepts* are therapeutic applications for the treatment of epilepsy, obesity related pathologies and neuropathic pain. In the last years CA inhibitors (CAIs) were validated for the treatment of hypoxic tumors.

Within the scope of this Thesis, we report new and more isoform selective modulators of CAs expressed in humans and/or in pathogenic organisms with the intent to pave the ways to the treatment of pathologies by means of innovative approaches.

The current Thesis is composed of seven chapters, each one dealing with the drug design, synthesis as well as *in vitro* kinetic assay of new CA modulators:

(i) Novel inhibitors against hCAs

(ii) Potential anticancer drugs targeting primarily hCA IX and XII that are predominantly expressed in tumor cells.

(iii) New class of agents for the prevention of diabetic cerebrovascular pathology (which probably target the mitochondrial isoforms hCA VA and/or hCA VB).

(iv) Potential drug leads for the treatment of different neurological disorders such as antiepileptic or neuropathic pain (probably targeting hCA II and VII).

(v) Agents that target various CAs from pathogenic microorganisms such as bacteria and protozoa.

(vi) New activators of hCAs

(vii) Kinetic activation studies on no human expressed CAs such as the α-, β-, γ-, δ-, ζ- and η-classes.

Chapter 1

The Carbonic Anhydrases

1.1 Introduction

Zinc plays a pivotal role in biochemistry and it is the second most abundant metal, after iron, in biological systems. The main advantages for this metal lie in its distinctive chemical properties, which among others combine Lewis acid strength, low redox potentials, fast ligand exchange and stable association with macromolecules. Moreover, the zinc coordination flexibility makes this metal highly adaptable to meet the catalytic needs of enzymes to carry out biological activities as well as to allow the correct folding of the proteic strains.[1,2] Zinc containing proteins are present within the six major classes of enzymes (i.e. oxidoreductases, transferases, hydrolases, lyases, isomerases, and ligases).[2,3] When present in enzymatic sites, zinc ions participate directly in the catalytic processes and exhibit a distorted tetrahedral or trigonal bipyramidal coordination geometry having the metal ion bound to three or four amino acid residues and/or a water molecule.[4-8] Among the amino acid residues coordinated to the metal ion the His, Glu, Asp, and Cys are the common ones.[6] The presence of water within the metal sphere coordination is a distinguishing feature that allows to differentiate a catalytic ion from a structural one.[9] As schematically reported in Figure 1, the water molecule can be involved in the catalytic process as hydroxide ion (i.e. activated as a nucleophile species by means of the polarizing effect played by the neighbouring amino acids) or may directly interact with the substrate itself. [5,6]

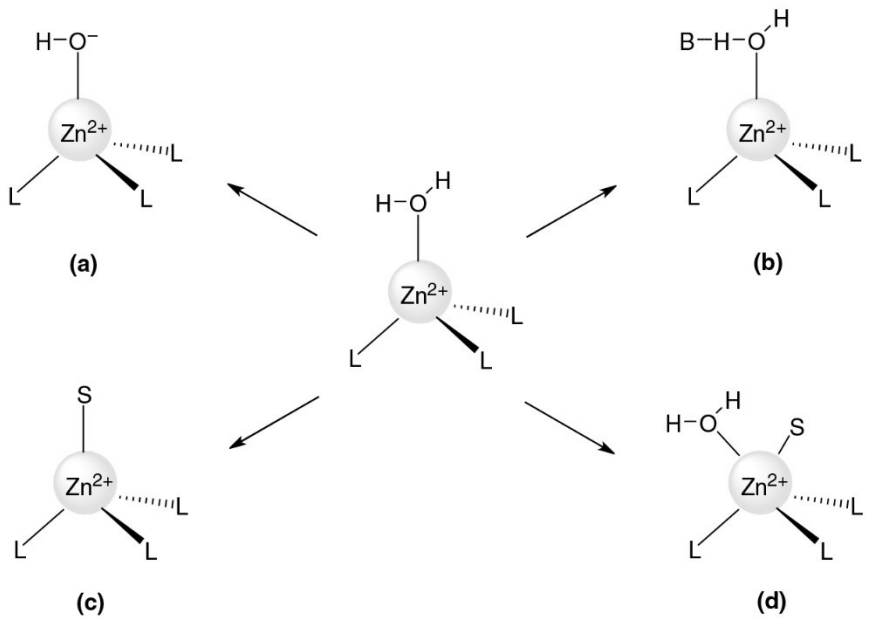

Figure 1. Role of the zinc-bound water molecule in catalysis: (**a**) ionization, (**b**) polarization, (**c**) displacement, and (**d**) expansion.

The relevance of zinc containing metalloenzymes to biomedical purposes is particularly increased in the past decades, as they represent convenient targets for designing, developing small-molecule drugs able to modulate their enzymatic activity. Nowadays modulators of this kind are largely used in modern medicine for the treatment of several human diseases such as cardiovascular, neurological, infectious and metabolic dysfunctions as well as cancer.[10,11]

1.2 Catalytic mechanism and reactions of Carbonic Anhydrases

Carbonic Anhydrases (CAs, EC 4.2.1.1) were first discovered in 1939, when the erythrocytes were found to contain stoichiometric amounts of zinc, which was also proved essential for the enzymatic activity to happen.[12] CAs are ubiquitously expressed within all kingdom life and are encoded by seven distinct and evolutionarily unrelated genes: the α-CAs (present in vertebrates, bacteria, algae, and cytoplasm of green plants), the β-CAs (predominantly expressed in bacteria, algae, and chloroplasts of both mono and di-

cotyledons), the γ-CAs (mainly found in archaea and some bacteria) and the δ-, ζ- and θ-CAs which are present in marine diatoms, whereas the η-CAs in protozoa belong to the *Plasmodium spp*.[13–18] α-CAs have been reported in vertebrates only and in humans 16 isozymes or CA-related proteins have been described. All of them differ for their catalytic activities, subcellular localizations and tissue distributions as schematically reported in **Table 1**).[19-20]

Table 1. Kinetic parameters for CO_2 hydration reaction catalyzed by the 16 vertebrate α-CA isozymes, at 20°C and pH 7.5, and their subcellular localization.[21]

Isozyme	k_{cat} (s^{-1})	K_m (mM)	k_{cat}/K_m ($M^{-1}\,s^{-1}$)	Subcellular Localization	Tissue/Organ Localization
hCA I	2.0×10^5	4.0	5.0×10^7	Cytosol	Erythrocytes, GI tract
hCA II	1.4×10^6	9.3	1.5×10^8	Cytosol	Erythrocytes, eye, GI tract, bone osteoclasts, kidney, lung, testis, brain
hCA III	1.0×10^4	33.3	3.0×10^5	Cytosol	Skeletal muscle, adipocytes
hCA IV	1.1×10^6	21.5	5.1×10^7	Membrane bound	Kidney, lung, pancreas, brain capillaries, colon, heart muscle
hCA VA	2.9×10^5	10.0	2.9×10^7	Mitochondria	Liver
hCA VB	9.5×10^5	9.7	9.8×10^7	Mitochondria	Heart and skeletal muscle, pancreas, kidney, spinal cord, GI tract
hCA VI	3.4×10^5	6.9	4.9×10^7	Secreted (saliva/milk)	Salivary and mammary glands
hCA VII	9.5×10^5	11.4	8.3×10^7	Cytosol	CNS
hCA VIII	—	—	—	Cytosol	CNS
hCA IX	3.8×10^5	6.9	5.5×10^7	Transmembrane	Tumors; GI mucosa
hCA X	—	—	—	Cytosol	CNS
hCA XI	—	—	—	Cytosol	CNS
hCA XII	4.2×10^5	12.0	3.5×10^7	Transmembrane	Renal, intestinal, reproductive epithelia, eye, tumors
hCA XIII	1.5×10^5	13.8	1.1×10^7	Cytosol	Kidney, brain, lung, gut, reproductive tract
hCA XIV	3.1×10^5	7.9	3.9×10^7	Transmembrane	Kidney, brain, liver
mCA XV	4.7×10^5	14.2	3.3×10^7	Membrane bound	Kidney

h, human; m, mouse enzyme. hCA VIII, X, and XI are devoid of catalytic activity.

Among the isoforms above reported, twelve isoforms showed catalytic activity. Five are located in the cellular cytosolic (CA I, CA II, CA III, CA VII and CA XIII), five are membrane-bound isozymes (CA IV, CA IX, CA XII, CA XIV and CA XV), two are mitochondrial forms (CA VA and CA VB), and one is secreted in saliva and tears (CA VI).[21]All the catalytically active CAs reversibly hydrate carbon dioxide to bicarbonate ion and proton. Although this reaction may also occur spontaneously at physiological pH values, still is too slow to meet metabolic needs of most organisms. The CAs catalytic mechanism occurs in two main steps according to the **Figure 2.**[22]

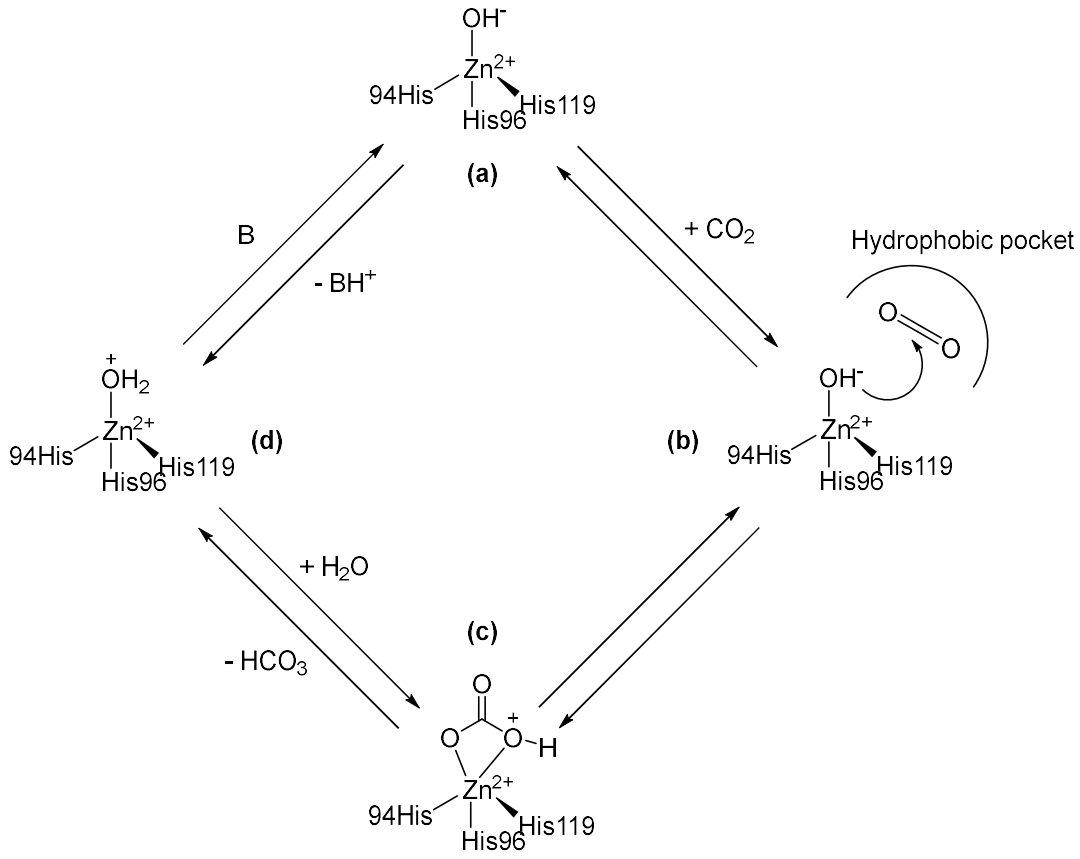

Figure 2. Catalytic mechanism of reversible hydration of CO_2 to $HCO_3^-$and proton.

The first one is the nucleophilic attack of the Zn^{2+}-bound hydroxide ion to a CO_2 with consequent formation of the enzyme-HCO_3 adduct (**b** to **c**), which is then displaced from the active site by a water molecule (**c** to **d**). The last step (**d** to **a**), which is the kinetically rate limiting step, regenerates the catalytically active Zn^{2+}-bound hydroxide ion through a proton transfer reaction from the Zn^{2+}-bound water molecule to an exogenous proton acceptor or to an active site residue (**Figure 2**).

In addition to the CO_2 hydration/bicarbonate dehydration processes (reaction 1 in **Table 2**), different α-CAs possess a certain catalytic versatility, with the possibility to hydrate small molecules similar to CO_2 such as COS (reaction 2),[23] CS_2 (reaction 3)[24] and cyanamide (reaction 4)[25,26] leading to H_2S (and CO_2) for the first reactions and urea for the last one. Aldehydes were also shown to be hydrated to *gem* diols (reaction 5),[27] whereas the esterase

activity with carboxylic acid esters (reaction 6),[28–30] sulfonic acid esters (reaction 7),[31,32] phosphate esters (reaction 8).[29,30,33] Some other less investigated hydrolytic processes (reactions 10 and 11 in **Table 2**) were also found.[35] Presently it is not known whether reactions other than the CO_2 hydration/bicarbonate dehydration may have physiological relevance, although the recently reported thioesterase activity[34] (reaction 13) may interfere with the generation/hydrolysis of acyl-coenzyme A derivatives, and thus possess relevant physiological role.

Table 2. Reactions catalysed by the α-Carbonic Anhydrases.

$O=C=O + H_2O \leftrightarrow HCO_3^- + H^+$	(1)
$O=C=S + H_2O \leftrightarrow H_2S + CO_2$	(2)
$S=C=S + 2H_2O \leftrightarrow 2H_2S + CO_2$	(3)
$HN=C=NH + 2H_2O \leftrightarrow H_2NCONH_2$	(4)
$RCHO + H_2O \leftrightarrow RCH(OH)_2$	(5)
$RCOOAr + H_2O \leftrightarrow RCOOH + ArOH$	(6)
$RSO_3Ar + H_2O \leftrightarrow RSO_3H + ArOH$	(7)
$ArOPO_3H_2 + H_2O \leftrightarrow RSO_3H + ArOH$	(8)
$ArOPO_3H_2 + H_2O \leftrightarrow ArOH + H_3PO_4$	(9)
$R_2NCSSR' + H_2O \leftrightarrow R_2NH + R'SH + COS$	(10)
$PhCH_2OCOCl + H_2O \leftrightarrow PhCH_2OH + CO_2 + HCl$	(11)
$RSO_2Cl + H_2O \leftrightarrow RSO_3H + HCl$	(12)
$RCOSAr + H_2O \leftrightarrow RCOOH + ArSH$	(13)

1.3 Characteristics of CA classes

1.3.1 α-Carbonic Anhydrases

Most *α*-class enzymes are organized as monomers but homodimers were also reported for some human and bacterial enzymes. The active site is placed deep down in a large, cone shaped cavity that reaches the centre of the protein, where the metal ion (which is Zn(II) in all *α*-CAs investigated up to now) is located.[14-16] In detail X-ray crystallographic data showed

the metal ion situated at the bottom of a 15 Å deep active site cleft and coordinated by three histidine residues His94, His96 and His119 (hCA II amino acid numbering system) and a water molecule/hydroxide ion (**Figure 3A**).[14-16]

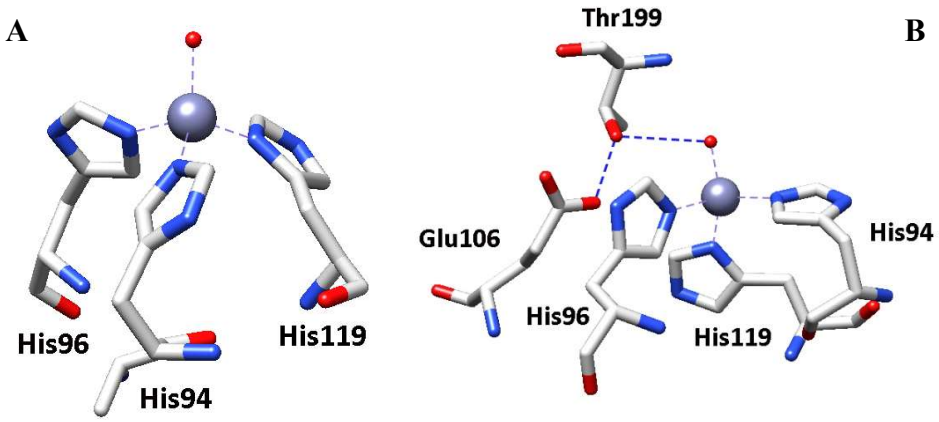

Figure 3. The Zn(II) ion coordination in the hCA II active site (**A**) and the gate-keeping residues (Thr199 and Glu106) (**B**) shown.

The zinc-bound water is also engaged in hydrogen bond interactions with the hydroxyl moiety of Thr199, which in turn is bridged to the carboxylate moiety of Glu106; these interactions enhance the nucleophilicity of the water molecule itself, and orient the substrate (CO_2) in a favourable place for the nucleophilic attack to occur (**Figure 3B**).[14-16] This is why the residues Thr199 and Glu106, an important catalytic dyad for all α-CAs, are called gate-keeping residues. Residues in position 121, 131, 141, 143, 198 and 207 delimit the hydrophobic region, whereas those in position 62, 64, 67 and 92 identify the hydrophilic one (**Figure 4**).

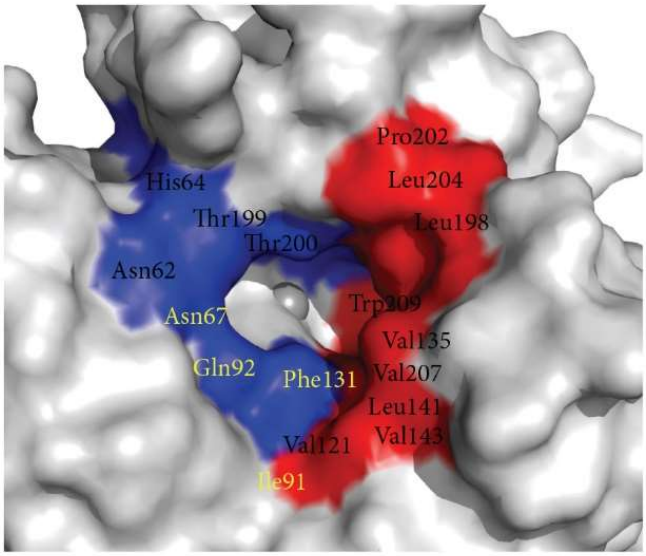

Figure 4. Solvent accessible residues in and around CA II active site. Hydrophilic cleft (blue) and hydrophobic cleft (red). Residues in yellow indicate residues of the "selective pocket."

Furthermore, the bulky Phe131 residue in hCA II, roughly in the middle of the hydrophobic half, subdivides this part of the active site in two sub-sites in which various classes of inhibitors bind in a specific manner.[14-16]

1.3.2 β-Carbonic Anhydrases

Many bacteria, archaea, algae and the chloroplasts of superior plants contain CAs belonging to the β-class.[13-16] The principal difference between these enzymes and the α-CAs discussed above consists in the fact that usually the β-CAs are organized as oligomers, generally formed by the assembly of 2-6 monomers each of 25-30 kDa. Although the Zn(II) ion is essential for catalysis, its coordination is different and rather variable when compared to α-CAs. The metal ion in the active site is coordinated by one His and two Cys residues, with a fourth coordination site occupied by water or analogue substrate (**Figure 5A**).

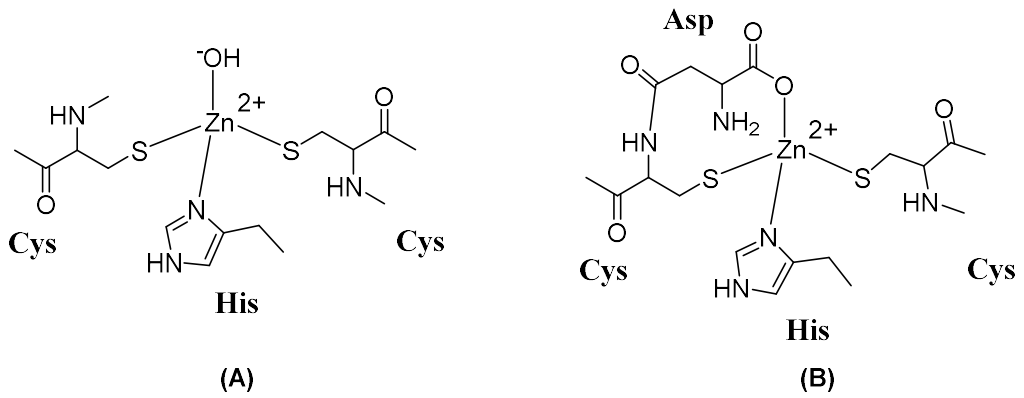

Figure 5 The metal ion coordination pattern in the β-CAs, opened active site (**A**) and β-CAs closed active site by an aspartate residues as the fourth zinc ligand (**B**).

Recently, it has been reported the β-CA active site at pH 7.5 or lower showed the carboxylate of an aspartic acid coordinated to Zn(II) ion as fourth ligand and "locked" the active site (**Figure 5B**).[57] However, at pH values over 8.3, an opening of the active site occurs, with the blocking aspartate forming a salt bridge with a conserved Arg residue so that a water molecule/hydroxide ion has finally access to coordinate the metal ion for completion of its tetrahedral geometry (**Figure 5A**).

1.3.3 γ-Carbonic Anhydrases

The prototype of the γ-class CAs, "Cam" has been isolated from the methanogenic archaeon *Methanosarcina thermophila*.[58-60] The active form of the enzyme is a trimer with three distinct zinc-containing active sites, each located at the interface between two monomers with the approximate molecular weight of 70 kDa. The Zn(II) ion within the active site is coordinated by three His residues, in analogy to α-CAs. The active cleft of γ-CA contains an additional metal-bound water ligand, when compared to the tetrahedral coordination geometry α- CAs, so that the resulting coordination geometry is trigonal bipyramidal. The catalytic mechanism of γ-CAs was proposed to be similar with the one presented for the α-class enzymes. Still, the finding that Zn(II) is not tetra-coordinated as originally reported but penta-coordinated,[59,60] with two water molecules bound to the metal ion, demonstrates that much is still to be understood regarding these enzymes.

1.3.4 δ- and ζ-Carbonic Anhydrases

Recently in the marine diatom *Thalassiosira weissflogii* have been identified two CA, TweCA (or TWCA1) and CDCA1, belonging respectively to classes δ and ζ.[61] TweCA is a 27 kDa protein, probably a monomer, which does not show significant sequence similarity with other carbonic anhydrases and may represent an example of convergent evolution at the molecular level. In the same diatom a rather perplexing discovery has been then made: the first cadmium-containing enzyme, which is a CA-type protein.[61] Purification of the CA-active fraction leads to the isolation of a Cd-containing protein of 43 kDa being clear that *T. weissflogii* expresses a Cd-specific CA, which, particularly under conditions of Zn limitation, can replace the Zn enzyme TWCA1 in its carbon-concentrating mechanism.

1.3.5 η-Carbonic Anhydrases

In 2004, Krungkrai and coworkers cloned a truncated form of *Plasmodium falciparum* CA gene (GenBank: AAN35994.2) encoding for an active CA (named PfCA1) with a primary structure of 235 amino acid residues.[62] Dipper investigations by means of sequence alignments of the full length PfCA1 compared with several members of the α-CA class, showed that the metal ion coordination pattern of this CA is unique (**Figure 6**).

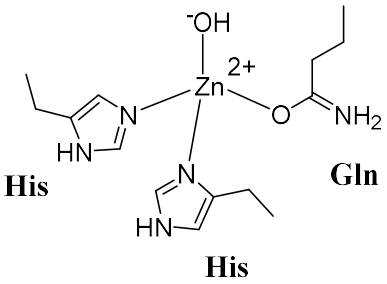

Figure 6. The metal ion coordination pattern in the η-CAs,

As above reported the metal ion is coordinated by two His and one Gln residues, in addition a water molecule/hydroxide ion. On the basis of these data, it was concluded that Plasmodia CAs were the result of modifications of an ancestral α-CA gene, which originated a new class of CA denominated as the η-class.[14-16]

1.3.6 θ-Carbonic Anhydrases

The θ-CA is a domain of the Cys-Gly-His–rich (CGHR) protein family.[17] It has been recently isolated into the lumen of the pyrenoid-penetrating thylakoid of the marine diatom *Phaeodactylum tricornutum,* where it seems to play an essential function in photosynthesis, although its reported that CO_2 hydration activity seems to be very low. Probably, its main physiological function is to control the pH gradient across the thylakoid membrane and to supply CO_2 to the Calvin cycle.[17] The detection of Zn in purified θ-CA strongly suggests that at least three residues of the highly conserved CGHR domain amino acid sequence are involved in Zn binding, such as Cys307, Asp309, His349, His363, and Cys387. On the basis of putative active-site amino acids, θ-CA is dissimilar to α- and δ-CAs and most similar to β- and ζ-CAs, which use Cys, His, and sometimes Asp to coordinate the metal ion. By contrast, the recombinant θ-CA exhibited esterase activity in addition to CA activity. Esterase activity is well known for α- and δ-CAs, thus, the biochemical properties of this θ-CA appear to be distinct from other known CAs.

1.4 Catalytic inhibition and activation mechanisms

The catalytic inhibition mechanisms of carbonic anhydrases are understood in great detail. For a long period, the only CA inhibition mechanism known involved primary sulfonamides and their isosters (sulfamates and sulfamides).[13-16] The primary sulfonamide moiety (R-SO_2NH_2) is the most important and extensively used zinc binding group (ZBG) in the design of Carbonic Anhydrase Inhibitors (CAIs). To date, X-ray crystallographic structures are available for many sulfonamide inhibitors in adducts with various CA isoforms.[36,37] All structures showed a ZBG in a deprotonated state with the nitrogen atom coordinated to Zn(II) ion in a tetrahedral geometry (**Figure 7A**). Moreover, the NH moiety forms, also, a hydrogen bond with the γ-O of Thr199, which in turn donates a hydrogen bond to the carboxylate group of Glu106. Finally, one of the oxygen atoms of the SO_2NH moiety participates in a hydrogen bond with the backbone NH moiety of Thr199.[38-40] Other classes of inhibitors which bind to the metal ion include carboxylates;[41] hydroxamates;[42] dithiocarbamates and isosteres.[43] However, this situation changed drastically in the last decade, with a large number of novel CA inhibition mechanisms reported here in **Figure 7** and new classes of

CAIs discovered apart from the zinc binders.[44] The second CA inhibition mechanism, involved inhibitors that anchoring the metal ion coordinated water molecule/hydroxide ion as shown in **Figure 7B**. These compounds incorporate an anchoring group (AG) which is hydrogen bonded to the metal ion coordinated nucleophile, eventually making additional hydrogen bonds with neighbouring residues such as the gate keeping ones (Thr199, Glu106) in the α-class enzymes. Phenol was the first inhibitor for which this mechanism was documented by X-ray crystallography,[45] followed thereafter by polyamines,[46] esters[47] and sulfocoumarins.[48]

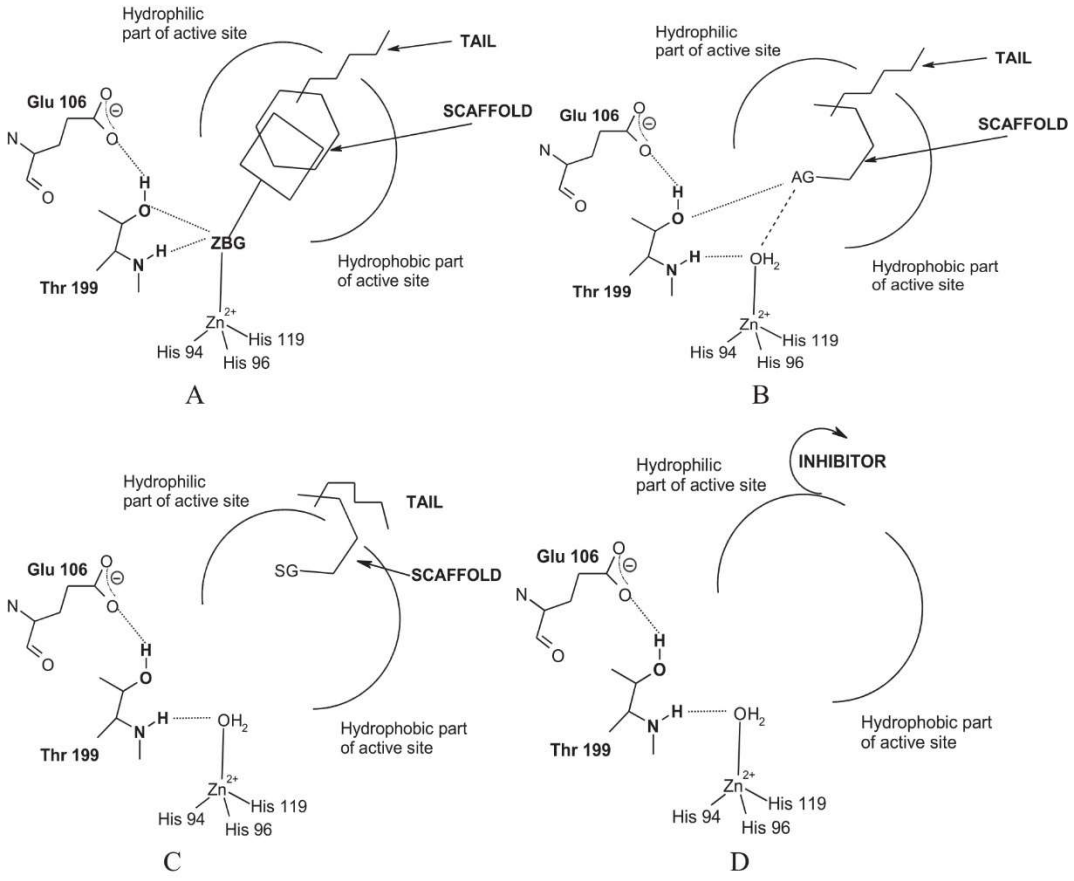

Figure 7. CA inhibition mechanisms: (**A**) Zinc binding. (**B**) Anchoring to the metal ion coordinated water. (**C**) Occlusion of the active site entrance. (**D**) Out of the active site binding.

The mechanism of inhibition discovered for coumarins[49,50] and other classes of structurally similar compounds (i.e the sulfocoumarins),[51,52] incorporate a sticky group (SG) which may be of the OH, amino, COOH and other types, and did not directly involve coordination of the metal ion. The SG moieties are created *in situ* upon hydrolysis of the coumarin or sulfocoumarin moiety and such a product relocates at the entrance of the CA active site occluding it (**Figure 7C**). The last and more recently CA inhibition mechanism (**Figure 7D**), documented by X-ray crystallography,[53] involved a particular benzoic acid derivative, which was observed bounded outside the CA cavity, and anchored in a hydrophobic pocket adjacent to the rim of the enzymatic cleft. In the latter the catalytic inhibition is achieved by fixing the proton shuttle residue (His64) in its out conformation, which leads to the collapse of the entire enzymatic cycle.[53] Traditionally the CA activation has been less investigated than the inhibitors. Only recently major interests in this area are present, thus contributing to reveal in detail the mechanisms of activation in CAs (at least for the α-class) by means of *in vitro* kinetic, spectroscopic and X-ray crystallographic studies.[54,55] All available reports in the literature exhibit CA activators (i.e. amines and amino acids) bound at the entrance of the CA active site and actively participating in the "proton shuttling" stage which is necessary to restore the enzymatic active form (**d** to **a** in **Figure 2**). Assuming as model the α-CA II, all X-ray co-crystallographic adducts showed CA activators bound at the entrance of the active site (distinct from the inhibitor binding pocket), and establishing hydrogen bond interactions with amino acids (i.e. Asn62, Asn67 and Gln92 among others) and water molecules (W129, 130 and 152) (**Figure 8**).

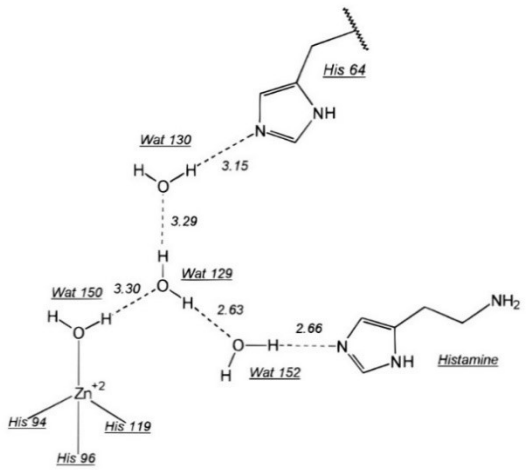

Figure 8. Scheme of the hydrogen-bonding pathways in the hCA II linking the zinc-bound Wat150 to the histamine molecule and to His64.

The formation of the complex activator-enzyme results in enhancing the enzyme regeneration rate which also is the kinetic limiting step of the entire cycle. In the absence of activators this step is assisted by the amino acid residue His64 situated in the middle of the active cavity, which also possess a pH-dependent mobility through a 64° ring-flipping.[54,56] Thy activation mechanism is in agreement with the equation below reported and since the species do interact intramolecularly, it is far more efficient than the corresponding process happening via the intermolecular fashion. [15,16]

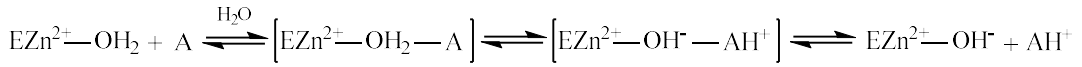

1.5 Physiological functions of carbonic anhydrases

Among the multitude of reactions reported in **Table 2** only the CO_2 hydration/bicarbonate dehydration has well established physiological relevance, being thoroughly investigated over the past 70 years in vertebrates, including *Homo sapiens*.[12,14,16,19,20] Specifically the hCA I, II, IV and XII isoforms are involved in respiration and regulation of the acid/base homeostasis.[20] The latter is involved in the transport of CO_2/bicarbonate between metabolizing tissues and excretion sites (lungs, kidneys), CO_2 elimination in capillaries and pulmonary microvasculature, elimination of H^+ ions in the renal tubules and collecting ducts as well as reabsorption of HCO_3^- in the brush border and thick ascending Henle loop in kidneys.[20] Usually, these isoforms are also expressed within the eyes by producing the bicarbonate-rich aqueous humor and their malfunction results in increase of the intraocular pressure.[19] hCA II is also involved in the bone development and function, such as the differentiation of osteoclasts or the provision of acid for bone resorption in osteoclasts.[16] Different CAs are involved in the secretion of electrolytes in many other tissues/organs, such as cerebrospinal fluid formation, by providing bicarbonate and by regulating the pH in the choroid plexus; saliva production in acinar and ductal cells; gastric acid production in the stomach parietal cells; bile production; pancreatic juice production; and intestinal ion transport.[14,19] CAs are also involved in gustation and olfaction, protection of gastrointestinal

tract from extreme pH conditions (too acidic or too basic), regulation of pH and bicarbonate concentration in the seminal fluid, muscle functions, and adaptation to cellular stress. Some isoforms such as hCA V are involved in molecular signalling processes, such as insulin secretion signalling in pancreas β cells.[14,19] hCA II and VA are involved in important metabolic processes, as they provide bicarbonate for gluconeogenesis, fatty acids *de novo* biosynthesis, or pyrimidine base synthesis. Finally, hCA IX and XII are quite abundant in tumors and are involved in oncogenesis and tumor progression.[13,14,16] Although the physiological function of some human isoforms such as hCA I and III are still unclear or poorly understood.

In this panorama, modulators, and in particular inhibitors of these enzymes, found a firm application in clinical medicine. Acetazolamide (**AAZ**) was the first nonmercurial diuretic agent introduced in clinical since 1954.[12] At present, CA inhibitors are widely used as antiglaucoma agents, diuretics, antiepileptics, for the treatment of gastric and duodenal ulcers, neurological disorders and osteoporosis.[14,16]

The aim of this work is the discovery of new and more specific modulators of CAs expressed in humans as well as in pathogenic organisms with the intent to pave the ways to the treatment of different pathologies by means of new approaches.

The current thesis is composed of seven chapters, each one dealing with the drug design, synthesis as well as *in vitro* kinetic assay of new CA modulators as potential tools for the treatment of various diseases as follows:

(i) Novel inhibitors against hCAs

(ii) Potential anticancer drugs targeting primarily hCA IX and XII that are predominantly present in tumor cells.

(iii) New class of agents for prevention of diabetic cerebrovascular pathology (which probably target the mitochondrial isoforms hCA VA and/or hCA VB).

(iv) Potential drug for the treatment of different neurological disorders such as antiepileptic or neuropathic pain (probably targeting hCA II and VII).

(v) Agents that target various CAs from pathogenic microorganisms such as the bacteria and protozoa.

(vi) New activators of hCAs

(vii) Kinetic activation studies on no human expressed CAs such as theα, β-, γ-, δ-, ζ- and η-classes.

References

1. Vallee B.L., Falchuk K. The biochemical basis of zinc physiology. *Physiol Rev.* 1993, 73, 79–118.
2. Andreini C., Bertini I., Cavallaro G. Minimal functional sites allow classification of zinc sites in proteins. *PLoS ONE.* 2011, 6, e26325.
3. Vallee B.L., Galdes A. The metallobiochemistry of zinc enzymes. *Adv Enzymol Relat Areas Mol Biol* 1984; 56, 283–430.
4. McCall K.A., Huang C.C., Fierke C.A. Function and mechanism of zinc metalloenzymes. *J. Nutr.* 2000, 130, 1437S–1446S
5. Auld D.S., Zinc enzymes. In Encyclopedia of Inorganic Chemistry, 2nd ed.; Bruce King, R., Ed.; John Wiley & Sons, Ltd: Chichester, 2005, Vol. IX, pp 5885–5927.
6. Auld D.S. Zinc coordination sphere in biochemical zinc sites. *BioMetals* 2001, 14, 271–313.
7. O'Dell B.L. Zinc plays both structural and catalytic roles in metalloproteins. *Nutr. Rev.* 1992, 50, 48–50.
8. Christianson D.W. Structural biology of zinc. *Adv. Protein Chem.* 1991, 42, 281–355.
9. Lee Y.-M., Lim C. Physical basis of structural and catalytic Zn-binding sites in proteins. *J. Mol. Biol.* 2008, 379, 545–553.
10. Anzellotti A.I., Farrell N.P. Zinc metalloproteins as medicinal targets. *Chem. Soc. Rev.* 2008, 37, 1629–1651.
11. Jacobsen F.E., Lewis J.A., Cohen S.E. The design of inhibitors for medicinally relevant metalloproteins. *ChemMedChem* 2007, 2, 152–171.
12. Keilin D., Mann T. Carbonic anhydrase. *Nature.* 1939, 144, 442–443.
13. Neri D., Supuran C.T. Interfering with pH regulation in tumours as a therapeutic strategy. *Nature Rev Drug Discov.* 2011, 10, 767–777.
14. Supuran C.T. Structure-based drug discovery of carbonic anhydrase inhibitors. *J Enzyme Inhib Med Chem.* 2012, 27, 759–772.
15. Capasso C., Supuran C.T. An overview of the alpha-, beta- and gamma-carbonic anhydrases from Bacteria: can bacterial carbonic anhydrases shed new light on evolution of bacteria? *J Enzyme Inhib Med Chem. 2015*, 30, 325–332.

16. Supuran C.T. Structure and function of carbonic anhydrases. *Biochem J.* 2016, 473, 2023–2032.
17. Kikutani S., Nakajima K., Nagasato C., Tsuji Y., Miyatake A., Matsuda Y. Thylakoid luminal θ-carbonic anhydrase critical for growth and photosynthesis in the marine diatom Phaeodactylum tricornutum. *Proc Natl Acad Sci USA.* 2016, 113, 9828–9833.
18. Del Prete S., Vullo D., Fisher G.M., Andrews K.T., Poulsen S.A., Capasso C., Supuran C.T. Discovery of a new family of carbonic anhydrases in the malaria pathogen Plasmodium falciparum–the η-carbonic anhydrases. *Bioorg Med Chem Lett.* 2014, 15, 4389–4396.
19. Supuran C.T. Carbonic anhydrases: novel therapeutic applications for inhibitors and activators. *Nature Rev Drug Discov.* 2008, 7, 168–181.
20. Supuran C.T. Structure and function of carbonic anhydrases. *Biochem J.* 2016, 473, 2023-2032.
21. Supuran C.T. Carbonic Anhydrases as drug tagets: general presentation, in Drug Design of Zinc-Enzyme Inhibitors: Functional, Structural, and Disease Applications; Supuran C.T., Winum J.-Y Eds.; Wiley: Hoboken, NJ, 2009; 15-38.
22. Supuran C.T. Advances in structure-based drug discovery of carbonic anhydrase inhibitors. *Expert Opin Drug Discov.* 2017, 12, 61-88.
23. Ogawa T., Noguchi K., Saito M., Nagahata Y., Kato H., Ohtaki A., Nakayama H., Dohmae N., Matsushita Y., Odaka M., Yohda M., Nyunoya H., Katayama Y. Carbonyl sulfide hydrolase from Thiobacillus thioparus strain THI115 is one of the *β*-carbonic anhydrase family enzymes. *J. Am. Chem. Soc.* 2013, 135, 3818–3825
24. Smeulders, M.J., Barends, T.R., Pol, A., Scherer, A., Zandvoort, M.H., Udvarhelyi, A., Khadem, A.F., Menzel, A., Hermans, J., Shoeman, R.L. et al. Evolution of a new enzyme for carbon disulphide conversion by an acidothermophilic archaeon. *Nature* 2011, 478, 412–416
25. Briganti F., Mangani S., Scozzafava A., Vernaglione G., Supuran C.T. Carbonic anhydrase catalyzes cyanamide hydration to urea: is it mimicking the physiological reaction? *J. Biol. Inorg. Chem.* 1999, 4, 528–536

26. Guerri A., Briganti F., Scozzafava A., Supuran C.T., Mangani S. Mechanism of cyanamide hydration catalyzed by carbonic anhydrase II suggested by cryogenic X-ray diffraction. *Biochemistry* 2000, 39, 12391–12397
27. Pocker Y., Meany, J.E. The catalytic versatility of carbonic anhydrase from erythrocytes. The enzymatic catalyzed hydration of acetaldehyde. *J. Am. Chem. Soc.* 1965, 87, 1809–1811.
28. Pocker Y., Stone J.T. The catalytic versatility of erythrocyte carbonic anhydrase. The enzyme-catalyzed hydrolysis of para -nitrophenyl acetate. *J. Am. Chem. Soc.* 1965, 87, 5497–5498.
29. Innocenti A., Supuran C.T. Paraoxon, 4-nitrophenyl phosphate and acetate are substrates of α- but not of β-, γ - and ζ -carbonic anhydrases. *Bioorg. Med. Chem. Lett.* 2010, 20, 6208–6212
30. Innocenti A., Scozzafava A., Parkkila S., Puccetti L., De Simone G., Supuran C.T. Investigations of the esterase, phosphatase, and sulfatase activities of the cytosolic mammalian carbonic anhydrase isoforms I, II, and XIII with 4-nitrophenyl esters as substrates. *Bioorg. Med. Chem. Lett.* 2008, 18, 2267–2271
31. Kazancioglu E.A., Guney M., Senturk M., Supuran, C.T. Simple methanesulfonates are hydrolyzed by the sulfatase carbonic anhydrase activity. *J. Enzyme Inhib. Med. Chem.* 2012, 27, 880–885
32. Cavdar H., Ekinci D., Talaz O., Saracoglu N., Senturk M., Supuran, C.T. α-Carbonic anhydrases are sulfatases with cyclic diol monosulfate esters. *J. Enzyme Inhib. Med. Chem.* 2012, 27, 148–154
33. Carta F., Maresca A., Scozzafava A., Supuran C.T. 5- and 6-membered (thio)lactones are prodrug type carbonic anhydrase inhibitors. *Bioorg. Med. Chem. Lett.* 2012, 22, 267–270
34. Tanc M., Carta F., Scozzafava A., Supuran C.T. α-Carbonic anhydrases possess thioesterase activity. *ACS Med. Chem. Lett.* 2015, 6, 292–295
35. Supuran C.T., Conroy C.W., Maren T.H. Is cyanate a carbonic anhydrase substrate? *Proteins* 1997, 27, 272–278
36. Supuran C.T. Carbonic anhydrase inhibitors. *Bioorg. Med. Chem. Lett.* 2010, 20, 3467–3474

37. De Simone, G., Supuran C.T. (In)organic anions as carbonic anhydrase inhibitors. *J. Inorg. Biochem*. 2012, 111, 117–129
38. Angeli A., Di Cesare Mannelli L., Lucarini E., Peat T.S., Ghelardini C., Supuran C.T. Design, synthesis and X-ray crystallography of selenides bearing benzenesulfonamide moiety with neuropathic pain modulating effects. *Eur J Med Chem.* 2018, 154, 210-219
39. Angeli A., Di Cesare Mannelli L., Trallori E., Peat T.S., Ghelardini C., Carta F., Supuran C.T. Design, Synthesis, and X-ray of Selenides as New Class of Agents for Prevention of Diabetic Cerebrovascular Pathology. *ACS Med Chem Lett.* 2018, 9, 462-467.
40. Angeli A., Tanini D., Peat T.S., Di Cesare Mannelli L., Bartolucci G., Capperucci A., Ghelardini C., Supuran C.T., Carta F. Discovery of New Selenoureido Analogues of 4-(4-Fluorophenylureido)benzenesulfonamide as Carbonic Anhydrase Inhibitors. *ACS Med Chem Lett.* 2017, 8, 963-968
41. Innocenti A., Vullo D., Scozzafava A., Casey J.R., Supuran C.T. Carbonic anhydrase inhibitors. Interaction of isozymes I, II, IV, V and IX with carboxylates. *Bioorg. Med. Chem. Lett.* 2005, 15, 573–578
42. Di Fiore A., Maresca A., Supuran C.T., De Simone G. Hydroxamate represents a versatile zinc binding group for the development of new carbonic anhydrase inhibitors. *Chem. Commun.* 2012, 48, 8838–8840
43. Carta F., Aggarwal M., Maresca A., Scozzafava A., McKenna R., Masini E., Supuran C.T. Dithiocarbamates strongly inhibit carbonic anhydrases and show antiglaucoma action in vivo. *J. Med. Chem.* 2012, 55, 1721–1730
44. Supuran C.T. How many carbonic anhydrase inhibition mechanisms exist? *J. Enzyme Inhib. Med. Chem.* 2016, 31, 345–360
45. Nair S.K., Ludwig P.A., Christianson D.W. Two-site binding of phenol in the active site of human carbonic anhydrase II: structural implications for substrate association. *J. Am. Chem. Soc.* 1994, 116, 3659–3660
46. Carta F., Temperini C., Innocenti A., Scozzafava A., Kaila K., Supuran, C.T. Polyamines inhibit carbonic anhydrases by anchoring to the zinc-coordinated water molecule. *J. Med. Chem.* (2010), 53, 5511–5522

47. Davis R.A., Hofmann A., Osman A., Hall R.A., Muhlschlegel F.A., Vullo D., Innocenti A., Supuran C.T., Poulsen S.A. Natural product-based phenols as novel probes for mycobacterial and fungal carbonic anhydrases. *J. Med. Chem.* 2011, 54, 1682–1692
48. Tars K., Vullo D., Kazaks A., Leitans J., Lends A., Grandane A., Zalubovskis R., Scozzafava A., Supuran C.T. Sulfocoumarins (1,2-benzoxathiine-2,2-dioxides): a class of potent and isoform-selective inhibitors of tumor-associated carbonic anhydrases. *J. Med. Chem.* 2013, 56, 293–300
49. Maresca A., Temperini C., Vu H., Pham N.B., Poulsen S.A., Scozzafava A., Quinn R.J., Supuran C.T. Non-zinc mediated inhibition of carbonic anhydrases: coumarins are a new class of suicide inhibitors. *J. Am. Chem. Soc.* 2009, 131, 3057–3062
50. Maresca A., Temperini C., Pochet L., Masereel B., Scozzafava A., Supuran C.T. Deciphering the mechanism of carbonic anhydrase inhibition with coumarins and thiocoumarins. *J. Med. Chem.* 2010, 53, 335–344
51. Touisni N., Maresca A., McDonald P.C., Lou Y., Scozzafava A., Dedhar S., Winum J.Y., Supuran C.T. Glycosylcoumarin carbonic anhydrase IX and XII inhibitors strongly attenuate the growth of primary breast tumors. *J. Med. Chem.* 2011, 54, 8271–8277
52. Bonneau A., Maresca A., Winum J.Y., Supuran, C.T. Metronidazole-coumarin conjugates and 3-cyano-7-hydroxy-coumarin act as isoform-selective carbonic anhydrase inhibitors. *J. Enzyme Inhib. Med. Chem.* 2013, 28, 397–401
53. D'Ambrosio K., Carradori S., Monti S.M., Buonanno M., Secci D., Vullo D., Supuran C.T., De Simone G. Out of the active site binding pocket for carbonic anhydrase inhibitors. *Chem. Commun.* 2015, 51, 302–305
54. Briganti F., Mangani S., Orioli P., Scozzafava A., Vernaglione G., Supuran C.T. Carbonic anhydrase activators: X-ray crystallographic and spectroscopic investigations for the interaction of isozymes I and II with histamine, *Biochemistry* 1997, 36, 10384–10392.
55. Clare B.W., Supuran C.T., Carbonic anhydrase activators. 3: structure-activity correlations for a series of isozyme II activators, *J. Pharm. Sci.* 1994, 83, 768–773.
56. Supuran C.T. Future Med Chem. 2018 10, 561-573. Carbonic anhydrase activators.

57. Cronk J.D., Rowlett R.S., Zhang K.Y., Tu C., Endrizzi J.A., Lee J., Gareiss P.C., Preiss J.R. Identification of a novel noncatalytic bicarbonate binding site in eubacterial beta-carbonic anhydrase. *Biochemistry* 2006, 45, 4351–4361
58. Alber B.E., Ferry J.G. A carbonic anhydrase from the archaeon Methanosarcina thermophile. *Proc. Natl. Acad. Sci. U.S.A.* 1994, 91, 6909-6913
59. Kisker C., Schindelin H., Alber B.E. Ferry, J.G., Rees, D.C. A left-hand beta-helix revealed by the crystal structure of a carbonic anhydrase from the archaeon Methanosarcina thermophila. *EMBO J.* 11996, 5, 2323–2330
60. Iverson T.M., Alber B.E., Kisker C., Ferry J.G., Rees D.C. A closer look at the active site of gamma-class carbonic anhydrases: high-resolution crystallographic studies of the carbonic anhydrase from Methanosarcina thermophila . *Biochemistry* 2000, 39, 9222–9231
61. Alterio V., Langella E., Viparelli F., Vullo D., Ascione G., Dathan N.A., Morel F.M., Supuran C.T., De Simone G., Monti S.M. Structural and inhibition insights into carbonic anhydrase CDCA1 from the marine diatom Thalassiosira weissflogii. *Biochimie.* 2012, 94, 1232-41.
62. Reungprapavut S., Krungkrai S.R., Krungkrai J. Plasmodium falciparum carbonic anhydrase is a possible target for malaria chemotherapy. *J Enzyme Inhib Med Chem.* 2004, 9, 249-56.

Chapter 2

Novel inhibitors against human carbonic anhydrases

2.1 Primary sulfonamides with subnanomolar carbonic anhydrase II and IX inhibitory activities and X-ray investigation

In order to synthesize chemically novel and sulfur-containing CA inhibitors we developed a synthetic procedure based on the reaction of the disulfide **2** with an electrophilic agents as below reported.

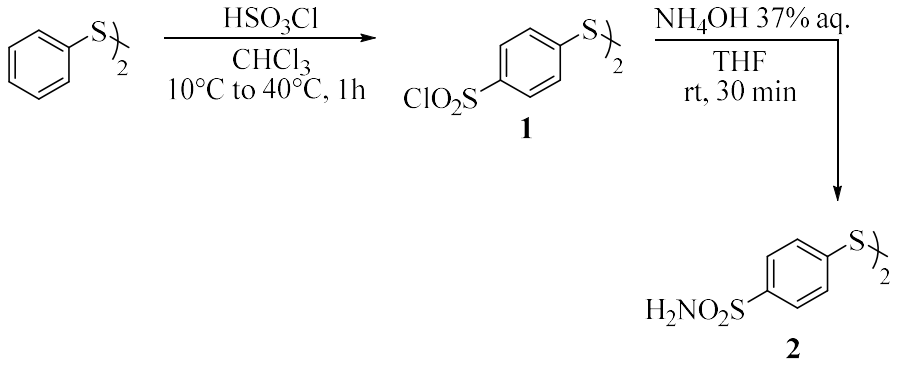

Scheme 1: Synthesis of disulfide **2**, bearing the benzenesulfonamide moiety

The disulfide **2** was conveniently obtained by treating the readily obtained disulfonylchloride **1** with a 37% aqueous ammonium hydroxide solution. The intermediate sulfonylchloride **1** was prepared according to reported procedures [1] using the commercially available diphenyl disulfide and chlorosulfonic acid (**Scheme 1**). In order to synthesize unsymmetrical sulfides incorporating the benzenesulfonamide moiety, compound **2** was reduced with $NaBH_4$, and the corresponding thiolate **3** was treated *in situ* with the appropriate electrophilic species **4a-e** to afford the sulfides **5a-e** in good yield, as reported in the **Scheme 2**.

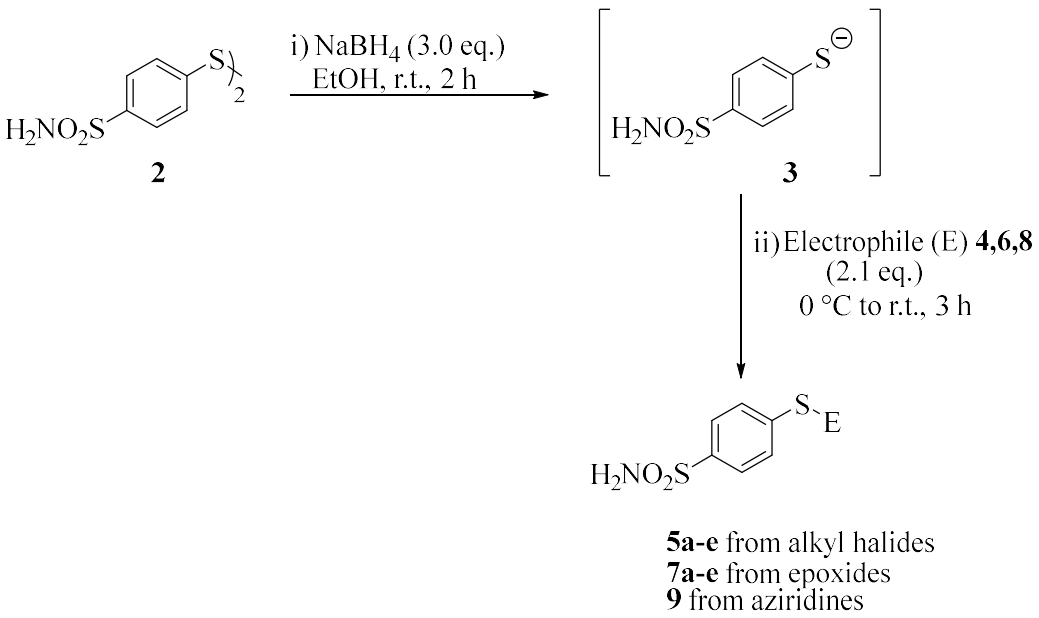

Scheme 2: Synthesis of sulfides bearing benzenesulfonamide moiety

Interestingly, the product **5e** (**Table 1**, entry 5) was selectively formed from methyl 3-bromopropionate **4e**, as no traces of compounds arising from substitution or reduction at the carbonyl position have been observed. Having explored the reactivity of **3** with alkyl halides, we turned our attention on the ring opening reaction of strained heterocycles. Thus, monosubstituted epoxides **6a-d** were treated with thiolate **3** under the above reported conditions affording the β-hydroxysulfides **7a-d** (**Table 1**, entries 6-9), bearing saturated or unsaturated carbon chains, and protected or free hydroxyl groups. Furthermore, the limonene derived sulfide **7e** was synthesised from the disubstituted epoxide **6e**. Finally, with the aim of enlarging the scope of such a procedure to another class of three-membered heterocycles, the enantio-enriched *N*-tosyl aziridine **8**, obtained from L-phenylalanine, afforded the β-amino substituted sulfide **9** (**Table 1**, entry 11).

Table 1. Sulphides **5-9** bearing benzenesulfonamide moiety

Entry	Electrophile		Product	
1	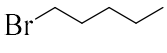	**4a**	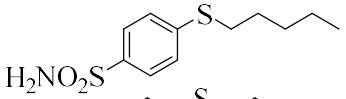	**5a**
2	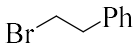	**4b**	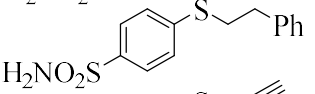	**5b**
3	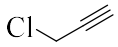	**4c**	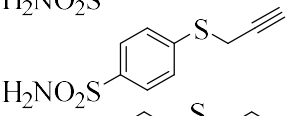	**5c**
4	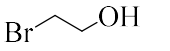	**4d**	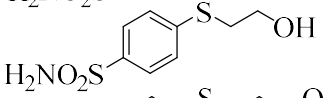	**5d**
5	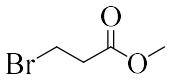	**4e**	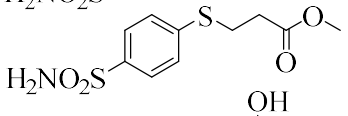	**5e**
6		**6a**	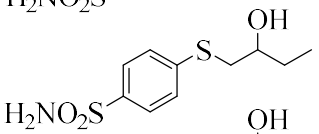	**7a**
7	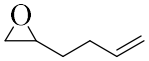	**6b**	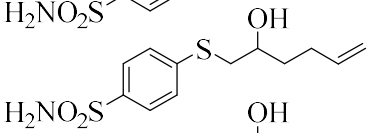	**7b**
8	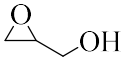	**6c**	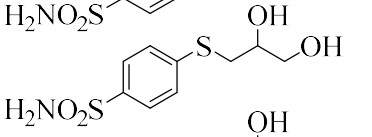	**7c**
9	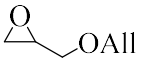	**6d**	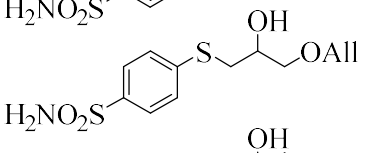	**7d**
10	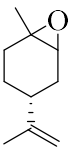	**6e**	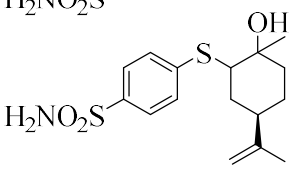	**7e**
11	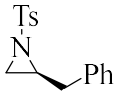	**8**	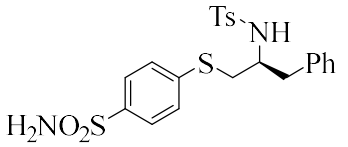	**9**

All the ring opening reactions here described were demonstrated to be highly regio-selective, as only the isomer arising from the nucleophilic attack at the less hindered carbon of the strained heterocycle was observed.[2,3] Having obtained a set of sulfides through the reaction of **2** with different electrophiles, we extended this procedure to the synthesis of thiol esters bearing the benzenesulfonamide moiety. Thus, the thiolate **3** was treated *in situ* with acyl

chlorides to afford the thiol esters **10a-e**. The reaction proved to be efficient, allowing the synthesis of saturated and unsaturated fatty acid derived thiol esters **10a-c** (i.e. caprylic, stearic, and oleic acids). Furthermore, α,β-unsaturated thiol ester **10d** and aromatic thiol esters **10e** were achieved from cinnamoyl chloride and 2,4-bis(trifluoromethyl)benzoyl chloride as reported in **Scheme 3**.

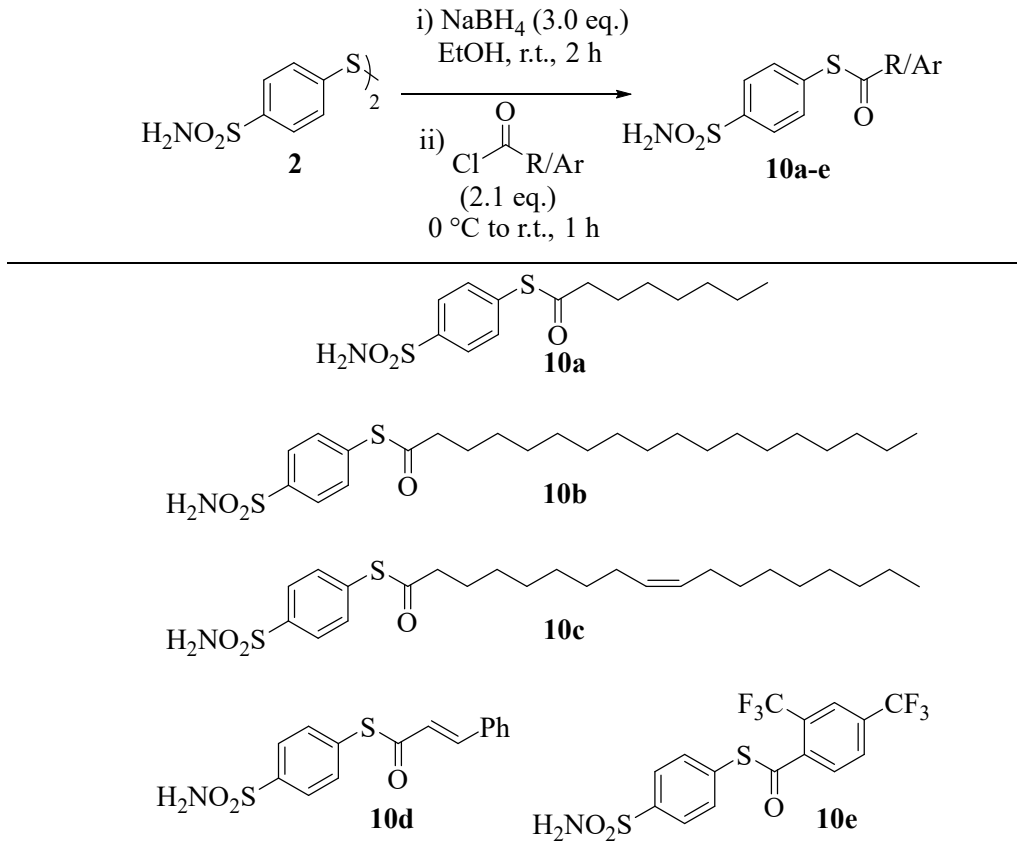

Scheme 3: Synthesis of thiol esters bearing benzenesulfonamide moiety

Having synthesised a representative series of functionalized sulfides and thiol esters encorporating the benzenesulfonamide moiety, we also prepared disulfides **11a-c**, bearing two primary and two secondary sulfonamide groups. Compounds **11a-c** could be easily achieved by reacting the disulphonylchloride **1** with the suitable amine in the presence of trimethylamine (**Scheme 4**).

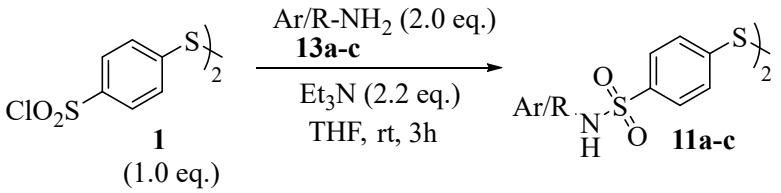

Entry	Electrophile	Product
1	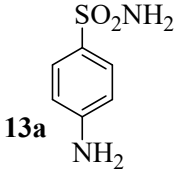	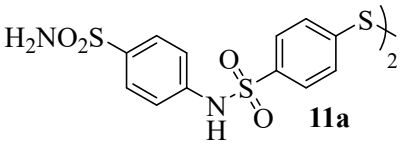
2	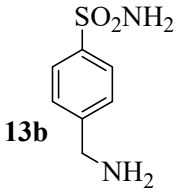	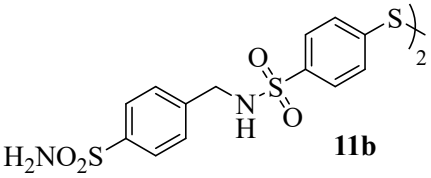
3	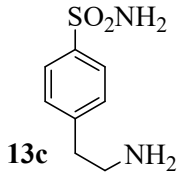	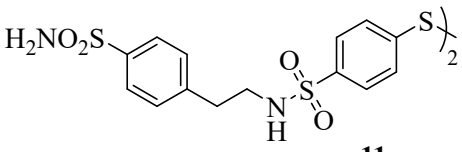

13a **11a**

13b **11b**

13c **11c**

Scheme 4: Synthesis of disulfides **11a-c**

All compounds **2**, **5a-e**, **7a-e**, **9**, **10a-e** and **11a-c** were tested in vitro for their inhibitory activity against the physiologically relevant hCA isoforms I, II, IV and IX by means of the stopped-flow carbon dioxide hydration assay[4] and their activities were compared to the standard CAI acetazolamide (**AAZ**) (**Table 2**).

Table 2. Inhibition constants of hCA I, hCA II, hCA IV and hCA IX with compounds **2**, **5a-g**, **7a-e**, **9**, **10a-e**, **11a-c** and **AAZ** by a stopped-flow CO_2 hydrase assay[4]

	K_i (nM)*			
Compound	hCA I	hCA II	hCA IV	hCA IX
2	412.7	0.9	368.3	0.5
5a	773.6	0.4	436.5	0.6
5b	227.5	0.4	80.9	0.9
5c	30.2	29.5	838.9	7.6
5d	135.6	37.2	878.0	36.7
5e	41.7	0.6	808.4	6.6
7a	138.1	0.8	683.6	2.0
7b	139.9	4.0	505.6	6.8
7c	74.8	31.0	552.6	41.7
7d	50.4	3.7	709.6	6.0
7e	9.8	1.4	87.7	0.6
9	685.2	197.2	2046	969.0
10a	76.7	47.0	5357	166.3
10b	513.3	663.5	9500	4687
10c	519.3	879.0	9647	37.3
10d	89.3	4.9	6888	268.9
10e	32.3	4.9	4933	5.2
11a	88.1	53.1	430.9	5.6
11b	542.5	69.0	752.8	55.4
11c	244.4	8.3	1985	139.3
AAZ	250	12.1	74.0	25.8

* Mean from three determinations by a stopped-flow, CO_2 hydrase method. Standard errors were in the range of 5–10% of the reported values.

The following structure–activity relationship (SAR) can be drawn from the data obtained and reported in **Table 2**:

i) The cytosolic isoform, hCA I, was inhibited by disulfide **2** with inhibition constant in the high nanomolar range (K_i 412.7 nM). Thioether scaffolds **5a-e** play a crucial role for the potency of inhibition. Compounds **5c** and **5e** showed an efficacy over 4 fold than the similar derivatives. On the other hand, β-hydroxysulfide from natural product limonene **7e** resulted the most potent inhibitor against this isoform. Like as

compounds mentioned above, thioesters tails lead to significant changes in the inhibition potency. Compounds **10b-c** with high hydrophobic moieties showed a significant decrease of the inhibitory potency in high nanomolar range (K_i 513.3 and 519.3 nM respectively), instead, the efficacy increased when the moiety was changed with short aliphatic chain (**10a** and **10e**) or cinnamic scaffold (**10d**). The potency of inhibition for disulfides **11a-c** can be modulate by changing the methylene chain length. Indeed, compound **11a** showed a potency over 2 times better than compound with an ethylene chain (**11c)** and over 6 times for compound with a single methylene (**11b**).

ii) The dominant cytosolic isoform, hCA II, was strong inhibited by disulfide **2** and most thioether compounds **5a-e** in sub-nanomolar range (K_i 0.4 to 0.9 nM). An interesting case is constituted by the thioesther compounds **10a-e**, for which the long hydrophobic tails led to a decrease of potency over 100 fold compared to the other similar products (K_i 663.5 and 879.0 nM for **10b**, **c** than 4.9 nM **10d, e**). Unlike the hCA I cytosolic isoform, the introduction of a methylene linker in compounds **11a-c** had diverse effects on the inhibition profile. A decrease of the potency was observed for a methylene linker with one or without a carbon atom (**11b**, a K_i of 69.0 nM and **11a** a K_i of 53.1 nM), whereas, a further chain elongation, as in **11c**, led to an increase of the potency, with a K_i of 8.2 nM.

iii) The membrane-bound hCA IV was inhibited by most of the compounds investigated here in the high nanomolar range or in the micromolar range. Thioethers **5a-e** and β-hydroxysulfides **7a-e** compounds showed an efficacy against this isoform, near ten times better than thioesters derivatives **10a-e** (K_i 0.4 to 37.2 nM for **5a-e** and **7a-e** than 4.9 to 879.0 nM for **10a-e**).

iv) hCA IX, the tumor-associated isoform, was effectively inhibited by many of the compounds reported here, especially thioether derivatives **5a-b**, **7e** and disulphide **2** in sub-nanomolar range (K_i 0.5 to 09 nM). On the other hand, compounds **10a-e** showed an over 100 times decrease in potency against this isoform. Unlike the other isoforms, the introduction of methylene chain in compounds **11a-c** had an almost linear effect on efficacy of inhibition. Indeed, increasing the linker led to loss of

potency near ten fold with one atom of carbon (**11b** K_i 55.4 nM) and over 20 fold with two atoms of carbon (**11c** K_i 139.3 nM).

To better understand the strong inhibition of thioether derivatives (**5a-e**) reported here against hCA II, we solved the X-ray structure of the compound **5b** bound to this isoform at 1.5 Å resolution, in order to identify the key interactions involved into protein-inhibitor interactions at the atomic level. Data collection and refinement of adduct was performed as described in the Experimental Section. Active site of hCA II showed the classic binding mode of sulfonamide inhibitors, where, the deprotonated nitrogen atom displaces the hydroxyl ion/water molecule present in the native enzyme and coordinates the zinc ion with a tetrahedral geometry by His94, His96 and His119, while additional hydrogen bond interactions with residue Thr199 further contribute to stabilize the binding (**Figure 1**).

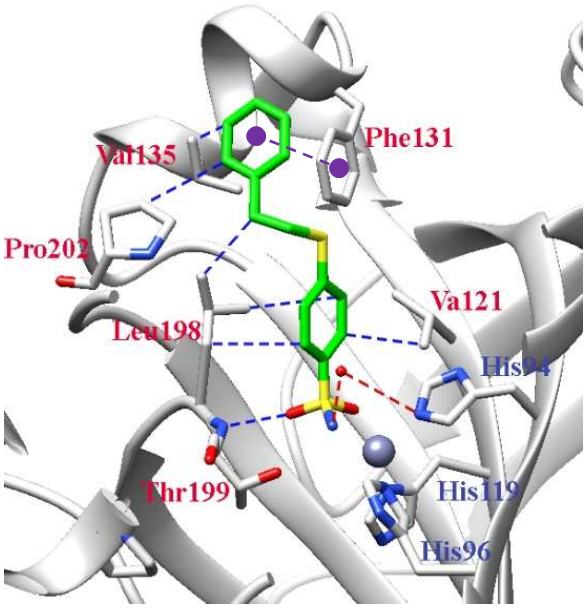

Figure 1: Ligand **5b** in the active site of hCA II (PDB: 6GOT) is shown in green. The zinc ion is the gray sphere with its protein ligands (His94, 96 and 119 in blue) shown as stick model, in CPK colors. Residues involved in the binding of inhibitors are also shown. Hydrophobic interactions and H-bonding are shown as blue dashed lines, π-Stacking as magenta and water bridges as red.

The hydrophobic tail of inhibitor **5b** is located in the hydrophobic region of the active site in a small pocket delimited by residues Phe131, Val135, Leu198, and Pro202 (**Figure 1**) and forms strong hydrophobic interactions with these residues. In addition to these contacts, a π-stacking interaction between Phe131 and the aromatic ring scaffold of inhibitor was evidenced.

2.2 Synthesis of Novel Selenides Bearing Benzenesulfonamide Moieties as Carbonic Anhydrase I, II, IV, VII, and IX Inhibitors.

Selenium has a long history of association with human health and disease.[5,6] Interest in the potential biological, pharmacological and therapeutic exploitation of synthetic organoselenium compounds started several decades ago. With the aim of synthesising a new series of hydroxy- and amino- functionalized selenium containing CAI, we sought to exploit the reactivity of three-membered ring, such as epoxides and aziridines, with a suitable selenolate, bearing the benzenesulfonamide moiety generated from the corresponding diselenide **14** and synthesized as shown in the **Scheme 5**. The diazonium salt of sulfanilamide was prepared by reaction of **12** with sodium nitrite in the presence of acid (Sandmeyer reaction) and used as key intermediate for the synthesis of compound **13**. Successively, the selenocyanate derivative **13** was converted easily into the diselenide **14** by reaction with $NaBH_4$ in ethanol.

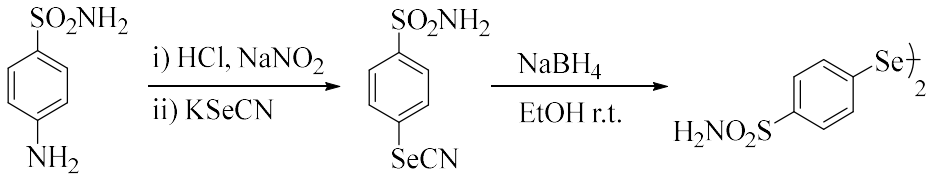

Scheme 5: Synthesis of selenocyanate and diselenide bearing benzenesulfonamide moiety

Having in our hands the diselenide **14**, we evaluated the possibility to access β-hydroxy selenides by using the ring opening reaction with epoxides.[7-9] Thus, **14** was reduced with $NaBH_4$ to the corresponding selenolate which was treated *in situ* with benzyl glycidyl ether

15a, affording the β-hydroxyselenide **16a** in good yield (**Table 3**, entry 1). The process proved to be highly regioselective, as only the isomer arising from the nucleophilic attack at the less hindered carbon of the oxirane was observed. On the basis of these results, and in order to study the generality of such a procedure, a series of epoxides was reacted with **14** under the same conditions, as reported in **Table 3**. Thus, differently substituted hydroxyl selenides **16b-g** were obtained from the corresponding epoxides **15b-g** through a regioselective ring opening route (**Table 3**, entries 2-4). Interestingly, (±) epibromohydrine **15e** was smoothly converted into **16e** in excellent yields; the nucleophilic attack occured exclusively on the epoxide since the halide was preserved on the side chain (**Table 3**, entry 5). Disubstituted hydroxy selenides **16f, g** were obtained by reacting **14** with cyclohexene oxide **15f** and limonene oxide **15g** (**Table 3**, entries 6, 7).

Table 3: Synthesis of β-hydroxy selenides bearing benzenesulfonamide moiety

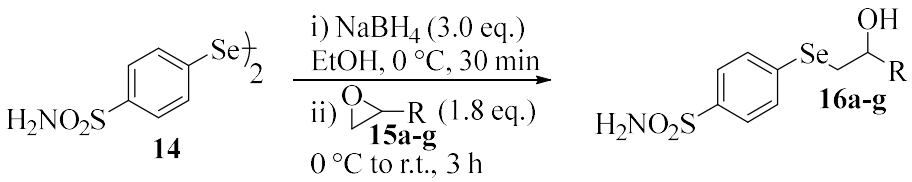

Entry	Epoxide		Product	
1	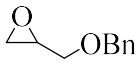	**15a**	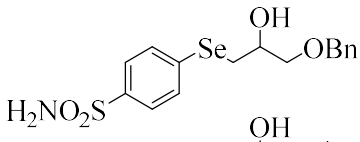	**16a**
2	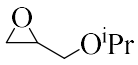	**15b**	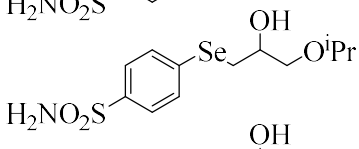	**16b**
3	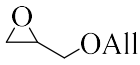	**15c**	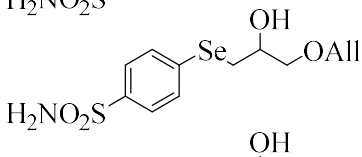	**16c**
4	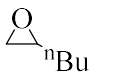	**15d**	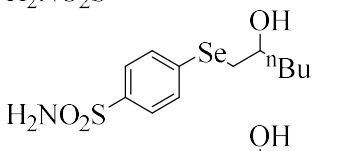	**16d**
5	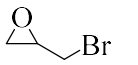	**15e**	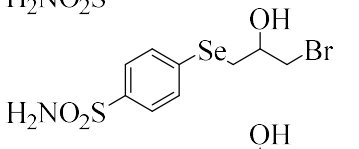	**16e**
6	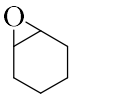	**15f**	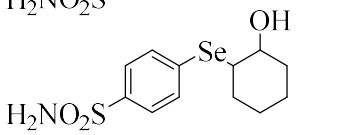	**16f**
7	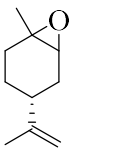	**15g**	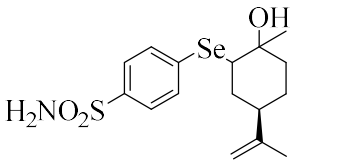	**16g**

In order to access benzenesulfonamide-substituted selenides bearing the amino group, the procedure was extended to differently N-protected aziridines **17**,[10,11] synthesised from natural aminoacids. As reported in the **Scheme 6**, enantioenriched *N*-Tosyl and *N*-Boc selenides **18a-c** were obtained in good yields from **17a-c** through a regio- and stereo-selective reaction.

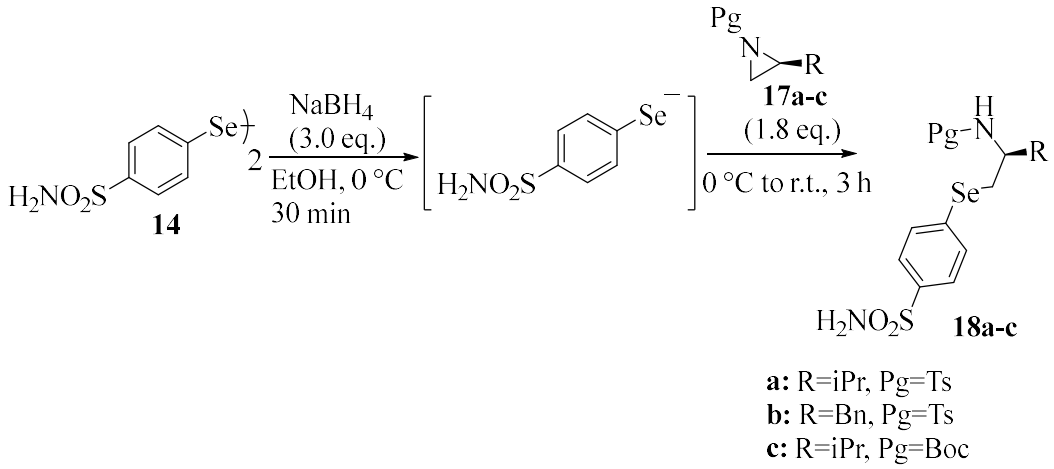

Scheme 6: Synthesis of *N*-protected β-amino selenides bearing benzenesulfonamide moiety

Finally, the free selenoamine **19** was obtained from the *N*-Boc derivative **18c** by the acetyl chloride promoted cleavage of the protecting group (**Scheme 7**).[12]

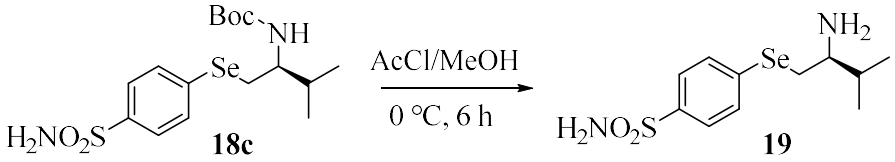

Scheme 7: Synthesis of β-amino selenide bearing benzenesulfonamide moiety

As a further investigation, in order to propose an alternative way to access the target compounds, we sought to achieve β-hydroxy- and β-amino- selenides from the selenocyanate **13**, thus avoiding the synthesis of the diselenide **14**. After having optimized the reaction conditions, we were pleased to observe that selenides **16a,b** and **18a** were obtained by ring opening of epoxides **15a,b** and aziridine **17a** with the selenolate, in situ generated by reducing **13**, as reported in the **Scheme 8.**

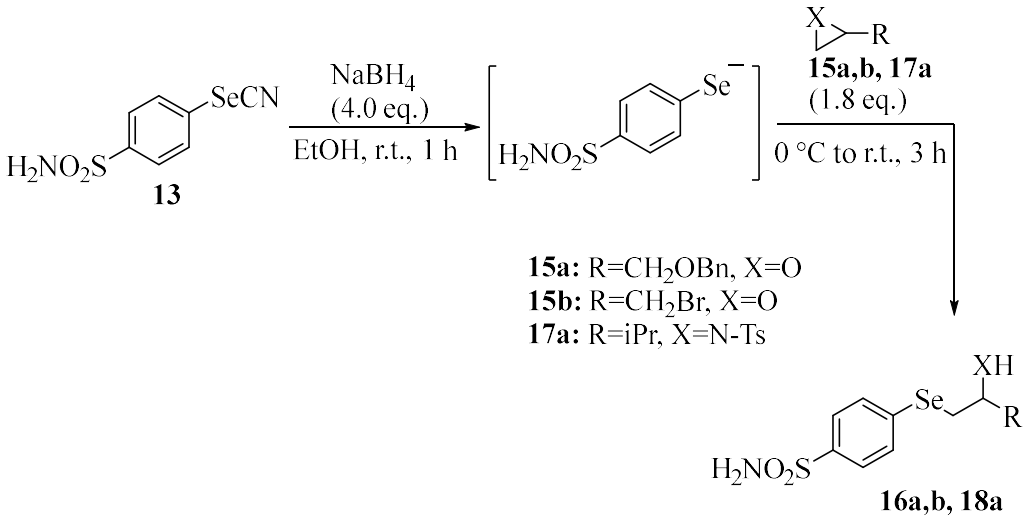

Scheme 8: Synthesis of selenides bearing benzenesulfonamide moiety

We investigated the CA inhibitory proprieties of compounds **13**, **14**, **16a-g**, **18a-c** and **19** against the physiologically relevant hCA isoforms I, II, IV, VII and IX by means of the stopped-flow carbon dioxide hydration assay[4] after a period of 15 min of incubation of the enzyme and inhibitor solutions. Their activities were compared to the standard CAI acetazolamide (**AAZ**) (**Table 4**).

Table 4. Inhibition constants of hCA I, hCA II, hCA IV, hCA VII and hCA IX with compounds **13**, **14**, **16a-g**, **18a-c**, **19** and **AAZ** by a stopped-flow CO_2 hydrase assay[4]

Compound	K_i (nM)*				
	hCA I	hCA II	hCA IV	hCA VII	hCA IX
13	95.6	53.1	30.6	7.1	9.3
14	1523	7.9	298.4	40.5	2.7
16a	193.8	1.4	377.7	1.9	10.1
16b	73.2	4.4	403.1	0.7	15.9
16c	8084	920.8	8133	74.2	11.9
16d	228.8	8.8	429.2	0.8	5.6
16e	127.2	4.9	319.3	7.4	6.5
16f	148.6	7.4	458.2	0.8	8.3
16g	8.4	0.2	34.8	0.7	2.4
18a	881.1	14.0	435.2	0.4	10.1
18b	4365	90.2	5601	3.4	2.4
18c	1471	15.9	2825	3.5	2.3
19	93.0	0.5	2321	36.2	2.4
AAZ	250.0	12.1	74.0	2.5	25.8

* Mean from three determinations by a stopped-flow, CO_2 hydrase method. Standard errors were in the range of 5–10% of the reported values.

The following structure activity relationship (SAR) may be noted regarding the inhibition data of **Table 4**:

i) The ubiquitous cytosolic hCA I was inhibited by all compounds with K_i spanning between low nanomolar range (K_i 8.4 nM) to high micromolar range (K_i 8084.3 nM). Selenocyanate derivative **13** inhibited hCA I in medium nanomolar range (K_i 95 nM) but, the next step, with the formation of diselenide **14**, showed a decreased potency of inhibition of almost 15 folds. β-Hydroxy selenides **16g** showed the best potency of inhibition with K_i of 8.4 nM. Moreover, a less bulky tail moiety such as cyclohexane (**16f**) decreased 16 folds the activity. Compound **19** inhibited this isoform in medium nanomolar range with K_i 93 nM. Same compound with different *N*- protecting groups **18a** and **18c** led to decrease the activity of inhibition near 9 times with tosyl group (**18a**) and 18 times for Boc group (**18c**).

ii) The dominant cytosolic human isoform, hCA II, was inhibited in low or low-medium nanomolar range by all compounds here considerated, except for derivative **5c** which acted in the high nanomolar range (K_i 920.8 nM). Selenocyanate derivate **13** was 6 folds less active compared to diselenide **14**. β-Hydroxy selenides compounds **16a-g** proved to be potent inhibitors for this isoform (with K_i between 0.18 to 8.8 nM) except for **16c** as mentioned earlier. In addition, β-amino selenide **19** showed a potent inhibition profile for hCA II. On the other hand, the introduction of N-protecting groups **18a** and **18c** led to a decrease the potency of inhibition nearly 29 times.

iii) The last cytosolic human isoform studied, hCA VII, was inhibited by all compounds in low or low-medium nanomolar range. This time, compound **13** led to be 6 times less potent compared to diselenide **14**. The presence of N-protecting groups for compounds **18a** and **18c**, increased the efficacy 10 times for Boc moiety and 100 times for tosyl moiety respect to the unprotected one (**19**).

iv) Almost all compounds here considerated, possessed low inhibitory activity for the membrane-bound hCA IV with K_is spanning between high nanomolar to micromolar range. Compound **13** showed the best activity against this isoform with K_i 30.6 nM but, the efficacy decreased with diselenide derivative **14** in high nanomolar range (K_i 298.4 nM). Different substituents on the β-hydroxy selenides **16a-g** did not effectively influenced the inhibition activity, except for compound **16c** which led to decrease of the efficacy up to the high micromolar range (K_i 8133 nM). Also for this isoform, compound **18a**, with the tosyl moiety as protectingd group, prove to have the better inhibition profile when compared to the other β-amino selenide.

v) The transmembrane tumor-associated hCA IX, was effectively inhibited by all compounds in low nanomolar range. Likewise to the other membrane isoform, substituents on β-hydroxy selenides **16a-g** did not influence the efficacy of inhibition. Moreover, N-protection for compounds **18a** and **18c** did not significantly change the profile of inhibition compared to the β-amino selenide **19**.

2.3 Synthesis of novel acyl selenoureido benzensulfonamides as carbonic anhydrase I, II, VII and IX inhibitors

Our interest towards organo-selenium compounds includes the development and synthesis of stable organo-selenium compounds that serve as antioxidant adjuvants against ROS damage. The rationale for the drug design for the compounds reported below is based on the bioisosteric replacement of the ureido moiety in the carbonic anhydrase inhibitor SLC-0111 [13] with a selenoureido group. Additionally, the tail end of the ureido moiety was changed with phenylacyl functionalities. This moiety possesses both high flexibility and potential to interact through multiple hydrogen bondings within the CA enzymatic cavity and thus may enhance the selectivity of compounds towards specific isforms.[14] With the same objective the zinc binding group (SO_2NH_2), the head section of the molecules was placed at different positions. The synthesis of the new compounds **25-29** is shown in **Scheme 9**. The acylselenoureido compounds were synthesized following the method of Koketsu *et al*.[15] We have obtained *in situ* the acyl isoselenocyanate (not isolated) and coupled it with the appropriate and commercially available amino benzensulfonamide (**12**, **21-24**).

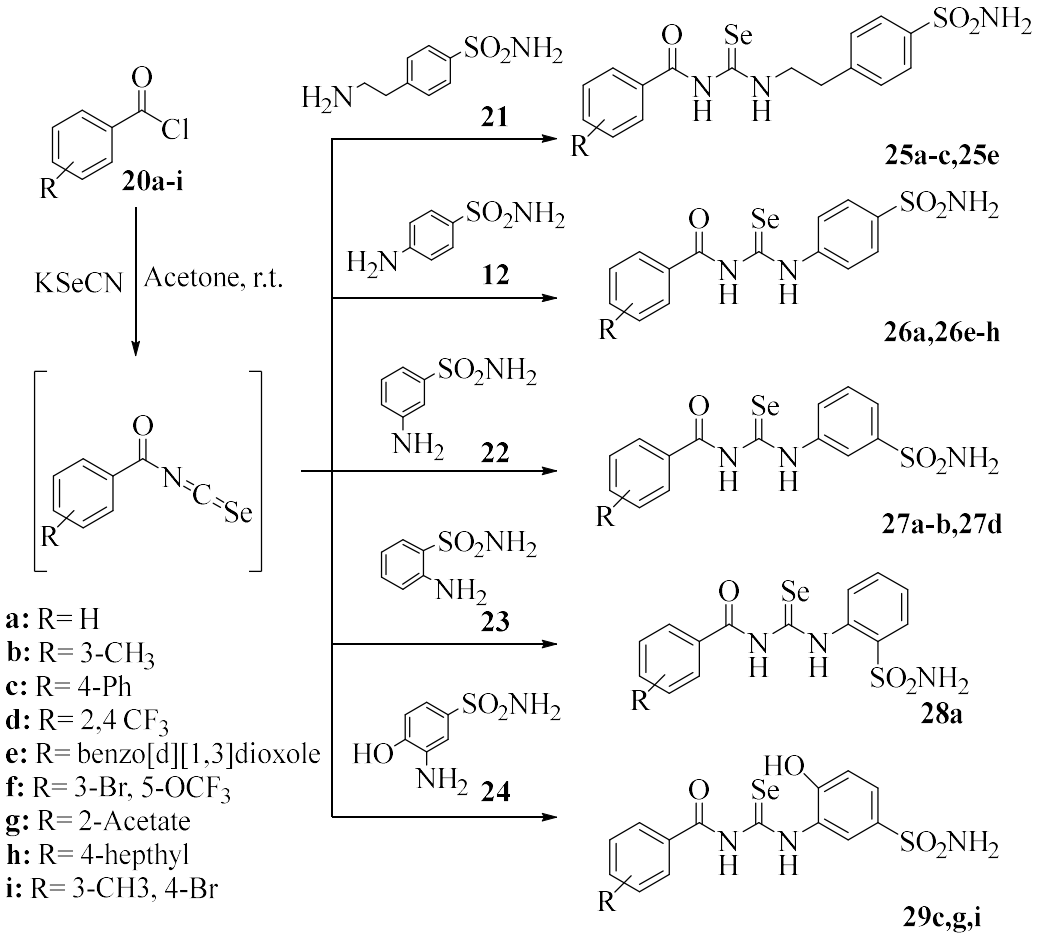

Scheme 9: General procedure for the synthesis of acyl selenoureido compounds **25-29**.

All compounds **25-29** were tested *in vitro* for their inhibitory activity against the physiologically relevant hCA isoforms I, II, VII and IX by means of the stopped-flow carbon dioxide hydration assay[4] and their activities were compared to the standard CA inhibitor (CAI) acetazolamide (**AAZ**) (**Table 5**).

Table 5. Inhibition constants of hCA I, hCA II, hCA VII and hCA IX with compounds **25-29** and **AAZ** by a stopped-flow CO_2 hydrase assay[4]

	K_i (nM)*			
Compound	hCA I	hCA II	hCA VII	hCA IX
25a	65.6	18.7	3.2	7.2
25b	514.9	21.8	138.4	145.9
25c	3746	9533	1881	4869
25e	523.7	26.9	27.8	105.2
26a	73.8	9.5	9.3	4.6
26e	8702	402.4	1885	128.6
26f	85.7	0.7	1.7	3.5
26g	85.7	9.1	6.8	13.6
26h	734.2	48.9	1.8	25.1
27a	521.2	247.4	1897	373.6
27b	81.6	6.6	15.2	43.9
27d	9381	6072	1907	4702
28a	61.5	66.9	100.4	283.7
29c	90.5	39.2	37.8	69.1
29g	44.7	3.9	55.5	80.8
29i	9.6	4.2	85.6	5.8
AAZ	250	12.1	2.5	25.8

* Mean from three determinations by a stopped-flow, CO_2 hydrase method. Standard errors were in the range of 5–10% of the reported values.

The following structure-activity-relationship (SAR) may be noted regarding the inhibition data of **Table 5**:

(i) The two dominant cytosolic isoforms, hCA I and hCAII, were inhibited by almost all compounds here reported with an inhibition constant in the nanomolar range, except for compounds **25c** and **26e,** which acted within the micromolar range for both isoforms (the same was valid for compound **27d** against hCA I). Substituents on the acyl selenoureido compounds **25a-c** and **25e**, incorporating 4-ethylamino benzensulfonamide, showed a decreased potency of inhibition of almost tenfold for hCA I. Instead, the introduction of small substituents on the acyl scaffold did not influence the potency for inhibition of hCA II. Furthermore, an addition of another

benzene ring at position 4 (**25e**) decreased the efficacy to micromolar range for both isoforms. For compounds **26a** and **26e-h**, incorporating the 4-amino benzenesulfonamide moiety, analogous to compounds **25a-c** and **25e**, the substitution on the acyl scaffold decreased the potency for the slow cytosolic isoform hCA I. An interesting case was how the ethyl linker between benzensulfonamide and acyl selenoureido moieties modulated the potency of inhibition for compounds **25e** and **26e,** with a benzo[d][1,3]dioxole scaffold. The presence of ethyl spacer increased the efficacy over 10 times with respect to compounds without it. A substitution at position 3 on the acyl scaffold, with the sulfonamide group in *meta* (**27a-b** and **27d**) increased the inhibition potency. On the other hand, the substitution at 2 and 4 with CF_3 groups (**27d**) decreased the efficacy to micromolar range. Compound **28a**, with SO_2NH_2 zinc binding group at position 2, resulted the most active inhibitor for isoforms hCA I compared to the others compounds previously reported without substituents on the acyl scaffold. Conversely, compound **26a**, with sulfonamide moiety at position 4, was the best inhibitor for hCA II.

(ii) The next cytosolic human isoform here studied, hCA VII, was inhibited by compounds **25c**, **26e**, **27a** and **27d** in micromolar range, whereas by the remaining compounds in nanomolar range. Substitutions on the acyl scaffold for compounds **25a-c** and **25e** decreased the potency of inhibition, as for the other two cytosolic isoforms discussed above. Compounds with 4-amino benzensulfonamide moiety (**26a** and **26e-h**) inhibited this isoform in the low nanomolar range except for compound **26e** (a micromolar inhibitor). The ethyl linker present in compound **26e**, decreased the efficacy nearly 60 times compared to the compound without it (**25e**).

(iii) The transmembrane isoform hCA IX was inhibited by all compounds (except **25c** and **27d**) in the nanomolar range. Substitution on the acyl scaffold for compounds **25a-c** and **25e** decreased the inhibition potency of such derivatives as for the other isoforms here considered. The presence or not of the ethyl linker in compounds **25e** and **26e**, did not influence the efficacy of inhibition for this isoform.

(iv) An interesting inhibition profile was observed for compounds **25e** and **26e**. The presence of the ethylene linker decreased the inhibition potency for all cytosolic isoforms but did not influence the transmembrane hCA IX inhibition, and the compounds showed selectivity for this isoform.

2.4 Intramolecular oxidative deselenization of acylselenoureas: a facile synthesis of benzoxazole amides and carbonic anhydrase inhibitors.

Benzoxazoles are scaffolds of particular interest in medicinal chemistry,[16] with additional applications including their use as laser dyes, photoluminescents[17] and whitening agents.[18] Despite their importance, the synthetic methods require multistep procedures, the use of metal catalysts,[19,20] hypervalent iodine[21] or strong oxidizing agents.[22] Herein we report for the first time a novel and easy procedure to obtain benzoxazoles substituted scaffolds. The starting material acylselenoureas **30a-h** were obtained according to the method of Koketsu *et al.* as mentioned above[15] using the commercially available 4-hydroxymetanilamide **24** (**Scheme 9**).

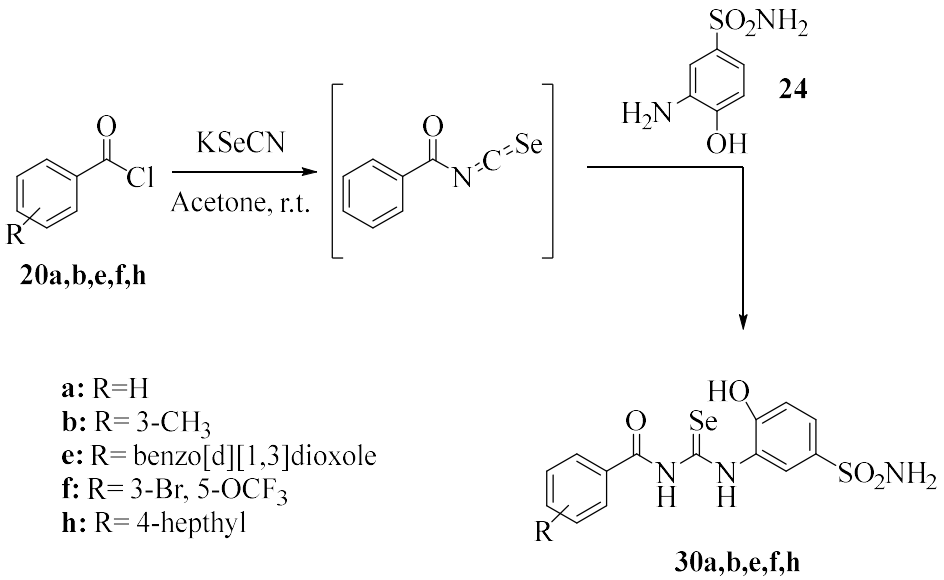

Scheme 9: General procedure for the synthesis of acyl selenoureido compounds **30a,b,e,f,h.**

We hypothesized the synthesis of benzoxazole scaffolds by means of an intramolecular cyclization of benzoylselenoureas in alkaline media (**Scheme 10**).

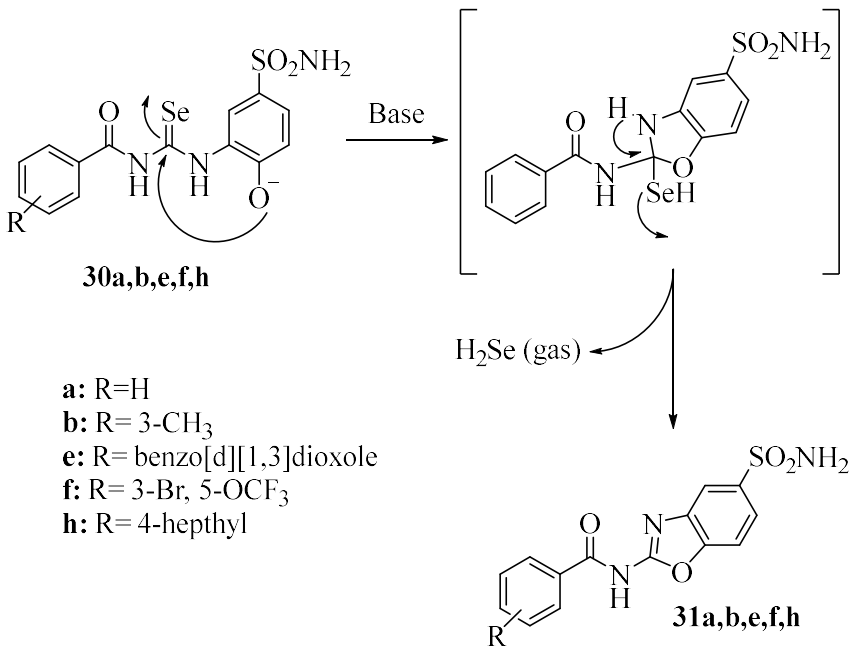

Scheme 10: Proposed reaction mechanism for the formation of benzoxazole **31**.

According to our proposal the *in situ* generated phenolate ion from **30a** might be able to trigger an intramolecular 5-membered ring cyclization to afford the corresponding tetrahedral intermediate, which upon release of selenhidric acid gas (H_2Se) forms the thermodynamically more stable aromatic benzoxazole amide **31a** (**Scheme 10**). In order to confirm the possible mechanism, we evaluated different variables. We investigated the role of the temperature in giving the desidered products. Thus, a solution of **30a** in 10% D_2O/DMSO-d_6 was heated into an open NMR tube at 60°C for 15 min, followed by 85°C for 1h. ^{1}H-NMR live monitoring neither showed formation of benzoxazole **31a** or decomposition of starting material **30a**. Conversely the treatment of a DMSO-d_6 solution of **30a** with a 1.0 M NaOD solution in D_2O (3.2 equivalents) revealed a 40% ^{1}H-NMR conversion of **30a** to the expected benzoxazole **31a** just after 24 h at r.t. (**Figure 2**).

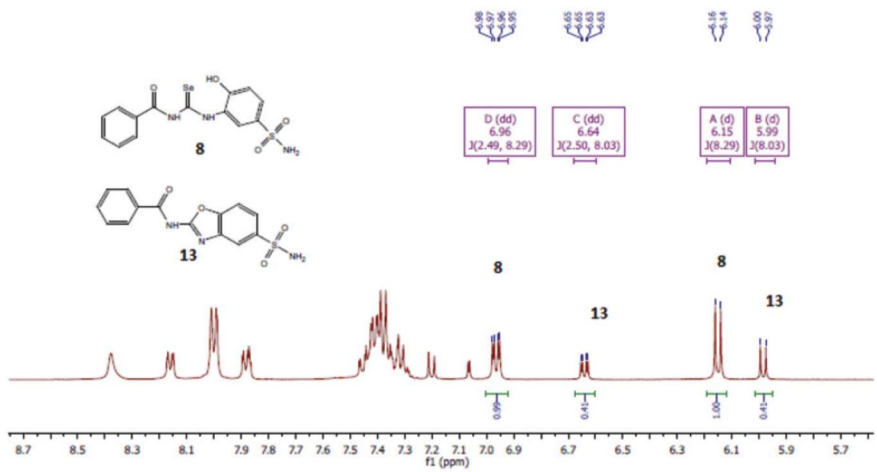

Figure 2: 400 MHz ^{1}H-NMR spectrum of **30a** treated with NaOD (3.2 eq.) after 24 h. Key signals of **30a** and **31a** are shown

The independence of the cyclization from the enzymatic activity was also assessed. Compound **30a** (10 mM) and hCA II (10 μM) were incubated at r.t. in a HEPES buffer solution at pH 7.4. The reaction progress was monitored by silica gel thin layer chromatography (TLC) (70:30 EtOAc/Hex) after 15, 30, 45, 120 min and 24 h, and showed the intact starting material **30a** still present. The pH dependence of the cyclization mechanism was also verified by means of Electrospray Ionization Mass Spectrometry (ESI-MS) experiments on water solution of **30a**. We created a pH gradient by means of proper modulation of both the intensity and polarity of the voltage applied to the terminal part of the capillary (Taylor cone).[19] Then we acquired the data in negative mode in the range between *m/z* 150 and 600 (**Figure 5**).

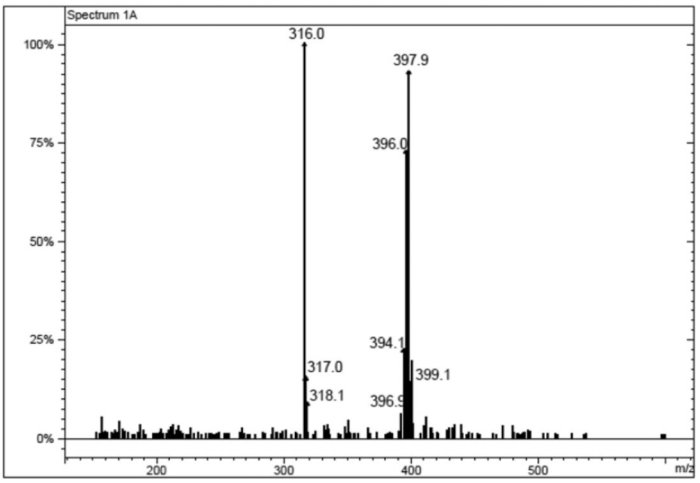

Figure 5: ESI-MS spectrum acquired in negative mode.

The MS spectrum obtained showed two principal cluster signals at *m/z* 316 and *m/z* 398. The latter represents the $[M-H]^-$ ion species of compound **30a**, as confirmed by the characteristic isotopic distribution of the selenium. The ions at *m/z* 316 belonged to the N-(5-sulfamoylbenzo[d]oxazol-2-yl)benzamide **31a**, which was formed by intramolecular cyclization of **30a**. It is worth considering that the cluster ions of **31a** did not show the isotopic pattern distribution of selenium, thus confirming its loss in agreement with our proposed mechanism. We turned our attention towards the optimization of the cyclization conditions of **30a**. The pH solvent played a crucial role in the mechanism. Indeed, the recovery of the product increased with the pH and the use of pyridine acting both as a solvent and a base gave the highest yield among all.

Acylselenoureas **30** previously obtained were all converted to the corresponding benzoxazole amides **31** in good yields and tested *in vitro* for their inhibition activity against the most relevant hCA isoforms (I, II, VII and IX), by means of the stopped flow carbon dioxide hydrase assay[4] and in comparison to the standard sulfonamide inhibitor acetazolamide (**AAZ**) (**Table 6**).

Table 6. Inhibition constants of hCA I, hCA II, hCA VII and hCA IX with compounds **30-31** and **AAZ** by a stopped-flow CO_2 hydrase assay[4]

	K_i (nM)*			
Compound	hCA I	hCA II	hCA VII	hCA IX
30a	9.1	36.5	9.1	7.0
30b	7.5	4.2	10.8	5.1
30e	149.2	270	11.9	9.3
30f	69.0	35.4	12.0	58.2
30h	27.3	47.4	11.4	5.0
31a	17.9	60.9	21.5	34.1
31b	57.6	75.2	62.5	217.8
31e	70.6	96.1	43.3	401.5
31f	30.3	75.7	90.8	455
31h	1558	8079	1262	5771
AAZ	250	12.1	2.5	25.8

* Mean from three determinations by a stopped-flow, CO_2 hydrase method. Standard errors were in the range of 5–10% of the reported values.

In general, all the compounds resulted to be effective in inhibiting the CA isoforms considered, with K_is values spanning from the low to medium nanomolar range. The only exception was the benzoxazole **31h** which was effective only at micromolar concentrations. As reported in **Table 6** the ubiquitous hCA I was strongly inhibited by the simple acylselenoureas **30a,b,h** (K_is 7.5-27.3 nM). The introduction of hindered tails, as in **30f** and **30e**, resulted in an increase of the K_i value (69.0 and 149.2 nM respectively). Cyclization of acylselenoureas **30a-h** to the corresponding benzoxazole amides **31a-h** led to a reduction of the inhibition potencies of the less hindered members of the series (**31a,b,h**). Conversely the bulky ones **31f** and **31e** were 2.3 and 2.1 fold more potent, respectively. The hCA II isoform, which is implicated in glaucoma,[22] was potently inhibited by **30b** (K_i 4.2 nM). Small modifications to the molecular tail, such as removal of the methyl group (**30a**) and introduction of linear alkyl chain (**30h**) or bulky moieties (**30e,f**) worsened the inhibition potency. In analogy, the benzoxazole derivatives **31a-h** were less potent when compared to their precursor acylselenoureas **30a-h** (**Table 6**). The acylselenoureas **30a-h** were all potent inhibitors of hCA VII with K_is in the range of 9.2-12.0 nM, and thus slightly less potent than

the standard **AAZ** (K_i 6.0 nM). Again the corresponding benzoxazole derivatives **31a-h** were poorer inhibitors (**Table 6**). Analogous results were also obtained for the tumor associated isoform hCA IX. The enhanced flexibility of the acylselenoureido **30-31** tails greatly improved the inhibition potency against hCA IX (K_is were between 5.0 and 9.3 nM) with the only exception of **30f** (K_i 58.2 nM). As expected, all the corresponding cyclic derivatives **31a-h** were far less potent compared to the non-cyclic ones.

The binding modes of such compounds within the human CA cavity, were assessed by means of co-crystallization experiments using the simple benzoylselenourea **30a** and hCA II (**Figure 6**).

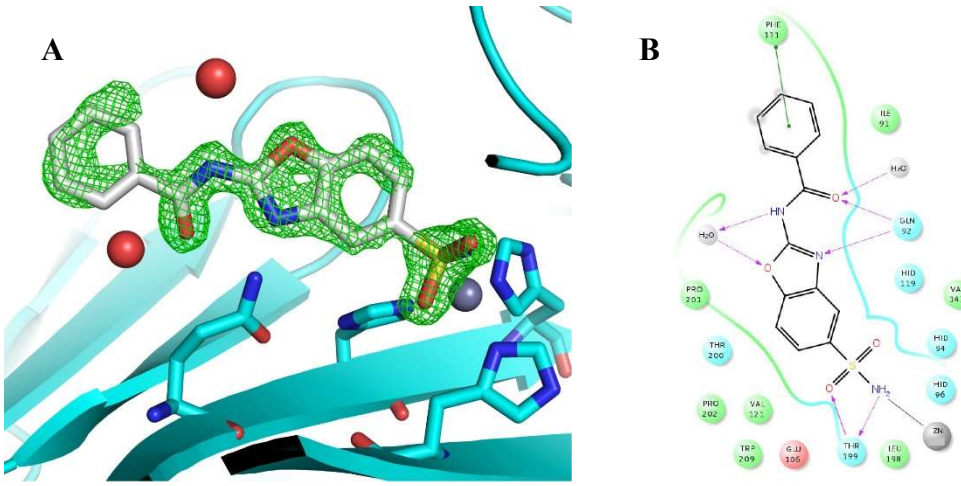

Figure 6: **A:** Fo–Fc electron density map is shown **B:** 2D Interaction Map of compound **31a** within the hCA II Catalytic Site

The Fo–Fc electron density maps showed a well defined density for all the atoms of the ligand N-(5-sulfamoylbenzo[d]oxazol-2-yl)benzamide **31a**. The sulfonamide SO_2NH^- moiety coordinated to the zinc ion buried at the low-edge of the enzymatic cavity and established the canonical interactions with Thr199 [18] (**Figure 6A**). The ligand occupied the entire available space inside the enzymatic cavity and was located at the center of the cleft. Strong hydrogen bonds were established between the Gln92 residue and both the oxazolyl nitrogen and the acetamidic oxygen. The latter is also engaged in hydrogen bonding with a water molecule. A slightly displaced π–π stacking interaction was established between the

benzoyl tail plane and Phe131 (**Figure 6B**). A second water molecule (W2 in **Figure 6B**) interacted both with the acetamidic nitrogen and the benzoxazolyl oxygen.

2.5 Selenols: a new class of Carbonic Anhydrase inhibitors

The biological significance of selenols are mainly related to their incorporation in proteins as selenocysteine (SeC). The different atomic structure and composition of selenium when compared to its isostere sulfur, makes the selenol (SeH) group in SeC (pKa ~5.8) more nucleophilic than the thiol in Cys (pKa ~8.3). Moreover, the low pKa value of selenol,[23] under physiological conditions (pH ~7.4), determines them to be almost fully present as the selenolate ion ($R\text{-}Se^-$), whereas the majority of thiols are present in the protonated form (R-SH). Thiophenols and phenols are well known inhibitors of Carbonic Anhydrases since 1970.[24,25] To date, no selenols have been investigated as CAIs since their low chemical stability in the presence of atmospheric oxygen. In this context, the synthesis of limited number of aryl selenols is reported in the literature, and the most used synthetic routes usually involve Grignard reagents or organolitium reagents. Conversely aryl selenolates can be easily obtained from reduction of the corresponding diselenides using $NaBH_4$ as the reagent of choice. We sought to evaluate the efficiency of different H^+ sources in order to protonate aryl selenolates and access stable selenols. Thus, diphenyl diselenide was treated with $NaBH_4$ in THF or EtOH, using different organic or inorganic proton sources. Results of this investigation are reported in **Table 7.** As can be noticed, higher isolated yields were found when the reaction was carried out at 0°C in dry EtOH, using citric acid as H^+ source.

Table 7: Optimization of the synthesis of aryl selenols

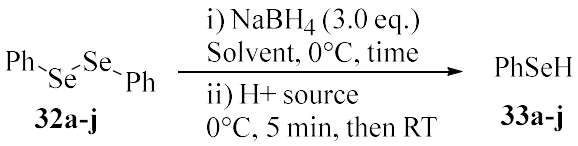

32a-j **33a-j**

Entry	Solvent	Time (min)	H+ source	Yield (%)
1	THF	30	HCl	15
2	THF	30	NH_4Cl	<5
3	THF	30	Citric acid	55
4	EtOH	10	HCl	10
5	EtOH	10	NH_4Cl	<5
6	EtOH	10	Citric acid	76
7	EtOH	10	Tartaric acid	<5
8	EtOH	10	Ascorbic acid	21

Having demonstrated the possibility to obtain stable aryl selenols through this easy and convenient procedure, we explored the scope of the reaction in order to obtain a series of differently substituted organoselenium compounds and evaluate their activity as hCAs inhibitors. On the basis of these considerations, we reacted under the conditions described in the **Scheme 11** a series of diaryl diselenides (**32a-j**), sinthesised according to literature reported procedures,[26] finding a clean and high yielding entry to aryl selenols **33a-j** bearing different groups at selected position of the aromatic ring (**Scheme 11**).

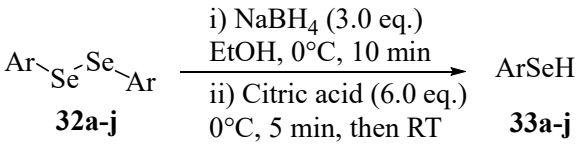

32a-j **33a-j**

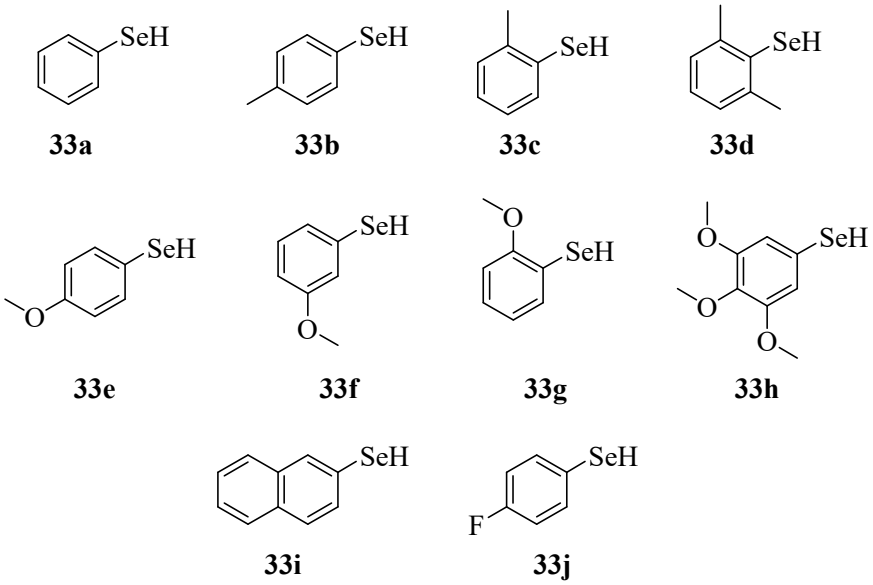

33a **33b** **33c** **33d**

33e **33f** **33g** **33h**

33i **33j**

Scheme 11: General procedure for the synthesis of aromatic selenols **33a-j**

We determined the inhibition kinetic constants for selenols **33a–j** against the most relevant hCA isoforms (I, II, VII and IX), by means of the stopped flow carbon dioxide hydrase assay[4] and in comparison to the standard sulfonamide inhibitor acetazolamide (**AAZ**) (**Table 8**).

Table 8. Inhibition constants of hCA I, hCA II, hCA VII and hCA IX with compounds **33a-j** and **AAZ** by a stopped-flow CO_2 hydrase assay[4]

	K_i (μM)*			
Compound	hCA I	hCA II	hCA VII	hCA IX
33a	6.7	2.2	93.8	0.44
33b	0.52	3.6	5.4	3.3
33c	0.87	0.72	0.84	0.20
33d	0.28	0.95	4.5	0.18
33e	7.5	3.2	6.1	3.0
33f	2.8	3.6	6.4	0.28
33g	0.85	0.49	0.76	0.20
33h	51.0	51.1	>60	9.6
33i	7.1	26.0	6.8	0.46
33j	3.7	3.9	18.2	22.4
AAZ	0.25	0.012	0.002	0.026

* Mean from three determinations by a stopped-flow, CO_2 hydrase method. Standard errors were in the range of 5–10% of the reported values.

One interesting result displayed in **Table 8** indicate the phenyl selenol (**33a**) is a promising scaffold to develop non classical inhibitors of the tumor associated CA (i.e. IX isoform). In fact, most of the tested derivatives inhibited hCAs IX at nanomolar concentrations. On the contrary, the cytosolic hCAs isoforms proved to be less active (micromolar range). Additional moieties on the benzene scaffold led to modulate the selectivity towards the different CA isoforms. Introduction of substituents at position 4, as compounds **33b**, **33e**, and 33j, generally led to lose selectivity against the membrane isoform hCA IX. 4-Methylbenzeneselenol **33b** showed remarkable inhibition for hCA I. On the other hand, replacement of the metyl moiety with the methoxyl one (**33e**), decreased the efficacy of inhibition for this isoform. The introduction of a fluorine atom at *para* position (**33j**) led to a 6 fold increase of the inhibition selectivity against the two dominant cytosolic isoforms hCA I and II over the tumor associated one (hCA IX). The inhibition potency increased for all isoforms here considerate, when the substituents were present at position 2 on phenyl ring (**33c** and **33g**). Moreover, these compounds resulted over 2 folds selective against the tumor-associated membrane isoform. An interesting inhibition profile was observed for compound **33f,** in which the methoxide moiety was placed at position 3 on the phenyl scaffold. This

placement led to the best result for obtaining selectivity against the hCA IX, which was over 10 folds when compared to the other isoforms here considerated. The presence of two additional methoxyl groups at 4 and 5 positions (compound **33h**) resulted in a remarkable decrease in inhibition potency for hCA I, II, IX and a complete loss of activity against hCA VII. On the other hand, compound **33d** with two methyl moieties at positions 2 and 6, resulted the best placement for increasing the potency of inhibition against hCA IX (K_i 0.18 μM). A further interesting inhibition profile was observed for the naphtyl scaffold **33i**. This compound showed a submicromolar activity (K_i 0.46 μM) for the membrane associated IX isoform also with remarkable selectivity since showed to be 50 folds more active over the hCA II (**Table 8**).

Next, the X-ray structure of **33a** in complex with both hCA I and II were determined at 1.64 and 1.44 Å resolution respectively, and compared to the structure of the same enzymes in complex with phenol and thiophenols as ligands.[24,25] Our adducts revealed the binding mode of selenol to be different than the typical binding mode of phenols.

A

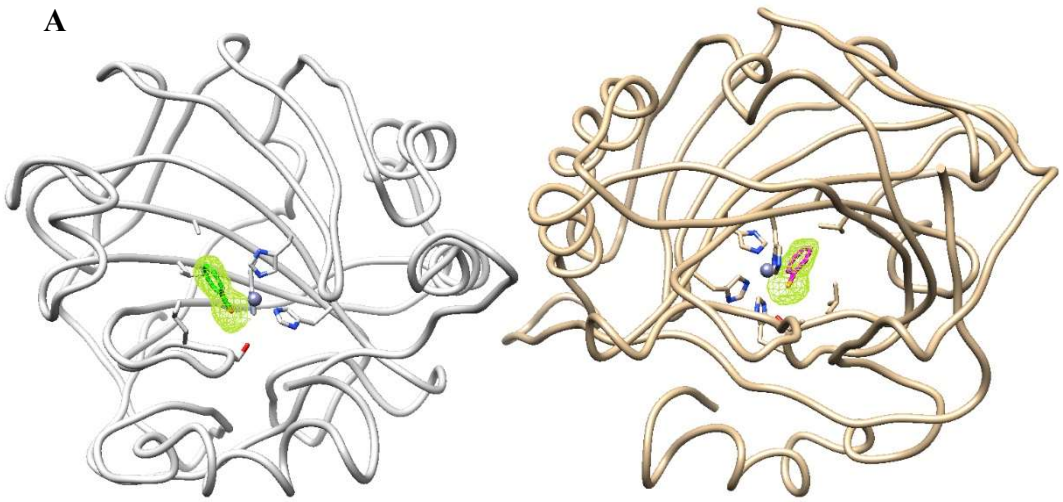

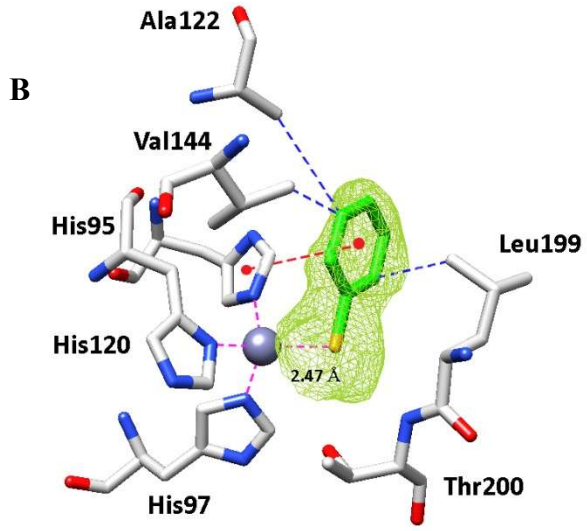

Figure 7: (**A**) Selenol **33a** in complex with hCA I. Inhibitor showed as σA-weighted $|F_o-F_c|$ density map at 2.0 σ. (**B**) Active site region of hCA I/**33a** adduct. Van der Waals interactions, and π-Stacking interactions are also shown (blue and red respectively)

According to the literature reported adducts, phenols were found anchored to the non-protein zinc ligand by a hydrogen bond involving the H atom of the inhibitor and the donor OH from the zinc hydroxide.[24] In addition, a second hydrogen bond involving the gate-keeping residue Thr199 has been observed to stabilize the enzyme–inhibitor adduct.[24] We showed that selenol was bound directly to the Zn(II) ion from the CAs active site with the usual tetrahedral geometry and similar to the thiolates.[25] We observed in crystal structure of hCA I two identical monomers with inside the active cleft a single ligand molecule (**Figure 7A**). Hydrophobic interactions were made by the selenol **33a** with Ala122, Val144 and Leu199 within the active site. Furthermore, the imidazole ring of His95 was also involved in a π-stacking interaction with the aromatic ring of inhibitor (**Figure 7B**).

Crystal structures of hCA II (**Figure 8**) also revealed similar binding mode for the selenol **33a**, even if the crystal structure appeared less ordered when compared to the hCA I (**Figure 8A**). This might be justified as **33a** was bound less strongly since a limited number of interactions among the ligand and the amino acid residues occurred (i.e. **33a** showed only three hydrophobic interaction with Val122 and Leu198; **Figure 8B**).

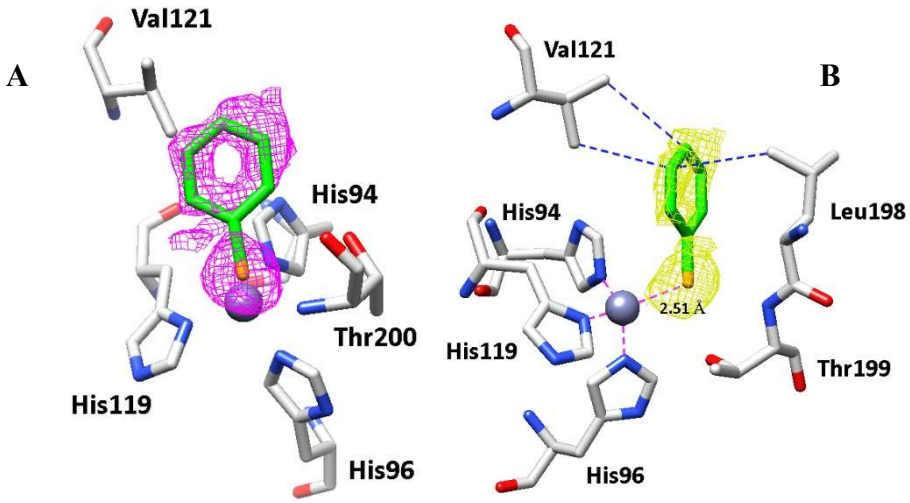

Figure 8: (**A**) Active site region of hCA II/**33a** adduct. Inhibitor showed as σA-weighted $|F_o-F_c|$ density map at 2.0 σ. (**B**) Van der Waals interactions, and the active site Zn^{2+}-ion coordination are also shown.

2.6 Conclusions

We developed new methods for the synthesis of novel series of CAs inhibitors worth of further development in Medicinal Chemistry. In particular we explored the three member ring opening by thiolate and selenolate bearing the sulfonamide moiety. Additional we reported a radical new synthetic approach to build benzoxazoles scaffolds. Finally the selenols were discovered as new chemotype of CAs inhibitors. On the last we investigated their mechanism of inhibition by means of *in vitro* kinetic and X-ray studies. hCAs binding modes comparison between the thiophenols and selenols showed close matching thus supporting a comparable inhibition mechanism for these chemical species. All compounds here reported were assayed on different human Carbonic Anhydrases of pharmacologic relevance such as the hCA I, II and IV as drug targets for the treatment of glaucoma symptoms, hCA VII as antiepileptic agents and the hCA IX which is an established target for the treatment of hypoxic tumors.

2.7 Experimental Data

General

All reactions were carried out in an oven-dried glassware under inert atmosphere (N_2). Ethanol was dried using a solvent purification system (Pure-Solv™). All commercial materials were used as received without further purification. Flash column chromatography purifications were performed with Silica gel 60 (230-400 mesh). Thin layer chromatography was performed with TLC plates Silica gel 60 F_{254}. NMR spectra were recorded in $CDCl_3$ or DMSO-*d*$_6$ with Mercury 400, and Bruker 400 Ultrashield spectrometers operating at 400 MHz (for ^{1}H), 100 MHz (for ^{13}C) and 376 MHz (for ^{19}F). NMR signals were referenced to nondeuterated residual solvent signals (7.26 and 2.50 ppm for ^{1}H, 77.0 and 40.5 ppm for ^{13}C). ^{1}H NMR data are reported as follows: chemical shift, integration, multiplicity (s= singlet, d= doublet, t= triplet, ap d= apparent doublet, m= multiplet, dd= doublet of doublet, bs= broad singlet, bd= broad doublet, ecc.), coupling constant (J), and assignment.

Synthesis of 4,4'-Disulfanediyldibenzenesulfonyl chloride 1:

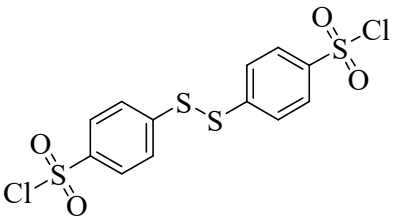

Disulfide **1** was synthesised following a reported procedure. A solution of 0.1 mol of diphenyldisulfide in chloroform (100 mL) was added to a solution of 0.3 mol chlorosulfonic acid in chloroform at 10 °C. Than, the mixture was stirred for one hour at 40 °C. After quenching on ice, the phases were separated, the organic phase washed twice with sodium bicarbonate solution and dried with Na_2SO_4. The solvent was eliminated and the product obtained as yellow powder with a yield of 74%. **^{1}H NMR** (400 MHz, $CDCl_3$) δ (ppm): 7.72 (4H, ap d, *J* = 8.7 Hz), 8.01 (4H, ap d, *J* = 8.7 Hz). **^{13}C NMR** (100 MHz, $CDCl_3$) δ (ppm): 127.1, 128.5, 143.6, 145.5.

Synthesis of 4,4'-Disulfanediyldibenzenesulfonamide 2:

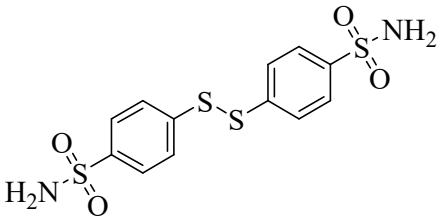

4,4'-Disulfanediyldibenzenesulfonyl chloride **1** (831 mg, 2.0 mmol) was solubilized in THF (50 mL) and treated with an excess of NH_4OH (37% *aq*. Solution, 10 eq.). The reaction was stirred at ambient temperature for 30 min; the solid was then filtered, washed with Et_2O (20 mL) and dried under vacuum to afford 4,4'-Disulfanediyldibenzenesulfonamide **2** (707 mg, 94%). **^{1}H NMR** (400 MHz, DMSO-d_6) δ (ppm): 7.45 (4H, bs), 7.78 (4H, ap d, J = 8.0 Hz), 7.88 (4H, ap d, J = 8.0 Hz). **^{13}C NMR** (100 MHz, DMSO-d_6) δ (ppm): 127.6, 127.7, 140.5, 144.0.

General Procedure for the preparation of sulfides 5a-e, 7a-e and 9 from disulfide 2:

$NaBH_4$ (23 mg, 0.60 mmol, 3.0 eq.) was portionwise added to a solution of 4,4'-disulfanediyldibenzenesulfonamide **2** (75 mg, 0.20 mmol, 1.0 eq.) in EtOH (2 mL) at ambient temperature under inert atmosphere (N_2). After 2 h, the suitable electrophile (0.42 mmol, 2.1 eq.) was slowly added and the reaction mixture was stirred at room temperature for 3 h, until complete consumption of the starting material was observed by TLC. The reaction was quenched by addition of saturated *aq*. NH_4Cl (2 mL) and diluted with EtOAc (5 mL), The layers were separated and the aqueous layer was extracted with EtOAc (2 x 5 mL), dried over Na_2SO_4, filtered and concentrated under vacuum. The crude material was purified by flash chromatography to yield sulfides **5**, **7** and **9** bearing benzenesulfonamide moiety.

4-(Pentylthio)benzenesulfonamide 5a:

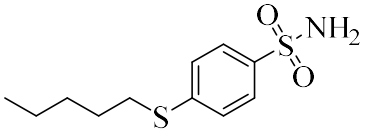

Following the general procedure, disulfide **2** (75 mg, 0.20 mmol) and bromopentane **4a** (63 mg, 0.42 mmol) gave 5a (76 mg, 74%) as a white solid. **^{1}H NMR** (400 MHz, DMSO-d_6) δ (ppm): 0.88 (3H, t, J = 7.2 Hz), 1.26-1.35 (2H, m), 1.37-1.44 (2H, m), 1.59-1.67 (2H, m), 3.06 (2H, ap t, J = 7.3 Hz, CH_2S), 7.31 (2H, bs, NH_2), 7.46 (2H, ap d, J = 8.7 Hz), 7.73 (2H, ap d, J = 8.7 Hz). **^{13}C NMR** (100 MHz, DMSO-d_6) δ (ppm): 14.9, 22.7, 29.0, 31.4, 32.0, 127.3, 127.6, 141.6, 143.2.

4-(Phenethylthio)benzenesulfonamide 5b:

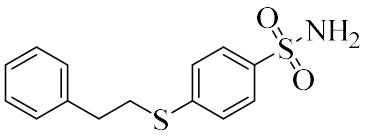

Following the general procedure, disulfide **2** (56 mg, 0.15 mmol) and (2-bromoethyl)benzene **4b** (58 mg, 0.32 mmol) gave **5b** (54 mg, 61%) as a white solid. **^{1}H NMR** (400 MHz, DMSO-d_6) δ (ppm): 2.92 (2H, t, *J*= 7.6 Hz), 3.34 (2H, t, *J* = 7.6 Hz), 7.21-7.27 (1H, m), 7.28-7.35 (6H, m), 7.50 (2H, ap d, *J* = 8.5 Hz), 7.74 (2H, ap d, *J* = 8.5 Hz). **^{13}C NMR** (100 MHz, DMSO-d_6) δ (ppm): 33.5, 35.4, 127.3, 127.5, 127.8, 129.4, 129.7, 140.8, 141.8, 142.8.

4-(Prop-2-yn-1-ylthio)benzenesulfonamide 5c:

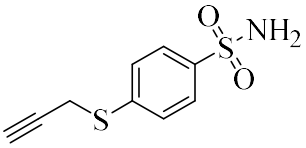

Following the general procedure, disulfide **2** (75 mg, 0.20 mmol) and propargyl chloride **4c** (31 mg, 0.42 mmol) gave **5c** (75 mg, 83%) as a white solid. **^{1}H NMR** (400 MHz, DMSO-d_6) δ (ppm): 3.21 (1H, t, *J* = 2.6 Hz, C≡CH), . 4.02 (2H, d, *J* = 2.6 Hz, CH_2C≡C), 7.38 (2H, bs, NH_2), 7.56 (2H, ap d, *J* = 8.6 Hz), 7.80 (2H, ap d, *J* = 8.6 Hz). **^{13}C NMR** (100 MHz, DMSO-d_6) δ (ppm): 20.6, 75.1, 80.8, 127.2, 128.2, 141.3, 142.3.

4-(Prop-2-yn-1-ylthio)benzenesulfonamide 5d:

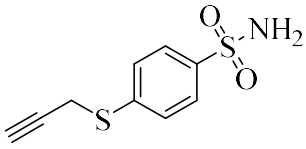

Following the general procedure, disulfide **2** (75 mg, 0.20 mmol) and 2-bromoethanol **4d** (53 mg, 0.42 mmol) gave **5d** (66 mg, 71%) as a white solid. **^{1}H NMR** (400 MHz, DMSO-d_6) δ (ppm): 3.11 (2H, t, *J* = 6.7 Hz, CH_2S), 3.55-3.62 (2H, m, CH_2O), 4.98 (1H, bs, OH), 7.29 (2H, bs, NH_2), 7.45 (2H, ap d, *J* = 8.6 Hz), 7.69 (2H, ap d, *J* = 8.6 Hz). **^{13}C NMR** (100 MHz, DMSO-d_6) δ (ppm): 34.4, 60.0, 126.6, 127.0, 141.0, 142.5. MS (ESI negative) *m/z* (%): 232 $[M-H]^-$, required $[M-H]^-$ 232.02.

Methyl 3-((4-sulfamoylphenyl)thio)propanoate 5e:

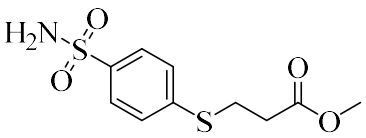

Following the general procedure, disulfide **2** (56 mg, 0.15 mmol) and 3-bromopropionate **4e** (54 mg, 0.32 mmol) gave **5e** (71 mg, 86%) as a white solid. **^{1}H NMR** (400 MHz, $CDCl_3$) δ (ppm): 2.69 (2H, t, *J* = 7.3 Hz), 3.26 (2H, t, *J* = 7.3 Hz), 3.71 (3H, s), 5.01 (2H, bs, NH_2), 7.37 (2H, ap d, *J* = 8.7 Hz), 7.81 (2H, ap d, *J* = 8.7 Hz). **^{13}C NMR** (100 MHz,

$CDCl_3$) δ (ppm): 27.3, 33.6, 52.0, 127.0, 127.6, 138.9, 143.0, 171.8. MS (ESI negative) *m/z* (%): 298 $[M+Na]^+$; required $[M+Na]^+$ 298.02.

4-((2-Hydroxybutyl)thio)benzenesulfonamide 7a:

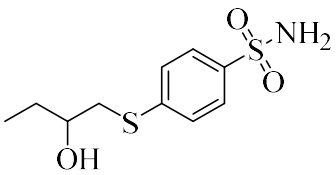

Following the general procedure, disulfide **2** (56 mg, 0.15 mmol) and 1,2-epoxybutane **6a** (23 mg, 0.32 mmol) gave **7a** (69 mg, 88%) as a white solid. **^{1}H NMR** (400 MHz, DMSO-d_6) δ (ppm): 0.89 (3H, t, J = 7.4Hz), 1.36-1.47 (1H, m), 1.52-1.66 (1H, m), 3.04 (1H, dd, J = 6.7, 13.1 Hz, CH_aH_bS), 3.10 (1H, dd, J = 5.4, 13.1 Hz, CH_aH_bS), 3.53-3.60 (1H, m, CHOH), 4.98 (1H, d, J = 5.3 Hz, CHOH), 7.32 (2H, bs, NH_2), 7.47 (2H, ap d, J = 8.5 Hz), 7.71 (2H, ap d, J = 8.5 Hz). **^{13}C NMR** (100 MHz, DMSO-d_6) δ (ppm): 11.0, 30.0, 39.4, 71.1, 127.2, 127.5, 141.4, 143.8. MS (ESI negative) *m/z* (%): 260 $[M-H]^-$, required $[M-H]^-$ 260.05.

4-((2-Hydroxyhex-5-en-1-yl)thio)benzenesulfonamide 7b:

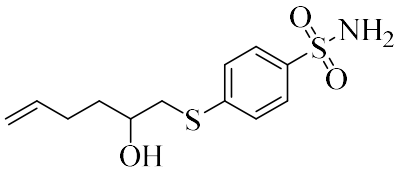

Following the general procedure, disulfide **2** (75 mg, 0.20 mmol) and 1,2-Epoxy-5-hexene **6b** (41 mg, 0.42 mmol) gave **7b** (108 mg, 94%) as a white solid. **^{1}H NMR** (400 MHz, $CDCl_3$) δ (ppm): 1.65-1.74 (2H, m), 1.92 (1H, bs, OH), 2.14-2.36 (2H, m), 3.02 (1H, dd, J = 8.2, 13.7 Hz, CH_aH_bS), 3.24 (1H, dd, J = 3.7, 13.7 Hz, CH_aH_bS), 3.81-3.87 (1H, m, CHOH), 4.92 (2H, bs, NH_2), 5.01-5.11 (2H, m), 5.78-5.90 (1H, m), 7.44 (2H, ap d, J = 8.4 Hz), 7.83 (2H, ap d, J = 8.4 Hz). **^{13}C NMR** (100 MHz, $CDCl_3$) δ (ppm): 30.5, 36.0, 40.9, 69.9, 116.0, 127.6, 128.4, 138.4, 139.5, 144.0. MS (ESI negative) *m/z* (%): 286 $[M-H]^-$, required $[MH]^-$ 286.06.

4-((2,3-Dihydroxypropyl)thio)benzenesulfonamide 7c:

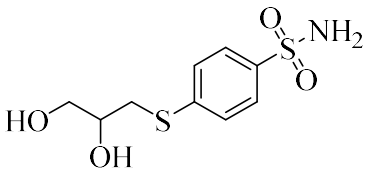

Following the general procedure, disulfide **2** (75 mg, 0.20 mmol) and glycidol **6c** (31 mg, 0.42 mmol) gave **7c** (80 mg, 76%) as a white solid. **^{1}H NMR** (400 MHz, DMSO-d_6) δ (ppm): 2.98 (1H, dd, J = 7.2, 13.2 Hz, CH_aH_bS), 3.23 (1H, dd, J = 4.6, 13.2 Hz, CH_aH_bS), 3.38 (1H, dd, J = 6.0, 12.9 Hz, CH_aH_bO), 3.43 (1H, dd, J = 5.3, 10.9 Hz, CH_aH_bO), 3.62-3.69 (1H, m, CHOH), 4.74 (1H, bt, J = 5.7 Hz, CH_2OH),

5.07 (1H, bd, *J* = 5.2 Hz, CHOH), 7.30 (2H, bs, NH2), 7.47 (2H, ap d, *J* = 8.6 Hz), 7.71 (2H, ap d, *J* = 8.6 Hz). **^{13}C NMR** (100 MHz, DMSO-d_6) δ (ppm): 36.6, 65.6, 71.3, 127.2, 127.5, 141.4, 143.9. MS (ESI negative) *m/z* (%): 262 $[M-H]^-$, required $[M-H]^-$ 262.03.

(*E*)-4-((2-Hydroxy-3-(prop-1-en-1-yloxy)propyl)thio)benzenesulfonamide 7d:

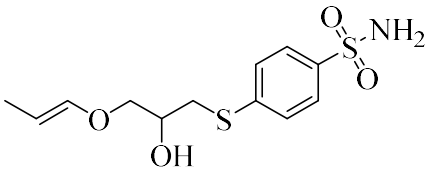

Following the general procedure, disulfide **2** (37.5 mg, 0.1 mmol) and allyl glycidyl ether **6d** (24 mg, 0.21 mmol) gave **7d** (54 mg, 89%) as a white solid. **^{1}H NMR** (400 MHz, $CDCl_3$) δ (ppm): 2.79 (1H, bs, OH), 3.09 (1H, dd, *J* = 6.7, 13.6 Hz, CH_aH_bS), 3.17 (1H, dd, *J* = 5.5, 13.6 Hz, CH_aH_bS), 3.49 (1H, dd, *J* = 5.9, 9.4 Hz, CH_aH_bO), 3.54 (1H, dd, *J* = 3.7, 9.4 Hz, CH_aH_bO), 3.93-3.98 (1H, m, CHOH), 3.98-4.03 (2H, m), 5.17- 5.28 (2H, m, $CH=CH_2$), 4.92 (2H, bs, NH_2), 5.82-5.92 (1H, m, $CH=CH_2$), 7.34-7.37 (2H, m), 7.73-7.75 (2H, m). **^{13}C NMR** (100 MHz, $CDCl_3$) δ (ppm): 35.7 (CH_2S), 69.0, 72.2, 72.3, 117.7, 126.8, 127.3, 134.1, 138.7, 143.3. MS (ESI negative) *m/z* (%): 302 $[M-H]^-$, required $[M-H]^-$ 302.06.

4-(((5*R*)-2-Hydroxy-2-methyl-5-(prop-1-en-2-yl)cyclohexyl)thio)benzene sulfonamide 7e:

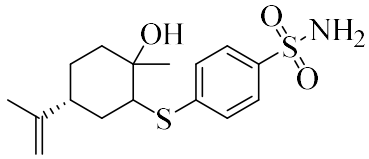

Following the general procedure, disulfide **2** (37.5 mg, 0.1 mmol) and limonene oxide **6e** (32 mg, 0.21 mmol) gave **7e** (53 mg, 78%) as a white solid. **^{1}H NMR** (400 MHz, $CDCl_3$) δ (ppm): 1.37 (3H, s), 1.58-1.68 (3H, m), 1.69 (3H, s), 1.73-1.81 (2H, m), 1.84 (1H, bs), 2.16-2.23 (1H, m), 2.28-2.37 (1H, m), 3.48-3.52 (1H, m, CHS), 4.72 (2H, ap d, *J* = 11.5 Hz), 5.12 (2H, bs, NH_2), 7.45 (2H, ap d, *J* = 8.4 Hz), 7.79 (2H, ap d, *J* = 8.4 Hz). **^{13}C NMR** (100 MHz, $CDCl_3$) δ (ppm): 21.8, 26.7, 29.3, 33.2, 35.7, 39.3, 55.1, 72.9, 110.0, 127.5, 129.7, 139.6, 144.3, 149.2. MS (ESI positive) *m/z* (%): 364 $[M+Na]^+$, required $[M+Na]^+$ 364.10.

(*S*)-4-Methyl-*N*-(1-phenyl-3-((4-sulfamoylphenyl)thio)propan-2-yl)benzene sulfonamide 9:

Following the general procedure, disulfide **2** (37.5 mg, 0.1 mmol) and (*S*)-2-benzyl-1-tosylaziridine **8** (60 mg, 0.21 mmol) gave 9 (60 mg, 62%) as a white solid. **^{1}H NMR** (400 MHz, DMSO-d_6) δ (ppm): 2.30 (3H, s), 2.66 (1H, dd, J = 6.7, 13.5 Hz), 2.81 (1H, dd, J = 6.5, 13.5 Hz), 2.96 (1H, dd, J = 5.8, 13.3 Hz), 3.01 (1H, dd, J = 5.1, 13.3 Hz), 3.28-3.39 (1H, m, CHNH, overlapped with H_2O), 7.03-7.04 (2H, m), 7.10 (2H, ap d, J = 8.5 Hz), 7.15-7.19 (5H, m), 7.32 (2H, bs, NH_2), 7.43 (2H, ap d, J = 8.2 Hz), 7.60 (2H, ap d, J = 8.5 Hz), 7.97 (1H, d, J = 7.5 Hz, NH). **^{13}C NMR** (100 MHz, DMSO-d_6) δ (ppm): 21.0, 35.7, 40.1 (overlapped with DMSO-d_6 signal), 54.2 (CHNH), 126.0, 126.3, 126.4, 126.5, 128.3, 129.2, 129.3, 137.4, 137.9, 140.8, 141.0, 142.4. MS (ESI negative) *m/z* (%): 475 $[M-H]^-$, required $[M-H]^-$ 475.09.

General Procedure for the preparation of thiol esters 10a-e from disulfide 2:

$NaBH_4$ (23 mg, 0.60 mmol, 3.0 eq.) was portionwise added to a solution of 4,4'-disulfanediyldibenzenesulfonamide **2** (75 mg, 0.20 mmol, 1.0 eq.) in EtOH (2 mL) at ambient temperature under inert atmosphere (N_2). After 2 h, the suitable acyl chloride (0.42 mmol, 2.1 eq.) was slowly added and the reaction mixture was stirred at room temperature for 1 h, until complete consumption of the starting material was observed by TLC. The reaction was quenched by addition of saturated *aq*. NH_4Cl (2 mL) and diluted with EtOAc (5 mL). The layers were separated and the aqueous layer was extracted with EtOAc (2 x 5 mL), dried over Na_2SO_4, filtered and concentrated under vacuum. The crude material was purified by flash chromatography to yield thiol esters **10a-e**.

***S*-(4-Sulfamoylphenyl) octanethioate 10a:**

According to general procedure, using disulfide **2** (37.5 mg, 0.1 mmol) and capryloyl chloride (34 mg, 0.21 mmol) **10a** (27 mg, 42%) was achieved as a white solid. **^{1}H NMR** (400 MHz, $CDCl_3$) δ (ppm): 0.89 (3H, t, J = 6.8 Hz), 1.22-1.39

(8H, m), 1.66-1.76 (2H, m), 2.69 (2H, t, J = 7.5 Hz, CH_2(CO)), 4.94 (2H, bs, NH_2), 7.56 (2H, ap d, J = 8.5 Hz), 7.94 (2H, ap d, J = 8.5 Hz). **^{13}C NMR** (100 MHz, $CDCl_3$) δ (ppm): 14.0, 22.6, 25.5, 28.9, 31.6, 44.1, 127.0, 134.0, 134.7, 142.4, 196.0. MS (ESI positive) *m/z* (%): 338 $[M+Na]^+$, required $[M+Na]^+$ 338.09.

_S_-(4-Sulfamoylphenyl) octadecanethioate 10b:

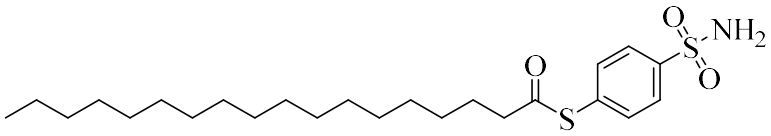

According to general procedure, using disulfide **2** (37.5 mg, 0.1 mmol) and stearoyl chloride (64 mg, 0.21 mmol) **10b** (49 mg, 54%) was achieved as a white solid. **^{1}H NMR** (400 MHz, $CDCl_3$) δ (ppm): 0.88 (3H, t, J = 6.7 Hz), 1.22-1.27 (28H, m), 1.67-1.78 (2H, m), 2.69 (2H, t, J = 7.5 Hz, CH_2(CO)), 4.93 (2H, bs, NH_2), 7.56 (2H, ap d, J = 8.4 Hz), 7.94 (2H, ap d, J = 8.4 Hz). **^{13}C NMR** (100 MHz, $CDCl_3$) δ (ppm): 14.1, 22.7, 28.9, 29.2, 29.3, 29.4, 29.5, 29.6, 29.7, 31.9, 44.1, 127.0, 128.7, 134.0, 134.2, 134.7, 142.4, 196.0. MS (ESI positive) *m/z* (%): 478 $[M+Na]^+$, required $[M+Na]^+$ 478.24.

_S_-(4-Sulfamoylphenyl) (_Z_)-octadec-9-enethioate 10c:

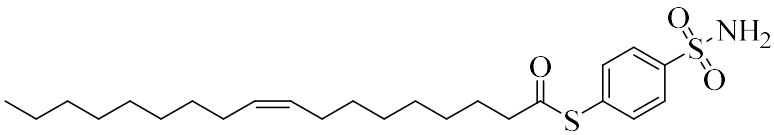

According to general procedure, using disulfide **2** (37.5 mg, 0.1 mmol) and oleoyl chloride (63 mg, 0.21 mmol) 10c (55 mg, 61%) was achieved as a waxy white solid. **^{1}H NMR** (400 MHz, $CDCl_3$) δ (ppm): 0.88 (3H, t, J = 6.7 Hz), 1.21-1.41 (20H, m), 1.66-1.75 (2H, m), 1.95-2.07 (4H, m), 2.68 (2H, t, J = 7.5 Hz, CH_2(CO)), 5.20 (2H, bs, NH_2), 5.30-5.40 (2H, m), 7.53 (2H, ap d, J = 8.3 Hz), 7.92 (2H, ap d, J = 8.3 Hz). **^{13}C NMR** (100 MHz, $CDCl_3$) δ (ppm): 14.1, 27.1, 27.2, 28.9, 29.0, 29.1, 29.3, 29.5, 29.6, 29.7, 31.9, 44.0, 126.9, 129.6, 130.0, 133.7, 134.7, 142.5, 196.2. MS (ESI positive) *m/z* (%): 476 $[M+Na]^+$, required $[M+Na]^+$ 476.23.

***S*-(4-Sulfamoylphenyl) (*E*)-3-phenylprop-2-enethioate 10d:**

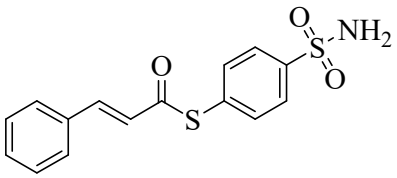

According to general procedure, using disulfide **2** (75 mg, 0.2 mmol) and cinnamoyl chloride (70 mg, 0.4 mmol) **10d** (74 mg, 58%) was achieved as a white solid. **^{1}H NMR** (400 MHz, DMSO-d_6) δ (ppm): 7.18 (1H, d, J = 15.8), 7.44-7.49 (3H, m), 7.51 (2H, bs), 7.70 (2H, ap d, J = 8.3 Hz), 7.72 (1H, d, J = 15.8), 7.81-7.83 (2H, m), 7.91 (2H, ap d, J = 8.3 Hz). **^{13}C NMR** (100 MHz, DMSO-d_6) δ (ppm): 124.1, 126.3, 129.0, 131.2, 131.6, 133.6, 134.8, 142.2, 144.9, 186.2. MS (ESI negative) *m/z* (%): 318 $[M-H]^-$, required $[M-H]^-$ 318.03.

***S*-(4-Sulfamoylphenyl) 2,4-bis(trifluoromethyl)benzothioate 10e:**

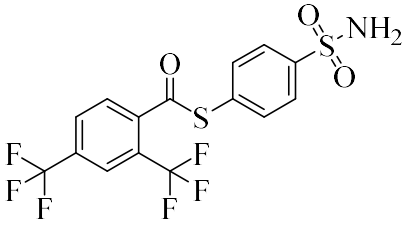

According to general procedure, using disulfide **2** (37.5 mg, 0.1 mmol) and 2,4-Bis(trifluoromethyl)benzoyl chloride (58 mg, 0.21 mmol), **10e** (40 mg, 46%) was achieved as white solid. **^{1}H NMR** (400 MHz, DMSO-d_6) δ (ppm): 7.56 (2H, bs NH_2), 7.80 (2H, ap d, J = 8.4 Hz), 7.99 (2H, ap d, J = 8.4 Hz), 8.26 (1H, ap d, J = 8.1 Hz), 8.34 (1H, ap d, J = 8.1 Hz), 8.31 (1H, s). **^{13}C NMR** (100 MHz, DMSO-d_6) δ (ppm): 123.0 (d, 1JC-F = 273 Hz, CF3), 125.2 (d, $^{1}J_{C\text{-}F}$ = 271 Hz, CF_3), 125.6 (bs), 127.6 (q, $^{2}J_{C\text{-}F}$ = 22 Hz, CCF_3), 127.8, 131.1, 131.2, 131.6 (bs), 133.4 (q, $^{2}J_{C\text{-}F}$ = 33 Hz, CCF_3), 136.1, 140.7, 146.8, 190.3. **^{19}F NMR** (376 MHz, DMSO-d_6) δ (ppm): -61.7, -57.5. MS (ESI negative) *m/z* (%): 428 $[M-H]^-$, required $[M-H]^-$ 427.99.

Synthesis of 4,4'-disulfanediylbis(N-(4-sulfamoylphenyl) benzenesulfonamide) 11a:

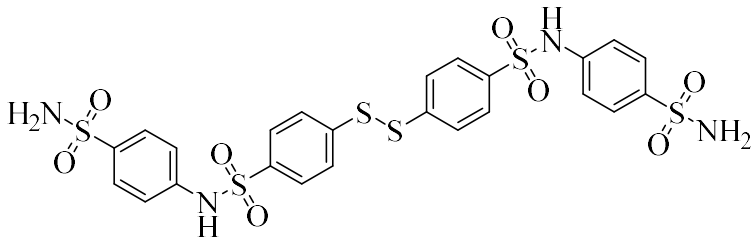

4,4'-Disulfanediyldibenzenesulfonyl chloride **1** (83 mg, 0.2 mmol) was solubilized in THF (5 mL) and treated with sulfanilamide (69 mg, 0.4 mmol). The reaction was stirred at

ambient temperature for 30 min; the solid was then filtered, washed with Et_2O (5 mL) and dried under vacuum to afford 11a (49 mg, 36%). **^{1}H NMR** (400 MHz, DMSO-*d_6*) δ (ppm): 7.40 (4H, bs, NH_2), 7.53-7.57 (10H, m), 7.85- 7.95 (8H, m). **^{13}C NMR** (100 MHz, DMSO-*d_6*) δ (ppm):123.7, 127.1, 128.1, 128.5, 130.4, 136.7, 140.3, 143.3.

Synthesis of 4,4'-Disulfanediylbis(*N*-(4-sulfamoylbenzyl)benzenesulfonamide) 11b:

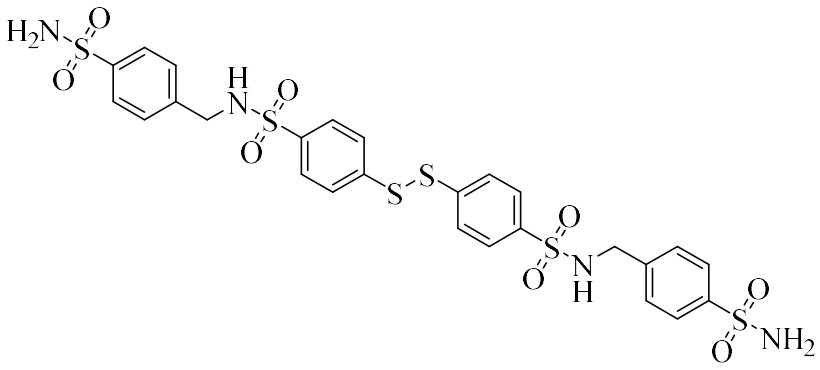

4,4'-Disulfanediyldibenzenesulfonyl chloride **1** (83 mg, 0.2 mmol) was solubilized in THF (5 mL) and treated with 4-aminomethylbenzenesulfonamide hydrochloride (89 mg, 0.4 mmol). The reaction was stirred at ambient temperature for 30 min; the solid was then filtered, washed with Et_2O (5 mL) and dried under vacuum to afford **11b** (75 mg, 53%). **^{1}H NMR** (400 MHz, DMSO-*d_6*) δ (ppm): 4.07 (4H, d, *J* = 6.2 Hz, CH_2N), 7.31 (4H, bs, NH_2), 7.43 (4H, d, *J* = 8.3 Hz), 7.75 (4H, d, *J* = 8.3 Hz), 7.75 (4H, d, *J* = 8.6 Hz), 7.83 (4H, d, *J* = 8.6 Hz), 8.31 (2H, t, *J* = 6.2 Hz, NH). **^{13}C NMR** (100 MHz, DMSO-*d_6*) δ (ppm): 46.6, 126.7, 127.8, 128.7, 128.9, 140.6, 141.6, 142.9, 144.1.

Synthesis of 4,4'-Disulfanediylbis(*N*-(4-sulfamoylphenethyl)benzene sulfonamide) 11c:

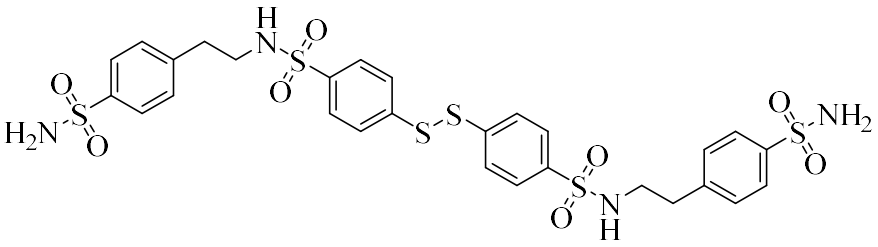

4,4'-Disulfanediyldibenzenesulfonyl chloride **1** (42 mg, 0.1 mmol) was solubilized in THF (3 mL) and treated with 4-(2-aminoethyl)benzenesulfonamide (40 mg, 0.2 mmol). The

reaction was stirred at ambient temperature for 30 min; the solid was then filtered, washed with Et_2O (5 mL) and dried under vacuum to afford **11c** (24 mg, 32%). **^{1}H NMR** (400 MHz, DMSO-*d_6*) δ (ppm): 2.76 (4H, t, *J* = 7.1 Hz), 2.97-3.02 (4H, m), 7.31 (4H, bs), 7.35 (4H, ap d, *J* = 8.3 Hz), 7.69-7.69 (12H, m), 7.80 (2H, bt, *J* = 5.6 Hz). **^{13}C NMR** (100 MHz, DMSO-*d_6*) δ (ppm): 36.0, 44.6, 126.7, 127.8, 128.7, 130.3, 140.3, 141.5, 143.3, 143.9.

Preparation 4-selenocyanatobenzenesulfonamide 13:

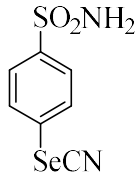

A suspension of 4-Aminonenzenesulfonamide **12** (1,72 g, 10 mmol) in H_2O (6 mL) with HCl (11 mL, 32 %) was cooled down to -5°C. Then, an aqueous solution of $NaNO_2$ (1.2 eq) was added dropwise and the mixture was kept stirring at the same temperature until a persistent pale yellow solution was formed (5–10 min). The resulting diazonium salt, kept at -5°C, was added KSeCN (1.2 eq). The reaction solution was stirred for 2 hours at the same temperature. The product was filtered off, washed with H_2O, dried under vacuo, and purified by flash column chromatography eluting with 1:1 mixture of hexane/ethyl acetate. (1.79 g, 83%). **^{1}H NMR** (400 MHz, DMSO-*d_6*) δ (ppm): 7.95 (2H, d, *J*=8.61), 7.89 (2H, d, *J*=8.68), 7.52 (2H, bs, N**H$_2$**, exchange with D_2O). **^{13}C NMR** (100 MHz, DMSO-*d_6*) δ (ppm): 145.5, 134.1, 129.8, 127.9, 105.9. **^{77}Se NMR** (76 MHz, DMSO-*d_6*) δ (ppm): 340.0. **MS** (ESI negative) *m/z* (%):261 $[M-H]^-$.

Preparation 4,4'-diselanediyldibenzenesulfonamide 14:

$NaBH_4$ (3 mmol) was added in small portions with caution to a solution of 4-selenocyanatobenzenesulfonamide **13** (3 mmol) in absolute ethanol (40 mL). The mixture was stirred at room temperature for 2 h. The solvents were removed under vacuum by rotary evaporation and the residue was treated with water. The mixture was extracted with ethyl acetate, dried with anhydrous Na_2SO_4, and purified by crystallization from EtOH. (529 mg, 75%). **^{1}H NMR** (400 MHz, DMSO-*d_6*) δ (ppm): 7.87 (2H, d, *J*=8.31), 7.79 (2H, d, *J*=8.36), 7.43 (2H, bs, N**H$_2$**, exchange with D_2O). **^{13}C NMR** (100 MHz, DMSO-*d_6*) δ (ppm): 144.3, 135.2, 131.5, 127.5. **^{77}Se NMR** (76 MHz, DMSO-*d_6*) δ (ppm): 446.7. **MS** (ESI negative) *m/z* (%):471 $[M-H]^-$.

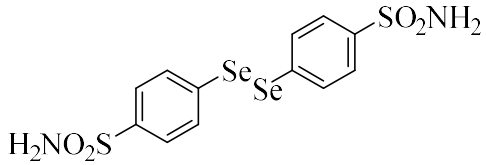

General Procedure for the preparation of β-hydroxy selenide 16a-g from diselenide 14:

$NaBH_4$ (23 mg, 0.60 mmol, 3.0 eq.) was portionwise added to a solution of 4,4'-diselanediyldibenzenesulfonamide **3** (94 mg, 0.20 mmol, 1.0 eq.) in EtOH (2 mL) at 0°C under inert atmosphere (N_2). After 30 min, the epoxide **15** (0.36 mmol, 1.8 eq.) was slowly added and the reaction mixture was stirred at room temperature for 2 h, until complete consumption of the starting material was observed by TLC. The reaction was quenched by addition of saturated aq. NH_4Cl (2 mL) and diluted with EtOAc (5 mL), The layers were separated and the aqueous layer was extracted with EtOAc (2 x 5 mL), dried over Na_2SO_4, filtered and concentrated under vacuum. The crude material was purified by flash chromatography to yield β-hydroxyselenides (**16**) bearing benzenesulfonamide moiety.

4-((3-(Benzyloxy)-2-hydroxypropyl)selanyl)benzenesulfonamide 16a:

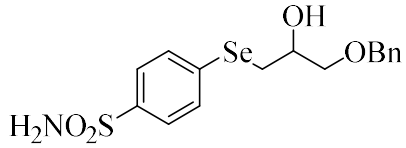

Following the general procedure, 4,4'-diselanediyldibenzenesulfonamide **14** (94 mg, 0.20 mmol) and 2-((benzyloxy)methyl)oxirane **15a** (59 mg, 0. 36 mmol) gave after flash chromatography (petroleum ether/EtOAc 1:1) **16a** (128 mg, 89%). **^{1}H NMR** (400 MHz, $CDCl_3$) δ (ppm): 2.63 (1H, bs, OH), 3.12 (1H, dd, *J* = 6.8, 12.8 Hz, C**H$_a$**H$_b$Se), 3.19 (1H, dd, *J* = 5.6, 12.8 Hz, CH$_a$**H$_b$**Se), 3.54 (1H, dd, *J* = 5.9, 9.5 Hz, C**H$_a$**H$_b$O), 3.59 (1H, dd, *J* = 4.2, 9.5 Hz, CH$_a$**H$_b$**O), 3.96-4.04 (1H, m, C**H**OH), 4.53 (2H, ap s, CH_2Ph), 4.82 (2H, bs, NH_2), 7.29-7.40 (5H, m), 7.59 (2H, d, *J* = 8.5 Hz), 7.76 (2H, d, *J* = 8.5 Hz). **^{13}C NMR** (100 MHz, $CDCl_3$) δ (ppm): 31.1 (CH_2Se), 69.5, 72.8, 73.5, 126.9, 127.8, 128.0, 128.5, 131.3, 137.5, 137.7, 139.9. **MS** (ESI positive) *m/z* (%): 401 $[M+H]^+$, (100). Elemental analysis: $C_{16}H_{19}NO_4SSe$ Calcd. C 48.00%, H 4.78%, N 3.50%. Found: C 48.11%, H 4.74%, N 3.46%.

4-((2-Hydroxy-3-isopropoxypropyl)selanyl)benzenesulfonamide 16b:

Following the general procedure, 4,4'-diselanediyldibenzenesulfonamide **14** (94 mg, 0.20 mmol) and 2-(isopropoxymethyl)oxirane **15b** (42 mg, 0. 36 mmol) gave after flash chromatography (petroleum ether/EtOAc 1:1) **16b** (121 mg, 96%). **^{1}H NMR** (400 MHz, $CDCl_3$) δ (ppm): 1.15 (6H, d, *J* = 6.1 Hz), 2.78 (1H, bs, OH), 3.11 (1H,

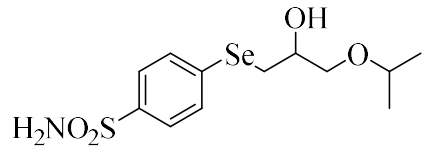

dd, *J* = 6.7, 12.7 Hz, C**H**$_a$H$_b$Se), 3.16 (1H, dd, *J* = 5.8, 12.7 Hz, CH$_a$**H**$_b$Se), 3.45 (1H, dd, *J* = 6.0, 9.4 Hz, C**H**$_a$H$_b$O), 3.53 (1H, dd, *J* = 4.1, 9.4 Hz, CH$_a$**H**$_b$O), 3.59 (1H, ept, *J* = 6.1 Hz, C**H**(CH$_3$)$_2$), 3.89-3.98 (1H, m, C**H**OH), 5.09 (2H, bs, NH$_2$), 7.58 (2H, d, *J* = 8.5 Hz), 7.75 (2H, d, *J* = 8.5 Hz). **^{13}C NMR** (100 MHz, CDCl$_3$) δ (ppm): 21.9, 22.0, 30.9 (CH$_2$Se), 69.6, 70.7, 72.4, 126.8, 131.2, 137.9, 139.9. **MS** (ESI positive) *m/z* (%): 375 [M+Na]$^+$, (100). Elemental analysis: $C_{12}H_{19}NO_4SSe$ Calcd. C 40.91%, H 5.44%, N 3.98%. Found: C 40.82%, H 5.49%, N 3.94%.

4-((3-(Allyloxy)-2-hydroxypropyl)selanyl)benzenesulfonamide 16c:

Following the general procedure, 4,4'-diselanediyldibenzenesulfonamide **14** (71 mg, 0.15 mmol) and 2-((allyloxy)methyl)oxirane **15c** (31 mg, 0. 27 mmol) gave after flash chromatography (petroleum ether/EtOAc 7:3) **16c** (70 mg, 74%). **^{1}H NMR** (400 MHz, CDCl$_3$) δ (ppm) 2.71 (1H, bs, OH), 3.12 (1H, dd, *J* = 6.8, 12.8 Hz, C**H**$_a$H$_b$Se), 3.18 (1H, dd, *J* = 5.7, 12.8 Hz, CH$_a$**H**$_b$Se), 3.49 (1H, dd, *J* = 6.0, 9.5 Hz, C**H**$_a$H$_b$O), 3.55 (1H, dd, *J* = 4.0, 9.5 Hz, CH$_a$**H**$_b$O), 3.94-4.06 (3H, m, C**H$_2$**CH=CH$_2$ overlapped wih C**H**OH), 5.04 (2H, bs, NH$_2$), 5.19-5.32 (2H, m), 5.83-5.93 (1H, m), 7.59 (2H, d, *J* = 8.2 Hz), 7.77 (2H, d, *J* = 8.2 Hz). **^{13}C NMR** (100 MHz, CDCl$_3$) δ (ppm): 31.0 (CH$_2$Se), 69.5, 72.3, 72.7, 117.6, 126.9, 131.2, 134.1, 137.7, 140.0. **MS** (ESI positive) *m/z* (%): 373 [M+Na]$^+$, (100). Elemental analysis: $C_{12}H_{17}NO_4SSe$ Calcd. C 41.15%, H 4.89%, N 4.00%. Found: C 41.07%, H 4.94%, N 4.05%.

4-((2-Hydroxyhexyl)selanyl)benzenesulfonamide 16d:

Following the general procedure, 4,4'-diselanediyldibenzenesulfonamide **14** (94 mg, 0.20 mmol) and 2-butyloxirane **15d** (36 mg, 0. 36 mmol) gave after flash chromatography (petroleum ether/EtOAc 1:1) **16d** (82 mg, 68%). **^{1}H NMR** (400 MHz, CDCl$_3$) δ (ppm) 0.92 (3H, t, *J* = 7.1 Hz), 1.29-1.49 (4H, m), 1.54-1.63 (2H, m), 1.97. (1H, bs, OH), 3.03 (1H, dd, *J* = 8.2, 12.8 Hz, C**H**$_a$H$_b$Se), 3.23 (1H, dd, *J* = 3.7, 12.8 Hz, CH$_a$**H**$_b$Se), 3.76-3.82 (1H, m, C**H**OH), 5.07 (2H, bs, NH$_2$), 7.61 (2H, d, *J* = 8.5 Hz), 7.78 (2H, d, *J* = 8.5 Hz). **^{13}C NMR** (100 MHz, CDCl$_3$) δ (ppm): 14.0, 22.6, 27.9, 36.2, 36.6, 70.3, 126.9, 131.5, 137.6, 140.0. **MS** (ESI

positive) *m/z* (%): 337 $[M+H]^+$, (100). Elemental analysis: $C_{12}H_{19}NO_3SSe$ Calcd. C 42.86%, H 5.69%, N 4.16%. Found: C 42.73%, H 5.76%, N 4.21%.

4-((3-Bromo-2-hydroxypropyl)selanyl)benzenesulfonamide 16e:

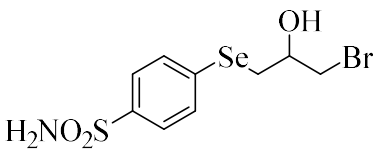

Following the general procedure, 4,4'-diselanediyldibenzenesulfonamide **14** (141 mg, 0.30 mmol) and 2-(bromomethyl)oxirane **15e** (74 mg, 0. 54 mmol) gave after flash chromatography (petroleum ether/EtOAc 3:2) **16e** (189 mg, 94%). **^{1}H NMR** (400 MHz, DMSO-d_6) δ (ppm) 3.15 (1H, dd, *J* = 7.1, 12.4 Hz, C**H$_a$**H$_b$Se), 3.24 (1H, dd, *J* = 5.1, 12.4 Hz, CH$_a$**H$_b$**Se), 3.54 (1H, dd, *J* = 5.6, 10.2 Hz, C**H$_a$**H$_b$O), 3.61 (1H, dd, *J* = 4.7, 10.2 Hz, CH$_a$**H$_b$**O), 3.85-3.92 (1H, m, C**H**OH), 5.68 (1H, d, *J* = 5.3 Hz, OH), 7.34 (2H, bs, NH_2), 7.65 (2H, d, *J* = 8.6 Hz), 7.69 (2H, d, *J* = 8.6 Hz). **^{13}C NMR** (100 MHz, DMSO-d_6) δ (ppm): 32.8, 39.8, 70.2, 127.1, 131.3, 137.1, 142.8. **MS** (ESI negative) *m/z* (%): 372 $[M-H]^-$, (100). Elemental analysis: $C_9H_{12}BrNO_3SSe$ Calcd. C 28.97%, H 3.24%, N 3.75%. Found: C 29.02%, H 3.19%, N 3.69%.

4-((2-Hydroxycyclohexyl)selanyl)benzenesulfonamide 16f:

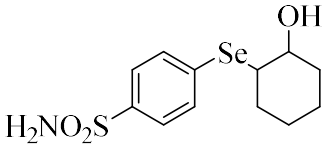

Following the general procedure, 4,4'-diselanediyldibenzenesulfonamide **14** (71 mg, 0.15 mmol) and 7-oxabicyclo[4.1.0]heptane **15f** (26 mg, 0. 27 mmol) gave after flash chromatography (petroleum ether/EtOAc 1:1) **16f** (37 mg, 41%). **^{1}H NMR** (400 MHz, $CDCl_3$) δ (ppm) 1.25-1.37 (4H, m), 1.63-1.72 (1H, m), 1.74-1.83 (1H, m), 2.12-2.26 (2H, m), 3.05-3.12 (1H, m, CHSe), 3.40-3.48 (1H, m, CHO), 4.91 (2H, bs, NH_2), 7.70 (2H, d, *J* = 8.4 Hz), 7.80 (2H, d, *J* = 8.4 Hz). **^{13}C NMR** (100 MHz, $CDCl_3$) δ (ppm): 24.4, 26.8, 33.5, 34.4, 53.9, 73.1, 126.6, 134.6, 138.2, 141.0. **MS** (ESI positive) *m/z* (%): 357 $[M+Na]^+$, (100). Elemental analysis: $C_{12}H_{17}NO_3SSe$ Calcd. C 43.12%, H 5.13%, N 4.19%. Found: C 43.05%, H 5.19%, N 4.23%.

4-(((5*R*)-2-Hydroxy-2-methyl-5-(prop-1-en-2-yl)cyclohexyl)selanyl)benzene sulfonamide 16g

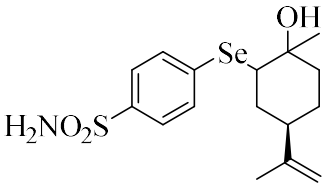

Following the general procedure, 4,4'-diselanediyldibenzenesulfonamide **14** (71 mg, 0.15 mmol) and (4*R*)-1-methyl-4-(prop-1-en-2-yl)-7-oxabicyclo[4.1.0]heptane **15g** (41 mg, 0. 27 mmol) gave after flash chromatography (petroleum ether/EtOAc 2:1) **16g** (51 mg, 56%). **^{1}H NMR** (400 MHz, $CDCl_3$) δ (ppm) 1.39 (3H, s), 1.63-1.66 (1H, m), 1.69 (3H, s), 1.72-1.90 (4H, m), 2.23-2.35 (2H, m), 3.54-3.59 (1H, m, CHSe), 4.72 (2H, ap d, *J* = 14.7 Hz), 5.14 (2H, bs, NH_2), 7.64 (2H, d, *J* = 8.3 Hz), 7.77 (2H, d, *J* = 8.3 Hz). **^{13}C NMR** (100 MHz, $CDCl_3$) δ (ppm): 21.3, 26.1, 29.6, 33.8, 35.4, 39.9, 54.1, 72.5, 109.5, 126.8, 132.8, 138.1, 140.2, 148.4. **MS** (ESI positive) *m/z* (%): 411 $[M+Na]^+$, (100). Elemental analysis: $C_{16}H_{23}NO_3SSe$ Calcd. C 49.48%, H 5.97%, N 3.61%. Found: C 49.36%, H 6.04%, N 3.65%.

General Procedure for the preparation of *N*- protected β-amino selenide 18a-c

$NaBH_4$ (23 mg, 0.60 mmol, 3.0 eq.) was portionwise added to a solution of 4,4'-diselanediyldibenzenesulfonamide **14** (94 mg, 0.20 mmol, 1.0 eq.) in EtOH (2 mL) at 0°C under inert atmosphere (N_2). After 30 min, a solution of aziridine **17** (0.36 mmol, 1.8 eq.) in THF (1 mL) was slowly added and the reaction mixture was stirred at room temperature for 12 h. The reaction was quenched by addition of saturated aq. NH_4Cl (2 mL) and diluted with EtOAc (5 mL), The layers were separated and the aqueous layer was extracted with EtOAc (2 x 5 mL), dried over Na_2SO_4, filtered and concentrated under vacuum. The crude material was purified by flash chromatography to yield *N*-protected β-aminoselenides **18a-c** bearing benzenesulfonamide moiety.

(*S*)-4-Methyl-*N*-(3-methyl-1-((4-sulfamoylphenyl)selanyl)butan-2-yl)benzene sulfonamide 18a:

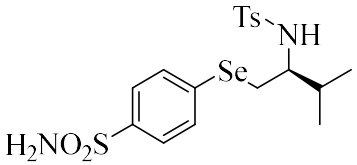

Following the general procedure, 4,4'-diselanediyldibenzenesulfonamide **14** (71 mg, 0.15 mmol) and (*S*)-2-isopropyl-1-tosylaziridine **17a** (65 mg, 0. 27 mmol) gave after flash chromatography (petroleum

ether/EtOAc 3:2) **18a** (94 mg, 73%). **^{1}H NMR** (400 MHz, DMSO-d_6) δ (ppm) 0.71 (6H, d, J = 6.8 Hz), 1.81-1.93 (1H, m), 2.36 (3H, s), 2.81 (1H, dd, J = 6.1, 12.2 Hz, $CH_a\mathbf{H_b}Se$), 3.03 (1H, dd, J = 6.9, 12.2 Hz, $CH_a\mathbf{H_b}Se$), 3.07-3.15 (1H, m, C**H**NH), 7.31 (2H, d, J = 8.0 Hz), 7.36 (2H, bs, NH_2), 7.39 (2H, d, J = 8.4 Hz), 7.61 (2H, d, J = 8.0 Hz), 7.64 (2H, d, J = 8.4 Hz), 7.71 (1H, bd, J = 7.8 Hz, NH). **^{13}C NMR** (100 MHz, DMSO-d_6) δ (ppm): 12.8, 19.6, 21.9, 31.3, 31.6, 58.9, 127.1, 127.5, 130.3, 131.5, 136.4, 139.6, 143.0, 143.3. **^{77}Se NMR** (76 MHz, DMSO-d_6) δ (ppm): 268.8. **MS** (ESI positive) *m/z* (%): 476 $[M+H]^+$, (100). Elemental analysis: $C_{18}H_{24}N_2O_4S_2Se$ Calcd. C 45.47%, H 5.09%, N 5.89%. Found: C 45.34%, H 5.15%, N 5.93%.

(*S*)-4-methyl-*N*-(1-phenyl-3-((4-sulfamoylphenyl)selanyl)propan-2-yl)benzene sulfonamide 18b:

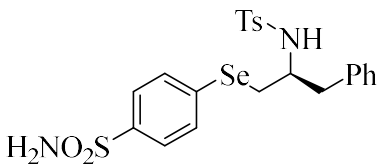

Following the general procedure, 4,4'-diselanediyldibenzenesulfonamide **14** (36 mg, 0.1 mmol) and (*S*)-2-benzyl-1-tosylaziridine **17b** (52 mg, 0. 18 mmol) gave after flash chromatography (petroleum ether/EtOAc 3:2) **18b** (65 mg, 69%). **^{1}H NMR** (400 MHz, DMSO-d_6) δ (ppm) 2.33 (3H, s), 2.66 (1H, dd, J = 6.9, 13.5 Hz, $C\mathbf{H_a}H_bPh$), 2.82 (1H, dd, J = 6.4, 13.5 Hz, $CH_a\mathbf{H_b}Ph$), 2.96 (1H, dd, J = 5.1, 11.6 Hz, $C\mathbf{H_a}H_bSe$), 3.01 (1H, dd, J = 4.9, 11.6 Hz, $CH_a\mathbf{H_b}Se$), 3.35-3.42 (1H, m, C**H**NH), 7.00-7.06 (2H, m), 7.15-7.22 (5H, m), 7.31 (2H, d, J = 8.4 Hz), 7.37 (2H, bs, NH_2), 7.44 (2H, d, J = 8.2 Hz), 7.60 (2H, d, J = 8.4 Hz), 7.97 (1H, bd, J = 5.8 Hz, NH). **^{13}C NMR** (100 MHz, DMSO-d_6) δ (ppm): 21.9, 32.1 (CH_2Se), 40.9 (CH_2Ph, partially overlapped with DMSO-d_6 signal), 55.9 (CHNH), 127.0, 127.1, 127.2, 129.1, 130.1, 130.3, 131.0, 136.4, 138.4, 138.8, 142.8, 143.3. **MS** (ESI positive) *m/z* (%): 547 $[M+Na]^+$, (100). Elemental analysis: $C_{22}H_{24}N_2O_4S_2Se$ Calcd. C 50.47%, H 4.62%, N 5.35%. Found: C 50.35%, H 4.68%, N 5.38%.

***tert*-Butyl (*S*)-(3-methyl-1-((4-sulfamoylphenyl)selanyl)butan-2-yl)carbamate 18c:**

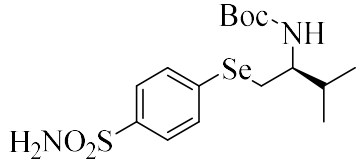

Following the general procedure, 4,4'-diselanediyldibenzenesulfonamide **14** (94 mg, 0.20 mmol) and *tert*-butyl (*S*)-2-isopropylaziridine-1-carboxylate **17c** (67 mg, 0. 36 mmol) gave after flash chromatography

(petroleum ether/EtOAc 3:1) **18c** (108 mg, 71%). **^{1}H NMR** (400 MHz, $CDCl_3$) δ (ppm) 0.91 (3H, d, *J* = 6.9 Hz), 0.94 (3H, d, *J* = 6.8 Hz), 1.42 (9H, s), 1.83-1.93 (1H, m), 3.13 (2H, ap d, *J* = 5.9 Hz, CH_2Se), 3.62-3.74 (1H, m, C**H**NH), 4.57 (1H, bd, *J* = 9.0 Hz, CHN**H**), 5.08 (2H, bs, NH_2), 7.58 (2H, d, *J* = 8.3 Hz), 7.76 (2H, d, *J* = 8.3 Hz). **^{13}C NMR** (100 MHz, $CDCl_3$) δ (ppm): 17.7, 19.6, 28.4, 31.6, 55.3, 79.5, 126.8, 131.5, 138.0, 140.0, 155.6. **^{77}Se NMR** (76 MHz, DMSO-*d*$_6$) δ (ppm): 265.6. **MS** (ESI positive) *m/z* (%): 422 $[M+H]^+$, (100). Elemental analysis: $C_{16}H_{26}N_2O_4SSe$ Calcd. C 45.60%, H 6.22%, N 6.65%. Found: C 45.71%, H 6.18%, N 6.60%.

Preparation of (*S*)-4-((2-Amino-3-methylbutyl)selanyl)benzenesulfonamide 19:

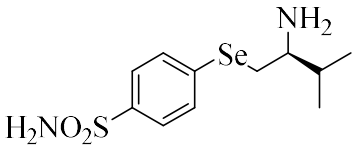

Following a reported procedure,[1] a solution of acetyl chloride (107µL, 1.5 mmol, 15 eq.) in MeOH (1 mL) was slowly added to a solution of *tert*-butyl (*S*)-(3-methyl-1-((4-sulfamoylphenyl)selanyl)butan-2-yl)carbamate **18c** (42 mg, 0.1 mmol, 1.0 eq.) in MeOH (1 mL) at 0 °C under inert atmosphere (N_2). The reaction mixture was stirred at 0 °C for 6 h and the solvent was removed under vacuum to afford the crude product. Flash column chromatography (petroleum ether/ethyl acetate 1:2) gave (*S*)-4-((2-amino-3-methylbutyl)selanyl)benzenesulfonamide **19** (17 mg, 52%). **^{1}H NMR** (400 MHz, DMSO-*d*$_6$) δ (ppm) 0.92 (6H, ap t, *J* = 6.3 Hz), 1.97-2.1 (1H, m), 3.01-3.13 (1H, m), 3.23 (1H, dd, *J* = 6.9, 13.1 Hz), 3.27-3.38 (1H, m), 7.38 (2H, bs), 7.67-7.74 (4H, m), (8.20 (2H, bs). **^{13}C NMR** (100 MHz, DMSO-*d*$_6$) δ (ppm): 18.2, 18.9, 27.6, 30.6, 56.5, 127.2, 132.0, 135.4, 143.4. **MS** (ESI positive) *m/z* (%): 320 $[M-H]^-$, (100). Elemental analysis: $C_{11}H_{18}N_2O_2SSe$ Calcd. C 41.12%, H 5.65%, N 8.72%. Found: C 41.22%, H 5.59%, N 8.67%.

General procedure for the synthesis of β-hydroxyselenides 16 and β-aminoselenides 18 from selenocyanate 13:

$NaBH_4$ (30 mg, 0.80 mmol, 4.0 eq.) was portionwise added to a solution of 4-selenocyanatobenzenesulfonamide **13** (52 mg, 0.20 mmol, 1.0 eq.) in EtOH (2 mL) at room temperature under inert atmosphere (N_2). After 1 h, the epoxide **15** or the aziridine **17** (0.18 mmol, 0.9 eq.) was slowly added and the reaction mixture was stirred at room temperature for 3 h, until complete consumption of the starting material was observed by TLC. The reaction was quenched by addition of saturated aq. NH_4Cl (2 mL) and diluted with EtOAc

(5 mL), The layers were separated and the aqueous layer was extracted with EtOAc (2 x 5 mL), dried over Na_2SO_4, filtered and concentrated under vacuum. The crude material was purified by flash chromatography to yield selenides **16** and **18**, bearing benzenesulfonamide moiety.

General procedure for preparation of acylselenoureido benzensolfonamide derivatives 25-29.

Potassium selenocyanate (0.14 g, 1.0 mmol) dissolved in acetone (5.0 mL) was treated with the appropriate acyl chloride **20a-i** (1.0 mmol). The reaction mixture was stirred at r.t. for 15 min, followed by addition of appropriate aminobenzensulfonamide (**12, 21-24**) (1.0 mmol) and stirred for 40 min at the same temperature. After this time the mixture was quenched with H_2O and the formed precipitate was filtered-off and dried on air. The obtained products **25-29** were used as they are.

***N*-((4-Sulfamoylphenethyl)carbamoselenoyl)benzamide 25a:**

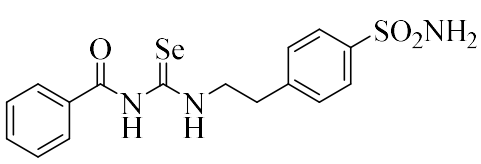

Yield 60%, 0.246 g; yellow solid, **^{1}H-NMR** (DMSO-*d_6*, 400 MHz): 11.63 (1H, brs, N**H**, exchange with D_2O), 11.47 (1H, apt, N**H**, exchange with D_2O), 7.94 (2H, d, *J*=8.52), 7.82 (2H, d, *J*=8.3), 7.68 (1H, t, *J*=7.4), 7.54 (4H, m), 7.35 (2H, brs, N**H$_2$**, exchange with D_2O), 3.98 (2H, apq), 3.13 (2H, t, J=7.36); **^{13}C-NMR** (DMSO-*d_6*, 100 MHz): 181.6 (**C**=Se), 168.9, 143.8, 143.3, 134.0, 132.8, 130.0, 129.6, 129.3, 126.8, 49.7, 34.1; *m/z* (ESI negative) 410.1 $[M-H]^-$.

3-Methyl-*N*-((4-sulfamoylphenethyl)carbamoselenoyl)benzamide 25b:

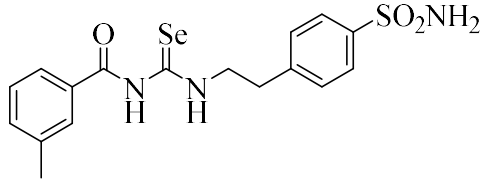

Yield 60%, 0.255 g; yellow solid, **^{1}H-NMR** (DMSO-*d_6*, 400 MHz): 11.57 (1H, brs, N**H**, exchange with D_2O), 11.48 (1H, apt, N**H**, exchange with D_2O), 7.81 (3H, m), 7.73 (1H, d, *J*=7.65), 7.54-7.41 (4H, m), 7.36 (2H, brs, N**H$_2$**, exchange with D_2O), 3.97 (2H, apq), 3.12 (2H, t, J=7.29), 2.41 (3H, s); **^{13}C-NMR** (DMSO-*d_6*, 100 MHz): 181.7 (**C**=Se), 169.0, 143.8, 143.3, 138.8, 134.7, 132.7, 130.1, 130.0, 129.3,

126.8, 126.7, 49.7, 34.1, 21.7; **^{77}Se-NMR** (DMSO-d_6, 76 MHz): 349; *m/z* (ESI positive) 426.1 $[M+H]^+$.

***N*-((4-Sulfamoylphenethyl)carbamoselenoyl)-[1,1'-biphenyl]-4-carboxamide 25c:**

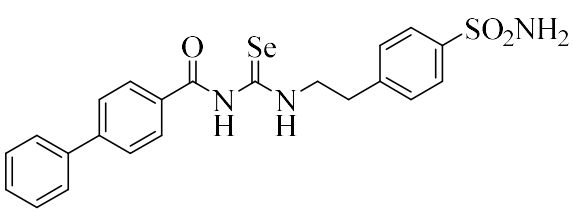

Yield 70%, 0.341 g; yellow solid, **^{1}H-NMR** (DMSO-d_6, 400 MHz): 11.86 (1H, brs, N**H**, exchange with D_2O), 11.54 (1H, apt, N**H**, exchange with D_2O), 8.23 (1H, s), 7.97 (1H, d, *J*=7.75), 7.92 (1H, d, *J*=8.04), 7.84 (4H, m), 7.65 (1H, t, *J*=7.77), 7.56 (4H, m), 7.46 (1H, t, *J*=7.34), 7.36 (2H, brs, N**H**$_2$, exchange with D_2O), 4.01 (2H, apq), 3.15 (2H, t, J=7.29); **^{13}C-NMR** (DMSO-d_6, 100 MHz): 181.8 (**C**=Se), 168.9, 143.8, 143.3, 141.1, 140.2, 133.5, 132.2, 130.1, 130.0, 129.9, 128.9, 128.7, 127.9, 127.8, 126.9, 49.7, 34.1; **^{77}Se-NMR** (DMSO-d_6, 76 MHz): 351; *m/z* (ESI positive) 488.0 $[M+H]^+$.

***N*-((4-Sulfamoylphenethyl)carbamoselenoyl)benzo[d][1,3]dioxole-5-carboxamide 25e:**

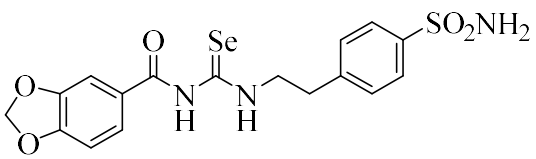

Yield 70%, 0.318 g; yellow solid, **^{1}H-NMR** (DMSO-d_6, 400 MHz): 11.47 (1H, apt, N**H,** exchange with D_2O), 11.39 (1H, brs, N**H**, exchange with D_2O), 7.82 (2H, d, *J*=8.35), 7.61 (1H, dd, *J*=8.24, 1.85), 7.52 (3H, m), 7.34 (2H, brs, N**H**, exchange with D_2O), 7.07 (1H, d, *J*=8.23), 6.18 (2H, s), 3.97 (2H, m), 3.12 (2H, t, *J*=7.34); **^{13}C-NMR** (DMSO-d_6, 100 MHz): 181.6 (**C**=Se), 167.7, 152.4, 148.3, 143.7, 143.3, 130.0, 126.8, 126.2, 125.7, 109.3, 108.9, 103.1, 49.6, 34.1; **^{77}Se-NMR** (DMSO-d_6, 76 MHz): 347; *m/z* (ESI positive) 456 $[M+H]^+$.

***N*-((4-Sulfamoylphenyl)carbamoselenoyl)benzamide 26a:**

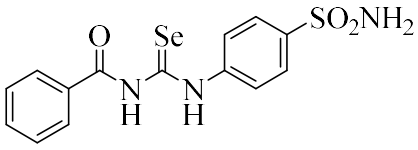

Yield 77%, 0.295 g; yellow solid, **^{1}H-NMR** (DMSO-d_6, 400 MHz): 13.10 (1H, brs, N**H**, exchange with D_2O), 11.94 (1H, brs, N**H**, exchange with D_2O), 8.02 (2H, d, *J*=7.40), 7.93 (4H, aps), 7.71 (1H, t, *J*=7.41), 7.59 (2H, t, *J*=7.79), 7.47 (2H, brs, N**H**$_2$, exchange with D_2O); **^{13}C-NMR** (DMSO-d_6, 100 MHz): 182.0 (**C**=Se), 169.0, 142.8,

134.2, 132.8, 130.2, 129.8, 129.4, 127.2, 126.4; **^{77}Se-NMR** (DMSO-d_6, 76 MHz): 435; *m/z* (ESI negative) 382 $[M-H]^-$

***N*-((4-Sulfamoylphenyl)carbamoselenoyl)benzo[d][1,3]dioxole-5-carboxamide 26e:**

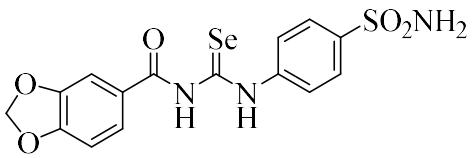

Yield 82%, 0.350 g; yellow solid, **^{1}H-NMR** (DMSO-d_6, 400 MHz): 13.10 (1H, brs, N**H**, exchange with D_2O), 11.72 (1H, brs, N**H**, exchange with D_2O), 7.90 (4H, aps), 7.69 (1H, dd, *J*=8.94, 1.72), 7.58 (1H, d, *J*=1.70), 7.45 (2H, brs, N**H**$_2$, exchange with D_2O), 7.10 (1H, d, *J*=8.23), 6.20 (2H, s); **^{13}C-NMR** (DMSO-d_6, 100 MHz): 181.9 (**C**=Se), 167.8, 152.6, 148.4, 142.8, 127.2, 126.4, 126.2, 126.0, 120.7, 109.4, 109.0, 103.2; **^{77}Se-NMR** (DMSO-d_6, 76 MHz): 430; *m/z* (ESI positive) 428 $[M+H]^+$.

3-Bromo-*N*-((4-sulfamoylphenyl)carbamoselenoyl)-5-(trifluoromethoxy) benzamide 26f:

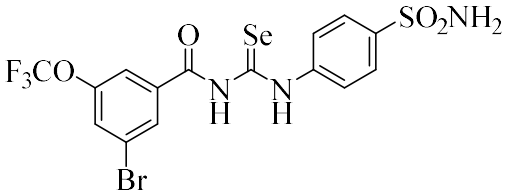

Yield 53%, 0.289 g; brown solid, **^{1}H-NMR** (DMSO-d_6, 400 MHz): 12.83 (1H, brs, N**H**, exchange with D_2O), 12.3 (1H, brs, N**H**, exchange with D_2O), 8.25 (1H, s), 8.04 (1H, s), 7.97 (1H, s), 7.91 (4H, aps), 7.47 (2H, brs, N**H**$_2$, exchange with D_2O); **^{13}C-NMR** (DMSO-d_6, 100 MHz): 181.8 (**C**=Se), 165.6, 149.3 (q, *J*=1.95), 142.8, 136.7, 131.8, 129.4, 127.2, 126.4, 123.1, 122.1, 121.5, 119.5; **^{19}F-NMR** (DMSO-d_6, 376 MHz): -56.90; **^{77}Se-NMR** (DMSO-d_6, 76 MHz): 452; *m/z* (ESI negative) 543.8 $[M-H]^-$.

2-(((4-Sulfamoylphenyl)carbamoselenoyl)carbamoyl)phenyl acetate 26g:

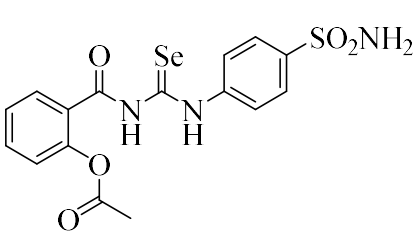

Yield 70%, 0.308 g; yellow solid, **^{1}H-NMR** (DMSO-d_6, 400 MHz): 12.82 (1H, brs, N**H**, exchange with D_2O), 11.97 (1H, brs, N**H**, exchange with D_2O), 7.90 (4H, aps), 7.79 (1H, dd, *J*=7.70, 1.33), 7.70 (1H, td, J=8.07, 1.52), 7.46 (3H, m), 7.34 (1H, d, *J*=8.03), 2.38 (3H, s); **^{13}C-NMR** (DMSO-d_6, 100 MHz): 181.7 (**C**=Se), 170.1, 167.1, 149.4, 143.1, 142.9,

134.7, 131.3, 127.4, 127.3, 127.2, 126.8, 124.5, 22.0; **^{77}Se-NMR** (DMSO-d_6, 76 MHz): 435; *m/z* (ESI positive) 442.0 $[M-H]^-$.

4-Heptyl-*N*-((4-sulfamoylphenyl)carbamoselenoyl)benzamide 26h:

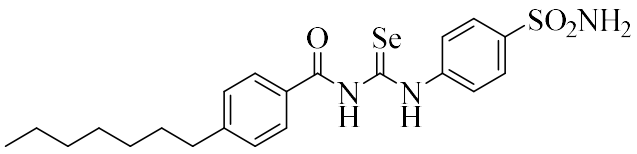

Yield 95%, 0.456 g; yellow solid, **^{1}H-NMR** (DMSO-d_6, 400 MHz): 13.14 (1H, brs, N**H**, exchange with D_2O), 11.83 (1H, brs, N**H**, exchange with D_2O), 7.96 (2H, d, J=8.07), 7.91 (4H, aps), 7.46 (2H, brs, N**H**, exchange with D_2O), 7.40 (2H, d, *J*=8.08), 2.70 (2H, t, J=7.48), 1.64 (2H, aps), 1.32 (8H, m), 0.89 (3H, t, *J*=6.53); **^{13}C-NMR** (DMSO-d_6, 100 MHz): 182.0 (**C**=Se), 168.8, 149.5, 142.9, 142.8, 130.1, 129.9, 129.3, 127.2, 126.3, 127.2, 38.0, 32.1, 31.5, 29.5, 29.4, 23.0, 14.9; *m/z* (ESI positive) 482.0 $[M+H]^+$.

***N*-((3-Sulfamoylphenyl)carbamoselenoyl)benzamide 27a:**

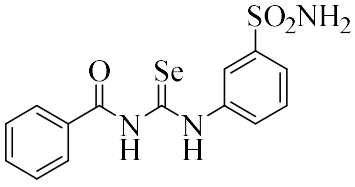

Yield 70%, 0.268 g; yellow/brown solid, **^{1}H-NMR** (DMSO-d_6, 400 MHz): 13.01 (1H, brs, N**H**, exchange with D_2O), 11.97 (1H, brs, N**H**, exchange with D_2O), 8.15 (1H, s), 8.02 (2H, d, *J*=7.45), 7.93 (1H, d, *J*=7.51), 7.80 (1H, d, J=7.56), 7.69 (2H, m), 7.59 (2H, t, *J*=7.64), 7.52 (2H, brs, NH_2, exchange with D_2O); **^{13}C-NMR** (DMSO-d_6, 100 MHz): 182.2 (**C**=Se), 168.9, 145.5, 140.5, 134.2, 132.8, 130.3, 129.7, 129.4, 124.9, 123.5; *m/z* (ESI positive) 384.1 $[M+H]^+$.

3-Methyl-*N*-((3-sulfamoylphenyl)carbamoselenoyl)benzamide 27b:

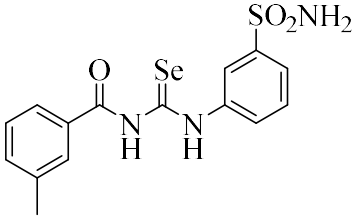

Yield 57%, 0.226 g; brown solid, **^{1}H-NMR** (DMSO-d_6, 400 MHz): 13.03 (1H, brs, N**H,** exchange with D_2O), 11.92 (1H, brs, N**H**, exchange with D_2O), 8.14 (1H, s), 7.93 (1H, d, *J*=7.83), 7.87 (1H, s), 7.81 (2H, m), 7.67 (1H, t, *J*=7.90), 7.55-7.46 (4H, m), 2.44 (3H, s); **^{13}C-NMR** (DMSO-d_6, 100 MHz): 182.2 (**C**=Se), 168.9, 145.5, 140.5, 138.9, 134.9, 132.7, 130.3, 130.2, 129.8, 129.3, 127.0, 124.9, 123.5, 21.7; *m/z* (ESI negative) 396.1 $[M-H]^-$.

***N*-((3-Sulfamoylphenyl)carbamoselenoyl)-2,4-bis(trifluoromethyl)benzamide 27d:**

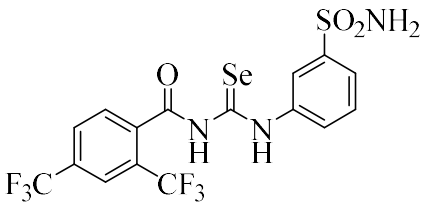

Yield 50%, 0.259 g; yellow solid, **^{1}H-NMR** (DMSO-d_6, 400 MHz): 12.59- 12.58 (2H, m, N**H**, exchange with D_2O), 8.28 (2H, m), 8.11 (2H, m), 7.92 (1H, d, *J*=7.92), 7.82 (1H, d, *J*=7.87), 7.68 (1H, t, *J*=7.68), 7.52 (2H, brs, N**H**$_2$, exchange with D_2O); **^{13}C-NMR** (DMSO-d_6, 100 MHz): 181.6 (**C**=Se), 167.3, 145.5, 140.4, 137.9, 132.3, 131.9, 131.2, 130.7, 130.4, 130.0, 128.0, 127.7, 125.3, 125.1, 125.0, 124.4, 123.7, 122.6, 122.4; **^{19}F-NMR** (DMSO-d_6, 376 MHz): -57.98, -61.51; *m/z* (ESI negative) 518.0 $[M-H]^-$.

***N*-((2-Sulfamoylphenyl)carbamoselenoyl)benzamide 28a:**

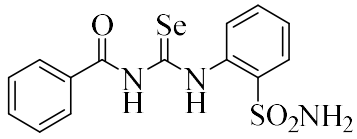

Yield 55%, 0.210 g; dark yellow solid, **^{1}H-NMR** (DMSO-d_6, 400 MHz): 13.17 (1H, brs, N**H**, exchange with D_2O), 11.98 (1H, brs, N**H**, exchange with D_2O), 8.08 (1H, d, *J*=7.88), 8.03 (2H, m), 7.94 (1H, dd, *J*=7.51, 1.41), 7.74-7.66 (4H, m), 7.61-7-52 (3H, m); **^{13}C-NMR** (DMSO-d_6, 100 MHz): 183.3 (**C**=Se), 168.9, 138.5, 137.0, 134.2, 132.8, 132.6, 131.2, 129.8, 129.3, 128.2, 128.1; *m/z* (ESI positive) 384.1 $[M+H]^+$.

***N*-((2-Hydroxy-5-sulfamoylphenyl)carbamoselenoyl)-[1,1'-biphenyl]-4-carboxamide 29c:**

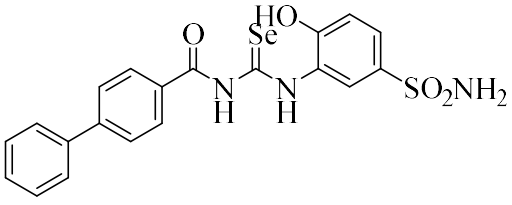

Yield 69%, 0.327 g; yellow solid, **^{1}H-NMR** (DMSO-d_6, 400 MHz): 13.46 (1H, brs, N**H**, exchange with D_2O), 12.14 (1H, brs, N**H**, exchange with D_2O), 11.17 (1H, s, OH, exchange with D_2O), 9.14 (1H, d, *J*=1.99), 8.30 (1H, s), 8.0 (2H, m), 7.86 (2H, d, *J*=7.35), 7.69 (2H, m), 7.57 (2H, t, *J*=7.57), 7.47 (1H, t, *J*=7.32), 7.27 (2H, brs, N**H**, exchange with D_2O), 7.14 (1H, d, *J*=8.56); **^{13}C-NMR** (DMSO-d_6, 100 MHz): 180.1 (**C**=Se), 169.2, 153.3, 141.1, 140.1, 135.0, 133.4, 132.3, 130.1, 129.9, 128.9, 128.0, 127.9, 127.2, 126.3, 123.1, 116.3; **^{77}Se-NMR** (DMSO-d_6, 76 MHz): 436; *m/z* (ESI positive) 476.1 $[M+H]^+$.

4-Bromo-*N*-((2-hydroxy-5-sulfamoylphenyl)carbamoselenoyl)-3-methylbenzamide 29g:

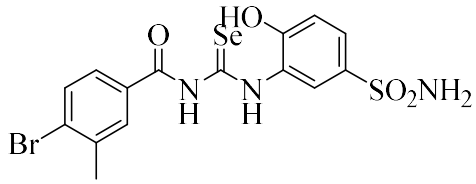

Yield 82%, 0.403 g; orange solid, **^{1}H-NMR** (DMSO-d_6, 400 MHz): 13.27 (1H, brs, N**H**, exchange with D_2O), 11.90 (1H, brs, N**H**, exchange with D_2O), 11.21 (1H, s, OH, exchange with D_2O), 9.15 (1H, d, *J*=2.08), 8.01 (1H, d, J=1.14), 7.77 (2H, m), 7.68 (1H, dd, *J*=8.56, 2.25), 7.27 (2H, brs, N**H**, exchange with D_2O), 7.14 (1H, d, *J*=8.57), 2.45(3H, s); **^{13}C-NMR** (DMSO-d_6, 100 MHz): 180.0 (**C**=Se), 168.5, 153.4, 138.7, 135.0, 133.3, 132.1, 132.0, 130.7, 129.0, 127.2, 126.4, 123.0, 116.3, 23.3; **^{77}Se-NMR** (DMSO-d_6, 76 MHz): 439; *m/z* (ESI positive) 492.0 $[M+H]^+$.

2-(((2-Hydroxy-5-sulfamoylphenyl)carbamoselenoyl)carbamoyl)phenyl acetate 29i:

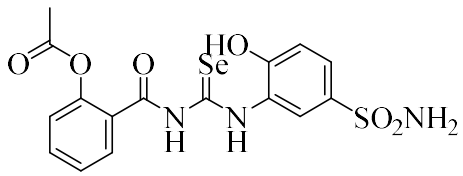

Yield 75%, 0.342 g; brown solid, **^{1}H-NMR** (DMSO-d_6, 400 MHz): 13.16 (1H, brs, N**H**, exchange with D_2O), 11.92 (1H, brs, N**H**, exchange with D_2O), 11.23 (1H, s, OH, exchange with D_2O), 9.18 (1H, d, *J*=1.91), 7.82 (1H, dd, J=7.66, 1.19), 7.71 (1H, m), 7.66 (1H, dd, *J*=8.56, 2.18), 7.46 (1H, t, *J*=7.37), 7.36 (1H, d, *J*=8.06), 7.26 (2H, brs, NH, exchange with D_2O), 7.12 (1H, d, *J*=8.56), 2.39(3H, s); **^{13}C-NMR** (DMSO-d_6, 100 MHz): 179.3 (**C**=Se), 169.7, 167.1, 153.1, 149.1, 135.0, 134.3, 131.1, 127.2, 127.1, 126.9, 126.3, 124.1, 122.6, 116.2, 21.8; **^{77}Se-NMR** (DMSO-d_6, 76 MHz): 441; *m/z* (ESI positive) 458.1 $[M+H]^+$.

Synthesis of *N*-((2-hydroxy-5-sulfamoylphenyl)carbamoselenoyl)benzamide 30a:

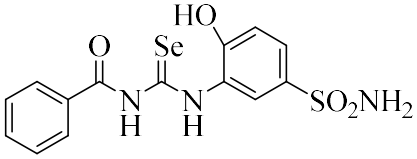

N-((2-Hydroxy-5-sulfamoylphenyl) carbamoselenoyl)benzamide **30a** was obtained according to the above reported general procedure using benzoyl chloride **20a** (0.14 g) and potassium selenocyanate (1.0 eq). Yield 63%, 0.25 g; yellow solid, **^{1}H-NMR** (DMSO-d_6, 400 MHz): 13.39 (1H, s, N**H**, exchange with D_2O), 11.89 (1H, s, N**H**, exchange with D_2O), 11.17 (1H, s, O**H**, exchange with D_2O), 9.12 (1H, d, *J*=1.98), 8.02 (2H, d, *J*=7.78), 7.72 (1H, t, *J*=7.42),

7.66 (1H, dd, *J*=8.55, *J*3=2.24), 7.59 (2H, t, *J*=7.71), 7.26 (2H, brs, N**H**$_2$, exchange with D_2O), 7.13 (1H, d, *J*=8.57); **^{13}CNMR** (DMSO-*d*$_6$, 100 MHz): 180.1 (*C*=Se), 169.3 (*C*=O), 153.3 (*C*OH), 134.9, 134.2, 132.7, 129.7, 129.3, 127.1, 126.2, 123.0, 116.2; **^{77}Se-NMR** (DMSO-*d*$_6$, 76 MHz): 435; HRMS *m/z* $[M+H]^+$ calcd for $C_{14}H_{14}N_3O_4SSe$, 399.9865; found, 399.9872.

Synthesis of N-((2-Hydroxy-5-sulfamoylphenyl)carbamoselenoyl)-3-methylbenzamide 30b:

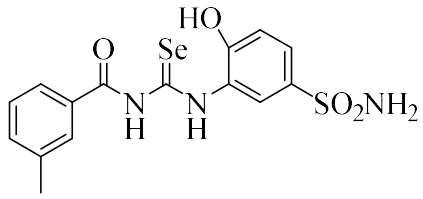

N-((2-Hydroxy-5-sulfamoylphenyl)carbamoselenoyl)-3-methylbenzamide **30b** was obtained according to the above reported general procedure using 3-methylbenzoyl chloride **20b** (0.15 g) and potassium selenocyanate (1.0 eq). Yield 77%, 0.32 g; yellow solid, **^{1}H-NMR** (DMSO-*d*$_6$, 400 MHz): 13.44 (1H, s, N**H**, exchange with D_2O), 11.82 (1H, s, N**H**, exchange with D_2O), 11.20 (1H, s, O**H**, exchange with D_2O), 9.16 (1H, d, *J*=1.43), 7.89 (1H, s), 7.83 (1H, d, *J*=7.51), 7.68 (1H, dd, *J*=8.50, *J*3=1.90), 7.55-7.46 (2H, m), 7.29 (2H, brs, N**H**$_2$, exchange with D_2O), 7.15(1H, d, *J*=8.55), 3.48 (3H,s); **^{13}C-NMR** (DMSO-*d*$_6$, 100 MHz): 180.1 (*C*=Se), 169.3 (*C*=O), 153.3 (*C*OH), 138.8, 135.0, 134.9, 132.6, 130.2, 129.3, 127.2, 126.9, 126.3, 123.0, 116.3, 21.7; **^{77}Se-NMR** (DMSO-*d*$_6$, 76 MHz): 434; HRMS *m/z* $[M+H]^+$ calcd for $C_{15}H_{16}N_3O_4SSe$, 414.0021; found, 414.0031.

Synthesis of 4-n-Heptyl-N-((2-hydroxy-5-sulfamoylphenyl)carbamoselenoyl) benzamide 30e:

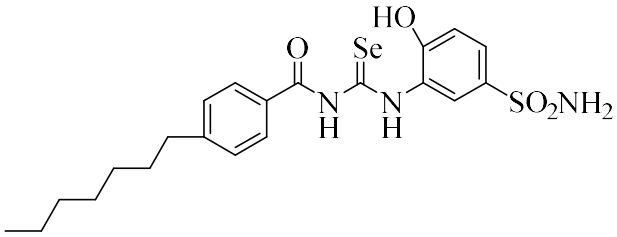

4-*n*-Heptyl-*N*-((2-hydroxy-5-sulfamoylphenyl)carbamoselenoyl) benzamide **30e** was obtained according to the above reported general procedure using 4-*n*-heptylbenzoyl chloride **20e** (0.24 g) and potassium selenocyanate (1.0 eq). Yield 91%, 0.45 g; yellow solid, **^{1}H-NMR** (DMSO-*d*$_6$, 400 MHz): 13.46 (1H, s, N**H**, exchange with D_2O), 11.72 (1H, s, N**H**, exchange with D_2O), 11.22 (1H, s, O**H**, exchange with D_2O), 9.17 (1H,

d, *J*=1.43), 7.96 (2H, d, *J*=8.15), 7.67 (1H, dd, *J*=8.51, *J*^{3}=1.89), 7.39 (2H, d, *J*=7.83), 7.26 (2H, brs, N**H**$_2$, exchange with D_2O), 7.14(1H, d, *J*=8.55), 2.68 (2H,t, *J*=7.27), 1.64 (2H, brs), 1.28-1.26 (8H, m), 0.87 (3H, t, *J*=6.73); **^{13}C-NMR** (DMSO-*d*$_6$, 100 MHz): 180.0 (*C*=Se), 169.1 (*C*=O), 153.3 (*C*OH), 149.5, 135.0, 129.9, 129.4, 128.5, 127.3, 126.3, 122.9, 116.3, 36.1, 32.2, 31.5, 29.6, 29.5, 23.1, 14.9; **^{77}Se-NMR** (DMSO-*d*$_6$, 76 MHz): 432; HRMS *m/z* $[M+H]^+$ calcd for $C_{21}H_{28}N_3O_4SSe$, 498.0961; found, 498.0972.

Synthesis of 3-Bromo-N-((2-hydroxy-5-sulfamoylphenyl)carbamoselenoyl) 5(trifluoromethoxy)benzamide 30f:

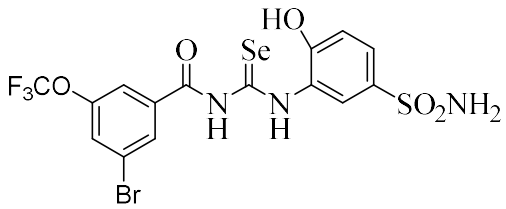

3-Bromo-*N*-((2-hydroxy-5-sulfamoylphenyl)carbamoselenoyl)-5-(trifluoromethoxy)benzamide **30f** was obtained according to the above reported general procedure using 3-bromo-5-(trifluoromethoxy)benzoyl chloride **20f** (0.30 g) and potassium selenocyanate (1.0 eq). Yield 84%, 0.47 g; yellow solid, **^{1}H-NMR** (DMSO-*d*$_6$, 400 MHz): 13.19 (1H, s, N**H**, exchange with D_2O), 12.27 (1H, s, N**H**, exchange with D_2O), 11.24 (1H, s, O**H**, exchange with D_2O), 9.13 (1H, d, *J*=2.10), 8.25 (1H, t, *J*=1.40), 8.03 (1H, s), 7.97 (1H, s), 7.66 (1H, dd, *J*=8.55, *J*3=2.26), 7.26 (2H, brs, N**H**$_2$, exchange with D_2O), 7.12 (1H,d, *J*=8.57); **^{13}C-NMR** (DMSO-*d*$_6$, 100 MHz): 179.8 (*C*=Se), 166.5 (*C*=O), 153.3 (*C*OH), 149.3, 136.7, 135.0, 131.9, 129.4, 127.1, 126.4, 123.0, 122.9, 121.7, 116.3; **^{19}F-NMR** (DMSO-*d*$_6$, 376 MHz): -56.86; HRMS *m/z* $[M+H]^+$ calcd for $C_{15}H_{12}BrF_3N_3O_5SSe$, 561.8790; found, 561.8810.

Synthesis of *N*-((2-Hydroxy-5 sulfamoylphenyl)carbamoselenoyl)benzo [d][1,3]dioxole-5-carboxamide 30h:

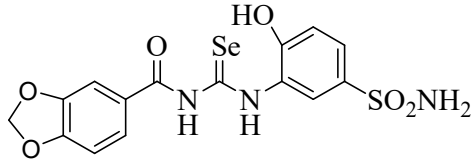

N-((2-Hydroxy-5-sulfamoylphenyl) carbamoselenoyl)benzo[d][1,3]dioxole-5-carboxamide **30h** was obtained according to the above reported general procedure using benzo[d][1,3]dioxole-5-carbonyl chloride **20h** (0.18 g) and potassium selenocyanate (1.0 eq). Yield 79%, 0.35 g; yellow solid, **^{1}H-NMR** (DMSO-*d*$_6$, 400 MHz): 13.40 (1H, s, N**H**, exchange with D_2O), 11.66 (1H, s, N**H**, exchange with D_2O), 11.13 (1H, s, O**H**, exchange

with D_2O), 9.11 (1H, d, *J*=1.82), 7.70-7.64 (2H, m), 7.58 (1H, d, *J*=1.43), 7.26 (2H, brs, N**H**$_2$, exchange with D_2O), 7.11 (2H, t, *J*=7.89), 6.20 (2H, s); **^{13}C-NMR** (DMSO-d_6, 100 MHz): 180.0 (*C*=Se), 168.1 (*C*=O), 153.3 (*C*OH), 152.6, 148.4, 134.9, 127.2, 126.2, 126.1, 126.0, 123.1, 116.3, 109.5, 108.9, 103.2; **^{77}Se-NMR** (DMSO-d_6, 76 MHz): 430; HRMS *m/z* $[M+H]^+$ calcd for $C_{15}H_{14}N_3O_6SSe$, 443.9763; found, 443.9774.

General procedure for Synthesis Compounds 31a-h:

Method A: The appropriate acylselenourea **30a-h** (0.5 mmol) was dissolved in a 1:1 biphasic mixture of acetonitrile and 3M NaOH aqueous solution, and was vigorously stirred overnight at r.t. The black solid residue (Se_0) was filtered-off and the reaction was quenched with a 3M HCl aqueous solution until a precipitate was formed, which was collected by filtration and dried on air and used as it is.

Method B: The appropriate acylselenourea **30a-h** (0.5 mmol) was dissolved in pyridine (5.0 ml) and stirred onernight at r.t. The black solid residue (Se_0) was filtered-off and the reaction was quenched with 3M HCl aqueous solution until a precipitate was formed, which was collected by filtration and dried on air and used as it is.

Synthesis of N-(5-Sulfamoylbenzo[d]oxazol-2-yl)benzamide 31a:

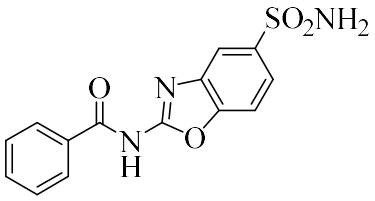

N-(5-Sulfamoylbenzo[d]oxazol-2-yl)benzamide **31a** was obtained according to the above reported general procedure using acylselenourea **30a** (0.20 g; 0.5 mmol). Yield 50%, 0.08 g; white solid, **^{1}H-NMR** (DMSO-d_6, 400 MHz): 12.32 (1H, s, N**H**, exchange with D_2O), 8.11-8.07 (3H, m), 7.90-7.83 (2H, m), 7.70 (1H, t, *J*=7.30), 7.60 (2H, t, *J*=7.57), 7.49 (2H, brs, N**H**$_2$, exchange with D_2O); **^{13}C-NMR** (DMSO-d_6, 100 MHz): 158.6, 150.2, 142.0, 133.8, 129.5, 129.4, 122.7, 116.7, 111.5; HRMS *m/z* $[M+H]^+$ calcd for $C_{14}H_{11}N_3O_4S$, 318.0543; found, 318.0550.

Synthesis of 3-Methyl-N-(5-sulfamoylbenzo[d]oxazol-2-yl)benzamide 31b:

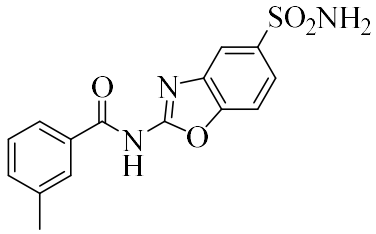

3-Methyl-*N*-(5-sulfamoylbenzo[d]oxazol-2-yl)benzamide **31b** was obtained according to the above reported general procedure using acylselenourea **30b** (0.20 g; 0.5 mmol). Yield 35%, 0.06 g; white solid, **^{1}H-NMR** (DMSO-d_6, 400 MHz): 12.25 (1H, s, N**H**, exchange with D_2O), 8.07 (1H, s), 7.90-7.82 (4H, m), 7.53-7.48 (2H, m), 7.46 (2H, brs, N**H**$_2$, exchange with D_2O), 2.45 (3H, s); **^{13}CNMR** (DMSO-d_6, 100 MHz): 165.8, 158.2, 150.4, 141.9, 138.8, 134.3, 133.7, 130.6, 129.8, 129.4, 126.5, 122.6, 116.8, 111.4, 21.8; HRMS *m/z* $[M+H]^+$ calcd for $C_{15}H_{14}N_3O_4S$, 332.0699; found, 332.0706.

Synthesis of 4-Heptyl-N-(5-sulfamoylbenzo[d]oxazol-2-yl)benzamide 31e:

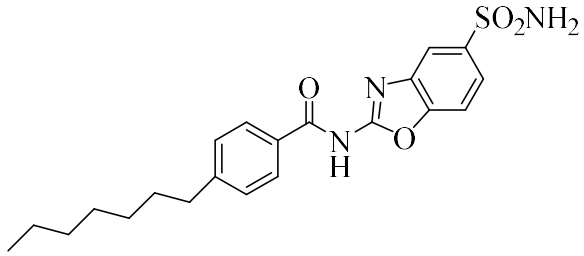

4-Heptyl-*N*-(5-sulfamoylbenzo[d]oxazol-2-yl) benzamide **31e** was obtained according to the above reported general procedure using acylselenourea **30e** (0.25 g, 0.5 mmol). Yield 29%, 0.06 g; white solid, **^{1}H-NMR** (DMSO-d_6, 400 MHz): 12.21 (1H, s, N**H**, exchange with D_2O), 8.08 (1H, s), 8.00 (2H, d, *J*=7.54), 7.90 (1H, d, *J*=8.44), 7.83 (1H, d, *J*=8.15), 7.46 (2H, brs, N**H**$_2$, exchange with D_2O), 7.42 (2H, d, *J*=7.82), 2.70 (2H, t, *J*=7.53), 1.64 (2H, t, *J*= 7.53), 1.33-1.29 (8H, m), 0.89 (3H, t, *J*=6.82); **^{13}C-NMR** (DMSO-d_6, 100 MHz): 165.5, 158.2, 150.4, 148.9, 141.9, 141.7, 130.9, 129.4, 122.6, 116.8, 111.4, 35.9, 32.1, 31.5, 29.5, 29.4, 22,9, 14.8; HRMS *m/z* $[M+H]^+$ calcd for $C_{21}H_{26}N_3O_4S$, 416.1638; found, 416.1650.

Synthesis of 3-Bromo-N-(5-sulfamoylbenzo[d]oxazol-2-yl)-5-(trifluoromethoxy)benzamide 31f:

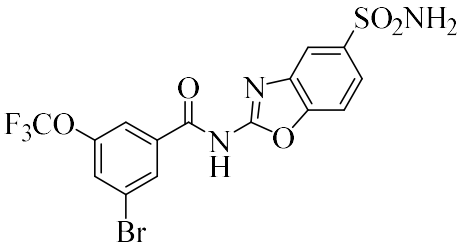

3-Bromo-*N*-(5-sulfamoylbenzo[d]oxazol-2-yl)-5-(trifluoromethoxy)benzamide **31f** was obtained according to the above reported general procedure using acylselenourea **30f** (0.28 g, 0.5 mmol). Yield 36%, 0.09 g; white solid, **^{1}H-NMR** (DMSO-d_6, 400 MHz): 8.30 (1H, s), 8.14 (1H, s), 8.03 (1H, s), 7.78 (1H, s), 7.62 (1H, m), 7.53 (1H, d, *J*=7.86), 7.28 (2H, brs, N**H**$_2$, exchange with D_2O); **^{13}C-NMR** (DMSO-d_6, 100 MHz): 168.9 (*C*=O), 149.4, 144.6, 139.9, 131.9, 131.3, 126.4, 125.6, 122.5, 122.2, 121.1, 120.3, 119.6, 115.6, 109.3; **^{19}F-NMR** (DMSO-d_6, 376 MHz): -56.93; HRMS *m/z* $[M+H]^+$ calcd for $C_{15}H_{10}BrF_3N_3O_5S$, 479.9471; found, 479.9490.

Synthesis of N-(5-Sulfamoylbenzo[d]oxazol-2-yl)benzo[d][1,3]dioxole-5-carboxamide 31h:

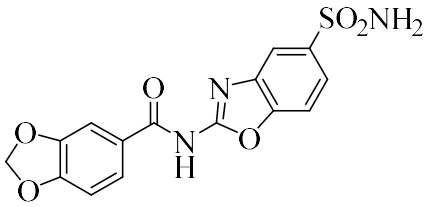

N-(5-Sulfamoylbenzo[d]oxazol-2-yl)benzo[d][1,3]dioxole-5-carboxamide **31h** was obtained according to the above reported general procedure using acylselenourea **30h** (0.22 g, 0.5 mmol). Yield 70%, 0,13 g; white solid, **^{1}H-NMR** (DMSO-d_6, 400 MHz): 8.04 (1H, s),7.88-7.81 (2H, m), 7.73 (1H, d, *J*=7.97), 7.60 (1H, d, *J*=1.62), 7.47 (2H, brs, N**H**$_2$, exchange with D_2O), 7.11 (1H, d, *J*= 8.24), 6.19 (2H, s, C**H**$_2$); **^{13}C-NMR** (DMSO-d_6, 100 MHz): 167.5 (*C*=O), 152.1, 148.5, 141.9, 125.9, 125.6, 125.3, 122.6, 111.4, 109.7, 109.2, 109.1, 109.0, 108.6, 103.0; HRMS *m/z* $[M+H]^+$ calcd for $C_{15}H_{12}N_3O_6S$, 362.0441; found, 362.0451.

General Procedure for preparation aryl selenols 33a-j from diselenides 32a-j:

$NaBH_4$ (23 mg, 0.6 mmol, 3.0 eq.) was portionwise added to a stirred solution or suspension (depending on the nature of the diselenide) of diselenide **32a-j** (0.2 mmol, 1.0 eq.) in EtOH (2 mL) at 0°C under inert atmosphere (N_2). After 15 solid citric acid (192 mg, 1.0 mmol, 5.0 eq.) was added and the reaction mixture was stirred at 0°C for 5 minutes. The mixture was

then diluted with Et_2O (5 mL) and H_2O (3 mL) was added. The layers were separated and the organic layer was washed with saturated *aq*. NH_4Cl (2 mL) and with brine (2 mL), dried over Na_2SO_4, filtered and concentrated under vacuum to afford aryl selenols **33a-j**, pure enough to be used without further purification.

Synthesis of 4-methylbenzeneselenol 33b:

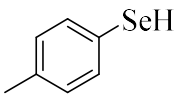

Following the general procedure, 1,2-di-*p*-tolyldiselane (75 mg, 0.22 mmol) gave 4-methylbenzeneselenol **33b** (45.3 mg, 60%). **^{1}H NMR** (400 MHz, $CDCl_3$) δ (ppm): 1.47 (1H, s, SeH), 2.31 (3H, s, CH_3), 7.04 (2H, ap. D, ls=8.0 Hz), 7.36 (2H, ap.d, ls=8.0 Hz). **^{13}C NMR** (100 MHz, $CDCl_3$) δ (ppm): 21.0, 120.1, 130.1, 133.0, 136.1.

Synthesis of 2-methylbenzeneselenol 33c:

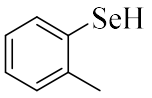

Following the general procedure, 1,2-di-*o*-tolyldiselane (75 mg, 0.22 mmol) gave 2-methylbenzeneselenol **33c** (49.8 mg, 66%). **^{1}H NMR** (400 MHz, $CDCl_3$) δ (ppm): 1.37 (1H, s, SeH), 2.36 (3H, s, CH_3), 7.02 (1H, ap t, *J*=7.4 Hz), 7.12-7.19 (2H, m), 7.46 (1H, ap d, *J*=7.7 Hz). **^{13}C NMR** (100 MHz, $CDCl_3$) δ (ppm): 23.0, 126.7, 126.9, 130.2, 133.2, 138.1.

Synthesis of 2,6-dimethylbenzeneselenol 33d:

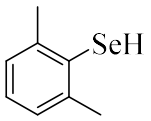

Following the general procedure, 1,2-bis(2,6-dimethylphenyl)diselane (75 mg, 0.20 mmol) gave 2,6-dimethylbenzeneselenol **33d** (58.8 mg, 78%). **^{1}H NMR** (400 MHz, $CDCl_3$) δ (ppm): 1.37 (1H, s, SeH); 2.39 (6H, s); 7.01-7.07 (3H, m). **^{13}C NMR** (100 MHz, $CDCl_3$) δ (ppm): 24.4; 125.8; 127.7; 138.1. **^{77}Se NMR** (76 MHz, $CDCl_3$) δ (ppm): 38.6.

Synthesis of 4-methoxybenzeneselenol 33e:

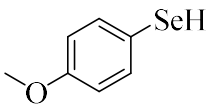

Following the general procedure, 1,2-bis(4-methoxyphenyl)diselane (75 mg, 0.20 mmol) gave 4-methoxybenzeneselenol **33e** (64.1 mg, 85%). **^{1}H NMR** (400 MHz, $CDCl_3$) δ (ppm): 1.45 (1H, s, SeH), 3.78 (3H, s, OCH_3), 6.79 (2H, ap d, ls=8.4 Hz), 7.41 (2H, ap d, ls=8.4 Hz). **^{13}C NMR** (100 MHz, $CDCl_3$) δ (ppm): 58.2; 112.9; 114.9, 135.3, 159.0.

Synthesis of 2-methoxybenzeneselenol 33f:

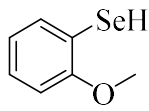

Following the general procedure, 1,2-bis(2-methoxyphenyl)diselane (75 mg, 0.20 mmol) gave 2-methoxybenzeneselenol **33f** (42.2 mg, 56%). **^{1}H NMR** (400 MHz, $CDCl_3$) δ (ppm): 1.53 (1H, s, Se**H**); 3.88 (3H, s); 6.80-6.85 (2H, m); 7.16-7.21 (1H, m); 7.39 (1H, dd, *J*=1.5, 7.5 Hz). **^{13}C NMR** (100 MHz, $CDCl_3$) δ (ppm): 55.8; 110.6; 115.7, 121.6, 127.4, 132.5, 156.4. **^{77}Se NMR** (76 MHz, $CDCl_3$) δ (ppm): 73.0.

Synthesis of 3-methoxybenzeneselenol 33g:

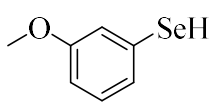

Following the general procedure, 1,2-bis(3-methoxyphenyl)diselane (75 mg, 0.20 mmol) gave 3-methoxybenzeneselenol **33g** (61.8 mg, 82%). **^{1}H NMR** (400 MHz, $CDCl_3$) δ (ppm): 1.58 (1H, s, SeH), 3.79 (3H, s, OCH_3), 6.76 (1H, ddd, *J*=0.8, 2.5, 8.3 Hz), 6.99-7.04 (2H, m), 7.13 (1H, ap t, *J*=8.3 Hz). **^{13}C NMR** (100 MHz, $CDCl_3$) δ (ppm): 55.2; 112.4; 118.1, 125.0, 125.4, 130.0, 159.9.

Synthesis of 3,4,5-trimethoxybenzeneselenol 33h:

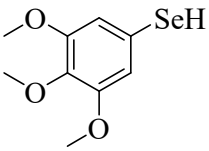

Following the general procedure, 1,2-bis(3,4,5-trimethoxyphenyl)diselane (75 mg, 0.15 mmol) gave 3,4,5-trimethoxybenzeneselenol **33h** (71.5 mg, 95%). **^{1}H NMR** (400 MHz, $CDCl_3$) δ (ppm): 1.62 (1H, s, SeH), 3.81 (3H, s, OCH_3), 3.84 (6H, s, OCH_3), 6.69 (2H, s). **^{13}C NMR** (100 MHz, $CDCl_3$) δ (ppm): 56.2; 60.9; 110.7; 117.7; 137. 3; 153.5.

Synthesis of naphthalene-2-selenol 33i:

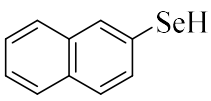

Following the general procedure, 1,2-di(naphthalen-2-yl)diselane (75 mg, 0.18 mmol) gave naphthalene-2-selenol **33i** (63.3 mg, 84%). **^{1}H NMR** (400 MHz, $CDCl_3$) δ (ppm): 1.69 (1H, s, SeH), 7.44-7.51 (3H, m), 7.68-7.74 (2H, m), 7.78-7.82 (1H, m), 7.94 (1H, s). **^{13}C NMR** (100 MHz, $CDCl_3$) δ (ppm): 122.0, 125.8, 126.6, 126.9, 127.8, 128.6, 130.6, 131.0, 131.8, 134.1.

Synthesis of 4-fluorobenzeneselenol 33j:

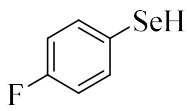

Following the general procedure, 1,2-bis(4-fluorophenyl)diselane (75 mg, 0.22 mmol) gave 4-fluorobenzeneselenol **33j** (48.3 mg, 64%). **^{1}H NMR** (400 MHz, $CDCl_3$) δ (ppm): 1.55 (1H, s, SeH); 6.89-7.03 (2H, m), 7.40-7.47 (2H, m). **^{13}C NMR** (100 MHz, $CDCl_3$) δ (ppm): 116.4 (d, $^2J_{C\text{-}F}$=21.7 Hz), 118.0, 135.2 (d, $^3J_{C\text{-}F}$=7.8 Hz), 162.2 (d, $^1J_{C\text{-}F}$=246.4 Hz).

Carbonic anhydrase inhibition

An Applied Photophysics stopped-flow instrument has been used for assaying the CA catalysed CO_2 hydration activity.[4] Phenol red (at a concentration of 0.2 mM) has been used as indicator, working at the absorbance maximum of 557 nm, with 20 mM Hepes (pH 7.5) as buffer, and 20 mM Na_2SO_4 (for maintaining constant the ionic strength), following the initial rates of the CA-catalyzed CO_2 hydration reaction for a period of 10–100 s. The CO_2 concentrations ranged from 1.7 to 17 mM for the determination of the kinetic parameters and inhibition constants. For each inhibitor at least six traces of the initial 5–10% of the reaction have been used for determining the initial velocity. The uncatalyzed rates were determined in the same manner and subtracted from the total observed rates. Stock solutions of inhibitor (0.1 mM) were prepared in distilled-deionized water and dilutions up to 0.01 nM were done thereafter with the assay buffer. Inhibitor and enzyme solutions were preincubated together for 15 min at room temperature prior to assay, in order to allow for the formation of the E-I complex. The inhibition constants were obtained by non-linear least-squares methods using PRISM 3 and the Cheng–Prusoff equation.

Crystallization and X-ray data collection

Crystals of hCAII were obtained using the hanging drop vapor diffusion method using 24 well Linbro plate. 2 µl of 10 mg/ml solution of hCA II in Tris-HCl 20 mM pH 8.0 were mixed with 2 µl of a solution of 1.5 M sodium citrate, 0.1 M Tris pH 8.0 and were equilibrated against the same solution at 296 K. Crystals of the protein grew in one week. Afterwards hCAII crystals were soaked in 5mM inhibitor solution for 3 days. The crystals were flash-frozen at 100K using a solution obtained by adding 15% (v/v) glycerol to the mother liquor solution as cryoprotectant. Data on crystals of the complexes were collected

using synchrotron radiation at the ID29 beamline at ESRF (Grenoble, France) with a wavelength of 0.827 Å and a PILATUS 6M Dectris CCD detector. Data were integrated and scaled using the program XDS.[27]

Structure determination

The crystal structure of hCA II (PDB accession code: 4FIK) without solvent molecules and other heteroatoms was used to obtain initial phases of the structures using Refmac5.[28] 5% of the unique reflections were selected randomly and excluded from the refinement data set for the purpose of Rfree calculations. The initial |Fo - Fc| difference electron density maps unambiguously showed the inhibitor molecules. The inhibitor was introduced in the model with 0.5 occupancy. In the |Fo - Fc| difference electron density map a spheric density was present close to the benezensulfonamide moiety and was interpreted as a solvent molecule at 0.5 occupancy. Atomic models for inhibitors were calculated and energy minimized using the program JLigand 1.0.40.[29] Refinements proceeded using normal protocols of positional, isotropic atomic displacement parameters alternating with manual building of the models using COOT.[30] Solvent molecules were introduced automatically using the program ARP.[31] The quality of the final models were assessed with COOT and RAMPAGE.[32] Graphical representations were generated with Chimera.[33]

Summary of Data Collection and Atomic Model Refinement Statistics

PDB	6GOT	5TFX
Compound	5b	31a
Space group	$P2_1$	$P2_1$
Cell dimensions		
a, b, c	42.4, 41.3, 72.1	42.6, 41.6, 72.3
alpha, beta, gamma	90, 104.3, 90	90, 104.6, 90
Resolution (Å)	41.1 - 1.56	41.6 - 1.50
Resolution-high (Å)	1.42 - 1.40	1.52 - 1.50
Rmerge	0.171 (0.805)	0.109 (0.783)
Rpim		0.044 (0.365)
CC ½	0.99 (0.536)	0.998 (0.668)
I/sigI	5.48 (1.26)	13.8 (2.0)
Completeness (%)	96.5 (96.1)	96.4 (66.2)
Redundancy		7.1 (5.3)
Refinement		
resolution (Å)	41.11 - 1.56	41.6 - 1.50
unique reflections	31883	36248
Rwork/Rfree (%)	19.8 / 22.33	18.7 / 24.6
# atoms		2427
Protein		2128
metal (Zn)	1	1
ligand		22
water		270
B-factors (Å²)	15.83	13,7
protein		12,8
metal (Zn)		6,3
ligand	16,7	13,7
water	21,22	24,9
r.m.s. deviations		
Bond length (Å)	0,015	0,016
Bond angle (°)	1,709	1,861

PDB	6HX5	6HWZ
Compound	**33a**-hCA II	**33a**-hCA I
Space group	P21	P212121
Cell dimensions		
a, b, c	42.31, 41.44, 72.11	62.38, 71.52, 120.69
alpha, beta, gamma	90.0, 104.3, 90.0	90.0, 90.0, 90.0
Resolution (Å)	41.00 -1.44	28.59 – 1.64
Resolution-high (Å)	1.58 – 1.44	1.73 - 1.64
Rsym (%)	9.9 (56.8)	15.0 (481.6)
Rmeas (%)	10.9 (65.0)	15.5 (499.3)
Redundancy	5.37 (4.17)	15.12 (13.87)
Completeness overall (%)	98.1 (92.9)	97.4 (83.6)
<I/σ(I)>	10.93 (2.85)	10.00 (0.40)
CC (1/2)	99.6 (84.3)	99.9 (28.4)
Unique reflections	43339 (9882)	66390 (9064)
Refinement		
Resolution range (Å)	41.0 – 1.44	28.59 – 1.64
Unique reflections, working/free	41176/2154	62499/3264
Rfactor (%)	18.82	22.45
Rfree(%)	20.98	26.91
r.m.s.d. bonds(Å)	0.018	0.0144
r.m.s.d. angles (°)	1.912	1.669
Ramachandran statistics (%)		
Most favored	96.9	96.5
additionally allowed	3.1	3.5
outlier regions	0.0	0.0
Average B factor (Å^2)		
All atoms	15.255	38.962
inhibitors	14.149	36.612
solvent	23.008	47.644
Resolution range (Å)	41.0 – 1.44	28.59 – 1.64
Unique reflections, working/free	41176/2154	62499/3264

References

1. Navarro R., Pérez Perrino M., García C., Elvira C., Gallardo A., Reinecke H., *Polymers* 2016, 8, 152.
2. Tanini D., Capperucci A., Degl'Innocenti A., *Eur. J. Org. Chem*, 2015, 2, 357.
3. Capperucci A., Tanini D., *Phosphorus Sulfur Silicon Relat. Elem*. 2015; 190, 1320.
4. Khalifah R.G., *J. Biol. Chem*., 1971, 246, 2561.
5. Olcott H.S., Brown W.D., Van Derveen J., Selenomethio-nine as an Antioxidant, *Nature.* 1961, 191, 1201.
6. Walter R., Schwartz I.L., Roy J., Can selenoamino ac-ids act as reversible biological antioxidants? *Ann N Y Acad Sci.* 1972, 192, 175-180.
7. Silva P.C., Borges E.L., Lima D.B., Jacob R.G., Lenardão E.J., Perin G., Silva M.S., A simple and non-conventional method for the synthesis of selected β-arylalkylchalcogeno substituted alcohols, amines and car-boxylic acids. *Arkivoc*, 2016, 5, 376-389.
8. Ganesh V., Chandrasekaran S., One-Pot Synthesis of β-Amino/β-Hydroxy Selenides and Sulfides from Aziri-dines and Epoxides. *Synthesis* 2009, 19, 3267-3278.
9. Tiecco M., Testaferri L., Marini F.,Sternativo S., Santi C., Bagnoli L., Temperini A., intramolecular addition of carbon radicals to aldehydes: synthesis of enantiopure tet-rahydrofuran-3-ols, *Tetrahedron*, 2007, 63, 5482-5489.
10. Tanini D., Barchielli G., Benelli F., Degl'Innocenti A., Capperucci A., Aziridines Ring Opening by Silyl Chalco-genides: a Stereoselective Access to Polyfunctionalized Molecules as Precursor of Sulfurated and Selenated Hetero-cycles. *Phosphorus, Sulfur, Silicon Relat. Elem.* 2015, 190, 1265-1270
11. Braga A.L., Schneider P.H., Paixao M.W., De-obald A.M., Peppe C., Bottega D.P., Chiral Seleno-Amines from Indium Selenolates. A Straightforward Synthesis of Seleno-cysteine Derivatives, *J. Org. Chem*., 2006, 71, 4305-4307.
12. Charrat C., Biscotti A., Godeau G., Greiner J., Vier-ling P., Guigonis J.M., Di Giorgio C., Formulation of highly functionalizable DNA nanoparticles based on 1,2-dithiolane derivatives, *ChemBioChem*, 2015; 16, 792-804.
13. https://clinicaltrials.gov/ct2/show/NCT02215850

14. Angeli A., Peat T.S., Bartolucci G., Nocentini A., Supuran C.T., Carta F. Intramolecular oxidative deselenization of acylselenoureas: a facile synthesis of benzoxazole amides and carbonic anhydrase inhibitors. *Org. Biomol. Chem.* 2016, 14, 11353
15. Koketsu M., Yamamura Y., Aoki H., Ishihara H. The preparation of acylselenourea and selenocarbamate using isoselenocyanate. *Phosphorus, Sulfur Silicon Relat. Elem.* 2006, 181, 2699–2708.
16. Boyer E., Arnoult M., Médebielle J., Guillemont J., Unge D., Jochmans D. Difluoromethylbenzoxazole pyrimidine thioether derivatives: a novel class of potent non-nucleoside HIV-1 reverse transcriptase inhibitors. *J. Med. Chem.*, 2011, 54, 7974-7985
17. Chipem F.A.S., Mishra A. Krishnamoorthy G. The role of hydrogen bonding in excited state intramolecular charge transfer *Phys. Chem. Chem. Phys.*, 2012, 14, 8775–8790.
18. Kawashita Y., Nakamichi N., Kawabata H., Hayashi M. Direct and practical synthesis of 2-arylbenzoxazoles promoted by activated carbon *Org. Lett.*, 2003, 5, 3713–3715.
19. Terashima M., Ishii M., Kanaoka Y. Direct and practical synthesis of 2-arylbenzoxazoles promoted by activated carbon. *Synthesis*, 1982, 484–485;
20. Altenhoff G., Glorius F., Domino A. Copper-Catalyzed C-N and C-O Cross-Coupling for the Conversion of Primary Amides into Benzoxazoles *Adv. Synth. Catal.*, 2004, 346, 1661–1664.
21. Nahakpam L., Chipem F.A.,. Chingakham B.S, Laitonjam W.S. Diacetoxyiodobenzene assisted C–O bond formation via sequential acylation and deacylation process: synthesis of benzoxazole amides and their mechanistic study by DFT *Org. Biomol. Chem.* 2016, 32, 7735–7745.
22. Fernández-Bolaños J.G., López Ó., Ulgar V., Maya I., Fuentes J., Synthesis of O-unprotected glycosyl selenoureas. A new access to bicyclic sugar isoureas. *Tetrahedron Lett.*, 2004, 45, 4081–4084.
23. R. E. Huber, R. S. Criddle, *Arch. Biochem. Biophys.* 1967, 122, 164.

24. Nair S.K., Ludwig P.A., Christianson D.W. Two-site binding of phenol in the active site of human carbonic anhydrase II: structural implications for substrate association. *J Am Chem Soc.* 1994;116, 3659–3660.
25. Olander J., Kaiser E.T. The binding of thiophenols to bovine carbonic anhydrase. *Biochem Biophys Res Commun.* 1971, 45, 1083–1088
26. Rizvi M.A., Guru S., Naqvi T., Kumar M., Kumbhar N., Akhoon S., Banday S., Singh S.K., Bhushan S., Mustafa Peerzada G., Shah B.A. An investigation of in vitro cytotoxicity and apoptotic potential of aromatic diselenides. *Bioorg Med Chem Lett*. 2014; 24, 3440-3446.
27. Leslie A.G.W., Powell H.R., Procesing diffraction data with mosflm. In: Read RJ, Sussman JL (eds) Evolving methods for macromolecular crystallography, vol 245, NATO Science series, Springer, Dordrecht, 2007, pp. 41-51.
28. Murshudov G.N., Vagin A.A., Dodson E.J., Refinement of macromolecular structures by the maximum-likelihood method. *Acta Crystallogr D Biol Crystallogr.* 1997, 53, 240-255.
29. Lebedev A.A., Young P., Isupov M.N., Moroz O.V., Vagin A.A., Murshudov G.N. JLigand: a graphical tool for the CCP4 template-restraint library. *Acta Crystallogr D Biol Crystallogr.* 2012, 68, 431-440.
30. Emsley P., Lohkamp B., Scott W., Cowtan K., Features and development of Coot. *Acta Crystallogr D Biol Crystallogr.* 2010, 66, 486-501.
31. Lamzin V.S., Perrakis A., Wilson K.S., The ARP/wARP suite for automated construction and refinement of protein models**,** M.G. Rossmann, E. Arnold (Eds.), Int. Tables for Crystallography. Vol. F: Crystallography of Biological Macromolecules, Kluwer Academic Publishers, Dordrecht, The Netherlands (2001), pp. 720-722
32. Lovell S.C., Davis I.W., Arendall III W.B., de Bakker P.I.W., Word J.M., Prisant M.G., Richardson J.S., Richardson D.C., Structure validation by Cα geometry: ϕ,ψ and Cβ deviation, *Proteins*, 2003, 50, 437-450.
33. Pettersen E.F., Goddard T.D., Huang C.C., Couch G.S., Greenblatt D.M., Meng E.C., Ferrin T.E., UCSF Chimera-a visualization system for exploratory research and analysis, *J. Comput. Chem.*, 2004, 25, 1605-161

Chapter 3

Carbonic Anhydrase Inhibitors as Antitumor Agents

3.1 Introduction

Hypoxia is defined as a physiological condition with reduced oxygen level and plays a key role in many types of solid cancers and results in cells spatial disorganization within the tissues involved, which in turn determine abnormal microvasculature formation and flow disruption of the fluids.[1] The low oxygen tension leads to the activation of the transcription factor hypoxia-inducible factors 1 and 2 (HIF-1/2)[2] (**Figure 1**).

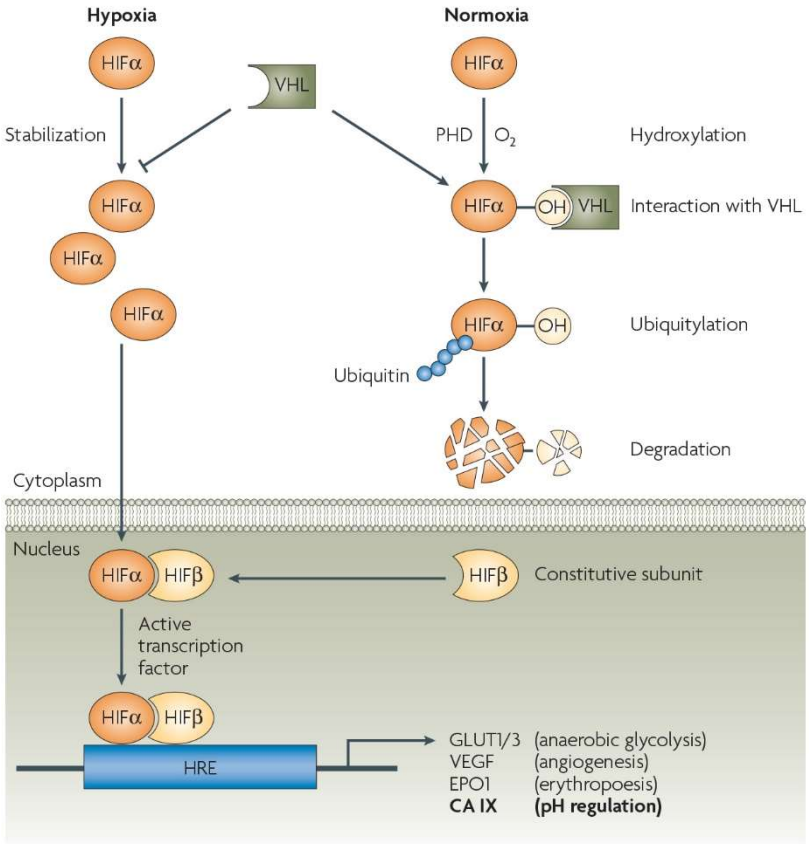

Figure 1 Mechanism of hypoxia-induced gene expression mediated by the HIF transcription factor.

Initiation of the hypoxia-induced signalling cascade results in the activation of a vast array of genes and signalling outputs that regulate a variety of processes aimed to adaptation of

tumor cells in conditions of low oxygen.[2] HIF-1α-activated tumor cells respond to this micro environmental stress by reprogramming their metabolism to the far less efficient glycolytic pathway. Such a metabolic change determines an increased production and export of acidic metabolites, such as lactic and carbonic acids to the extracellular space. The low extracellular pH created a selective advantage for tumor cells, the only ones able to survive to such harsh conditions.[3] The maintenance of pH homeostasis by tumor cells relies on a set of complex molecular mechanisms involving a variety of proteins and buffer systems with the central aim of maintaining a moderately intracellular alkaline pH, while generating a markedly acidic extracellular environment.[3,4] One set of proteins important to this pH regulatory system is the family of the carbonic anhydrases (CAs).[3,5] Among the 16 human CAs, the IX isoform (and marginally the XII) is directly linked to cancer progression, metastasis.[4,6-8]

The overexpression of hCA IX triggered from HIF-1α involves the formation of stable HIF-αβ complex which translocates to the nucleus and interacts with an Hypoxia Responsive Element (HRE) region located immediately upstream of the DNA transcription start site (**Figure 1**).[6] Indeed, HIF-1α is the exclusive regulator of hCA IX activity and often the most strongly upregulated gene in response to hypoxic stimuli.[5,9]

The recent resolution of the hCA IX catalytic domain architecture [10] has provided detailed structural confirmation of its observed catalytic activity and has aided in more rational drug design (**Figure 2**).[11-13]

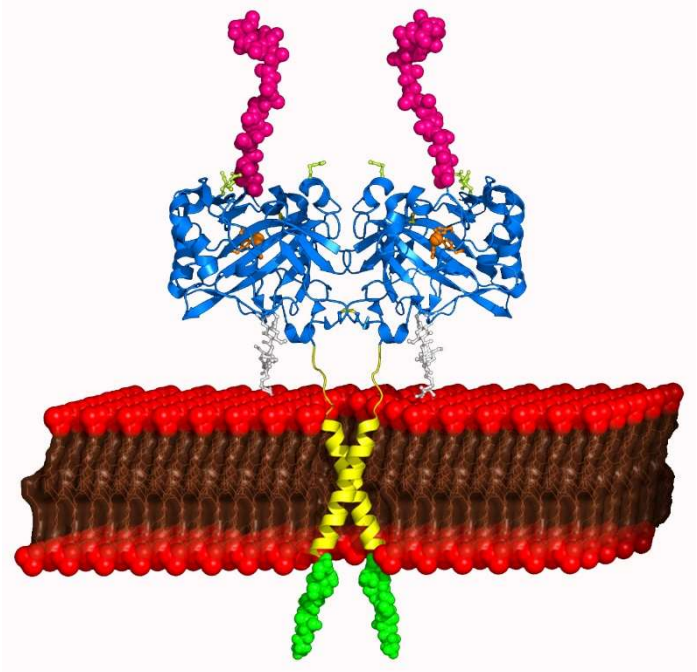

Figure 2. Proposed model showing the structural arrangement of the full-length hCA IX dimer on the cellular membrane. The X-ray structure of the dimeric catalytic domain is reported in cyan, with Arg58, Arg60, and Arg130 in green and the glycan moieties in white. The hypothetical arrangements of the PG domains, the transmembrane helices and the cytoplasmic portions are schematically reported in magenta, yellow, and green, respectively.

From the structural viewpoint hCA IX is dimeric,[13] contains a proteoglycan (PG)- like domain immediately adjacent to the catalytic domain, the presence of which may allow the enzyme to function most efficiently at more acidic pH values [12-14]

In this context, hCA IX has become an attractive target as anticancer therapy for several reasons. The first is represented by its selective overexpression in tumor cells (constitutive expression of hCA IX is reported in the guts). The second one is related to the direct connection of the hCA IX functions to tumor growth and metastasis processes. Indeed, a change in the pH ratio of 0.1-0.2 pH units can have important consequences in vital biological processes including ATP synthesis, proliferation, migration, survival and metastasis.[3-5] Additionally the hCA IX positioning on the extracellular surface of cell membranes allows efficient targeting by antibodies or small molecule inhibitors. Recent

studies have now demonstrated that hCA IX-selective inhibitors can directly and specifically inhibit the growth of hypoxic, hCA IX-positive tumors in preclinical animal models. Several approaches were reported for obtaining compounds that specifically target the tumor-associated isoforms CA IX (**Figure 3**) among which are:

- ureido sulfonamides (e.g., compound **A** and **B**), used in clinical trials against hypoxic tumors (**A**)[15] and for imaging purposes (**B**)[16]
- Positively (such as **C**)[17] or negatively charged compounds, which cannot cross plasma membranes due to their charged character and thus selectively inhibit only extracellular CAs.

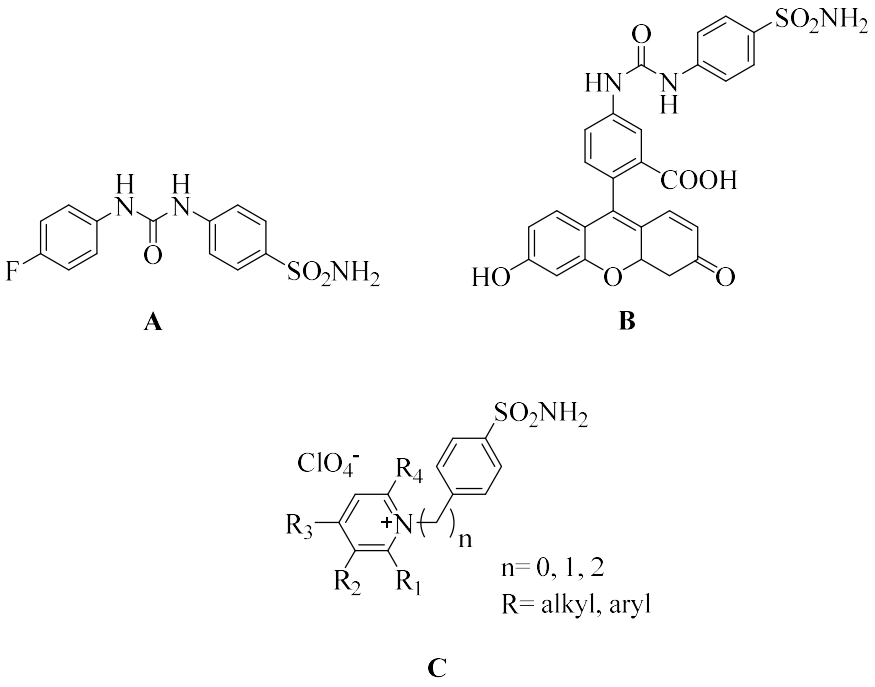

Figure 3. Chemical structures ureido derivative of sulphanilamide (SLC-0111) **A**, fluorescent inhibitor **B** and pyridinium derivatives of sulphanilamide **C.**

3.2 New Selenoureido Analogues of 4-(4-Fluorophenylureido)benzene sulfonamide as Carbonic Anhydrase Inhibitors

Isosteric replacement is a commonly used approach in Medicinal Chemistry. It consists in the introduction, within selected lead compounds, of structural modifications (named bioisosteric groups or elements) able to retain the desired biological activity.[18,19] We recently applied the isosteric replacement to the compound **A** in **Figure 3** (SLC-0111),[3] which successfully ended Phase I clinical programs for the treatment of patients with advanced hypoxic tumors overexpressing the human carbonic anhydrase IX.[20,21] The selenoureido containing compounds **7−21** were obtained by standard coupling reactions of the aromatic isoselenocyanates **3a−i** with commercially available benzenesulfonamides **4−6** in acetonitrile as solvent (**Scheme 1**).[15]

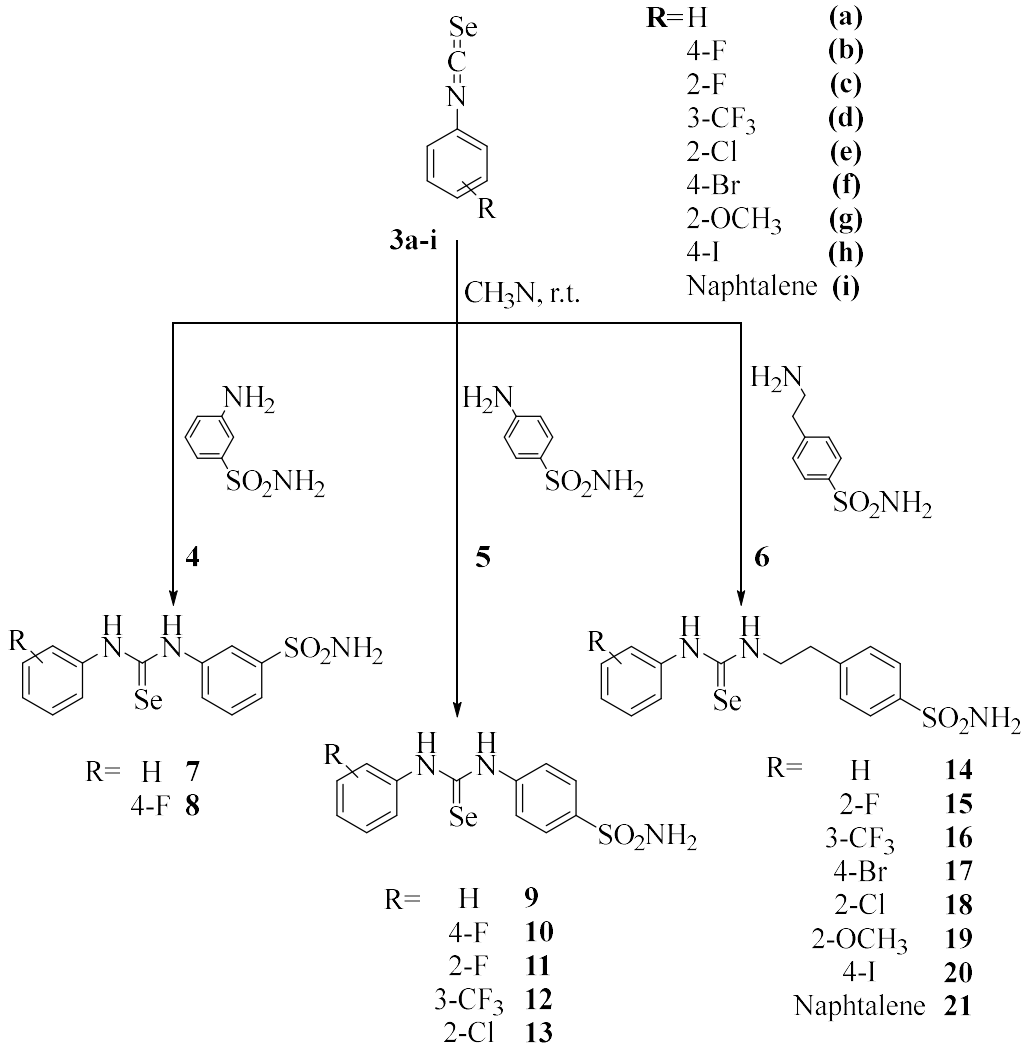

Scheme 1. General synthetic procedure for compounds **7-21**

The proper isoselenocyanates **3a−i** were obtained in a two-step synthetic procedure which involved as first step *N*-formylation in high yields of the commercially available aromatic amines **1a−i** using catalytic zinc chloride and formic acid under neat conditions[24] and subsequently the conversion of the formylanilines **2a−i** to the corresponding isoselenocyanates **3a−i** using the modified Barton's procedure as outlined in **Scheme 2**.[25]

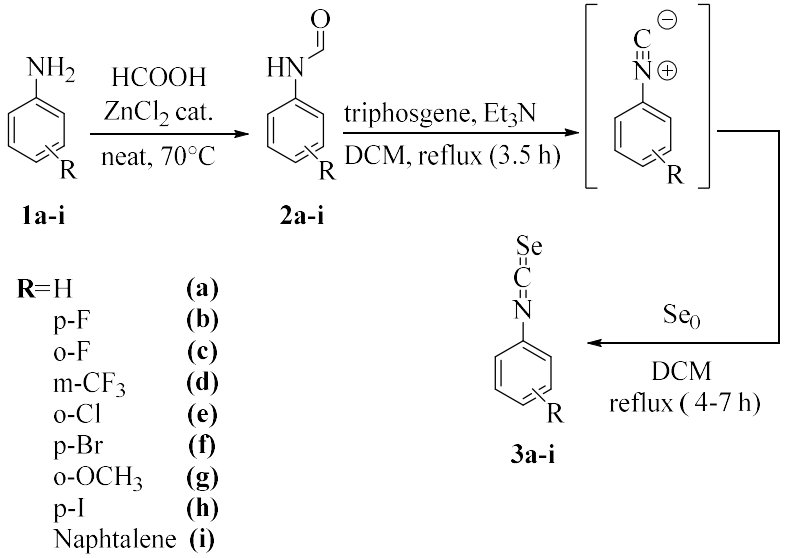

Scheme 2. General synthetic scheme of compounds **3a-i**

It is noteworthy that the dehydration of formylanilines **2a−i** was successfully conducted by the use of the safer and handy solid triphosgene,[26,27] and the *in situ* obtained isocyanides (not isolated) were treated with an excess of elemental selenium to afford the desired isoselenocyanates **3a−i**.[28] In order to asses a proper structure−activity relationship (SAR), the synthesis of the SLC-0111 thioureido analogue **22** was also carried out according to standard procedures (**Scheme 3**).[20]

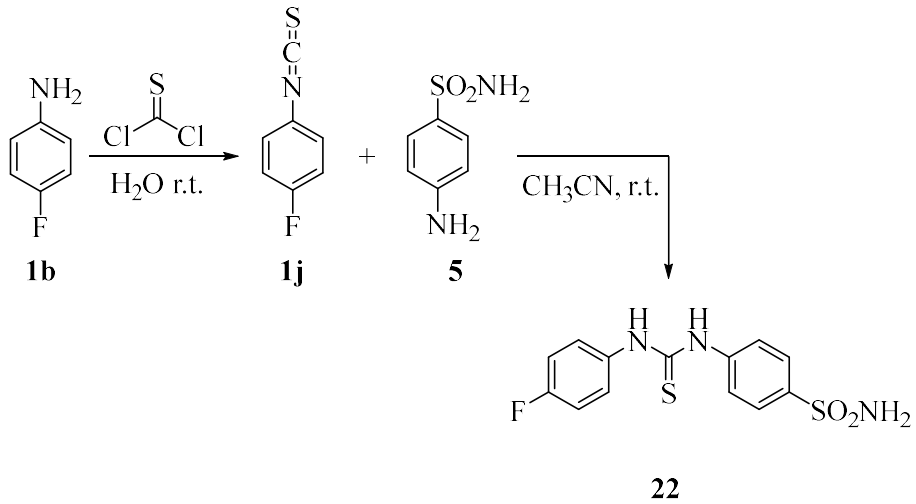

Scheme 3. Synthesis of the thioureido derivative **22.**

All synthesized compounds, **7−22**, were tested *in vitro* for the inhibitory properties against the physiological relevant isoforms hCA I, II, IV, and IX by means of the stopped-flow carbon dioxide hydration assay,[29] and their activities were compared to the standard carbonic anhydrase inhibitor acetazolamide (**AAZ**) (**Table 1**).

Table 1. Inhibition constants of hCA I, hCA II, hCA IV and hCA IX with compounds **7–22**, SLC-0111 and **AAZ** by a stopped-flow CO_2 hydrase assay[29]

	K_i (nM)*			
Compound	hCA I	hCA II	hCA IV	hCA IX[a]
7	483.8	343.2	908.7	329.7
8	435.3	388.9	765.9	97.8
9	132.5	54.3	8627	78.9
10	152.3	66.3	7557	63.0
11	5.9	6.3	902.1	5.8
12	32.7	6.1	734.4	15.9
13	7.9	4.0	268.8	3.9
14	6.7	5.5	1782	5.3
15	44.1	7.9	898.2	8.7
16	8.5	4.4	928.9	5.8
17	51.7	1.8	1409	4.8
18	8.3	3.5	731.2	4.8
19	6.0	4.5	765.9	3.1
20	267.4	57.6	6760	54.9
21	501.7	91.2	5423	93.1
22	35.0	14.2	4797	32.
SLC-0111	5080	960.0	286.0	45.0
AAZ	250	12.1	74	25.8

* Mean from three determinations by a stopped-flow, CO_2 hydrase method. Standard errors were in the range of 5–10% of the reported values.

[a] Catalytic domain

The following SARs for the hCA isoforms considered are reported:

The ubiquitous cytosolic hCA I was inhibited by all compounds with K_is spanning between 5.9 and 501.7 nM. Within the series reported, the compounds bearing the sulfonamide moiety at position 3 of the ring, compounds **7** and **8**, or the bulky naphthyl tail moiety **21**,

resulted the least active with K_i values respectively 1.9, 1.7 and 2.0 fold higher when compared to the standard Acetazolamide (**AAZ**) (**Table 1**). Relocation of the primary sulfonamide moiety in compound **7** from the *meta* to the *para* position, to afford **9**, resulted in a significant enhancement of the inhibitory potency (K_is of 483.8 and 132.5 nM respectively). The introduction in **9** of the *para*-fluoro moiety, compound **10**, slightly enhanced the K_i value of 1.15 fold. It is noteworthy that the inhibition potency was greatly improved when the fluoro was introduced at the *ortho* position (compound **11** K_i 5.9 nM). The nature of the halide didn't affect the inhibition potency against the hCA I as the introduction in *ortho* of the chloro atom instead of the fluoro, to afford **13**, determined only a slight increase of the K_i value to 7.9 nM. Conversely the introduction of the CF_3 group at the *meta* position spoiled the inhibition value to 32.7 nM. Among the ethylamino benzenesulfonamides **14-21**, the phenyl and the *ortho* methoxy substituted derivatives **14** and **19** resulted the most active in the series, with K_is of 6.7 and 6.0 nM respectively. Interestingly the *meta* CF_3 and the *ortho* Chloro substituted derivatives **16** and **18** slightly differed for their inhibition potencies (K_is 8.5 and 8.3 nM) respectively. Among the phenyl halide derivatives, the *ortho* fluoro **15** and the *para* bromo **17** resulted similar potencies in inhibiting the hCA I with K_is of 44.1 and 51.7 nM respectively. Substitution of the bromine with the iodine, as in compound **20**, was detrimental for the inhibition activity (K_i 267.4 nM). The bioisosteric substitution in SLC-0111 of the oxygen within the ureido moiety with a sulfur or selenium atom instead (compounds **22** and **10** respectively) resulted in an increase of the inhibition potency against the hCA I isoform of 145.1 and 33.4 fold respectively (**Table 1**).

The cytosolic and highly efficient hCA II isoform, was effectively inhibited by all compounds synthesized (K_i comprised between 3.5 and 388.9 nM), and in analogy to the hCA I the metanilamide derivatives **7** and **8** were the least potent (K_i 343.2 and 388.9 nM respectively). Among the sulfanilamide series, the introduction of the *para*-fluoro moiety within the simple phenyl ring, conversion of **9** to **10**, slightly spoiled the inhibition potency (K_is 54.3 and 66.3 nM respectively). Placement of the fluoro atom in the *ortho* position, compound **11**, resulted in a 10.5 fold increase of the inhibition potency, which was retained when the *meta*-CF_3 group was introduced instead (compound **12** K_i 6.1 nM) or even reinforced when a *ortho*-chloro moiety was placed (compound **13** K_i 4.0 nM). Among the

ethylaminobenzene sulfonamide series **14-21**, all compounds were quite effective in inhibiting the hCA II isoform (K_is spanning between 1.8 and 7.9 nM), with the only exceptions represented by the bulky *para*-iodo **20** and the naphtyl derivative **21** (K_is 57.6 and 91.2 nM respectively). As for the hCA II, the bioisosteric substitution of the oxygen atom within the ureido group in SLC-0111 (K_i 960 nM) resulted in enhancement of the inhibition potency. As reported in **Table 1**, K_is of 66.3 and 14.2 nM were obtained when the selenium, compound **10** or the sulfur, compound **22**, were introduced.

The membrane bound hCA IV was the least inhibited among the enzymatic isoforms herein considered, and showed K_is spanning between 8627 and 268.8 nM. The introduction in **7** of the fluoro atom in *para* position, to afford **8**, resulted in a 1.2 fold enhancement of the inhibition potency. In analogy, a 1.1 fold inhibition potency increase was reported when the *para*-fluoro substitution was operated in **9** to afford **10** (K_is of 8627 and 7557 nM respectively), and it was further improved when a *meta*-CF_3 (K_i 734.4 nM) or an *ortho*-chloro moiety (K_i 268.8 nM) were introduced. Among the ethylaminobenzene sulfonamide series the introduction within the phenyl tail of **14** in *ortho* position either of a fluoro **15**, chloro **18** , methoxy **19** or a *meta*-CF_3 moiety, as in **16**, resulted in a significant enhancement of the inhibition potency with K_is of 1782, 898.2, 731.2, 765.9 and 928.9 nM respectively (**Table 1**). The introduction in **14** of the para bromo moiety determined only a slight reduction of the inhibition activity against the hCA IV. The bulky *para*-iodo **20** and naphthyl **21** were the least effective in the series (K_is 6760 and 5423 nM respectively). The effects of the divalent isosteric substitution in SLC-0111 were detrimental for the inhibition properties against the hCA IV isoform. As reported in **Table 1**, the parent SLC-0111 showed a K_i value of 286 nM, the introduction of the sulfur and the selenium atom within the ureido moiety enhanced the K_i value 16.8 and 26.4 fold, respectively.

The transmembrane and tumor associated hCA IX was effectively inhibited by the compounds herein reported and showed K_i values comprised between 3.1 and 329.7 nM. In particular, the introduction of the *para*-fluoro moiety in **7**, to afford **8**, resulted in a 3.4 fold decrease of the inhibition value. A slight lower potency increase (1.3 fold) was observed when the *para*-fluoro moiety was introduced within the sulfanilamide series (conversion of **9** to **10**). In analogy to the other enzymes herein considered, the inhibition data showed

strictly related to the fluoro regioisomerism. Kinetic data in **Table 1** account for a 10.9 fold potency increase when the fluoro moiety was shifted from the *para* to the *ortho* position (conversion of **10** to **11**). Interestingly, the replacement of the fluoro atom in **11** with the chloro instead, to afford **13**, resulted in an increase of the inhibition potency (K_is of 5.8 and 3.9 nM respectively). The introduction of the *meta*-CF_3 moiety within the simple phenyl tail on compound **9** to afford **12**, was beneficial for the inhibition potency which showed a 5.0 fold increase (K_is of 78.9 and 15.9 nM for **9** and **12** respectively). With the exception of the bulky *para*-iodo **20** and naphthyl derivative **21** (K_is 54.9 and 93.1 nM respectively), all compounds within the ethylbenzene sulfonamide series were quite effective in inhibiting the hCA IX and showed K_is spanning between 3.1 and 8.7 nM, thus far more active when compared to the standard **AAZ** (K_i 25.8 nM). In particular, the introduction in **14** of the *ortho*-fluoro moiety to afford **15**, slightly spoiled the inhibition potency (K_i of 5.3 and 8.7 nM respectively). Conversely the introduction within the phenyl tail in **14** of a *meta*-CF_3 **16**, or *para*-bromo **17**, *ortho*-chloro **18** and *ortho*-methoxy **19** moiety, clearly resulted in enhancement of the inhibition potency (K_is of 5.8, 4.8, 4.8 and 3.1 nM respectively). SAR relative to the isosteric substitution of the oxygen within the SLC-0111 ureido moiety accounted for an increase of the inhibition potency when the sulfur was introduced (compound **22**; K_i 32.1 nM). Conversely, the K_i value was 1.4 fold decreased when the selenium was introduced instead (compound **10**; K_i 63 nM). In general, the divalent bioisosteric replacement of the ureido oxygen on SLC-0111 with a sulfur or selenium, compounds **22** and **10** respectively, determined powerful enhancements of the inhibition potencies against the hCA I and II isoforms (**Table 1**). Any modification at the ureido moiety resulted in a suppression of the inhibition activity against the membrane associated hCA IV (K_is of 4797 and 7557 for **22** and **10** respectively). Interestingly, the sulfur derivative **22** resulted in only a slight increase of the inhibition potency against hCA IX (K_is of 45.0 and 32.1 nM for SLC-0111 and **22** respectively). Conversely, the introduction of the selenium, as in **10**, was detrimental for the activity (K_i 63.0 nM). Although the inhibition potency of the selenium derivative **10** was only 1.4 fold less potent when compared to the parent SLC-0111, it is worth mentioning that the selectivity ratio hCA II/hCA IX of this compound was heavily spoiled (21.3 for SLC-0111 and 1.1 for **10**).

The antioxidant activity of the selenoureido congener of SLC-0111 (compound **10**) was evaluated according to literature procedures in catalysing the reaction between hydrogen peroxide (H_2O_2) and two different thiols such as dithiothreitol (DTT)[30,31] and glutathione (GSH).[32,33] A preliminary investigation of the GPx-like activity of compound **10** was carried out following the oxidation of DTT in CD_3OD by means of ^1H NMR. A control experiment was performed in the absence of catalyst. The catalytic activity of $(PhSe)_2$ against DTT^{red} under these conditions was also determined, to compare the activity of the title compound with commonly used standard materials for the GPx assays.28-30 As depicted in **Figure 4**, when the reaction was performed in the absence of catalyst, 98% of DTT^{red} remained unreacted after 60 min. Conversely, DTT oxidation was complete within 35 min when 10% of the substituted selenourea **10** was added. Under these conditions, the time required to halve the initial concentration of DTT^{red} (T_{50}) was 8 min. Interestingly, according to this test, **10** proved to behave as a better catalyst than $(PhSe)_2$, in that it exhibited a longer reaction time and higher T_{50} values. Compounds SLC-0111 and **22**, did not catalyse the DTT oxidation under the studied conditions, being the kinetic profile comparable with that of the control experiment.

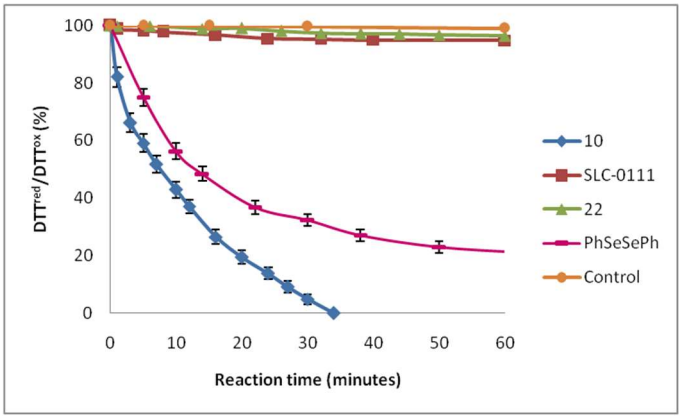

Figure 4. Oxidation of DTT^{red} with H_2O_2 in the presence of compounds **10**, **SLC-0111** and **22**. Reaction conditions: $[DTT^{red}]_0$=0.14 mM, $[H_2O_2]_0$=0.14 mM, [catalyst]=0.014 mM), CD_3OD (1.1 mL). ^1H NMR spectra were measured at variable reaction time at 25 °C. The relative populations of DTT^{red} and DTT^{ox} were determined by integration of the ^1H NMR signals. In the control experiment the reaction was run with no catalyst. Reported are the mean ± SD values of three separate experiments.

The GPx-like properties of **10** were further confirmed by using the nicotinamide adenine dinucleotide phosphate (NADPH)-coupled assay. In this experiment GSH was used as a substrate and H_2O_2 as an oxidant in the presence of NADPH and glutathione reductase (GR).[32,33] The reaction was carried out in H_2O and its progress was monitored by UV spectroscopy, measuring the absorbance decreasing at 340 nm due to the consumption of NADPH (**Figure 5**).

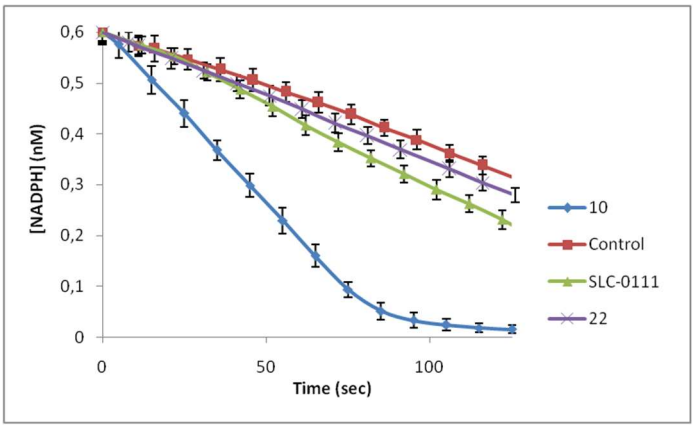

Figure 5. NADPH-coupled GPx assay for compounds **10**, **SLC-0111**and **22**. Reaction conditions: $[NADPH]_0$=0.6 mM, $[GSH]_0$=2.0 mM, $[H_2O_2]_0$=5 mM, [GR]=8 units/mL, [catalyst]=0.2 mM in pH 7.4 phosphate buffer at ambient temperature. Reported are the mean ± SD values of three separate experiments.

As above reported the NADPH was completely consumed within 100 s in the presence of the selenium containing compound **10**. Conversely the NADPH consumption rate was only slightly higher with respect to the control experiment (no catalyst used) when the sulfur- and oxygen-containing analogues **22** and SLC-0111 were used instead.

The water soluble selenoureido containing compounds **10**, **15** and **20** were evaluated for their viability effects on human prostate (PC3), breast (MDA-MB-231) and colon cancer (HT-29) cells lines at 30, 100 and 300 μM concentration, incubated for 48 h both under normoxic and hypoxic conditions and using the CA inhibitor SLC-0111 as a reference compound (**Figure 6**).

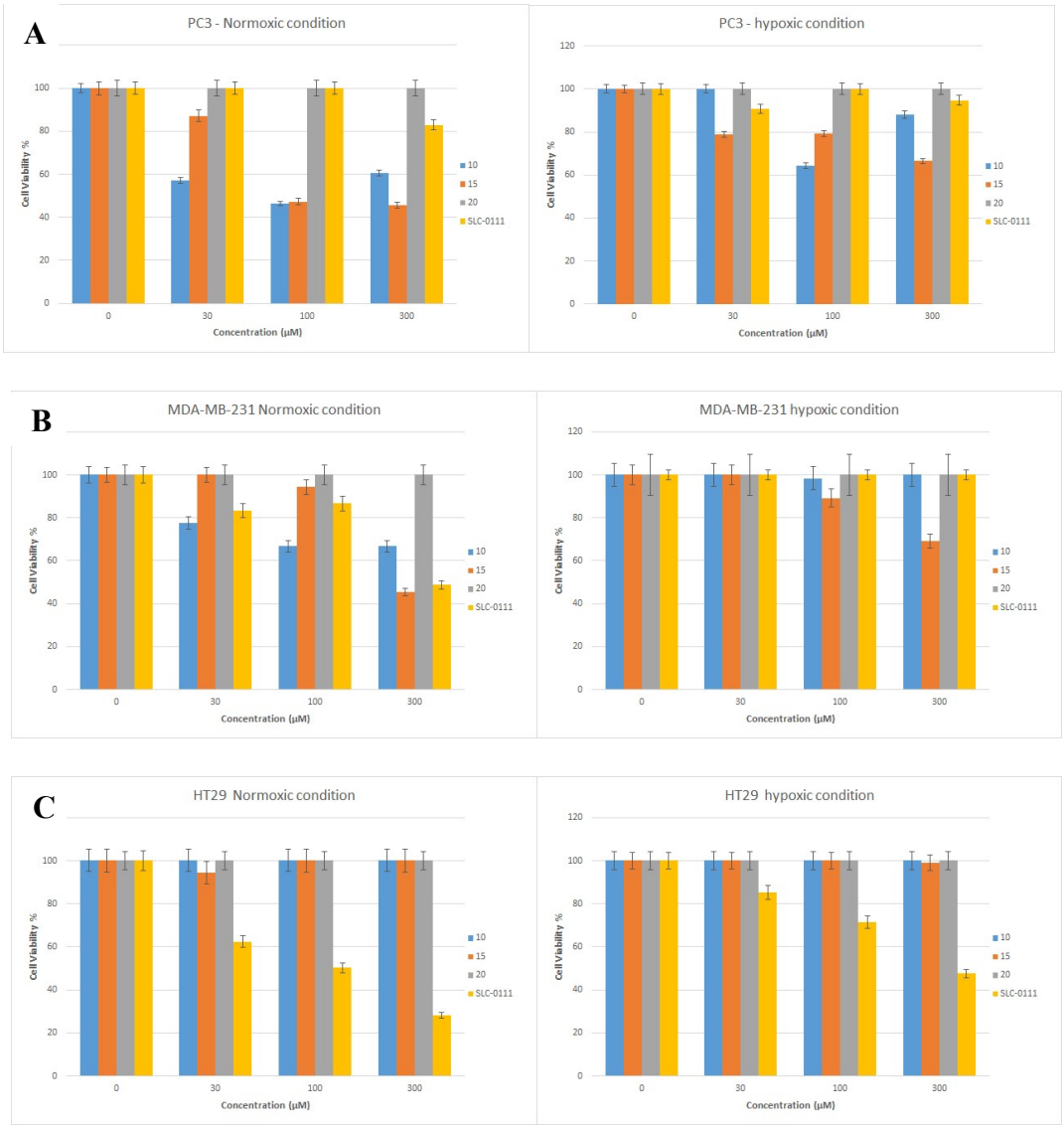

Figure 6. PC3 (**A**), MDA-MB-231 (**B**) and HT-29 (**C**) were plated at 1 10^4/well, incubation was allowed for 48h in normoxic (20% O_2) and hypoxic conditions (0.1% O_2). Compounds **10**, **15** and **20** in comparison with SLC-0111 were tested in the 30–300 μM concentration range. Control condition was arbitrarily set as 100% and values are expressed as the mean ± S.E.M. of three experiments.

In PC3 cells the selenoureido derivative of SLC-0111 (compounds **10**) and its longer *ortho* fluoro derivative **15** significantly reduced cell viability in normoxia (20 % Oxygen), whereas their effects resulted lower when the experiments were carried out under hypoxic conditions

(0.1 % Oxygen). Compound **20** was ineffective in all set of experiments, whereas the reference ureido derivative SLC-0111 induced modest mortality and only at the highest concentration (300 μM) in normoxia (**Figure 6 A**). Interestingly, in MDA-MB-231 cells, compound **10** was effective in normoxia at 30 μM and with a profile comparable to the reference SLC-0111. The elongated derivative **15** was successful in reducing cells viability in both conditions of oxygenation but only at the highest concentration (300 μM). Finally compound **20** was ineffective on the breast cancer cell lines (**Figure 6 B**). As for colon cancer HT-29 cells, all compounds considered (**10**, **15** and **20**) were ineffective in inducing mortality, whereas the reference compounds SLC-0111 strongly reduced cell viability at all concentrations in normoxic and hypoxic conditions (**Figure 6 C**).

The binding modes of both selenium and sulfur analogues of SLC-0111 (compound **10** and **22** respectively) were determined by means of their X-ray co-crystallographic adducts with the hCA II (**Figure 7**). The difference |Fo−Fc| electron density maps of the hCA II−**10** complex revealed a well ordered structure of the benzenesulfonamide section, which became weaker in electron density for the seleno ureido and *para*-fluorobenzene moieties (**figure 7C**). Instead the hCA II−**22** complex showed clear electron density all through the molecule, thus suggesting a better ordered structure within the enzymatic cleft (**Figure 7D**). In both cases **10** and **22** showed almost identical allocations within the enzyme cavity, with average distances between the two structures (RMSD) of just 0.12 Å across the whole protein.

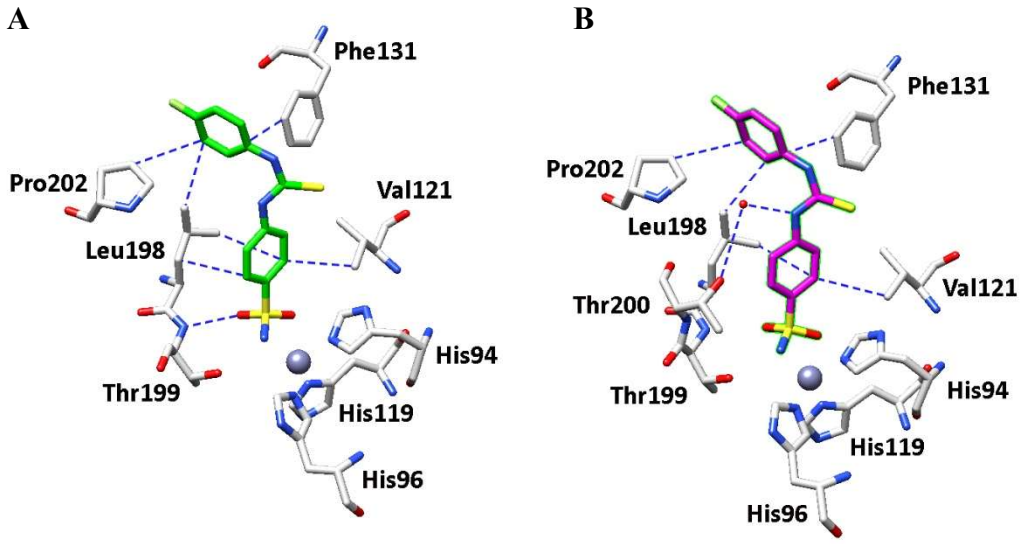

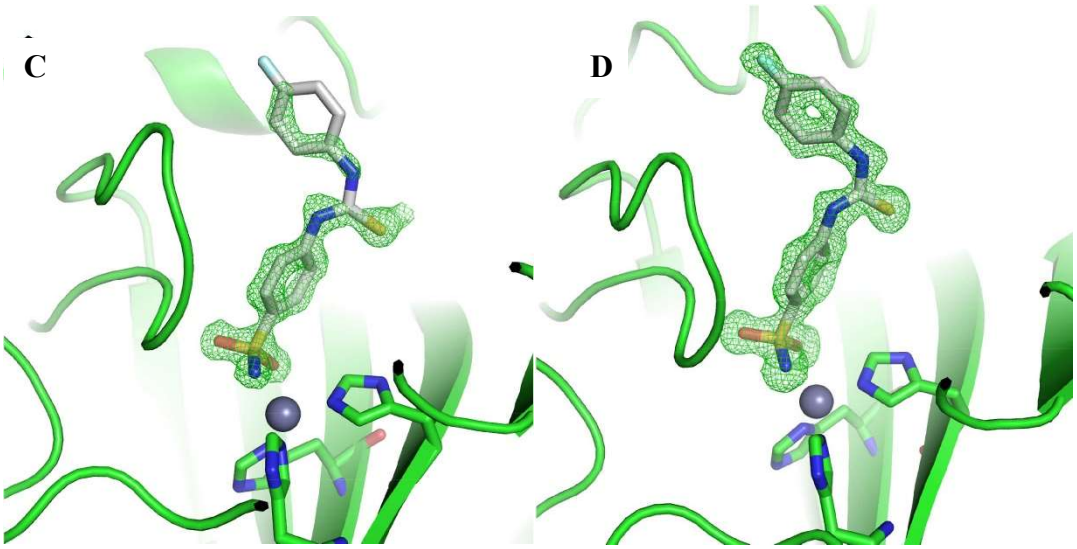

Figure 7. (**A**) Active site region of the hCA II−**10** complex (PDB 5WEX) and (**B**) hCA II−**22** complex (PDB code: 5ULN); Hydrogen bonds and van der Waals interactions are also shown. Compound **10** (**C**) and **22** (**D**) showed as σA-weighted $|F_o-F_c|$ density map at 2.0 σ.

The compounds were buried within the enzyme active site, being coordinated to the Zn (II) ion through the sulfonamide group and orientated towards the hydrophobic half of the pocket. Compound **10** showed several hydrophobic interactions with Val121, Phe131, Leu198 and Pro202. Moreover, one oxygen of sulfonamide showed a hydrogen bond with Thr199 (**Figure 7A**). In the same way, compound **22** showed similar hydrophobic interaction with the side chain of residues in the active site, but also, a water bridge between the ureido moiety of **22** and Thr200 (**Figure 7B**). We also determined the binding mode of the longer selenoureido derivative **14** (**Figure 8**).

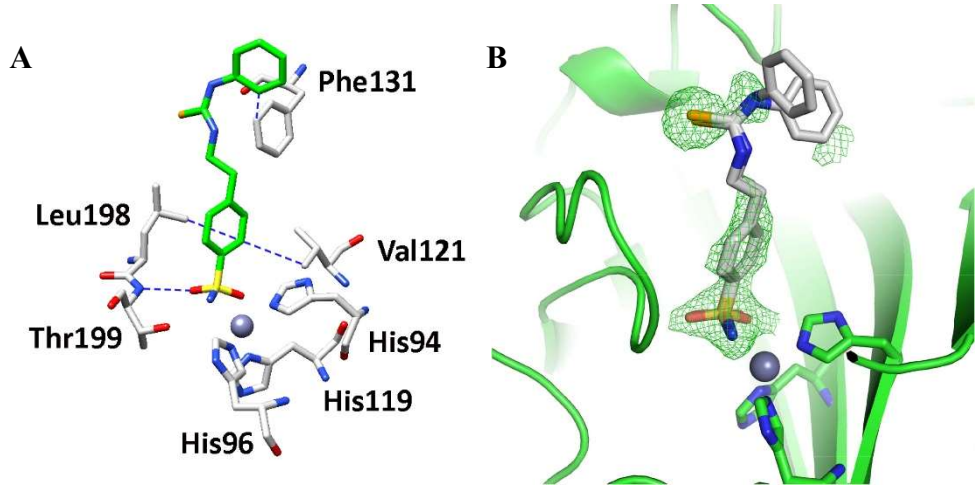

Figure 8. (**A**) Active site region of the hCA II−**14** complex (PDB 5UMC) and Hydrogen bond and van der Waals interactions are also shown. (**B**) Compound **14** showed as σA-weighted $|F_o-F_c|$ density map at 2.0 σ.

The difference |Fo−Fc| electron density maps showed that **14** is buried within the enzyme cavity. The *N*-phenyl moiety was modelled with two different conformations due to the diffuse electron density present in this region (**Figure 8B**).The sulfonamide moiety is tightly coordinated to the Zn(II) ion by means of the canonical interactions of all CAs-sulfonamide compounds. Conversely, the tail fragment of **14** was somewhat disordered. Only one conformation showed three hydrophobic interaction whit Val121, Phe131 and Leu198 in addition to hydrogen bond among the oxygen of sulfonamide and Thr199 (**Figure 8A**).

3.3 Discovery of new 2, 5-disubstituted 1,3-selenazoles as selective human carbonic anhydrase IX inhibitors with potent anti-tumor activity

Given our interest in the study of chalcogen-containing compounds, we designed and synthesized a series of selenazole derivatives with the aim to identify novel hCA IX selective inhibitors.[34,36] Selenazoles are an important class of heterocycles with significant biological effects and considerable pharmacological relevance.[37,38] Moreover, these five membered selenium heterocycles are easily synthetized from primary selenoamide as starting materials. Thus, our attention focused on the synthesis of primary selenoamide containing sulfonamide moiety, as shown in **Scheme 4**. First step was the synthesis of 4-cyanobenzenesulfonamide

(**24**) by reaction of the corresponding sulfonyl chloride (**23**) with an aqueous solution of ammonium hydroxide. Successively, 4-sulfamoylbenzoselenoamide (**25**) was prepared by the reaction of nitrile compound **24** with Na_2Se as selenating reagent in refluxing ethanol, for 6h.

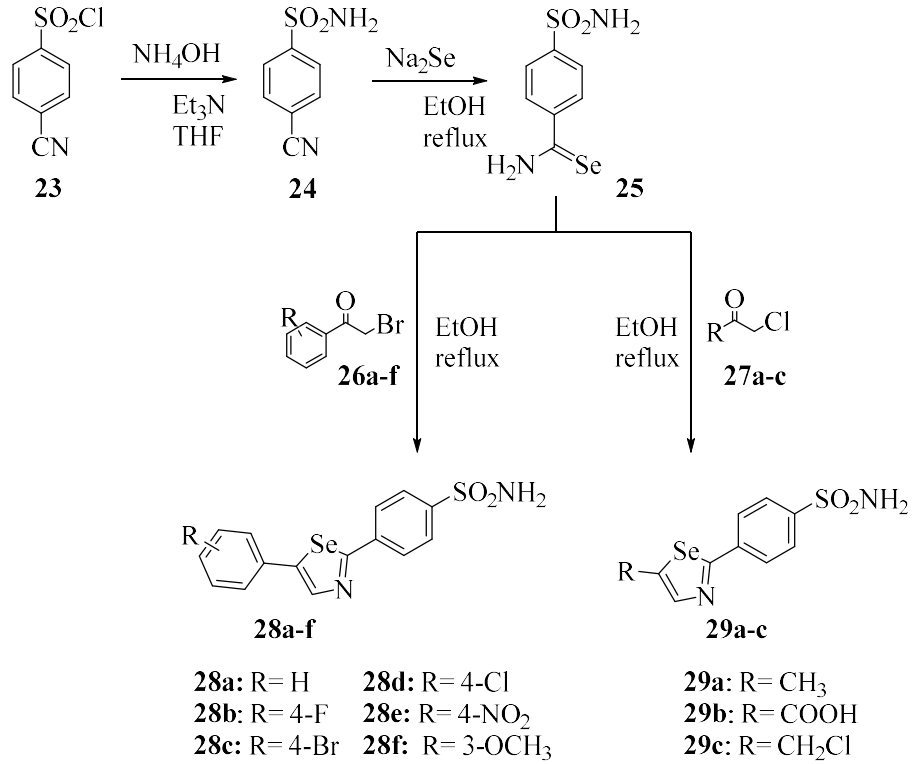

Scheme 4: Synthesis of primary selenoamide incorporating a sulfonamide moiety **25** and the corresponding functionalized selenazoles **26a-f** and **29a-c**. Na_2Se was generated *in situ* from elemental Se (0.5 eq.) and $NaBH_4$ (1.0 eq.).

Finally, the reaction of primary selenobenzamide (**25**) with different α-haloketones incorporating aromatic **26a-f** or aliphatic **27a-c** moieties, in refluxing ethanol, gave various 2,5-disubstituted 1,3-selenazoles **28a-f** and **29a-c**. In addition, herein, we report the synthesis of a variety of double-functionalized and ionic 1,3-selenazoles by nucleophilic displacement reactions of 4-halomethyl-1,3-selenazoles **29c** as shown in **Scheme 5.**

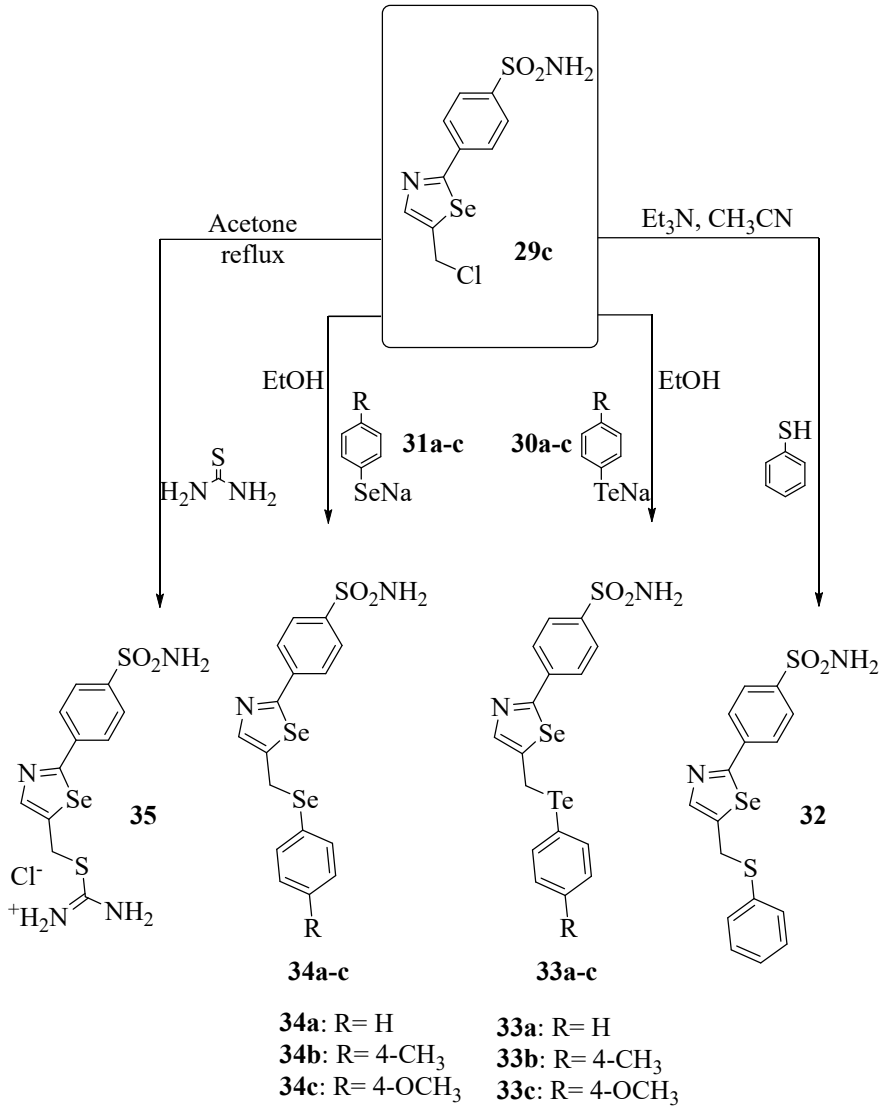

Scheme 5: Synthesis of substituted 2,5-selenazoles **32-35.**

Treatment of **29c** with thiophenol and Et_3N in acetonitrile afforded in excellent yields the corresponding functionalized 1,3-selenazoles **32**. A number of 1,3-selenazoles containing aromatic chalcogenide side chains were also prepared (**33a-c** and **34a-c**). The reaction started with the reduction of the appropriate dichalcogenide and $NaBH_4$ to afford the corresponding chalcogenate (**30a-c** and **31a-c**), which was treated *in situ* with 4-halomethyl-1,3-selenazoles **29c** leading to the corresponding functionalized 1,3-selenazoles **33a-c** and **34a-c** in good

yield (**Scheme 5**). Finally, 1,3-selenazole containing the pharmacologically relevant isothiouronium moiety (**35**) was prepared from **29c** and thiourea.

All compounds **25**, **28a-f**, **29a-c**, **32**, **33a-c**, **34a-c** and **35** were tested *in vitro* for their inhibitory activity against the physiologically relevant hCA isoforms I, II, IV, VA, VB and IX by means of the stopped-flow carbon dioxide hydration assay[29] and their activities were compared to the standard acetazolamide (**AAZ**) (**Table 2**).

Table 2. Inhibition constants of hCA I, hCA II, hCA IV, hCA VA, hCA VB and hCA IX with compounds **25**, **28a-f**, **29a-c**, **32-35** and **AAZ** by a stopped-flow CO_2 hydrase assay[29]

	K_i (nM)*					
Compound	hCA I	hCA II	hCA IV	hCA VA	hCA VA	hCA IX[a]
25	44.2	84.8	941.1	63.4	552.7	7.6
28a	33.5	29.6	652.3	9.7	703.1	6.5
28b	637.9	85.8	6353	75.3	724.2	7.5
28c	206.0	88.6	3098	86.6	620.4	0.87
28d	414.1	67.9	873.1	82.2	730.0	8.4
28e	539.7	245.1	9386	85.7	757.3	8.2
28f	42.2	70.9	359.5	82.5	808.7	56.3
29a	15.8	47.3	384.7	82.3	600.0	6.9
29b	41.6	77.0	392.4	42.5	460.0	9.0
29c	7.3	73.2	326.2	58.4	90.9	2.8
32	935.0	74.6	6860	55.8	550.0	5.4
33a	135.2	79.7	5155	56.3	81.0	7.2
33b	8.2	186.7	2695	56.8	809.5	2.6
33c	47.7	9.5	853.9	40.0	85.0	0.89
34a	289.1	9.8	751.0	68.3	517.0	9.1
34b	30.3	9.6	203.9	75.6	54.1	7.1
34c	7.1	7.7	120.8	47.1	319.1	0.55
35	14.6	80.4	216.5	57.3	700.0	7.0
AAZ	250	12.1	74.0	63.0	54.0	25.8

* Mean from three determinations by a stopped-flow, CO_2 hydrase method. Standard errors were in the range of 5–10% of the reported values.

[a] Catalytic domain

We have investigated a range of various kinds of 2,5-disubstituted 1,3-selenazole derivatives for their interaction with the six hCAs here considered, after a period of 15 min of incubation of the enzyme.[39–41] The following structure-activity relationship (SAR) may be noted from the inhibition data in **Table 2**:

i) The cytosolic hCA I was inhibited by primary selenoamide **25** in the medium nanomolar range (K_i 44.2 nM). On the other hand, the inhibition profile of selenazole derivatives varied according to the substituent at position 5. The benzene moiety (**28a**) led to a slight increase in the activity (K_i 33.5 nM) and substitutions at positions 3 or 4 led to a decrease of the potency. An interesting inhibition profile was observed for compounds **28b-d** incorporating halogens. The dimension of this substituent proved to be crucial for the inhibition potency. Indeed, replacement of fluorine (**28b**) by bromine (**28c**) caused an increase of activity for hCA I (K_i 637.9 nM *vs*. K_i 206.0 nM). Moreover, substitution in position 3 (**28f**) led to a better activity than the corresponding compounds with *para* groups (**28b-e**). Aliphatic moieties at position 5 of selenazoles (**29a-c**) increased the efficacy compared to aromatic compounds (**28a-f**). **29c** showed an inhibition constant in the low nanomolar range (K_i 7.3 nM). Another interesting point was the further substitution of the side chain in compound **29c** with chalcogen aromatic moiety. Going down along the chalcogen group of the periodic table (from sulphur **32** to tellurium **33a**) the activity increased (K_i 935.0 nM to K_i 135.2 nM) as the chalcogen group element increased from sulphur (**32**) to tellurium (**33a**). The second dominant cytosolic isoform, hCA II, was inhibited by all these compounds in the medium nanomolar range except for compounds **33c** and **34a-c** which showed low nanomolar inhibition (K_i 7.7 to 9.8 nM). The different moieties at position 5 of the selenazole scaffold did not influence significantly the inhibition constant. On the other hand, the further functionalization of 4-halomethyl-1,3-selenazoles **29c** with different selenites **34a-c** and tellurate **33c** moieties led to an increase of potency near ten folds compared to the other compounds here considered.

ii) Almost all compounds investigated here, possessed low inhibitory activity for the membrane-bound isoform hCA IV with ranges spanning between the high

nanomolar to the micromolar (K_i 120.8 to 9386 nM). Aliphatic substituents at position 5 proved to be better than the aromatic ones, with inhibition constants K_is spanning from 326.2 to 392.4 nM. Indeed, as for the previously discussed isoform hCA II mentioned above, the functionalization of 4-halomethyl-1,3-selenazoles **29c** with selenolate (**34a-c**) and tellurate **33c** moieties increased the efficacy.

iii) An interesting inhibition pattern was observed for the mitochondrial hCA VA and hCA VB isoforms. All compounds here considered, except **34a**, exhibited a preference of inhibition for the isoform hCA VA over hCA VB and, selenazole **28a** showed this preference with an activity 70 folds more potent for hCA VA (K_i 9.7 nM) compared to hCA VB (K_i 703.1 nM). On the other hand, the different moieties at position 5 of the selenazole scaffold did not influence significantly the inhibition potency.

iv) The membrane-bound, tumor-associated, hCA IX, is effectively inhibited by selenazoles in low nanomolar to sub-nanomolar range (K_i 0.55 nM to 9 nM) except for compound **28f** (K_i 56.3 nM). An interesting case was constituted by the isosteric substitution of the halogen atom in the aromatic moiety of **28c-d** and **28f**. The transition from fluorine atom (**28f**) to bromine (**28b**) led to a significant increase of the inhibitory potency (K_i 56.3 to 0.87 nM). The activity was influenced also for the other chalcogen moieties (**33a-c** and **34a-c**), especially for methoxyl substituent, which led to a subnanomolar inhibition (K_i 0.89 and 0.55 nM).

X-Ray crystallography was used to determine the mode of binding of compound **29c** in complex with hCA II. Structural analysis of the initial $|F_o-F_c|$ electron density map of the active site showed well defined electron densities, fully compatible with the presence of inhibitor **29c,** instead electron density for chlorine atom was not present (**Figure 9A**). The sulfonamide moiety coordinates the catalytic zinc ion of hCA II with a tetrahedral geometry, by means of one nitrogen atom of the sulfonamide group and displacing the zinc bound water molecule/hydroxide ion similarly to other sulfonamide and sulfamide derivatives investigated earlier.[42]

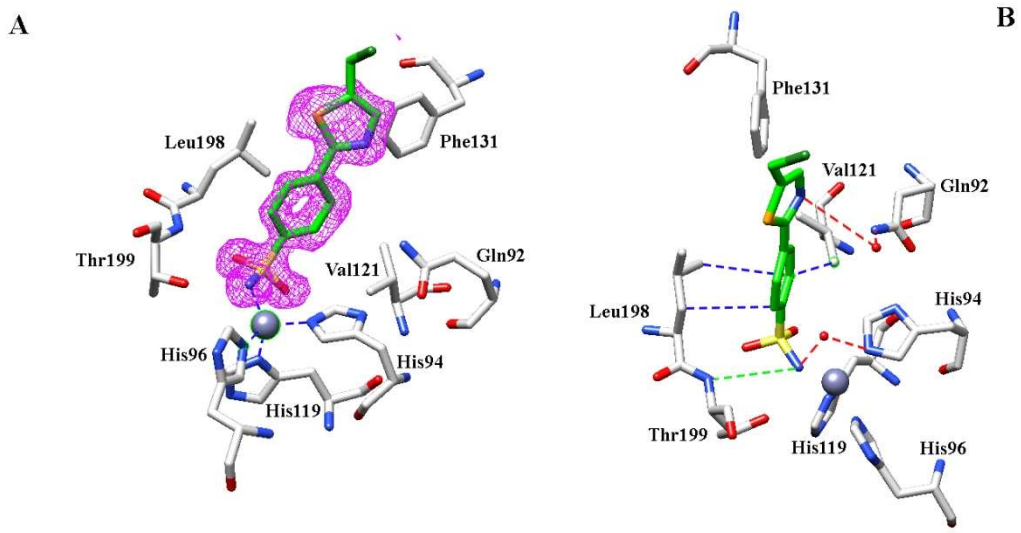

Figure 9. Active site region of hCA II/**29c** adduct (PDB 6H3Q). Inhibitor showing the σA-weighted $|F_o-F_c|$ map (at 2.5 σ) (**A**). Hydrogen bonds, van der Waals interactions and Water Bridges are shown and labelled in green, blue and red respectively (**B**).

The deprotonated nitrogen atom of the sulfonamide moiety forms a hydrogen bond with the NH moiety of Thr199. Furthermore, a hydrogen bond is involved with a water molecule showing a well-defined solvent network that contributes to stabilize the inhibitor within the active site (**Figure 9B**). The phenyl ring of inhibitor **29c** is located in the active site channel, where it is involved in a number of hydrophobic interaction with the side chains of residues Val121 and Leu198. The medium potency of inhibition against hCA II (K_i 73 nM) could be explained with the rigid structure conferred by two consecutive aromatic rings; this scaffold prevented the inhibitor from locating its tail in a small hydrophobic pocket delimited by residues Phe131 and which strongly correlates with the inhibition potency against this isoform. On the other hand, nitrogen of selenazole moiety is involved in a water bridge with residue Gln92 (**Figure 9B**).

We focused our attention on the *ex vivo* activity of compounds **28e**, **33c** and **34c**, which were evaluated for their effects on cell viability against the human prostate (PC3) and breast (MDA-MB-231) cancer cell lines. All compounds were low/sub nanomolar hCA IX inhibitors, and were used at different concentrations, being incubated for 48 h in both normoxic and hypoxic conditions, when overexpression of high amounts of CA IX occurs.[17]

In PC3 cells, selenazole derivative **28e**, with a 4-NO_2 phenyl moiety, reduced the cell viability to 60% at 1µM. Its efficacy increased significantly at 10 µM reducing the viability to 10% (**Figure 10**). In the hypoxic conditions, compound **28e** showed significantly more effects on cytotoxicity which reached 32% at 1µM. At higher concentration the compound was comparable to its effects in normoxic condition. Chalcogenide atom in the side chain of compounds **33c** and **34c** proved to play a crucial role for cytotoxicity. Compound **33c**, whit tellurium atom in the side chain, showed a strong activity against this cancer cell line in normoxic condition with a viability of 23% at 1 µM. On the other hand, in hypoxic condition compound **33c** showed an efficacy two times lower than in the normoxia. Finally, compound **34c**, with selenium in the side chain, proved to be inactive at lower doses against PC3 cell line, but the efficacy increased at 30 and 100 µM showing a cell viability in normoxic condition of 59% and 11% respectively. In hypoxic condition compound **34c** exhibited more cytotoxic effects at low concentration (77% at 10 µM) whereas at higher doses exhibited an efficacy comparable to that in normoxic condition.

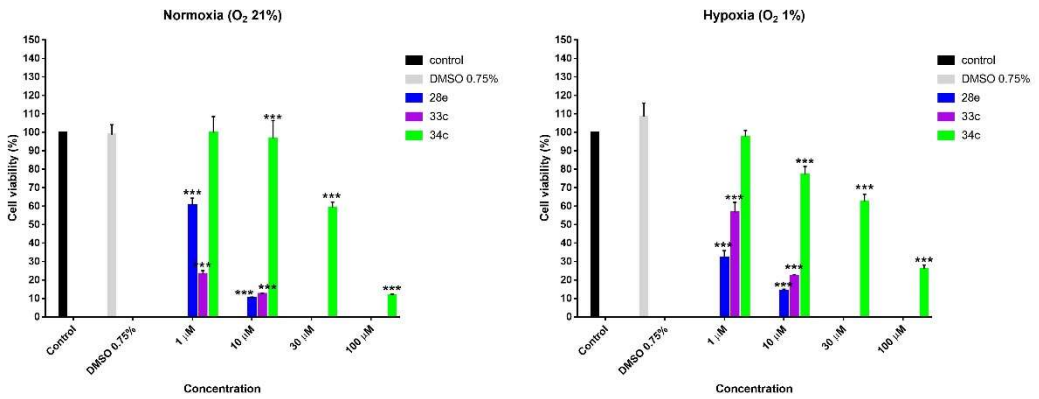

Figure 10. Effects of newly synthetized compounds **28e**, **34c** and **33c** on viability of the human prostatic cancer cell line PC3 following 48h treatment in normoxic and hypoxic (1% O_2) conditions. ***p<0.001 *versus* control.

In the MDA-MB231 cell line, the derivative **28e** at the lower concentration showed a weak activity with viability of 73%. On the other hand, at 10 µM the potency against this cancer cell line increased drastically killing over 90% of the cells. Also for MDA-MB231 cell line the different chalcogenide in the side chain of compound **33c** and **34c** played an important

role on the viability (**Figure 11**). Indeed, tellurium atom in **33c** exhibited a strong cytotoxicity in normoxic conditions, already at lower concentration (16% at 1 μM). Also this time, the potency decreased over two time in hypoxic condition. Compound **34c** did not show any activity in this *ex vivo* normoxia assay at 1 and 10 μM concentration. A reduced cell viability was observed for this compound only at high concentration (30 μM and 100 μM). In the hypoxic conditions the selenium derivative **34c** did not show any significant activity, only at higher concentration of 100 μM the cell viability reached 46%.

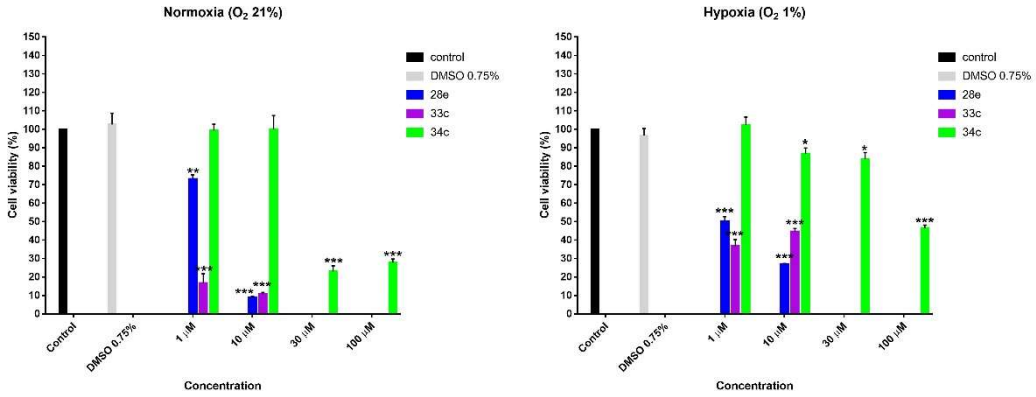

Figure 11. Effects of the newly synthetized compounds **28e**, **34c** and **33c** on viability of the human adenocarcinoma breast cell line MDA-MB231 following 48h treatment in normoxic (21% O_2) and hypoxic (1% O_2) conditions. *p<0.05, ** p<0.01, ***p<0.001 *versus* control.

3.4 Novel telluride bearing benzensulfonamide moiety as Carbonic Anhydrase inhibitors with potent antitumor activity

Oxidative stress has been found to play a crucial role in numerous disease conditions.[43,44] During the last decades a growing interest in selenium- and tellurium-containing agents with potential redox-modulating properties has been reported.[45-47] Several organotellurium compounds possessing a range of unique and interestingly properties such as activity against pathogenic microorganisms,[48,49] inhibition cancer cells growth,[50-52] potent caspase and cathepsin inhibitory propieties[53] and antioxidant activity were developed to date. For the latter many of them were reported superior to that of the selenium analogues.[54,55] For this reason we decided to synthesize various Te(II) derivatives as hCA inhibitors. Diaryl

ditellurides **36a-g** were prepared from aryl bromides via lithiation, tellurium insertion, and air oxidation according to, or in analogy to literature procedures (**scheme 6**).[56]

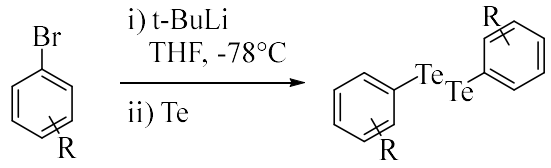

36a-g **37a-g**

36a: R= H
36b: R= 2-CH_3
36c: R= 4-CH_3
36d: R= 4-OCH_3
36e: R= 2-Napthyl
36f: R= 2,6-CH_3
36g: R= 3,4,5-OCH_3

37a: R= H
37b: R= 2-CH_3
37c: R= 4-CH_3
37d: R= 4-OCH_3
37e: R= 2-Napthyl
37f: R= 2,6-CH_3
37g: R= 3,4,5-OCH_3

Scheme 6: Synthesis of aryl ditellurides **37a-g**

The tellurides **39a-g** synthesized in this study were prepared by *in situ* reduction of the corresponding aromatic ditellurides followed by reaction with 4-(bromomethyl) benzenesulfonamide **38** dissolved in THF as outlined in **Scheme 7**.

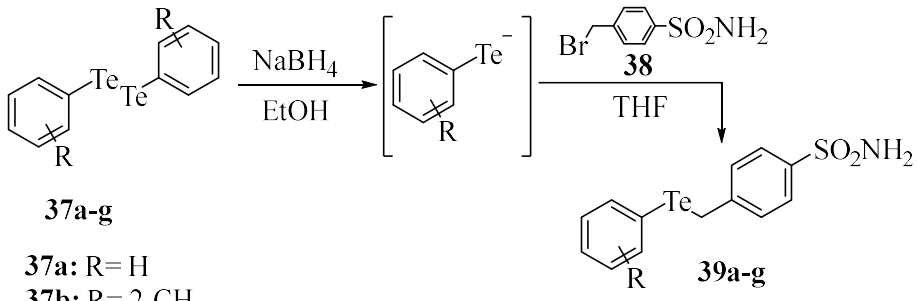

37a-g

37a: R= H
37b: R= 2-CH_3
37c: R= 4-CH_3
37d: R= 4-OCH_3
37e: R= 2-Napthyl
37f: R= 2,6-CH_3
37g: R= 3,4,5-OCH_3

39a-g

39a: R= H
39b: R= 2-CH_3
39c: R= 4-CH_3
39d: R= 4-OCH_3
39e: R= 2-Napthyl
39f: R= 2,6-CH_3
39g: R= 3,4,5-OCH_3

Scheme 7: Synthesis of tellurides bearing benzenesulfonamide moiety **39a-g**

On the basis of our experience on the chemistry of three-membered heterocycles and chalcogen containing nucleophiles,[57,58] we sought to study the reactivity of epoxide **40** with tellurium-containing nucleophiles, thus allowing us to enlarge the scope of the present work aiming to access the β-hydroxy substituted tellurides incorporating the benzenesulfonamide moiety. Having synthesized the epoxide **40**,[59] we evaluated its reactivity with aryl tellurolates generated *in situ* by reduction of the corresponding ditellurides. Thus, diphenyl ditelluride **37a** was treated with $NaBH_4$ and then reacted with **40** to afford the tellurium containing *N*-sulfonylformamidine **41** as the major product. The cleavage of the protecting group[60] led to the formation of the desired β-hydroxy telluride **42a** (**Scheme 8**).

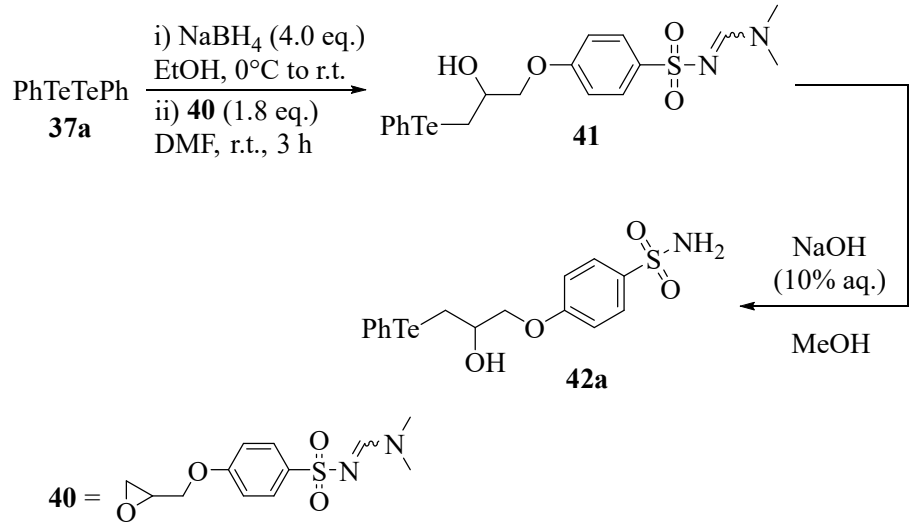

Scheme 8: Synthesis of β-hydroxy telluride **42a** from epoxide **40**

In order to investigate whether the ring opening reaction and the cleavage of the sulfonamide protecting group could be achieved in *one pot*, the epoxide **40** was reacted with $PhTe^-$, generated by treating diphenyl ditellurides **37a-e** with a large excess of $NaBH_4$ (4.0 eq.) in the presence of NaOH (2.0 eq.) (**Scheme 9**).[61] We were glad to observe that, under these conditions a direct formation of the β-hydroxyl-substituted telluride **42a-e** was achieved in rather good yield (**Scheme 9**).

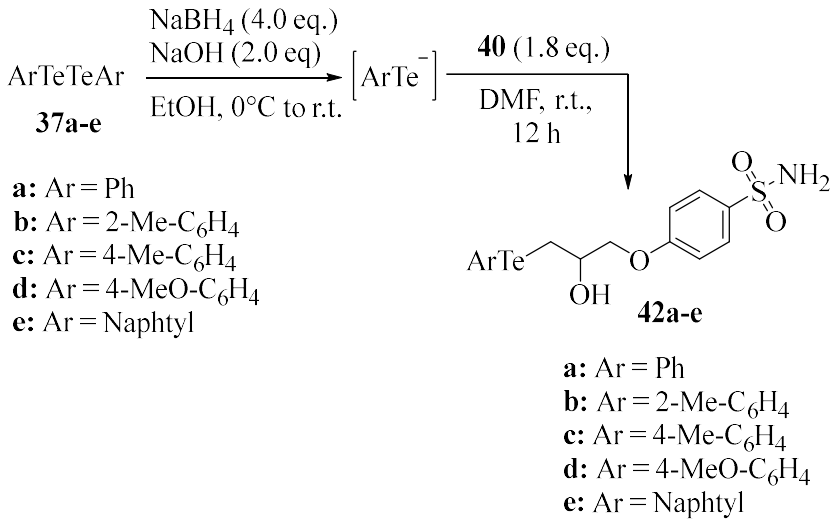

Scheme 9: *One pot* synthesis of β-hydroxy tellurides **42a-e** from epoxide **40**

With the aim to further investigate the activity of β-hydroxy tellurides bearing the benzensulfonamide moiety, the symmetric dialkyl telluride **43** was synthesised from the epoxide **40** and Li_2Te, generated from elemental tellurium and $LiEt_3BH$, following a slightly modified reported procedure[57] (**Scheme 10**).

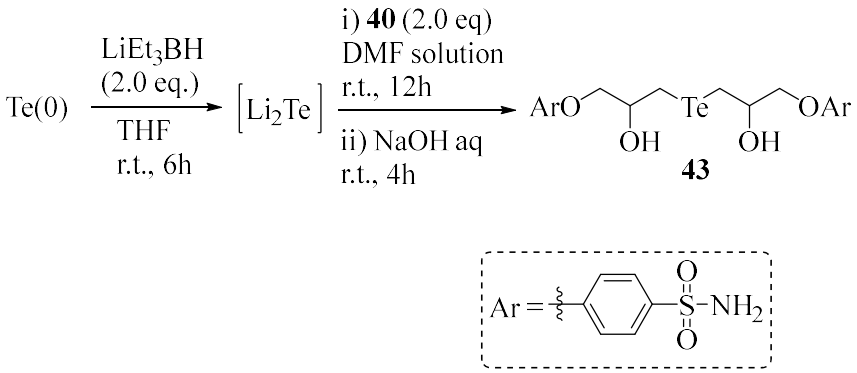

Scheme 10: Synthesis of symmetric β-hydroxy telluride **43** from elemental tellurium

The CA inhibition data for compounds **39a-g**, **42a-e, 43** using **AAZ** as a reference compound was measured for the hCA isoforms I, II, IV, VII and IX by means of the stopped-flow carbon dioxide hydration assay[29]and the results are presented in **Table 3**.

Table 3. Inhibition constants of hCA I, hCA II, hCA IV, hCA VII and hCA IX with compounds **39a-g**, **42a-e**, **43** and **AAZ** by a stopped-flow CO_2 hydrase assay[29]

Compound	K_i (nM)*				
	hCA I	hCA II	hCA IV	hCA VII	hCA IX[a]
39a	209.8	12.1	52.0	8.4	2.4
39b	24.0	4.4	1.9	0.54	2.2
39c	1.5	2.0	2.1	0.3	2.6
39d	2402	182.3	828.2	62.7	2.9
39e	18.0	0.67	1.8	0.76	2.6
39f	256.6	3.3	5.1	2.7	2.5
39g	377.1	13.2	6925	55.4	2.4
42a	46.8	0.42	6.8	0.78	14.8
42b	36.5	0.64	192.1	0.72	9.5
42c	83.9	0.56	1.7	2.7	118.1
42d	394.4	4.4	42.1	11.9	7.8
42e	8798	8.5	183.2	261.9	6.4
43	67.4	0.62	18.1	0.8	808.9
AAZ	250.0	12.1	74.0	2.5	25.8

* Mean from three determinations by a stopped-flow, CO_2 hydrase method. Standard errors were in the range of 5–10% of the reported values.

[a] Catalytic domain

As for the hCA I, the K_i values for compounds **39a-g** were strong influenced by different aromatic scaffolds. Indeed, compound **39b** with the 2-CH_3 moiety showed an efficacy about 9 fold lower when compared to the unsubstituted phenyl **39a** (K_is 24.0 and 209.8 nM respectively) and the introduction of the CH_3 at position 4 (**39c**) resulted over 10 fold more potent (K_i 1.5 nM). On the other hand, the replacement at position 4 of the CH_3 with the methoxyl group (**39d**) led to a drastically decrease of the activity up to the micromolar range (K_i 2402 nM). The inhibition data for compounds with more complex scaffold such as **39f** and **39g** were equipotent to **39a** (K_is 256.6, 377.1 and 209.8 nM respectively). In analogy, the 4-OCH_3 moiety in β-hydroxy telluride **42d** showed adverse effect on the potency compared to **42a** (K_i 394.4 and 46.8 nM). In addition, for these compounds the naphtyl scaffold **42e** led to decrease the potency in the micromolar range (K_i 8798 nM). The second dominant cytosolic isoform, hCA II, showed a strong inhibition pattern by these compounds

and in particular **39e, 42a-c** and **43** exhibited inhibition potencies in the subnanomolar range (K_i 0.42-0.67 nM). The 4-OCH_3 moiety in compounds **39d** and **42d**, such as for hCA I, showed an adverse effect on the efficacy. On the other hand, for this isoform, the disubstituited molecule **39f** proved to be more potent than **39a** without substituent (K_i 3.3 and 12.1 nM, respectively). An interesting inhibition pattern is observed for compounds **39e** and **42e** against the last cytosolic isoform study here (i.e. hCA VII). The bulky naphtyl moiety for derivative **39e** led to strong inhibition activity (K_i 0.67 nM). Contrary, when this substituent is present in β-hydroxyl tellurides (**42e**) the inhibition drastically decreased (K_i 261.9 nM). The transmembrane tumor-associated hCA IX, was effectively inhibited by tellurides derivatives **39a-g** in the low nanomolar range (K_i 2.4-2.9 nM). The interesting point for these compounds was that the various moieties present in the scaffold did not influence the efficacy against the hCA IX. On the other hand, β-hydroxy tellurides **42a-e** showed different inhibition activity and depending on the tail moiety, and among them compound **42c** (i.e. bearing the 4-CH_3) proved to be the least potent (K_i 118.1 nM). Also, the divalent symmetric dialkyl telluride **43** showed a low inhibition efficacy against hCA IX in high nanomolar range (K_i 808.9 nM).

The binding modes of both classes of telluride derivatives (compound **39a** and **43** respectively) were determined by means of their adducts with the hCA II studied by means of X-ray crystallography (**Figure 12**). The |Fo−Fc| electron density maps for the hCA II−**39a** complex revealed a well ordered structure of the benzenesulfonamide section, which instead became weaker in electron density when the telluride moiety was present (**Figure 12A**).

The hCA II−**43** complex showed clear electron density all through the molecule, thus suggesting a better ordered structure within the enzymatic cleft (**Figure 12B**). Both **39a** and **43** showed almost identical allocations within the enzyme cavity.

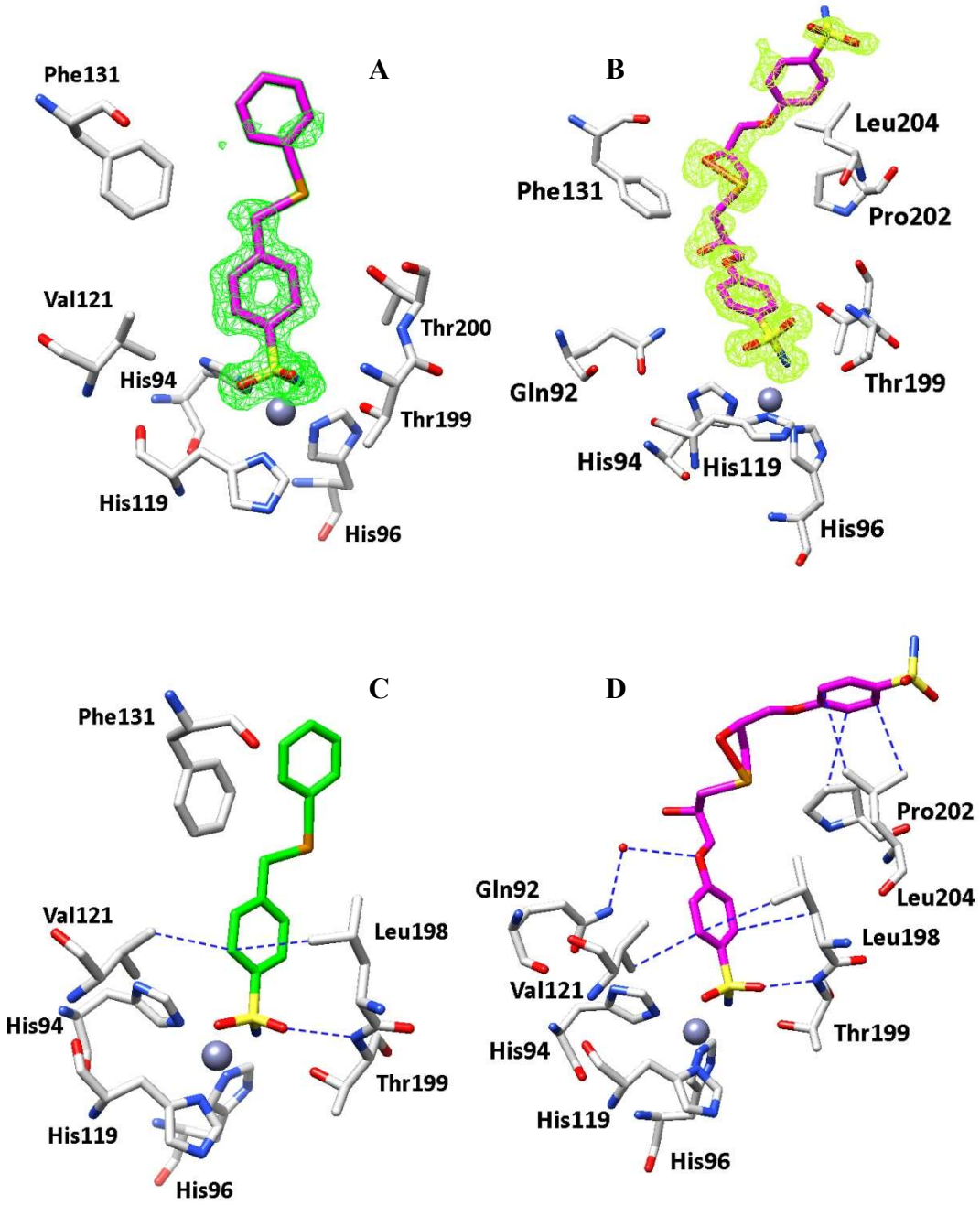

Figure 12: Active site region of hCA II/**39a (A)** or hCA II/**43** (**B**) adduct. Hydrogen bonds, van der Waals interactions and water bridges are shown and labelled in blue for inhibitor **39a** (**C**) and **43** (**D**).

For both complexes, the deprotonated nitrogen atom of the sulfonamide moiety forms a hydrogen bond with the NH moiety of Thr199 that contributes to stabilize the inhibitor within the active site (**Figure 12C, D**). Compound **39a** is located in the active site channel where is involved in a very few number of hydrophobic interactions such as the side chains of residues Val121 and Leu198. On the other hand, compound **43** is involved in several hydrophobic interaction with Val121 and Leu198 in the same manner **39a**, in addition, Pro202 and Leu204 are involved in several hydrophobic interactions with the second sulfonamide ring. Moreover, is present a water bridge with residue Gln92 (**Figure 12D**). This different pattern of interactions with hCA II could be explained the dissimilar activity against it. Indeed, the high number of contacts with **43** agree with strong inhibition data (K_i 0.62 nM), on the contrary, the few interactions as for **39e** resulted in reduced potency (K_i 21.2 nM).

The low nanomolar hCA IX inhibitors, compounds **39a**,**g** and **42b**,**e** were evaluated for their effects on cell viability against the human breast (MDA-MB-231) cancer cell lines at different concentrations and in both normoxic and hypoxic conditions. All derivatives in normoxia showed strong efficacy at 10 μM concentration by killing almost completely the tumor cells. When used at 1 μM concentration different activities among the two classes of compounds (**39** and **42**) can be discriminated. The telluride **39g** and in particular **39a**, still exhibited strong cytotoxicity with viabilities of 17.7% and 5.2% respectively. On the other hand, compounds **42b** and **42e** at the same concentration proved to be less potent (36.2% and 42.6% respectively). In hypoxic conditions the potencies drastically decreased at 1 μM as for compounds **42b,e** killing only 30% of the tumor cells. A reduced cell viability was observed also for the tellurides **39a,g**, where the potency decreased over 3 times for **39a** and almost 2 times for **39g.** At higher concentrations (30 μM and 100 μM) all compounds, with the exception of **42b**, showed significant activity as over the 80% of tumor cells were killed.

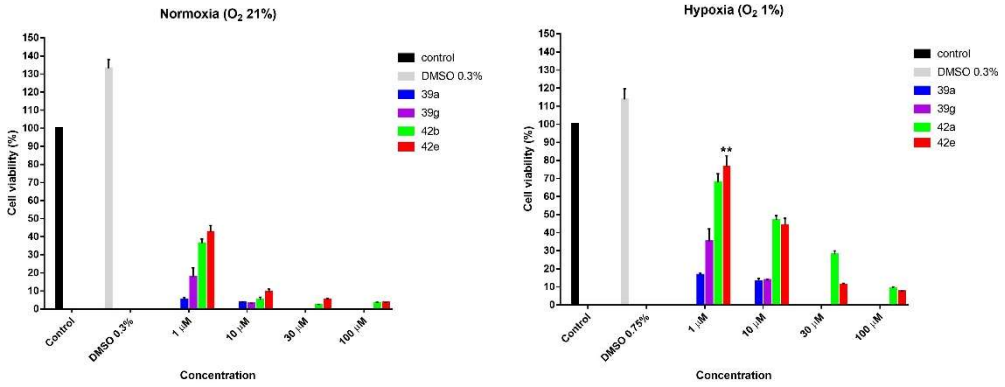

Figure 13. Effects of the newly synthetized compounds **39a**,g and **42b,e** on viability of the human adenocarcinoma breast cell line MDA-MB231 following 48h treatment in normoxic (21% O_2) and hypoxic (1% O_2) conditions. $p<0.001$ *versus* control, ** $p<0.01$.

3.5 Heterocoumarins are selective Carbonic Anhydrase IX and XII Inhibitors with Cytotoxic effects against Cancer Cell lines

Coumarin derivatives showed a large number of biological activities, including anticoagulant,[62] antibacterial,[63] antiviral,[64] and recently many different derivatives have been reported possessing anti-tumor properties *in vitro* and *in vivo*.[65-67] The interesting heterocyclic system of coumarin derivatives, with their wide range of biological functions, has made them an excellent starting point for further chemical derivatization useful to identify novel therapeutic agents. In this context, recently, several coumarin derivatives have shown to constitute a new class of selective inhibitors against the human tumor-associate carbonic anhydrase isoforms hCA IX and hCA XII.[68,69] For this reason, we developed potent and selective inhibitors with the aim to identify new CAIs structurally related to the natural coumarins. In continuation of our research on the preparation of potentially useful chalcogen derivatives, herein we report a facile and convenient access to synthetic strategies for the replacement of the endocyclic oxygen atom by selenium (**Scheme 11**)

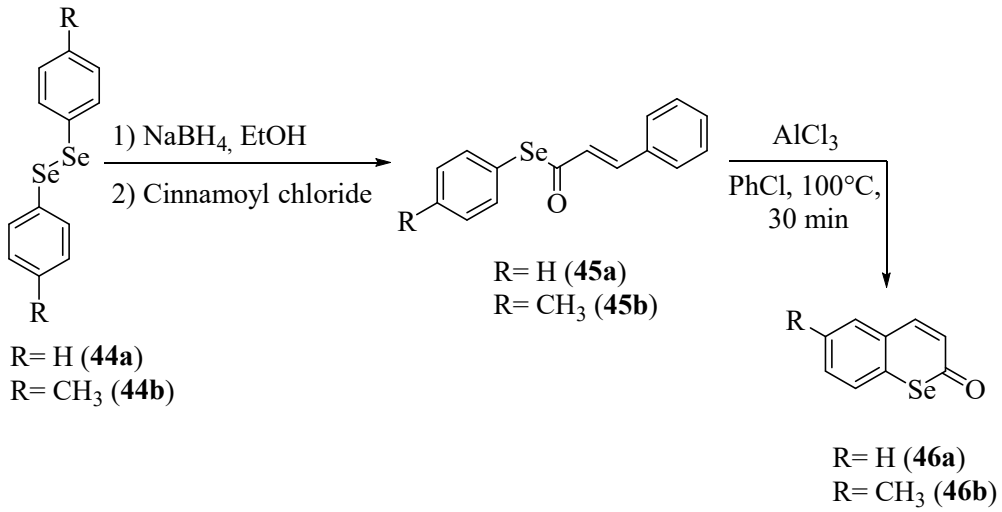

R= H (**44a**)
R= CH_3 (**44b**)

R= H (**45a**)
R= CH_3 (**45b**)

R= H (**46a**)
R= CH_3 (**46b**)

Scheme 11. Synthesis of selenocoumarins **46a-b.**

The selenophenyl cinnamate (**45a-b**) needed for the synthesis of selenocoumarins was prepared by reduction of diselenides **44a-b** with $NaBH_4$ to the corresponding selenolate which was treated in situ with cinnamoyl chloride, affording the compounds **45a-b** in excellent yield. Thus derivatives **45a-b** were treated with anhydrous $AlCl_3$ in chlorobenzene at 100°C for 30 minutes to afford a red reaction mixture, which after work-up furnished compounds **46a-b** in good yield [70] (**Scheme 11**). In order to access further heterocoumarins, we evaluated the replacement of the carbonyl group with the isosteric thiocarbonyl moiety by using an excess of Lawesson's reagent (2.0 eq.) in refluxing toluene for 4h. Compounds **47a-b** were obtained in excellent yields as reported in the **Scheme 12.**

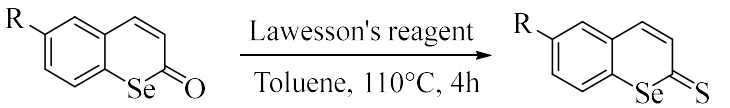

R= H (**46a**)
R= CH_3 (**46b**)

R= H (**47a**)
R= CH_3 (**47b**)

Scheme 12. Synthesis of thioseleno coumarins **47a-b**

We explored the replacement of the coumarin exocyclic oxygen atom with a selenium with negative results.

Furthermore our study has been extended to nitrogen endocyclic systems as outlined in **Scheme 13**.

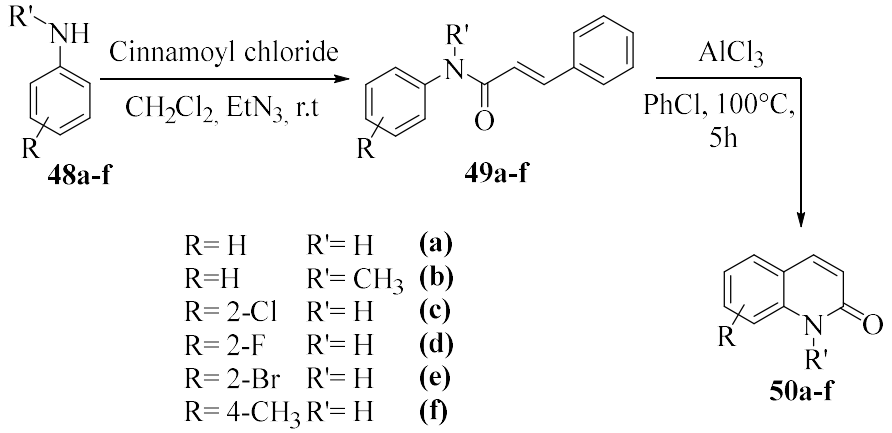

Scheme 13. Synthesis of different quinolin-2(1H)-one derivatives **50a-f**

Cinnamoyl amides differently substituted **49a-f** were obtained from the corresponding amines **48a-f** with cinnamoyl chloride in dichloromethane at room temperature in quantitative yields. Treatment of compounds **49a-f** with anhydrous $AlCl_3$ in chlorobenzene at 100°C for 5h afforded the corresponding quinolin-2(1*H*)-one derivatives **50a-f** with similar mechanistic pathway of compounds **46a-b**. Moreover, the reaction proceeded efficiently with substituents on the nitrogen (**50b**) or on the aryl group (**50a**, **50c-f**) as reported in **Scheme 13**.[71] The exocyclic selenium was inserted in a one-pot procedure by selenation reaction with Wollins' reagent (WR) (**Scheme 14**).

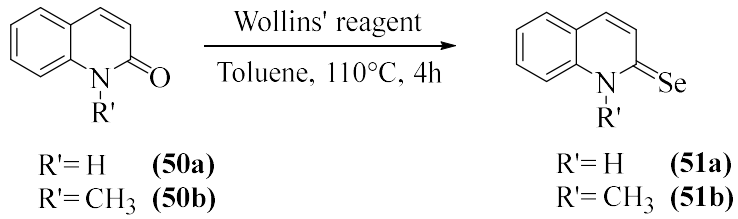

Scheme 14. Synthesis of seleno quinolin-2(1*H*)-one derivatives **51a-b**.

Compounds **50a-b** were readily converted to seleno quinolin-2(1*H*)-one derivatives **51a-b** with an excess of WR (1.5 eq.) in refluxing toluene for 4h affording the desiderate compounds in good yields.

Our attempts to synthesize endocyclic tellurium coumarins with it proved to be difficult by using an analogue synthetic strategy, since the telluro esters proved particularly instable. Therefore we used an alternative synthetic pathway based on the cinnamic acid derivative **57** (**Scheme 15**).

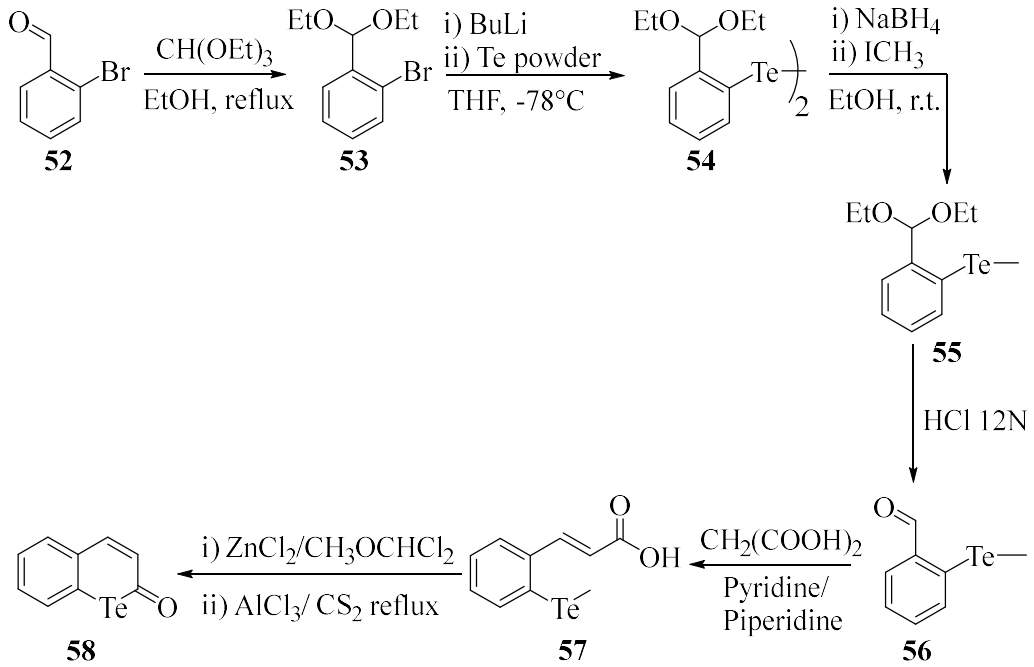

Scheme 15. Synthesis of tellurocoumarin **58**

The aldehyde group of in compound **52** was protected by with triethyl orthoformate in refluxing ethanolic solution. Diaryl ditelluride **54** was prepared from aryl bromide **53** via lithiation, tellurium insertion and oxidation in analogy with the literature procedure.[72] Then the ditelluride acetal derivative **54** was hydrolyzed with concentrated aqueous HCl and the resulting aldehyde **56** was subjected to Knoevenagel condensation with malonic acid to afford the corresponding cinnamoyl acid derivative **57**. Finally, cyclization into telluro-coumarin **58** was obtained by converting compound **57** the corresponding acyl chloride which was subsequently treated with $AlCl_3$ as reported previously. [73]

All synthesized compounds **46a-b**, **47a-b, 50a-f, 51a-b** and **58**, were tested *in vitro* for their inhibitory properties against the physiologically relevant hCA isoforms (I, II, IX, and XII) by means of a stopped-flow carbon dioxide hydration assay [29] after a period of 6h of

incubation. Their activities were compared to the standard carbonic anhydrase inhibitor (CAI) acetazolamide (**AAZ**) (**Table 4**).

Table 4. Inhibition constants of hCA I, hCA II, hCA IX and hCA XII with compounds **46a-b, 47a-b, 50a-f, 51a-b, 58** and **AAZ** by a stopped-flow CO_2 hydrase assay[29]

	K_i (nM)*			
Compound	hCA I	hCA II	hCA IX	hCA XII
46a	>10000	>10000	26.3	22.9
46b	>10000	>10000	56.1	7.6
47a	>10000	>10000	39.5	25.8
47b	>10000	>10000	59.9	7.4
50a	>10000	>10000	82.0	93.0
50b	>10000	>10000	44.6	83.5
50c	>10000	>10000	23.0	6.8
50d	>10000	>10000	58.8	6.8
50e	>10000	>10000	23.4	8.4
50f	>10000	>10000	123.1	8.7
51a	>10000	>10000	54.4	7.6
51b	>10000	>10000	172.0	86.4
58	>10000	>10000	59.0	8.2
AAZ	250	12.1	25.8	5.7

* Mean from three determinations by a stopped-flow, CO_2 hydrase method. Standard errors were in the range of 5–10% of the reported values.

From the analysis of inhibition costant values reported in **Table 4**, we observed that all compounds, according to previous report,[74,75] were ineffective inhibitors of two dominant cytosolic hCA I and hCA II showing high selectivity against tumor-associated isoforms hCA IX and hCA XII. In terms of structure-activity relationships it could be observed that methyl moiety at position 6 of seleno-coumarins **46a-b** and **47a-b** played a crucial role for the activity. This moiety increased near 2 times the potency against hCA IX and over 3 times for hCA XII. Moreover, the isosteric substitution of carbonyl with thiocarbonyl group did not significantly influence the activity. Methyl substituent on nitrogen of quinolin-2(1*H*)-one **50b** led to increase the activity by 2 folds against the hCA IX than compound **50a** (K_i 44 nM to 82 nM). On the other hand, different substituents at position 8 (**50c-e**) increased the potency for both the tumor associated isoforms. The replacement of carbonyl group with

selenocarbonyl moiety (**51a-b**) influenced the activity especially for compound **51b** showing a decrease of near 4 times when compared to **50b** (K_i 44 nM to 172 nM). Finally the telluro-coumarin **58** showed an interesting inhibition pattern compared to seleno-coumarin **46a**. The biggest chalcogen atom for compound **15** led to a decrease potency near two times than **46a** for hCA IX (K_i 59 nM to 26.3 nM). However for the other membrane isoform hCA XII the activity of **58** was increased near 3 times than the seleno-coumarin **46a** (K_i 8.2 nM to 22.9 nM).

The high isoforms selectivity coupled to the upregulated expression of hCA IX and XII in hypoxic tumors, makes these compounds highly desirable for targeting the tumor-associated enzymes. We focused our attention on the activity of compounds **46a**, **47b**, **51a** and **58**, which were evaluated for their effects on cell viability against human prostate (PC3) and breast (MDA-MB-231) cancer cell lines. All compounds were high selective hCA IX and XII inhibitors, and were used at different concentrations (1, 10 100 and 300 μM), being incubated for 48 h in both normoxic and hypoxic conditions.[15] In PC3 cells, seleno quinolin-2(1*H*)-one **51a** did not show any cytotoxic activity in normoxic and hypoxic conditions. On the other hand, the seleno-coumarin **46a** showed reduction of cell viability to 68% only when the maximum concentration (300 μM) was used and in both oxygenated conditions. Its efficacy increased significantly when the endocyclic selenium was replaced by tellurium (i.e. compound **58**). In normoxic conditions such an isosteric substitution led to reduction of the cell viability to 54% at 30 μM and increased up to 19% at higher concentrations (**Figure 14**). In the hypoxic condition, compound **58** showed less effects on cytotoxicity which reached 71% at 30μM and 38% at 100-300 μM. Moreover, the thioseleno-coumarin derivative **47b** showed at 30 μM similar cytotoxicity effects to compound **58** in normoxic and hypoxic conditions (51% and 79% respectively).

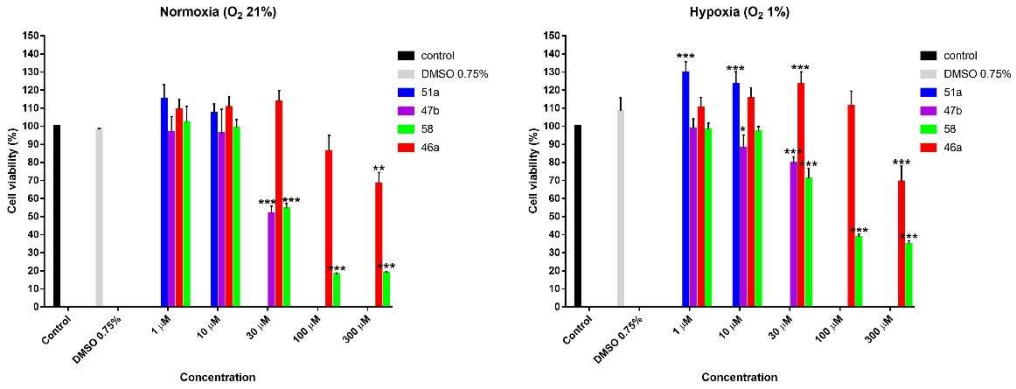

Figure 14. Effects of newly synthetized compounds **46a**, **47b**, **51a** and **58** on viability of the human prostatic cancer cell line PC3 following 48h treatment in normoxic (21% O_2) and hypoxic (1% O_2) conditions. *p<0.05, ** p<0.01, ***p<0.001 *versus* control.

Derivative **51a** also in the MDA-MB231 cell line, did not show any activity in these assays. On the other hand, seleno-coumarin **46a** showed only at 300 μM a good cytotoxic activity in normoxia (28%). The potency against this cancer cell line increased drastically when compound **46a** was used in hypoxic condition. Indeed, this compound reduced cell viability already at 30 μM more than 50% and reached to kill over 90% at 300 μM (**Figure 15**). Also this time, telluro-coumarin **58** exhibited a strong cytotoxicity in normoxic conditions, already at 30 μM (15.9%). The potency decreased over 3 times in hypoxic condition reducing the cell viability at 22% using a concentration of 300 μM. A reduced cell viability (61%) was observed also for compound **47b** only at 30 μM. In the hypoxic conditions this compound did not show any significant activity.

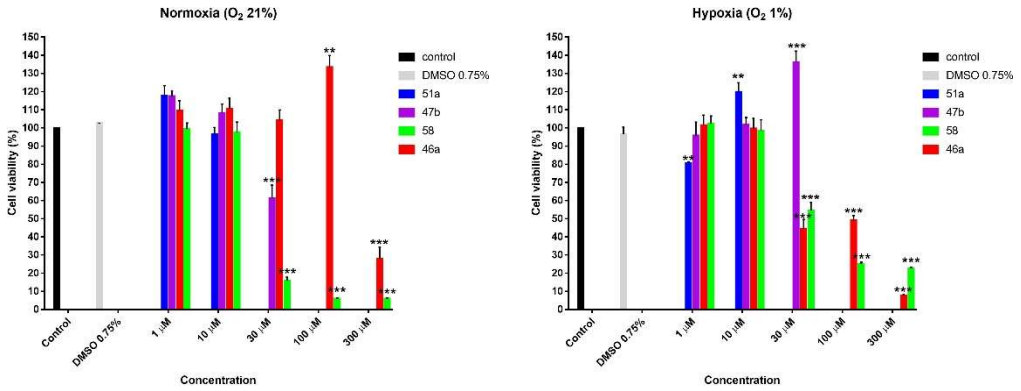

Figure 15. Effects of the newly synthetized compounds **46a**, **47b**, **51a** and **58** on viability of the human adenocarcinoma breast cell line MDA-MB231 following 48h treatment in normoxic and hypoxic (1% O_2) conditions. ** $p<0.01$, ***$p<0.001$ *versus* control.

3.7 Conclusions

We reported for the first time the synthesis of new series of chalcogenide derivatives as inhibitors of the Carbonic Anhydrases. These kind of scaffold are a rarely investigated chemotype in the CA field, and for this reason we focused by determining their binding modes in adduct with the hCA II. The unique proprieties of selenium and tellurium contacting compounds particularly emerged in the last years thus making them of particular interest in Medicinal Chemistry fields. A preliminary cytotoxic assay of selected compounds on prostate, breast, and colon cell lines was also reported for the first time. The obtained results suggested that multiple mechanisms of action, not yet identified, may take place and are responsible for exerting the compounds' cytotoxic effects. In the whole, this study clearly opens new perspectives within the CA-dependent diseases and in particular to tumors.

3.6 Experimental Data

General

Anhydrous solvents and all reagents were purchased from Sigma-Aldrich, Alfa Aesar and TCI. All reactions involving air- or moisture-sensitive compounds were performed under a nitrogen atmosphere using dried glassware and syringes techniques to transfer solutions. Nuclear magnetic resonance (^{1}H-NMR, ^{13}C-NMR, ^{19}F-NMR, ^{77}Se-NMR, ^{125}Te-NMR) spectra were recorded using a Bruker Advance III 400 MHz spectrometer in DMSO-d_6. or $CDCl_3$. $(PhSe)_2$ and $(PhTe)_2$were used as an external references for ^{77}Se NMR (δ = 461 ppm) and ^{125}Te NMR (δ = 420 ppm). Chemical shifts are reported in parts per million (ppm) and the coupling constants (*J*) are expressed in Hertz (Hz). Splitting patterns are designated as follows: s, singlet; d, doublet; t, triplet; q, quadruplet; m, multiplet; brs, broad singlet; dd, double of doublets. The assignment of exchangeable protons (O*H* and N*H*) was confirmed by the addition of D_2O. Analytical thin-layer chromatography (TLC) was carried out on Merck silica gel F-254 plates. Flash chromatography purifications were performed on Merck Silica gel 60 (230-400 mesh ASTM) as the stationary phase and ethyl acetate/*n*-hexane were used as eluents. Melting points (mp) were measured in open capillary tubes with a Gallenkamp MPD350.BM3.5 apparatus and are uncorrected. The solvents used in MS measures were acetone, acetonitrile (Chromasolv grade), purchased from Sigma-Aldrich (Milan - Italy), and mQ water 18 MΩ, obtained from Millipore's Simplicity system (Milan-Italy). The mass spectra were obtained using a Varian 1200L triple quadrupole system (Palo Alto, CA, USA) equipped by Electrospray Source (ESI) operating in both positive and negative ions. Stock solutions of analytes were prepared in acetone at 1.0 mg mL^{-1} and stored at 4°C. Working solutions of each analyte were freshly prepared by diluting stock solutions in a mixture of mQ H_2O/ACN 1/1 (*v/v*) up to a concentration of 1.0 µg mL^{-1} The mass spectra of each analyte were acquired by introducing, via syringe pump at 10 µL min^{-1}, of the its working solution. Raw-data were collected and processed by Varian Workstation Vers. 6.8 software.

General procedure for the synthesis of *N*-formyl compounds 2a-i.

The appropriate aromatic amine (**1a-i**) (1.0 mmol) and anhydrous $ZnCl_2$ (0.1 mmol) were placed under N_2 atmosphere and treated dropwise with formic acid (3.0 mmol) with constant

stirring for 10 min. This mixture was heated at 70°C and the progress of reaction was monitored by TLC. When the reaction was completed, the mixture was cooled to r.t. and diluted with ethyl acetate. The organic layer was washed with a saturated solution of Na_2CO_3, water, brine and dried over Na_2SO_4. The solvent was removed under reduced pressure and the resulting crude product was purified by silica gel column chromatography to obtain the titled *N*-formyl derivate (**2a-i**).

General procedure for the synthesis of isoselenocyanate 3a-i.

The appropriate formamide **2a-i** (1.5 mmol) was dissolved in DCM (5 mL) and treated with Et_3N (6.4 mmol) and 4Å molecular sieves. Then a solution of triphosgene (0.8 mmol) in DCM (2 mL) was added drop-wise for a period of 1 h followed by reflux for 2.5 h. Then selenium powder (3.0 mmol) was added and the resulting mixture was refluxed for 4-7 h; conventional work-up and silica gel column chromatography afforded the titled isoselenocyanate **3a-i**.

General procedure for the synthesis of selenoureido derivatives 7-21.

The appropriate isoselenocyanate **3a-i** (1.0 mmol) was dissolved in CH_3CN (5 mL) and treated with the corresponding benzenesulfonamide **4-6** (1.0 mmol). The mixture was stirred overnight at r.t, quenched with H_2O and the readily formed precipitate was collected by filtration and dried on air to afford the titled selenourea **7-21**.

3-(3-Phenylselenoureido)benzenesulfonamide 7:

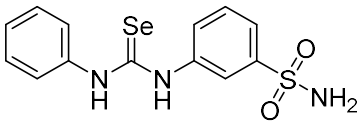

3-(3-Phenylselenoureido)benzenesulfonamide **7** was obtained according to the above reported general procedure using compound **3a** (0.09 g, 0.5 mmol). Yield 53%, 0.094 g; orange solid, M.p.180-183°C; **^{1}H-NMR** (DMSO-d_6, 400 MHz): 10.44 (1H, brs, N**H**, exchange with D_2O), 10.33 (1H, brs, N**H**, exchange with D_2O),7.43-7.38 (4H, m), 7.42 (2H, brs, N**H$_2$**, exchange with D_2O), 7.24 (1H, t, *J*= 6.8), 6.98 (2H, d, *J*= 6.8), 6.40 (2H, d, *J*= 6.8); **^{13}C-NMR** (DMSO-d_6, 100 MHz): 180.2 (*C*=Se), 145.2, 141.4, 130.8, 1329.8, 129.7, 129.2, 126.4, 125.5, 125.3, 123.0, 122.6; HRMS *m/z* $[M+H]^+$ calcd for $C_{13}H_{14}N_3O_2SSe$, 355.9966; found, 355.9972.

3-(3-(4-Fluorophenyl)selenoureido)benzenesulfonamide carboxamide 8:

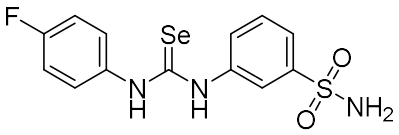

3-(3-(4-Fluorophenyl)selenoureido)benzene sulfonamide carboxamide **8** was obtained according to the above reported general procedure using compound **3b** (0.1 g, 0.5 mmol). Yield 52%, 0,097 g; white solid, M.p. 187-190°C; **^{1}H-NMR** (DMSO-d_6, 400 MHz): 10.38 (1H, brs, N**H**, exchange with D_2O), 10.31 (1H, brs, N**H**, exchange with D_2O), 7.86 (1H, s), 7.71 (1H, d, *J*=7.96),7.65 (1H, d, *J*=7.91), 7.55 (1H, t, *J*=7.87), 7.45-7.42 (2H, m), 7.44 (2H, brs, N**H$_2$**, exchange with D_2O), 7.24 (2H, apt); **^{13}C-NMR** (DMSO-d_6, 100 MHz): 180.6 (*C*=Se), 160.7 (d, *J*= 242.32), 145.2, 141.3, 136.7, 129.9, 129.2, 128.1 (d, *J*= 8.44), 123.1, 122.7, 116.3 (d, *J*= 22.75); **^{19}F-NMR** (DMSO-d_6, 376 MHz): -116.68; HRMS *m/z* $[M+H]^+$ calcd for $C_{13}H_{13}FN_3O_2SSe$, 373.9872; found, 373.9866.

4-(3-Phenylselenoureido)benzenesulfonamide 9:

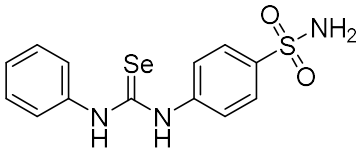

4-(3-Phenylselenoureido)benzenesulfonamide **9** was obtained according to the above reported general procedure using compound **3a** (0.09 g, 0.5 mmol). Yield 55%, 0.098 g; white solid, M.p. 181-183°C; **^{1}H-NMR** (DMSO-d_6, 400 MHz): 10.50 (1H, brs, N**H**, exchange with D_2O), 10.40 (1H, brs, N**H**, exchange with D_2O), 7.79 (2H, d, *J*=8.54), 7.65 (2H, d, *J*=8.51), 7.46-7.38 (4H, m), 7.36 (2H, brs, N**H$_2$**, exchange with D_2O), 7.24 (1H, t, *J*=7.12); **^{13}C-NMR** (DMSO-d_6, 100 MHz): 180.1 (*C*=Se), 143.8, 140.8, 140.4, 129.5, 127.0, 126.3, 125.4, 124.9; HRMS *m/z* $[M+H]^+$ calcd for $C_{13}H_{14}N_3O_2SSe$, 355.9966; found, 355.9975.

4-(3-(4-Fluorophenyl)selenoureido)benzenesulfonamide 10:

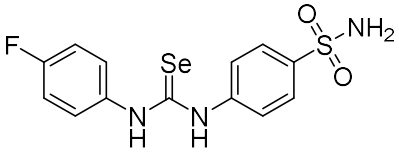

4-(3-(4-Fluorophenyl)selenoureido)benzene sulfonamide **10** was obtained according to the above reported general procedure using compound **3b** (0.1 g, 0.5 mmol). Yield 53%, 0.099 g; white solid, M.p. 187-190°C; **^{1}H-NMR** (DMSO-d_6, 400 MHz): 10.38 (2H, brs, N**H**, exchange with D_2O), 7.80 (2H, d, *J*= 8.65), 7.64 (2H, d, *J*=8.35), 7.46 (2H, m), 7.35 (2H, brs, N**H$_2$**, exchange with D_2O), 7.23 (2H, apt); **^{13}C-NMR** (DMSO-d_6, 100 MHz): 180.4 (*C*=Se), 160.7 (d, *J*= 242.58),

143.8, 140.9, 136.9, 128.1 (d, *J*= 7.90), 127.1, 125.0, 116.2 (d, *J*= 22.76); **^{19}F-NMR** (DMSO-d_6, 376 MHz): -116.83; HRMS *m/z* $[M+H]^+$ calcd for $C_{13}H_{13}FN_3O_2SSe$, 373.9872; found, 373.9868.

4-(3-(2-Fluorophenyl)selenoureido)benzenesulfonamide 11:

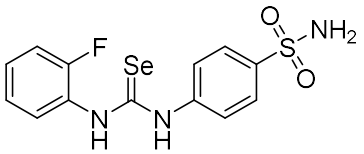

4-(3-(2-Fluorophenyl)selenoureido)benzene sulfonamide **11** was obtained according to the above reported general procedure using compound **3c** (0.1 g, 0.5 mmol). Yield 72%, 0,134 g; white solid, M.p. 188-191°C; **^{1}H-NMR** (DMSO-d_6, 400 MHz): 10.50 (1H, brs, N**H**, exchange with D_2O), 10.20 (1H, brs, N**H**, exchange with D2O), 7.83 (2H, d, *J*= 8.66), 7.67 (2H, d, *J*=8.65), 7.49 (1H, td, *J*=7.85, *J3*= 1.58), 7.38 (2H, brs, N**H**$_2$, exchange with D_2O), 7.33 (2H, m), 7.25 (1H, td, *J*= 7.67, *J3*=1.52); **^{13}C-NMR** (DMSO-d_6, 100 MHz): 181.5 (*C*=Se), 157.7 (d, *J*= 247.36), 143.6, 141.1, 130.3, 127.1, 125.4, 125.3, 117.0 (d, *J*= 19.80); **^{19}F-NMR** (DMSO-d_6, 376 MHz): -120.49; **^{77}Se-NMR** (DMSO-d_6, 76 MHz): 295; HRMS *m/z* $[M+H]^+$ calcd for $C_{13}H_{13}FN_3O_2SSe$, 373.9872; found, 373.9865.

4-(3-(3-(Trifluoromethyl)phenyl)selenoureido)benzenesulfonamide 12:

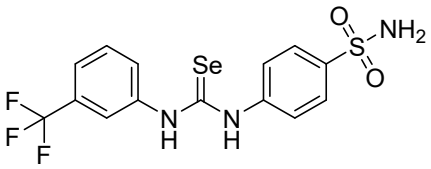

4-(3-(3-(Trifluoromethyl)phenyl)selenoureido) benzenesulfonamide **12** was obtained according to the above reported general procedure using compound **3d** (0.125 g, 0.5 mmol). Yield 62%, 0.131 g; white solid, M.p. 195-198°C; **^{1}H-NMR** (DMSO-d_6, 400 MHz): 10.65 (2H, brs, N**H**, exchange with D_2O), 7.90 (1H, s), 7.83 (2H, d, *J*= 8.67), 7.78 (1H, d, *J*= 7.92), 7.76 (2H, d, *J*= 8.70), 7.59 (2H, m),7.39 (2H, brs, N**H**$_2$, exchange with D_2O); **^{13}C-NMR** (DMSO-d_6, 100 MHz): 180.6 (*C*=Se), 143.4, 141.7, 141.1, 130.6, 130.2, 129.9, 129.5, 127.3, 126.3, 125.0, 123.6, 122.6, 122.2; **^{19}F-NMR** (DMSO-d_6, 376 MHz): -61.18; HRMS *m/z* $[M+H]^+$ calcd for $C_{14}H_{13}F_3N_3O_2SSe$, 423.9840; found, 423.9833.

4-(3-(2-Chlorophenyl)selenoureido)benzenesulfonamide 13:

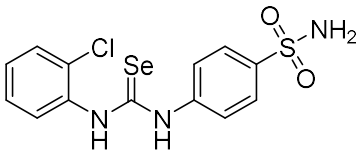

4-(3-(2-Chlorophenyl)selenoureido)benzene sulfonamide **13** was obtained according to the above reported general procedure using compound **3e** (0.108 g, 0.5 mmol). Yield 50%, 0.097 g; yellow solid, M.p. 198-201°C; **^{1}H-NMR** (DMSO-d_6, 400 MHz): 10.47 (1H, brs, N**H**, exchange with D_2O), 10.23 (1H, brs, N**H**, exchange with D_2O), 7.83 (2H, d, *J*= 8.32), 7.70 (2H, d, *J*= 8.27), 7.58 (1H, d, J= 7.28), 7.52 (1H, d, *J*= 7.14), 7.39 (2H, brs, N**H**$_2$, exchange with D_2O), 7.40 (2H, m); **^{13}C-NMR** (DMSO-d_6, 100 MHz): 181.1 (*C*=Se), 143.4, 141.1, 137.9, 131.9, 131.3, 130.6, 129.4, 128.4, 127.1, 125.3; HRMS *m/z* $[M]^+$ calcd for $C_{13}H_{12}ClN_3O_2SSe$, 388.9574 ; found, 388.9581.

4-(2-(3-Phenylselenoureido)ethyl)benzenesulfonamide 14:

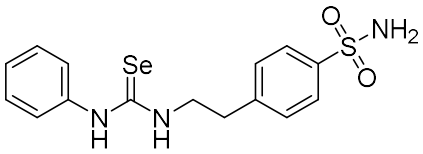

4-(2-(3-Phenylselenoureido)ethyl)benzene sulfonamide **14** was obtained according to the above reported general procedure using compound **3a** (0.09 g; 0.5 mmol). Yield 60%, 0.115 g; white solid, M.p. 210-213°C; **^{1}H-NMR** (DMSO-d_6, 400 MHz): 10.02 (1H, s, N**H**, exchange with D_2O), 8.14 (1H, brs, N**H**, exchange with D_2O), 7.81 (2H, d, *J*= 8.37), 7.48 (2H, d, *J*= 7.98), 7.39(2H, m), 7.36 (2H, brs, N**H$_2$**, exchange with D_2O), 7.22 (3H, m), 3.83 (2H, brs), 3.02 (2H, t, *J*= 7.38); **^{13}C-NMR** (DMSO-d_6, 100 MHz): 179.4 (*C*=Se), 144.3, 143.1, 139.2, 130.1, 130.0, 126.7, 126.2, 124.9, 48.7, 35.2; **^{77}Se-NMR** (DMSO-d_6, 76 MHz): 216; HRMS *m/z* $[M+H]^+$ calcd for $C_{15}H_{18}N_3O_2SSe$, 384.0279 ; found, 384.0284.

4-(2-(3-(2-Fluorophenyl)selenoureido)ethyl)benzenesulfonamide 15:

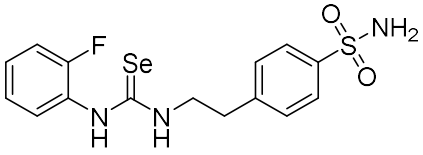

4-(2-(3-(2-Fluorophenyl)selenoureido)ethyl) benzenesulfonamide **15** was obtained according to the above reported general procedure using compound **3c** (0.1 g, 0.5 mmol). Yield 92%, 0.184 g; white solid, M.p. 202 - 205°C; **^{1}H-NMR** (DMSO-d_6, 400 MHz): 9.74 (1H, brs, N**H**, exchange with D_2O), 8.18 (1H, brs, N**H**, exchange with D_2O), 7.81 (2H, d, *J*= 8.20), 7.38 (2H, d, *J*= 8.20), 7.45 (3H, m), 7.34 (2H, brs, N**H**$_2$, exchange with D_2O), 7.25 (1H, m), 3.82 (2H, q, *J*= 5.23), 3.01

(2H, t, *J*= 7.35); **^{13}C-NMR** (DMSO-d_6, 100 MHz): 180.9 (*C*=Se), 157.2 (d, *J*= 246.73), 144.2, 143.1, 130.0, 129.9, 129.1 (d, *J*= 7.72), 127.0 (d, *J*= 13.01), 126.7, 125.4, 117.2 (d, *J*= 20.14), 48.8, 35.2; **^{19}F-NMR** (DMSO-d_6, 376 MHz): -121.28; **^{77}Se-NMR** (DMSO-d_6, 76 MHz): 207; HRMS *m/z* $[M+H]^+$ calcd for $C_{15}H_{17}FN_3O_2SSe$, 402.0185 ; found, 402.0177.

4-(2-(3-(3-(Trifluoromethyl)phenyl)selenoureido)ethyl)benzenesulfonamide 16:

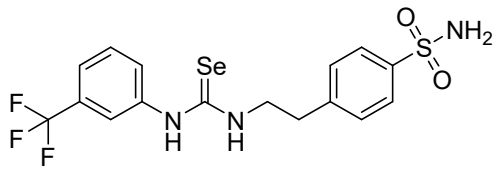

4-(2-(3-(3-(Trifluoromethyl)phenyl) selenoureido)ethyl)benzenesulfonamide **16** was obtained according to the above reported general procedure using compound **3d** (0.125 g, 0.5 mmol). Yield 65%, 0.146 g; orange solid, M.p. 202-205°C; **^{1}H-NMR** (DMSO-d_6, 400 MHz): 10.19 (1H, brs, N**H**, exchange with D_2O), 8.48 (1H, brs, N**H**, exchange with D_2O), 7.85 (1H, s), 7.83 (2H, brs), 7.58 (2H, m), 7.51 (3H, m), 7.36 (2H, brs, N**H**$_2$, exchange with D_2O), 3.89 (2H, q, *J*= 5.70), 3.06 (2H, t, *J*= 7.25); **^{13}C-NMR** (DMSO-d_6, 100 MHz): 180.4 (*C*=Se), 144.3, 143.2, 140.8, 130.9, 130.1, 128.5, 126.8, 122.1, 121.1, 48.6, 35.1; **^{19}F-NMR** (DMSO-d_6, 376 MHz): -61.26; **^{77}Se-NMR** (DMSO-d_6, 76 MHz): 225; HRMS *m/z* $[M+H]^+$ calcd for $C_{16}H_{17}F_3N_3O_2SSe$, 452.0153; found, 452.0146.

4-(2-(3-(4-Bromophenyl)selenoureido)ethyl)benzenesulfonamide 17:

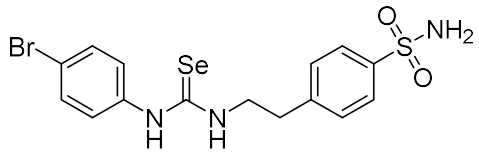

4-(2-(3-(4-Bromophenyl)selenoureido) ethyl)benzenesulfonamide **17** was obtained according to the above reported general procedure using compound **3f** (0.131 g, 0.5 mmol). Yield 60%, 0.138 g; white solid, M.p. 207-210°C; **^{1}H-NMR** (DMSO-d_6, 400 MHz): 10.02 (1H, brs, N**H**, exchange with D_2O), 8.28 (1H, brs, N**H**, exchange with D_2O), 7.82 (2H, d, *J*= 8.21), 7.54 (2H, d, *J*= 8.72), 7.48 (2H, d, J= 8.12), 7.35 (2H, brs, N**H**$_2$, exchange with D_2O), 7.21 (2H, d, *J*= 8.33), 3.83 (2H, brs), 3.03 (2H, t, *J*= 7.27); **^{13}C-NMR** (DMSO-d_6, 100 MHz): 179.9 (*C*=Se), 144.3, 143.1, 138.9, 132.7, 130.1, 127.0, 126.7, 118.2, 48.7, 35.0; HRMS *m/z* $[M+H]^+$ calcd for $C_{15}H_{17}BrN_3O_2SSe$, 461.9381; found, 461.9390.

4-(2-(3-(2-Chlorophenyl)selenoureido)ethyl)benzenesulfonamide 18:

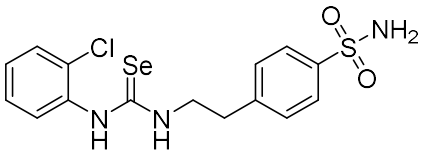

4-(2-(3-(2-Chlorophenyl)selenoureido) ethyl)benzenesulfonamide **18** was obtained according to the above reported general procedure using compound **3e** (0.108 g, 0.5 mmol). Yield 73%, 0.152 g; white solid, M.p. 206 - 209°C; **^{1}H-NMR** (DMSO-d_6, 400 MHz): 9.74 (1H, brs, N**H**, exchange with D_2O), 8.15 (1H, brs, N**H**, exchange with D_2O), 7.81 (2H, d, *J*= 8.20), 7.56 (1H, d, *J*= 7.57), 7.47 (3H, m), 7.38 (2H, m), 7.35 (2H, brs, N**H**$_2$, exchange with D_2O), 3.82 (2H, brs), 3.02 (2H, t, *J*=7.14); **^{13}C-NMR** (DMSO-d_6, 100 MHz): 180.9 (*C*=Se), 144.3, 143.1, 136.7, 131.3, 130.9, 130.7, 130.0, 129.2, 128.5, 126.7, 48.7, 35.3; HRMS *m/z* $[M+H]^+$ calcd for $C_{15}H_{17}ClN_3O_2SSe$, 417.9887; found, 417.9895.

4-(2-(3-(2-Methoxyphenyl)selenoureido)ethyl)benzenesulfonamide 19:

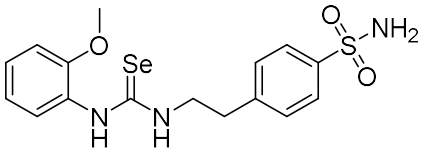

4-(2-(3-(2-Methoxyphenyl)selenoureido) ethyl)benzenesulfonamide **19** was obtained according to the above reported general procedure using compound **3g** (0.106 g, 0.5 mmol). Yield 55%, 0.113 g; white solid, M.p. 200 - 203°C; **^{1}H-NMR** (DMSO-d_6, 400 MHz): 9.42 (1H, brs, N**H**, exchange with D_2O), 7.88 (1H, brs, N**H**, exchange with D_2O), 7.80 (2H, d, *J*= 8.04), 7.46 (2H, d, *J*= 8.00), 7.41 (2H, d, *J*= 7.55), 7.33 (2H, brs, N**H**$_2$, exchange with D_2O), 7.28 (1H, t, *J*= 7.82), 7.11 (1H, d, *J*=8.16), 6.96 (1H, t, *J*= 7.58), 3.81 (4H, m), 2.99 (2H, t, *J*= 7.29); **^{13}C-NMR** (DMSO-d_6, 100 MHz): 179.5 (*C*=Se), 154.1, 144.3, 143.0, 130.0, 128.3, 128.2, 127.4, 126.7, 121.1, 113.1, 56.4, 48.6, 35.4; **^{77}Se-NMR** (DMSO-d_6, 76 MHz): 197; HRMS *m/z* $[M+H]^+$ calcd for $C_{16}H_{20}N_3O_3SSe$, 414.0385; found, 414.0391.

4-(2-(3-(4-Iodophenyl)selenoureido)ethyl)benzenesulfonamide 20:

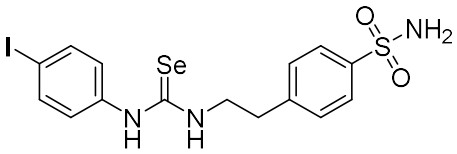

4-(2-(3-(4-Iodophenyl)selenoureido) ethyl)benzenesulfonamide **20** was obtained according to the above reported general procedure using compound **3h** (0.154 g, 0.5 mmol). Yield 81%, 0.206 g; white solid, M.p. 209-211°C; **^{1}H-NMR** (DMSO-d_6, 400 MHz): 9.99 (1H, brs,

N**H**, exchange with D_2O), 8.27 (1H, brs, N**H**, exchange with D_2O), 7.83 (2H, d, *J*= 8.18), 7.70 (2H, d, *J*= 8.59), 7.49 (2H, d, *J*= 8.12), 7.35 (2H, brs, NH_2, exchange with D_2O), 7.09 (2H, d, *J*= 8.06), 3.84 (2H, brs), 3.03 (2H, t, *J*= 7.19); **^{13}C-NMR** (DMSO-d_6, 100 MHz): 179.8 (*C*=Se), 144.3, 143.1, 139.3, 138.5, 130.1, 127.1, 126.7, 90.5, 48.7, 35.0; **^{77}Se-NMR** (DMSO-d_6, 76 MHz): 224; HRMS *m/z* $[M+H]^+$ calcd for $C_{15}H_{17}IN_3O_2SSe$, 509.9246; found, 509.9254.

4-(2-(3-(Naphthalen-2-yl)selenoureido)ethyl)benzenesulfonamide 21:

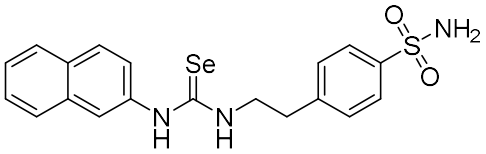

4-(2-(3-(Naphthalen-2-yl)selenoureido)ethyl)benzenesulfonamide **21** was obtained according to the above reported general procedure using compound **3i** (0.116 g, 0.5 mmol). Yield 82%, 0.177 g; white solid, M.p. 208 - 210°C; **^{1}H-NMR** (DMSO-d_6, 400 MHz): 10.19 (1H, brs, N**H**, exchange with D_2O), 8.30 (1H, brs, N**H**, exchange with D_2O), 7.92 (2H, d, *J*= 6.92), 7.85 (3H, d, *J*= 8.17), 7.74 (1H, s), 7.52 (4H,m), 7.36 (3H, brs), 3.89 (2H, brs), 3.07 (2H, t, *J*= 7.27); **^{13}C-NMR** (DMSO-d_6, 100 MHz): 179.7 (*C*=Se), 144.4, 143.1, 136.8, 134.2, 131.8, 130.1, 129.6, 128.5, 128.4, 127.4, 126.7, 126.5, 124.8, 122.2, 48.8, 35.2; **^{77}Se-NMR** (DMSO-d_6, 76 MHz): 221; HRMS *m/z* $[M+H]^+$ calcd for $C_{19}H_{20}N_3O_2SSe$, 434.0436; found, 434.0443.

General procedure for the synthesis of thioureido derivative 22:

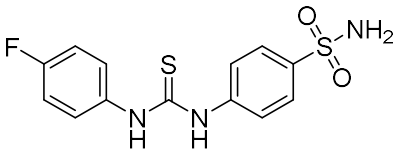

A solution of 4-fluroroaniline **1b** (1 mmol) in H_2O was treated with thiophosgene (1.5 mmol) at r.t. The mixture was stirred for 2h, was extracted with chloroform and the organic layers were dried over Na_2SO_4 and filtered. The solvent was evaporated under vacuo to afford the corresponding thioisocyanate which was immediately dissolved in CH_3CN and treated with sulphanilamide **5**. The mixture was quenched with H_2O and the precipitate formed was collected by filtration, dried on air to afford the titled thioureido derivate **22**. Yield 62%, 0.101 g; white solid, M.p. 185-188 °C; **^{1}H-NMR** (DMSO-d_6, 400 MHz): 10.11 (1H, brs, N**H**, exchange with D_2O), 10.30 (1H, brs, N**H**, exchange with D_2O), 7.80 (2H, d, *J*= 8.77), 7.72 (2H, d, *J*= 8.78), 7.52 (2H, m), 7.32 (2H, brs, N*H*, exchange with D_2O), 7.23 (2H, t, *J*= 8.87); **^{13}C-NMR** (DMSO-d_6, 100 MHz):

180.9 (*C*=Se), 160.2 (d, *J*= 241.6) , 143.5, 140.0, 136.4, 127.2, 127.1 (d, *J*=8.36), 123.6, 116.1 (d, *J*= 22.52), **^{19}F-NMR** (DMSO-d_6, 76 MHz): -117.54; HRMS *m/z* $[M+H]^+$ calcd for $C_{13}H_{13}FN_3O_2S_2$, 326.0428 ; found, 326.0425.

Procedure for the synthesis of 4-cyanobenzenesulfonamide 24:

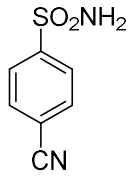

4-cyanobenzenesulfonyl chloride **23** (10 mmol) was added to a solution of anhydrous THF (40 mL). An aqueous solution of ammonium hydroxide (30%) (3mL) was added to the mixture at 0°C and stirred at room temperature for 1 h. The mixture was extracted with ethyl acetate, dried with anhydrous Na_2SO_4, and triturated with diethyl ether (1.6 g, 88%). **^{1}H NMR** (400 MHz, DMSO- d_6) δ(ppm): 8.11 (2H, d, *J*=8.58 Hz), 8.02 (2H, d, *J*=8.62 Hz), 7.69 (2H, bs, N**H$_2$**, exchange with D_2O). **^{13}C NMR** (100 MHz, DMSO- d_6) δ(ppm): 148.9, 134.2, 127.4, 118.8, 115.3.

Procedure for the synthesis of 4-sulfamoylbenzoselenoamide 25:

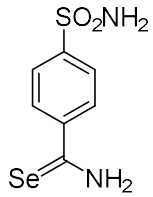

$NaBH_4$ (626 mg, 16.47 mmol, 3.0 eq.) was portion wise added to a solution of elemental selenium (650mg, 8.24 mmol, 1.5 eq.) in EtOH (20 mL) at 0°C under inert atmosphere (N_2). After 30 min, 4-cyanobenzenesulfonamide **24** (1 g, 5.49 mmol, 1.0 eq.) was added and the reaction mixture was stirred at reflux for 6h. When the starting 4-cyanobenzenesulfonamide **24** had completely reacted (monitored by TLC), cooling to room temperature and hydrochloric acid (6N, 2 ml) was added and the solution was stirred for about an hour. The organic phase was extracted with EtOAc, washed with brine (1 x 5 mL), dried over Na_2SO_4, filtered and concentrated under vacuum. The crude material was purified by flash chromatography (1:1 hexane/ethyl acetate) to yield 4-sulfamoylbenzoselenoamide (**25**) as orange solid (1.1 g, 76%). **^{1}H NMR** (400 MHz, DMSO- d_6) δ(ppm): 11.05 (1H, bs, N**H**, exchange with D_2O), 10.42 (1H, bs, N**H**, exchange with D_2O), 7.99 (2H, d, *J*=8.65 Hz), 7.85 (2H, d, *J*=8.65 Hz), 7.51 (2H, bs, N**H$_2$**, exchange with D_2O). **^{13}C NMR** (100 MHz, DMSO- d_6) δ(ppm): 203.7, 146.6, 146.3, 128.5, 126.1. **^{77}Se NMR** (76 MHz, DMSO-d_6) δ (ppm): 627.5. MS (ESI negative) *m/z* (%): 263.0 $[M-H]^-$.

General procedure for the synthesis of 2, 5 substitutes 1, 3-selenazoles (28a-f and 29a-c).

An EtOH solution (20 mL) of 4-sulfamoylbenzoselenoamide (**25**) (100 mg, 0.38 mmol) and appropriate ω-halo derivatives **26a-f** or **27a-c** (0.38 mmol, 1 Eq.) was stirred at reflux for 20 min. After cooling, the mixture was poured into H_2O (20 mL), which resulted in the formation of a precipitate. This was filtered off and recrystallized (EtOH) to give the corresponded 2,5 subtitutes 1, 3-selenazoles (**28a-f** and **29a-c**).

4-(5-phenyl-1,3-selenazol-2-yl)benzenesulfonamide 28a:

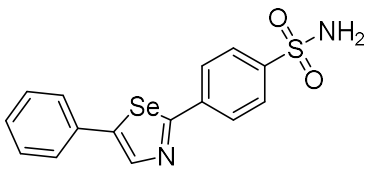

Following the general procedure, 4-sulfamoylbenzoselenoamide (**25**) (100 mg, 0.38 mmol) and 2-Bromoacetophenone **26a** (76 mg, 0.38 mmol) gave **28a** as white solid (115 mg, 83%). **^{1}H NMR** (400 MHz, DMSO- d_6) δ (ppm): 8.83 (1H, s), 8.25 (2H, d, J = 8.62 Hz), 8.11 (2H, dd, J = 8.31, 1.21 Hz), 7.99 (2H, d, J = 8.63 Hz), 7.54-7.50 (4H, m), 7.42 (1H, t, J = 7.33 Hz). **^{13}C NMR** (100 MHz, DMSO-d_6) δ (ppm): 172.6, 156.9, 146.2, 139.2, 135.6, 129.7, 129.0, 128.1, 127.6, 127.3, 123.3; **^{77}Se NMR** (76 MHz, DMSO-d_6) δ (ppm): 738.9. **MS** (ESI negative) *m/z*: 363.1 $[M-H]^-$.

4-(5-(4-fluorophenyl)-1,3-selenazol-2-yl)benzenesulfonamide 28b:

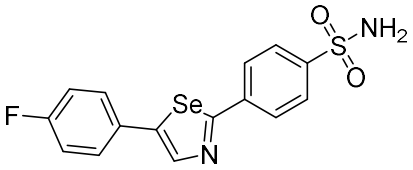

Following the general procedure, 4-sulfamoylbenzoselenoamide (**25**) (100 mg, 0.38 mmol) and 2-Bromo-4'-fluoroacetophenone **26b** (83 mg, 0.38 mmol) gave **28b** as pink solid (93 mg, 64%). **^{1}H NMR** (400 MHz, DMSO- d_6) δ (ppm): 8.81 (1H, s), 8.25 (2H, d, J = 8.42 Hz), 8.15 (2H, dd, J = 8.79, 5.54 Hz), 7.99 (2H, d, J = 8.41 Hz), 7.54 (2H, bs, N**H$_2$**, exchange with D_2O), 7.35 (2H, t, J = 8.86 Hz). **^{13}C NMR** (100 MHz, DMSO-d_6) δ (ppm): 172.7, 162.8 (d, J = 245.19 Hz), 155.8, 146.3, 139.2, 132.2, 129.4 (d, J = 8.25 Hz), 128.1, 127.6, 123.0, 116.6 (d, J = 21.55 Hz); **^{19}F-NMR** (376 MHz, DMSO-d_6) δ (ppm): -113.89; **^{77}Se NMR** (76 MHz, DMSO-d_6) δ (ppm): 741.0. **MS** (ESI negative) *m/z*: 381.1 $[M-H]^-$.

4-(5-(4-bromophenyl)-1,3-selenazol-2-yl)benzenesulfonamide 28c:

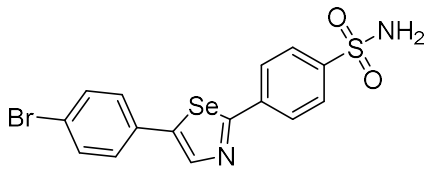

Following the general procedure, 4-sulfamoylbenzoselenoamide (**25**) (100 mg, 0.38 mmol) and 2-Bromo-4'-bromoacetophenone **26c** (106 mg, 0.38 mmol) gave **28c** as white solid(101 mg, 60%). **^{1}H NMR** (400 MHz, DMSO- d_6) δ (ppm): 8.90 (1H, s), 8.25 (2H, d, J = 8.21 Hz), 8.07 (2H, d, J = 8.38 Hz), 7.98 (2H, d, J = 8.23 Hz), 7.71 (2H, d, J = 8.35 Hz), 7.55 (2H, bs, N**H$_2$**, exchange with D_2O). **^{13}C NMR** (100 MHz, DMSO-d_6) δ (ppm): 172.9, 155.6, 146.3, 139.1, 134.8, 132.7, 129.3, 128.1, 127.6, 124.2, 122.1; **^{77}Se NMR** (76 MHz, DMSO-d_6) δ (ppm): 744.8. **MS** (ESI negative) *m/z*: 441.1 $[M-H]^-$.

4-(5-(4-chlorophenyl)-1,3-selenazol-2-yl)benzenesulfonamide 28d:

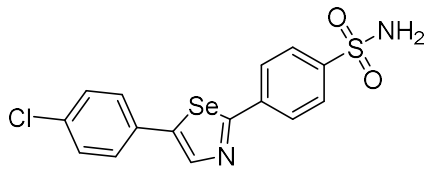

Following the general procedure, 4-sulfamoylbenzoselenoamide (**25**) (100 mg, 0.38 mmol) and 2-Bromo-4'-chloroacetophenone **26d** (89 mg, 0.38 mmol) gave **28d** as white solid(92 mg, 61%). **^{1}H NMR** (400 MHz, DMSO- d_6) δ (ppm): 8.89 (1H, s), 8.25 (2H, d, J = 8.40 Hz), 8.14 (2H, d, J = 8.55 Hz), 7.99 (2H, d, J = 8.40 Hz), 7.59-7.54 (4H, m). **^{13}C NMR** (100 MHz, DMSO-d_6) δ (ppm): 172.9, 155.6, 146.3, 139.1, 134.4, 133.5, 129.8, 129.1, 128.1, 127.6, 124.1; **^{77}Se NMR** (76 MHz, DMSO-d_6) δ (ppm): 744.2. **MS** (ESI negative) *m/z*: 397.1 $[M-H]^-$.

4-(5-(4-nitrophenyl)-1,3-selenazol-2-yl)benzenesulfonamide 28e:

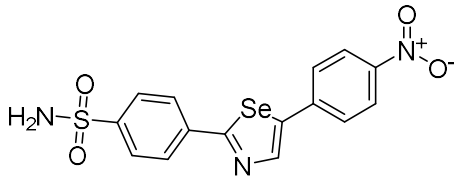

Following the general procedure, 4-sulfamoylbenzoselenoamide (**25**) (100 mg, 0.38 mmol) and 2-Bromo-4'-nitroacetophenone **26e** (93 mg, 0.38 mmol) gave **28e** as yellow solid(85 mg, 55%). **^{1}H NMR** (400 MHz, DMSO- d_6) δ (ppm): 9.19 (1H, s), 8.38 (4H, aps), 8.28 (2H, d, J = 8.48 Hz), 8.00 (2H, d, J = 8.53 Hz), 7.56 (2H, bs, N**H$_2$**, exchange with D_2O). **^{13}C NMR** (100 MHz, DMSO-d_6) δ (ppm): 173.6, 154.6, 147.6, 146.5, 141.5, 138.9, 128.3, 128.2,

127.9, 127.6, 125.2; **^{77}Se NMR** (76 MHz, DMSO-d_6) δ (ppm): 757.4. **MS** (ESI negative) *m/z*: 408.1 $[M-H]^-$.

4-(5-(3-methoxyphenyl)-1,3-selenazol-2-yl)benzenesulfonamide 28f:

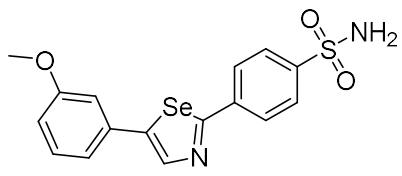

Following the general procedure, 4-sulfamoylbenzoselenoamide (**25**) (100 mg, 0.38 mmol) and 2-Bromo-3'-methoxyacetophenone **26f** (87 mg, 0.38 mmol) gave **28f** (120 mg, 80%). **^{1}H NMR** (400 MHz, DMSO- d_6) δ (ppm): 8.86 (1H, s), 8.25 (2H, d, J = 8.53 Hz), 7.99 (2H, d, J = 8.53 Hz), 7.68-7.66 (2H, m), 7.55 (2H, bs, N**H$_2$**, exchange with D_2O), 7.43 (1H, t, J = 7.94 Hz), 7.00 (1H, ddd, J = 8.53 Hz), 3.88 (3H, s). **^{13}C NMR** (100 MHz, DMSO-d_6) δ (ppm): 172.4, 160.6, 156.7, 146.2, 139.2, 136.9, 130.8, 128.1, 127.6, 123.6, 119.8, 114.5,112.9, 56.1 **^{77}Se NMR** (76 MHz, DMSO-d_6) δ (ppm): 757.4. **MS** (ESI positive) *m/z*: 395.0 $[M+H]^+$.

4-(5-methyl-1,3-selenazol-2-yl)benzenesulfonamide 29a:

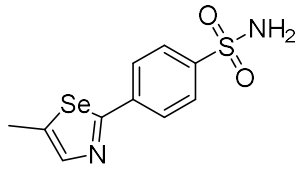

Following the general procedure, 4-sulfamoylbenzoselenoamide (**25**) (100 mg, 0.38 mmol) and Chloroacetone **27a** (31 µl, 0.38 mmol) gave **29a** as yellow solid (70 mg, 61%). **^{1}H NMR** (400 MHz, DMSO- d_6) δ (ppm): 8.12 (2H, d, J = 8.61 Hz), 7.94 (3H, m), 7.50 (2H, bs, N**H$_2$**, exchange with D_2O), 2.49 (3H, s). **^{13}C NMR** (100 MHz, DMSO-d_6) δ (ppm): 172.1, 154.8, 145.9, 139.3, 127.8, 127.5, 122.7, 18.9; **^{77}Se NMR** (76 MHz, DMSO-d_6) δ (ppm): 711.9. **MS** (ESI negative) *m/z*: 301.0 $[M-H]^-$.

2-(4-sulfamoylphenyl)-1,3-selenazole-5-carboxylic acid 29b:

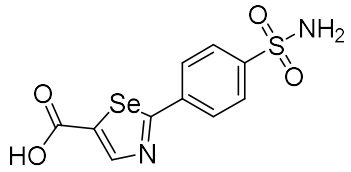

Following the general procedure, 4-sulfamoylbenzoselenoamide (**25**) (100 mg, 0.38 mmol) and Chloroacetic acid **27b** (64 mg, 0.38 mmol) gave **29b** as white solid (69 mg, 55%). **^{1}H NMR** (400 MHz, DMSO- d_6) δ (ppm): 13.07 (1H, bs, COO**H**), 9.22 (1H, apd), 8.20 (2H, d, J = 8.48 Hz), 7.98 (2H, d, J = 8.44 Hz), 7.54 (2H, bs, N**H$_2$**, exchange with D_2O). **^{13}C NMR** (100 MHz, DMSO-d_6) δ (ppm):

173.6, 173.2, 163.1, 149.1, 146.5, 138.8, 128.3, 127.6; **^{77}Se NMR** (76 MHz, DMSO-d_6) δ (ppm): 763.7. **MS** (ESI negative) *m/z*: 331.0 $[M-H]^-$.

4-(5-(chloromethyl)-1,3-selenazol-2-yl)benzenesulfonamide 29c:

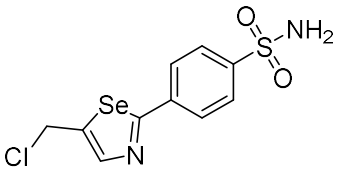

Following the general procedure, 4-sulfamoylbenzoselenoamide (**25**) (100 mg, 0.38 mmol) and 1,3 Chloroacetone **27c** (48 mg, 0.38 mmol) gave **29c** as white solid (89 mg, 70%). **^{1}H NMR** (400 MHz, DMSO- d_6) δ (ppm): 8.47 (1H, s), 8.16 (2H, d, *J* = 8.62 Hz), 7.96 (2H, d, *J* = 8.62 Hz), 7.53 (2H, bs, N**H$_2$**, exchange with D_2O), 4.93 (2H, s). **^{13}C NMR** (100 MHz, DMSO-d_6) δ (ppm): 173.8, 154.5, 146.3, 138.9, 128.3, 128.0, 127.6, 42.7; **^{77}Se NMR** (76 MHz, DMSO-d_6) δ (ppm): 728.4. **MS** (ESI negative) *m/z*: 335.0 $[M-H]^-$.

Procedure for the synthesis of 4-(5-((phenylthio)methyl)-1,3-selenazol-2-yl) benzenesulfonamide 32:

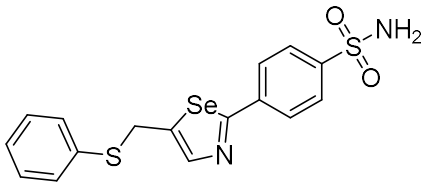

An acetonitrile solution (10 mL) of 2,5 substituted 1,3 selenazole (**29c**) (100 mg, 0.298 mmol), thiophenol (36 µL, 1.2 Eq) and Et_3N (79 µL, 2Eq) were stirred overnight at room temperature. The mixture was extracted with ethyl acetate, dried with anhydrous Na_2SO_4 and the crude material was purified by flash chromatography (1:1 hexane/ethyl acetate) to yield compound **32** as white solid (98 mg, 80%). **^{1}H NMR** (400 MHz, DMSO- d_6) δ (ppm): 8.16 (1H, s), 8.10 (2H, d, *J* = 8.36 Hz), 7.94 (2H, d, *J* = 8.34 Hz), 7.52 (2H, bs, N**H$_2$**, exchange with D_2O), 7.45 (2H, d, *J* = 7.62 Hz), 7.36 (2H, t, *J* = 7.66 Hz), 7.24 (1H, t, *J* = 7.33 Hz), 4.43 (2H, s). **^{13}C NMR** (100 MHz, DMSO-d_6) δ (ppm): 172.9, 154.8, 146.1, 139.1, 136.8, 129.9, 129.4, 127.9, 127.5, 126.8, 125.5, 34.4; **^{77}Se NMR** (76 MHz, DMSO-d_6) δ (ppm): 720.9. **MS** (ESI positive) *m/z*: 411.0 $[M+H]^+$.

4.1.14 General procedure for the synthesis of 2, 5 substitutes 1, 3-selenazoles 33a-c and 34a-c.

$NaBH_4$ (43 mg, 1.14 mmol, 3.0 eq.) was portionwise added to a solution of appropriate chalcogenide **30a-c** or **31a-c** (0.5 eq.) in EtOH (10 mL) at room temperature under inert

atmosphere (N_2). After 30 min, 2,5 substituted 1,3 selenazole **29c** (127 mg, 0.38 mmol, 1.0 eq.) was slowly added and the reaction mixture was stirred at room temperature for 3 h, until complete consumption of the starting material was observed by TLC. The reaction was quenched by addition of saturated aq. NH_4Cl (2 mL) and diluted with EtOAc (5 mL). The layers were separated and the aqueous layer was extracted with EtOAc (2 x 5 mL), dried over Na_2SO_4, filtered and concentrated under vacuum. The crude material was purified by flash chromatography (hexane/EtOAc 1:1) to yield the corresponded chalcogenide **33a-c** or **34a-c**.

4-(5-((phenyltellanyl)methyl)-1,3-selenazol-2-yl)benzenesulfonamide 33a:

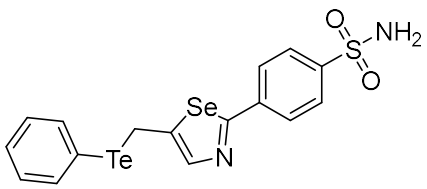

Following the general procedure, 4-(5-(chloromethyl)-1,3-selenazol-2-yl)benzene sulfonamide **29c** (127 mg, 0.38 mmol) and diphenyl ditelluride **30a** (78 mg, 0.19 mmol) gave **33a** as yellow solid (96 mg, 50%). **^{1}H NMR** (400 MHz, DMSO- d_6) δ (ppm): 8.05 (2H, d, J = 8.52 Hz), 7.93 (2H, d, J = 8.54 Hz), 7.89 (1H, s), 7.75 (2H, dd, J = 1.32, 8.06 Hz), 7.52 (2H, bs, N**H$_2$**, exchange with D_2O), 7.33-7.25 (3H, m), 4.45 (2H, s). **^{13}C NMR** (100 MHz, DMSO-d_6) δ (ppm): 172.2, 157.5, 146.0, 139.2, 138.6, 130.1, 128.4, 127.8, 127.5, 122.5, 114.4, 8.0; **^{77}Se NMR** (76 MHz, DMSO-d_6) δ (ppm): 717.6. **^{125}Te NMR** (126 MHz, DMSO-d_6) δ(ppm): 608.3. **MS** (ESI negative) *m/z*: 506.9 $[M-H]^-$.

4-(5-((p-tolyltellanyl)methyl)-1,3-selenazol-2-yl)benzenesulfonamide 33b:

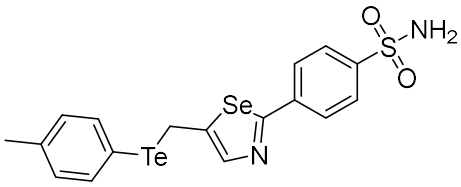

Following the general procedure, 4-(5-(chloromethyl)-1,3-selenazol-2-yl)benzenesulfonamide **29c** (127 mg, 0.38 mmol) and *p*-tolyl ditelluride **30b** (83 mg, 0.19 mmol) gave **33b** as yellow solid (154 mg, 78%). **^{1}H NMR** (400 MHz, DMSO- d_6) δ (ppm): 8.05 (2H, d, J = 8.59 Hz), 7.93 (2H, d, J = 8.60 Hz), 7.85 (1H, s), 7.63 (2H, d, J = 7.96 Hz), 7.51 (2H, bs, N**H$_2$**, exchange with D_2O), 7.09 (2H, d, J = 7.61 Hz), 4.40 (2H, s), 2.32 (3H, s). **^{13}C NMR** (100 MHz, DMSO-d_6) δ (ppm): 172.1, 157.6, 146.0, 139.2, 139.1, 138.1, 130.9, 127.8, 127.5, 122.5, 110.1, 21.6, 8.0; **^{77}Se NMR** (76 MHz, DMSO-d_6) δ (ppm): 717.0. **^{125}Te NMR** (126 MHz, DMSO-d_6) δ (ppm): 600.6. **MS** (ESI negative) *m/z*: 520.9 $[M-H]^-$.

4-(5-(((4-methoxyphenyl)tellanyl)methyl)-1,3-selenazol-2-yl)benzenesulfonamide 33c:

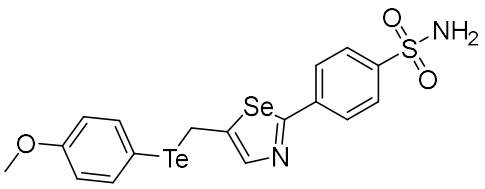

Following the general procedure, 4-(5-(chloromethyl)-1,3-selenazol-2-yl)benzenesulfonamide **29c** (127 mg, 0.38 mmol) and 4-methoxyphenyl ditelluride **30c** (89 mg, 0.19 mmol) gave **33c** as yellow solid (153 mg, 75%). **^{1}H NMR** (400 MHz, DMSO- d_6) δ (ppm): 8.05 (2H, d, J = 8.59 Hz), 7.93 (2H, d, J = 8.58 Hz), 7.85 (1H, s), 7.78 (1H, s), 7.64 (2H, d, J = 8.75 Hz), 7.51 (2H, bs, N**H$_2$**, exchange with D_2O), 6.84 (2H, d, J = 8.77 Hz), 4.35 (2H, s), 3.76 (3H, s). **^{13}C NMR** (100 MHz, DMSO-d_6) δ (ppm): 172.1, 160.3, 157.2, 146.0, 141.6, 139.2, 127.8, 127.5, 122.4, 116.1, 103.0, 55.9, 8.3; **^{77}Se NMR** (76 MHz, DMSO-d_6) δ (ppm): 716.1. **^{125}Te NMR** (126 MHz, DMSO-d_6) δ (ppm): 600.9. **MS** (ESI negative) *m/z*: 536.9 $[M-H]^-$.

4-(5-((phenylselanyl)methyl)-1,3-selenazol-2-yl)benzenesulfonamide 34a:

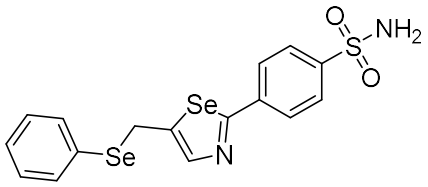

Following the general procedure, 4-(5-(chloromethyl)-1,3-selenazol-2-yl)benzenesulfonamide **29c** (127 mg, 0.38 mmol) and phenyl diselenide **31a** (59 mg, 0.19 mmol) gave **34a** as white solid (128 mg, 74%). **^{1}H NMR** (400 MHz, DMSO- d_6) δ (ppm): 8.09-8.06 (3H, m), 7.94 (2H, d, J = 8.41 Hz), 7.57 (2H, dd, J = 1.36, 8.01 Hz), 7.56 (2H, bs, N**H$_2$**, exchange with D_2O), 7.36-7.30 (3H, m), 4.41 (2H, s). **^{13}C NMR** (100 MHz, DMSO-d_6) δ (ppm): 172.7, 155.8, 146.1, 139.1, 132.9, 131.2, 130.0, 127.9, 127.8, 127.5, 124.8, 27.5; **^{77}Se NMR** (76 MHz, DMSO-d_6) δ (ppm): 719.4, 347.3. **MS** (ESI positive) *m/z*: 459.0 $[M+H]^+$.

4-(5-((p-tolylselanyl)methyl)-1,3-selenazol-2-yl)benzenesulfonamide 34b:

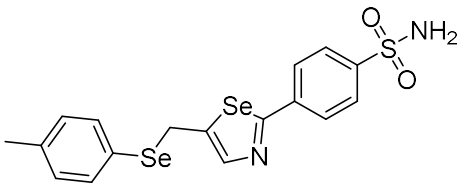

Following the general procedure, 4-(5-(chloromethyl)-1,3-selenazol-2-yl)benzenesulfonamide **29c** (127 mg, 0.38 mmol) and *p*-tolyl diselenide **31b** (65 mg, 0.19 mmol) gave **34b** as white solid (143 mg, 80%). **^{1}H NMR** (400 MHz, DMSO- d_6) δ (ppm): 8.08 (2H, d, J = 8.63 Hz), 8.01 (1H, s), 7.94 (2H, d, J = 8.63 Hz), 7.52 (2H, bs, N**H$_2$**, exchange with

D_2O), 7.44 (2H, d, *J* = 8.05 Hz), 7.16 (2H, d, *J* = 7.81 Hz), 4.35 (2H, s), 2.31 (3H, s). **^{13}C NMR** (100 MHz, DMSO-*d_6*) δ (ppm): 172.6, 156.0, 146.1, 139.2, 137.4, 133.5, 130.7, 127.8, 127.5, 127.2, 124.7, 27.9, 21.5; **^{77}Se NMR** (76 MHz, DMSO-*d_6*) δ (ppm): 722.2 **MS** (ESI positive) *m/z*: 473.0 $[M+H]^+$.

4-(5-(((4-methoxyphenyl)selanyl)methyl)-1,3-selenazol-2-yl)benzene sulfonamide 34c:

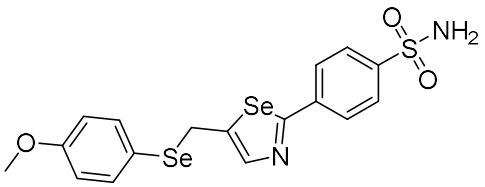

Following the general procedure, 4-(5-(chloromethyl)-1,3-selenazol-2-yl)benzenesulfonamide **29c** (127 mg, 0.38 mmol) and 4-methoxyphenyl diselenide **31c** (71 mg, 0.19 mmol) gave **34c** as white solid (129 mg, 70%). **^{1}H NMR** (400 MHz, DMSO- *d_6*) δ (ppm): 8.08 (2H, d, *J* = 8.54 Hz), 7.95-7.92 (3H, m), 7.51 (2H, bs, N**H$_2$**, exchange with D_2O), 7.46 (2H, d, *J* = 8.80 Hz), 6.91 (2H, d, *J* = 8.80 Hz), 4.28 (2H, s), 3.77 (3H, s). **^{13}C NMR** (100 MHz, DMSO-*d_6*) δ (ppm): 172.6, 159.9, 156.0, 146.0, 139.2, 136.3, 127.8, 127.5, 124.5, 120.5, 115.7, 56.0, 28.7; **^{77}Se NMR** (76 MHz, DMSO-*d_6*) δ (ppm): 717.8, 341.4. **MS** (ESI negative) *m/z*: 485.1 $[M-H]^-$.

Procedure for the synthesis of 2-((2-(4-sulfamoylphenyl)-1,3-selenazol-5-yl)methyl) isothiouronium chloride 35:

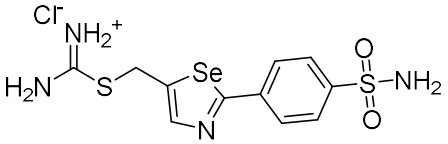

4-(5-(chloromethyl)-1,3-selenazol-2-yl)benzenesulfonamide **29c** (127 mg, 0.38 mmol) and Thiourea (29mg, 0.38 mmol) were dissolved in dry acetone. The mixture was stirred at reflux for 1h and after cooling, the precipitate was filtered off and washed with cold acetone to yield compound **35** as grey solid (78 mg, 50%). **^{1}H NMR** (400 MHz, DMSO- *d_6*) δ (ppm): 9.37 (2H, bs, N**H$_2$**, exchange with D_2O), 8.37 (1H, s), 8.14 (2H, d, *J* = 8.41 Hz), 7.96 (2H, d, *J* = 8.40 Hz), 7.56 (2H, bs, N**H$_2$**, exchange with D_2O), 7.13 (2H, bs, N**H$_2$**, exchange with D_2O), 4.71 (2H, s). **^{13}C NMR** (100 MHz, DMSO-*d_6*) δ (ppm): 174.2, 170.4, 152.3, 146.4, 138.7, 128.0, 127.6, 127.1, 32.0; **^{77}Se NMR** (76 MHz, DMSO-*d_6*) δ (ppm): 731.5. **MS** (ESI positive) *m/z*: 377.0 $[M+H]^+$.

General procedure for the synthesis of aryl ditellurides 37a-g:

To a stirred solution of appropriate bromo derivatives **36a-g** (8.5 mmol) in dry THF (40 mL) under N_2 at -78°C was added butyllithium (7.5 mL, 1.7 M; 12.75 mmol). After 1 h, the cooling bath was removed and freshly crushed finely ground elemental tellurium (8.5 mmol) was added while a brisk stream of nitrogen was passed through the open system. After 1 hour, when only trace amounts of tellurium remained, the dark solution was quenched with a saturate solution of NH_4Cl. After extraction with diethyl ether, separation, drying of the organic phase with $NaSO_4$ and evaporation, the pure product was obtained by flash chromatography with appropriate mixture of hexane/ethyl acetate.

1, 2-bis (3,4,5-trimethoxyphenyl) ditellane 37g:

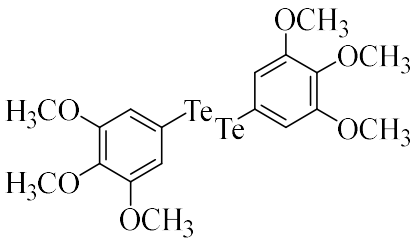

Following the general procedure, the product was gave after flash chromatography (hexane/ethyl acetate 70:30)as a red solid **37g** (2 g, 80%). **^{1}H NMR** (400 MHz, $CDCl_3$) δ(ppm): 6.99 (2H, s), 3.86 (3H, s), 3.79 (6H, s) **^{13}C NMR** (100 MHz, $CDCl_3$) δ(ppm): 153.4, 145.4, 116.0, 102.2, 61.3, 56.5 **^{125}Te NMR** (126 MHz, $CDCl_3$) δ(ppm) : 489.5 MS (ESI positive) *m/z*: $[M+H]^+$: 595

General Procedure for the synthesis of 39a-g

$NaBH_4$ (57 mg, 1.5 mmol, 3.0 eq.) was portionwise added to a solution of appropriate ditelluride **39a-g** (0.5 mmol, 0.5 eq.) in EtOH (10 mL) at room temperature under inert atmosphere (N_2). After 30 min, 4-(Bromomethyl) benzenesulfonamide **38** (250 mg, 1 mmol, 1.0 eq.) was slowly added and the reaction mixture was stirred at room temperature for 3 h, until complete consumption of the starting material was observed by TLC. The reaction was quenched by addition of saturated aq. NH_4Cl (2 mL) and diluted with EtOAc (5 mL). The layers were separated and the aqueous layer was extracted with EtOAc (2 x 5 mL), dried over Na_2SO_4, filtered and concentrated under vacuum. The crude material was purified by flash chromatography (hexane/EtOAc 1:1) to yield the corresponded telluride **39a-g**.

4-((phenyltellanyl)methyl)benzenesulfonamide 39a:

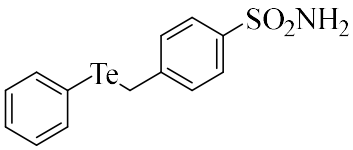

Following the general procedure, **37a** (0.5 mmol) and **38** (1 mmol) gave after flash chromatography (Hex/EtOAc 1:1) **39a** (236 mg, 63%). **^{1}H NMR** (400 MHz, DMSO) δ(ppm): 7.69-7.64 (4H, m), 7.34-7-25 (7H, m), 4.37 (2H, s) **^{13}C NMR** (100 MHz, DMSO) δ(ppm): 147.0, 142.5, 138.8, 130.2, 129.3, 128.7, 126.5, 114.1, 11.6. **^{125}Te NMR** (126 MHz, DMSO) δ(ppm) : 682.3 MS (ESI positive) *m/z*: 395 $[M+NH_4]^+$

4-((o-tolyltellanyl)methyl)benzenesulfonamide 39b:

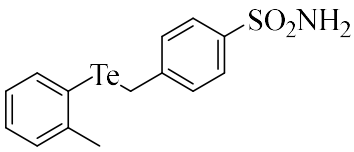

Following the general procedure, **37b** (0.5 mmol) and **38** (1 mmol) gave after flash chromatography (Hex/EtOAc 1:1) **39b** (236 mg, 63%). **^{1}H NMR** (400 MHz, DMSO) δ(ppm): 7.75-7.72 (2H, m), 7.66 (2H, d, *J*=8.32), 7.38 (2H, d, *J*=8.39), 7.29-7.10 (3H, m),7.08 (1H, td, *J*=7.36, 1.18), 4.36 (2H, s), 2.31 (3H, s). **^{13}C NMR** (100 MHz, DMSO) δ(ppm): 146.5, 138.6, 130.2, 130.0, 129.5, 127.6, 127.3, 126.5, 118.3, 26.8, 11.2. **^{125}Te NMR** (126 MHz, DMSO) δ(ppm) : 564.0 MS (ESI positive) *m/z*: 396 $[M+Li]^+$

4-((p-tolyltellanyl)methyl)benzenesulfonamide (39c)

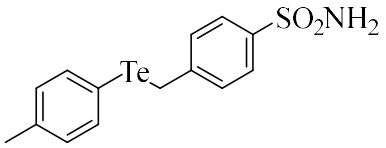

Following the general procedure, **37c** (0.5 mmol) and **38** (1 mmol) gave after flash chromatography (Hex/EtOAc 1:1) **39c** (257 mg, 66%). **^{1}H NMR** (400 MHz, DMSO) δ(ppm): 7.65 (2H, d, *J*=8.3 Hz), 7.57 (2H, d, *J*=7.9 Hz), 7.32-7.29 (5H, m), 7.10 (2H, d, *J*=7.7 Hz), 4.32 (2H, s), 2.33 (3H, s) **^{13}C NMR** (100 MHz, DMSO) δ(ppm): 147.1, 142.5, 139.2, 138.3, 131.1, 129.3, 126.5, 109.8, 21.7, 11.7. **^{125}Te NMR** (126 MHz, DMSO) δ(ppm): 672.9 MS (ESI positive) *m/z*: 407 $[M+NH_4]^+$

4-(((4-methoxyphenyl)tellanyl)methyl)benzenesulfonamide 39d:

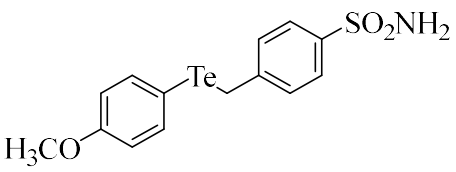

Following the general procedure, **37d** (0.5 mmol) and **38** (1 mmol) gave after flash chromatography (Hex/EtOAc 1:1) **39d** (271 mg, 67%). **^{1}H NMR**

(400 MHz, DMSO) δ(ppm): 7.64 (2H, d, *J*=8.3 Hz), 7.58 (2H, d, *J*=8.7 Hz), 7.29 (2H, brs, N**H**$_2$, exchange with D_2O), 7.25 (2H, d, *J*=8.3 Hz), 6.85 (2H, d, *J*=8.7 Hz), 4.27 (2H, s), 3.79 (3H, s) **^{13}C NMR** (100 MHz, DMSO) δ(ppm): 160.4, 147.1, 141.6, 130.2, 129.2, 126.4, 116.2, 102.7, 55.9, 12.0. **^{125}Te NMR** (126 MHz, DMSO) δ(ppm) : 672.9 MS (ESI positive) *m/z*: 425 $[M+NH_4]^+$

4-((naphthalen-2-yltellanyl)methyl)benzenesulfonamide 39e:

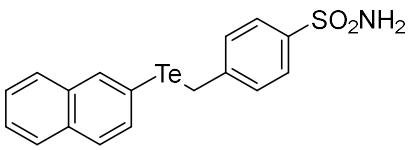

Following the general procedure, **37e** (0.5 mmol) and **38** (1 mmol) gave after flash chromatography (Hex/EtOAc 1:1) **39e** (259 mg, 61%). **^{1}H NMR** (400 MHz, DMSO) δ(ppm): 8.26 (1H, s), 7.93 (1H, dd, *J*=6.1, 2.9 Hz), 7.87 (1H, dd, *J*=6.2, 2.9 Hz) 7.82-7.76 (2H, m), 7.64 (2H, d, *J*=8.3 Hz), 7.57-7.54 (2H, m), 7.38 (2H, d, *J*=8.3 Hz), 7.24 (2H, brs, N**H**$_2$, exchange with D_2O), 4.47 (2H, s) **^{13}C NMR** (100 MHz, DMSO) δ(ppm): 147.1, 142.5, 137.9, 135.4, 134.7, 133.0, 129.4, 129.1, 128.5, 128.0, 127.4, 127.3, 126.5, 11.8. **^{125}Te NMR** (126 MHz, DMSO) δ(ppm) : 684.5 MS (ESI positive) *m/z*: 428 $[M+H]^+$

4-(((2,6-dimethylphenyl)tellanyl)methyl)benzenesulfonamide 39f:

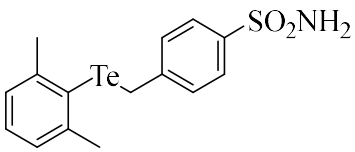

Following the general procedure, **37f** (0.5 mmol) and **38** (1 mmol) gave after flash chromatography (Hex/EtOAc 1:1) **39f** (278 mg, 69%). **^{1}H NMR** (400 MHz, DMSO) δ(ppm): 7.59 (2H, d, *J*=8.35 Hz), 7.28 (2H, brs, N**H**$_2$, exchange with D_2O), 7.21-7.17 (3H, m), 7.13 (2H, d, *J*=8.36 Hz), 4.13 (2H, s), 2.47 (6H, s). **^{13}C NMR** (100 MHz, DMSO) δ(ppm): 146.9, 146.0, 130.2, 128.9, 127.0, 126.3, 122.1, 30.2, 11.0. **^{125}Te NMR** (126 MHz, DMSO) δ(ppm) : 460.4 MS (ESI positive) *m/z*: 412 $[M+Li]^+$

4-(((3,4,5-trimethoxyphenyl)tellanyl)methyl)benzenesulfonamide 39g:

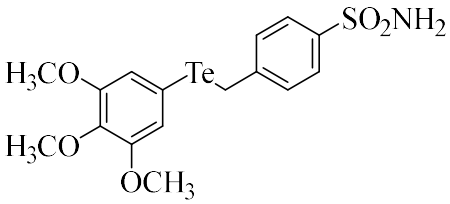

Following the general procedure, **37g** (0.5 mmol) and **38** (1 mmol) gave after flash chromatography (Hex/EtOAc 1:1) **39g** (335 mg, 72%). **^{1}H NMR** (400 MHz, DMSO) δ(ppm): 7.68 (2H, d, *J*=8.36 Hz), 7.36 (2H, d, *J*=8.38 Hz), 7.29 (2H, brs, N**H**$_2$, exchange with D_2O), 6.85 (2H, s), 4.39 (2H, s), 3.75 (6H, s), 3.68 (3H, s). **^{13}C NMR** (100

MHz, DMSO) δ(ppm): 154.0, 146.9, 142.5, 138.6, 129.6, 126.5, 116.6, 106.9, 61.0, 56.9, 12.2. **^{125}Te NMR** (126 MHz, DMSO) δ(ppm) : 719.5 MS (ESI positive) *m/z*: 485 $[M+Na]^+$

General procedure for the synthesis of □-hydroxy aryltellurides 42a-e

$NaBH_4$ (30 mg, 0.80 mmol, 4.0 eq.) was portionwise added to ditelluride **37** (0.20 mmol, 1.0 eq.) and NaOH (0.40 mmol, 2.0 eq.) in EtOH (5 mL) at 0°C under inert atmosphere (N_2). After 10 min, the epoxide **40** (102 mg, 0.36 mmol, 1.8 eq.) was slowly added and the reaction mixture was stirred at room temperature for 12 h. The reaction was quenched by addition of saturated aq. NH_4Cl (5 mL) and diluted with EtOAc (10 mL), The layers were separated and the aqueous layer was extracted with EtOAc (2 x 5 mL), dried over Na_2SO_4, filtered and concentrated under vacuum. The crude material was purified by flash chromatography to yield β-hydroxy aryltellurides (**42a-e**).

4-(2-Hydroxy-3-(phenyltellanyl)propoxy)benzenesulfonamide 42a:

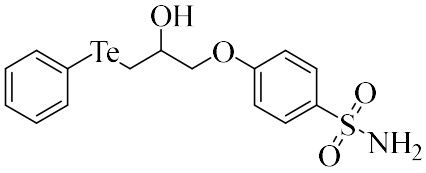

Following the general procedure, **37a** (66 mg, 0.16 mmol) and **40** (82 mg, 0.29 mmol) gave, after flash column chromatography (petroleum ether/EtOAc 1:1), telluride **42a** (81, 64%). **^{1}H NMR** (400 MHz, $CDCl_3$) δ (ppm): 2.61 (1H, bd, *J* = 4.6 Hz, OH), 3.15 (1H, dd, *J* = 6.8, 12.6 Hz, C**H$_a$**H$_b$Te), 3.20 (1H, dd, *J* = 6.1, 12.6 Hz, CH$_a$**H$_b$**Te), 4.04 (1H, dd, *J* = 6.0, 9.4 Hz, C**H$_a$**H$_b$O), 4.08 (1H, dd, *J* = 4.1, 9.4 Hz, CH$_a$**H$_b$**O), 4.15-4.23 (1H, m, C**H**OH), 4.78 (2H, bs, NH_2), 6.90 (2H, ap d, *J* = 8.9 Hz), 7.19 (2H, ap t, *J* = 7.4 Hz), 7.26-7.30 (1H, m), 7.45-7.78 (2H, m), 7.83 (2H, ap d, *J* = 8.9 Hz). **^{13}C NMR** (100 MHz, $CDCl_3$) δ (ppm): 13.7, 69.8, 71.9, 111.0, 114.7, 128.1, 128.6, 129.4, 134.2, 138.6, 161.7. **^{125}Te NMR** (126 MHz, $CDCl_3$) δ (ppm): 392.1. **MS** (ESI negative) *m/z* (%): 436 $[M-H]^-$ (100).

4-(2-Hydroxy-3-(*o*-tolyltellanyl)propoxy)benzenesulfonamide 42b:

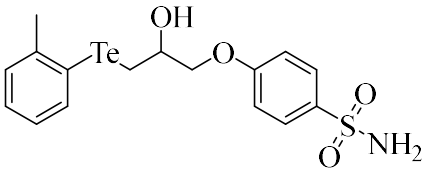

Following the general procedure, **37b** (52 mg, 0.12 mmol) and **40** (61 mg, 0.22 mmol) gave, after flash column chromatography (petroleum ether/EtOAc 1:1), telluride **42b** (48 mg, 48%). **^{1}H NMR** (400 MHz, $CDCl_3$) δ (ppm): 2.46 (3H, s), 2.87 (1H, bs, OH), 3.10-3.18 (2H, m, CH_2Te), 3.99-

4.07 (2H, m, CH_2O), 4.14-4.24 (1H, m, C**H**OH), 5.11 (2H, bs, NH_2), 6.86 (2H, ap d, *J* = 8.4 Hz), 6.97 (1H, t, *J* = 7.2 Hz), 7.15-7.21 (2H, m), 7.69 (1H, d, *J* = 7.5 Hz), 7.78 (2H, d, *J* = 8.4 Hz). **^{13}C NMR** (100 MHz, $CDCl_3$) δ (ppm): 12.5, 26.6, 69.9, 71.9, 114.7, 126.7, 128.3, 128.5, 129.3, 134.2, 134.2, 137.8, 142.6, 161.6. **^{125}Te NMR** (126 MHz, $CDCl_3$) δ (ppm): 283.6. **MS** (ESI negative) *m/z* (%): 450 $[M-H]^-$ (100).

4-(2-hydroxy-3-(*p*-tolyltellanyl)propoxy)benzenesulfonamide 42c:

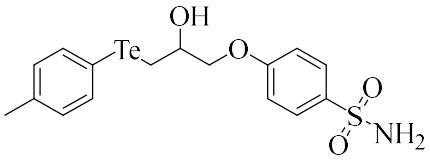

Following the general procedure, **37c** (52 mg, 0.12 mmol) and **40** (61 mg, 0.22 mmol) gave, after flash column chromatography (petroleum ether/EtOAc 3:1), telluride **42c** (53 mg, 54%). **^{1}H NMR** (400 MHz, $CDCl_3$) δ (ppm): 2.31 (3H, s), 2.60 (1H, bs, OH), 3.11 (1H, dd, *J* = 6.6, 12.5 Hz, C**H$_a$**H$_b$Te), 3.16 (1H, dd, *J* = 5.9, 12.5 Hz, CH$_a$**H$_b$**Te), 4.02 (1H, dd, *J* = 6.0, 9.4 Hz, C**H$_a$**H$_b$O), 4.06 (1H, dd, *J* = 4.1, 9.4 Hz, CH$_a$**H$_b$**O), 4.11-4.20 (1H, m, C**H**OH), 4.76 (2H, bs, NH_2), 6.89 (2H, ap d, *J* = 9.0 Hz), 6.99 (2H, ap d, *J* = 7.6 Hz), 7.65 (2H, ap d, *J* = 7.6 Hz), 7.82 (2H, ap d, *J* = 9.0 Hz). **^{13}C NMR** (100 MHz, $CDCl_3$) δ (ppm): 13.8, 21.2, 69.8, 71.7, 106.8, 114.7, 128.6, 130.4, 134.1, 138.4, 139.0, 161.7. **^{125}Te NMR** (126 MHz, $CDCl_3$) δ (ppm): 376.5. **MS** (ESI negative) *m/z* (%): 450 $[M-H]^-$ (100).

4-(2-Hydroxy-3-((4-methoxyphenyl)tellanyl)propoxy)benzenesulfonamide 42d:

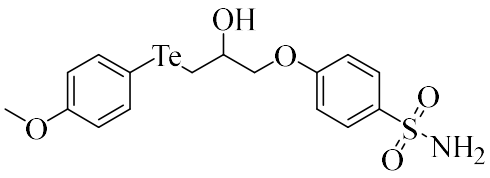

Following the general procedure, **37d** (47 mg, 0.10 mmol) and **40** (51 mg, 0.18 mmol) gave, after flash column chromatography (petroleum ether/EtOAc 1:1), telluride **42d** (43, 51%). **^{1}H NMR** (400 MHz, $CDCl_3$) δ (ppm): 2.64 (1H, bd, *J* = 5.1 Hz, OH), 3.05 (1H, dd, *J* = 6.5, 12.5 Hz, C**H$_a$**H$_b$Te), 3.13 (1H, dd, *J* = 6.0, 12.5 Hz, CH$_a$**H$_b$**Te), 3.77 (3H, s, CH_3O), 4.01 (1H, dd, *J* = 4.6, 8.2 Hz, C**H$_a$**H$_b$O), 4.04 (1H, dd, *J* = 3.1, 8.2 Hz, CH$_a$**H$_b$**O), 4.10-4.17 (1H, m, C**H**OH), 4.92 (2H, bs, NH_2), 6.68 (2H, ap d, *J* = 8.7 Hz), 6.85 (2H, ap d, *J* = 9.0 Hz), 7.67 (2H, ap d, *J* = 8.7 Hz), 7.79 (2H, ap d, *J* = 9.0 Hz). **^{13}C NMR** (100 MHz, $CDCl_3$) δ (ppm): 14.1, 55.2, 69.9, 71.5, 99.9, 114.7, 115.3, 128.5, 134.1, 141.0, 159.9, 161.6. **^{125}Te NMR** (126 MHz, $CDCl_3$) δ (ppm): 369.4. **MS** (ESI negative) *m/z* (%): 466 $[M-H]^-$ (100).

4-(2-Hydroxy-3-(naphthalen-2-yltellanyl)propoxy)benzenesulfonamide 42e:

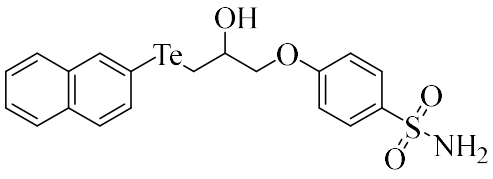

Following the general procedure, **37e** (51 mg, 0.10 mmol) and **40** (51 mg, 0.18 mmol) gave, after flash column chromatography (petroleum ether/EtOAc 1:1), telluride **42e** (38 mg, 43%). **^{1}H NMR** (400 MHz, $CDCl_3$) δ (ppm): 2.65 (1H, bd, *J* = 5.3 Hz, OH), 3.22 (1H, dd, *J* = 6.5, 12.6 Hz, C**H$_a$**H$_b$Te), 3.28 (1H, dd, *J* = 6.0, 12.5 Hz, CH$_a$**H$_b$**Te), 4.02 (1H, dd, *J* = 4.4, 8.2 Hz, C**H$_a$**H$_b$O), 4.06 (1H, dd, *J* = 3.0, 8.2 Hz, CH$_a$**H$_b$**O), 4.17-4.25 (1H, m, C**H**OH), 4.78 (2H, bs, NH_2), 6.79 (2H, ap d, *J* = 8.8 Hz), 7.44-7.51 (2H, m), 7.62 (1H, d, *J* = 8.4 Hz), 7.68-7.63 (1H, m), 7.71 (2H, ap d, *J* = 8.8 Hz), 7.76-7.79 (2H, m), 8.26 (1H, s). **^{13}C NMR** (100 MHz, $CDCl_3$) δ (ppm): 13.9, 69.9, 71.6, 108.3, 114.6, 126.5, 126.6, 127.2, 127.8, 128.5, 128.6, 132.6, 134.1, 135.0, 138.4, 161.5. **^{125}Te NMR** (126 MHz, $CDCl_3$) δ (ppm): 393.6. **MS** (ESI negative) *m/z* (%): 486 $[M-H]^-$ (100).

4,4'-((Tellurobis(2-hydroxypropane-3,1-diyl))bis(oxy))dibenzenesulfonamide 43:

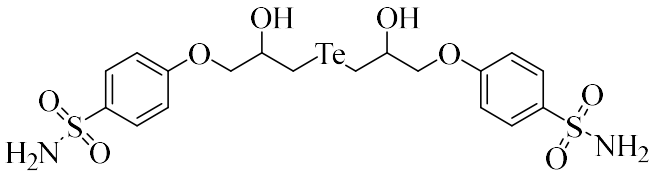

A solution of the epoxide **40** (141 mg, 0.5 mmol, 2.0 eq.) in dry DMF was slowly added to a suspension of Li_2Te in THF, generated *in situ* according to literature from elemental tellurium (32 mg, 0.25 mmol., 1.0 eq.) and $LiEt_3BH$ (1.0 mL of a 1M THF solution; 1.0 mmol, 4.0 eq.). The reaction was stirred for 12 h at ambient temperature and then treated with a NaOH 1M solution. The reaction mixture was stirred at ambient temperature for 4 h and then diluted with EtOAc (10 mL), filtered through a short pad of celite, washed with NH_4Cl and with H_2O (2 x 5 mL). The organic phase was dried over Na_2SO_4, filtered and evaporated under reduced pressure. The crude material was purified by flash column chromatography (petroleum ether/EtOAc 1:1) to afford □-hydroxy telluride **43** as a pale yellow solid (79 mg, 74%). **^{1}H NMR** (400 MHz, DMSO-*d$_6$*) δ (ppm) 2.84 (4H, dd, *J* = 5.5, 12.0 Hz, C**H$_a$**H$_b$Te), 2.90 (4H, dd, *J* = 3.9, 12.0 Hz, CH$_a$**H$_b$**Te), 3.97-4.08 (12H, m, CH_2O and C**H**OH), 5.32 (4H, bd, *J* = 3.8 Hz, OH), 7.08 (2H, ap d, *J* = 8.9 Hz), 7.18 (2H, bs, NH_2), 7.75 (2H, ap d, *J* = 8.9 Hz). **^{13}C NMR** (100 MHz,

DMSO-d_6) δ (ppm): 9.8, 70.5, 73.7, 115.6, 128.7, 137.3, 162.0. **^{125}Te NMR** (126 MHz, DMSO-d_6) δ (ppm): 117.5, 118.5. **MS** (ESI negative) *m/z* (%): 589 $[M-H]^-$ (100).

General procedure for the synthesis of compounds 45a-b:

$NaBH_4$ (3.0 eq.) was portionwise added to a solution of appropriate diselenides **44a-b** (1 eq.) in EtOH at room temperature under inert atmosphere (N_2). After 30 min, cinnamoyl chloride (2.0 eq.) was slowly added and the reaction mixture was stirred at room temperature for 2 h, until complete consumption of the starting material was observed by TLC. The reaction was quenched by addition of saturated aq. NH_4Cl and diluted with EtOAc (5 mL). The layers were separated and the aqueous layer was extracted with EtOAc, dried over Na_2SO_4, filtered and concentrated under vacuum. The crude material was purified by flash chromatography (hexane/EtOAc 90:10) to yield the corresponded compounds **45a-b**.

General procedure for the synthesis of compounds 46a-b:

Selenophenylcinnamates (**45a-b**) were mixed with anhydrous $AlCl_3$ (5 eq) in chlorobenzene and heated at 100°C for 30 minutes. When the colour of the reaction mixture changed from yellow to red and TLC indicated the disappearance of starting materials, the reaction mixture was quenched with ice-cold diluted HCl and extracted with chloroform. The organic layer was dried over magnesium sulfate, filtered and evaporated under reduced pressure. The residue was purified by column chromatography (benzene/hexane 50:50) to give the title compounds **46a-b**.

2H-selenochromen-2-one 46a:

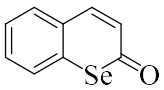

Following the general procedure, **45a** (1 equiv) and $AlCl_3$ (5 equiv) gave **46a** as yellow solid (yield 70%). **^{1}H NMR** (400 MHz, $CDCl_3$) δ (ppm): 6.24 (1H, d, *J*= 11.00 Hz), 7.38 (1H, m), 7.45 (1H, td, *J*= 7.61, 1.48 Hz), 7.59 (1H, dd, *J*= 7.90, 1.30 Hz), 7.65 (1H, dd, *J*= 7.71, 1.18 Hz), 7.69 (1H, d, *J*= 11.01 Hz). **^{13}C NMR** (100 MHz, $CDCl_3$) δ (ppm): 123.9, 126.8, 127.9, 129.2, 130.3, 133.7, 138.0, 145.1, 189.9 **^{77}Se NMR** (76 MHz, $CDCl_3$) δ (ppm): 628.8 **MS** (ESI positive) *m/z*: 211.1 $[M+H]^+$ ($[M+H]^+$ 210.96 required).

6-methyl-2H-selenochromen-2-one 46b:

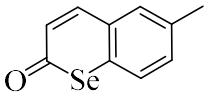

Following the general procedure, **46b** (1 equiv) and $AlCl_3$ (5 equiv) gave **47b** as yellow solid (yield 50%). **^{1}H NMR** (400 MHz, $CDCl_3$) δ (ppm): 2.41 (3H, s), 6.16 (1H, d, *J*= 10.97 Hz), 7.17 (1H, dd, *J*= 7.96, 0.98 Hz), 7.38 (1H, s), 7.51 (1H, d, *J*= 7.97), 7.63 (1H, d, *J*= 10.97). **^{13}C NMR** (100 MHz, $CDCl_3$) δ (ppm): 21.8, 122.8, 125.4, 128.1, 129.3, 133.5, 138.0, 141.1, 145.0, 190.0 **^{77}Se NMR** (76 MHz, $CDCl_3$) δ (ppm): 624.7 **MS** (ESI positive) *m/z*: 225.1 $[M+H]^+$ ($[M+H]^+$ 224.97 required).

General procedure for the synthesis of compounds 47a-b:

Seleno-coumarin **46a-b** and Lawesson's reagent (2 eq) in dry toluene were refluxed for 4h. Upon cooling to room temperature, water was added and extracted with ethyl acetate (20 mL x 3). The organic layer was dried over magnesium sulfate, filtered and evaporated under reduced pressure. The residue was purified by column chromatography (hexane/ethyl acetate 90:10) to give the title compounds **47a-b**.

2H-selenochromene-2-thione 47a:

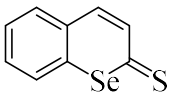

Following the general procedure, **46a** (1 equiv) and Lawesson's reagent (2 equiv) gave **47a** as red solid (87%). **^{1}H NMR** (400 MHz, $CDCl_3$) δ (ppm): 7.10 (1H, d, *J*= 10.54 Hz), 7.37-7.42 (2H, m), 7.55-7.48 (2H, m), 7.72 (1H, dd, *J*= 7.79, 0.95). **^{13}C NMR** (100 MHz, $CDCl_3$) δ (ppm): 126.5, 127.9, 129.5, 130.5, 133.5, 135.6, 137.0, 141.1, 216.2 **^{77}Se NMR** (76 MHz, $CDCl_3$) δ (ppm): 771.6 **MS** (ESI positive) *m/z*: 225.8 $[M]^+$. ($[M]^+$ 225.94 required).

6-methyl-2H-selenochromene-2-thione 47b:

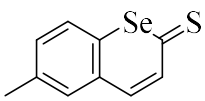

Following the general procedure, **46b** (1 equiv) and Lawesson's reagent (2 equiv) gave **47b** as red solid (80%). **^{1}H NMR** (400 MHz, $CDCl_3$) δ (ppm): 2.41 (3H, s) 7.06 (1H, d, *J*= 10.46 Hz), 7.20 (1H, d, *J*= 7.99 Hz) 7.35-7.41 (2H, m), 7.60 (1H, d, *J*= 8.01). **^{13}C NMR** (100 MHz, $CDCl_3$) δ (ppm): 21.9, 126.7, 129.3, 130.5, 132.3, 135.7, 136.2, 136.9, 141.6, 215.9 **^{77}Se NMR** (76 MHz, $CDCl_3$) δ (ppm): 767.7 **MS** (ESI positive) *m/z*: 241.1 $[M+H]^+$ ($[M+H]^+$ 240.95 required).

General procedure for the synthesis of compounds 49a-f:

Appropriate amines **48a-f** (1.0 eq.) were added to a solution of cinnamoyl chloride (1 eq.) in DCM at room temperature under inert atmosphere (N_2) and Et_3N was added drop by drop. The reaction was quenched by addition of saturated aq. NH_4Cl and diluted with EtOAc (5 mL). The layers were separated and the aqueous layer was extracted with EtOAc, dried over Na_2SO_4, filtered and concentrated under vacuum. The crude material was purified by flash chromatography (hexane/EtOAc 70:30) to yield the corresponded compounds **49a-f**.

General procedure for the synthesis of compounds 50a-f:

Compounds **49a-f** were mixed with anhydrous $AlCl_3$ (5 eq) in chlorobenzene and heated at 100°C for 5h. When TLC indicated the disappearance of starting materials, the reaction mixture was quenched with ice-cold diluted HCl and extracted with chloroform. The organic layer was dried over magnesium sulfate, filtered and evaporated under reduced pressure. The residue was purified by column chromatography (hexane/ethyl acetate= 50:50) to give the title compounds **50a-f**.

Quinolin-2(1H)-one 50a:

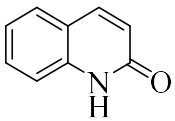

^{1}H NMR (400 MHz, $CDCl_3$) δ (ppm): 6.75 (1H, d, *J*= 9.46), 7.22 (1H, m), 7.23-7.58 (3H, m), 7.83 (1H, d, *J*= 9.47), 12.81 (1H, bs). **^{13}C NMR** (100 MHz, $CDCl_3$) δ (ppm): 116.7, 120.3, 121.5, 123.1, 128.1, 131.1, 138.8, 141.5, 165.6 **MS** (ESI positive) *m/z*: 146.0 $[M+H]^+$ ($[M+H]^+$ 146.05 required).

1-Methylquinolin-2(1H)-one 50b:

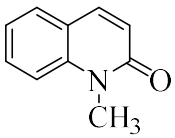

^{1}H NMR (400 MHz, $CDCl_3$) δ (ppm): 3.77 (3H, s), 6.80 (1H, d, *J*= 9.45), 7.28-7.30 (1H, m), 7.41 (1H, d, *J*= 8.61), 7.59-7.63 (2H, m), 7.72 (1H, d, *J*= 9.45). **^{13}C NMR** (100 MHz, $CDCl_3$) δ (ppm): 29.7, 14.4, 121.1, 122.1, 122.4, 129.1, 131.0, 139.3, 140.4, 162.7 **MS** (ESI positive) *m/z*: 160.0 $[M+H]^+$ ($[M+H]^+$ 160.07 required).

8-Chloroquinolin-2(1H)-one 50c:

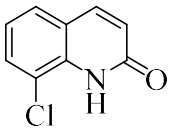

^{1}H NMR (400 MHz, $CDCl_3$) δ (ppm): 6.69 (1H, d, *J*= 9.57), 7.16 (1H, t, *J*= 7.88), 7.48 (1H, dd, *J*= 0.78, 7.83), 7.56 (1H, dd, *J*= 0.93, 7.87), 7.74 (1H, d, d, *J*= 9.58) 9.10 (1H, bs). **^{13}C NMR** (100 MHz, $CDCl_3$) δ (ppm): 119.7, 121.3, 123.1, 123.3, 127.1, 130.7, 134.9, 140.7, 162.4 **MS** (ESI positive) *m/z*: 180.0 $[M+H]^+$ ($[M+H]^+$ 180.01 required).

8-Fluoroquinolin-2(1H)-one 50d:

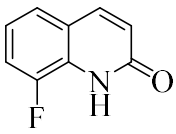

^{1}H NMR (400 MHz, $CDCl_3$) δ (ppm): 6.75 (1H, d, *J*= 9.60), 7.12-7.17 (1H, m), 7.25-7.30 (1H, m), 7.35 (1H, d, *J*= 7.88), 7.78 (1H, d, *J*= 9.61), 10.65 (1H, bs). **^{13}C NMR** (100 MHz, $CDCl_3$) δ (ppm): 115.9 (d, *J*= 17.18), 121.9 (d, *J*= 2.99), 122.6 (d, *J*= 6.75), 123.3, 123.6 (d, *J*= 3.74), 127.7 (d, *J*= 12.84), 140.6, 149.7 (d, *J*= 246.56), 163.0 **^{19}F NMR** (103 MHz, $CDCl_3$) δ (ppm): -134.16 **MS** (ESI positive) *m/z*: 164.0 $[M+H]^+$ ($[M+H]^+$ 164.04 required).

8-Bromoquinolin-2(1H)-one 50e:

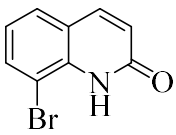

^{1}H NMR (400 MHz, $CDCl_3$) δ (ppm): 6.68 (1H, d, *J*= 9.55), 7.11 (1H, t, *J*= 7.85), 7.53 (1H, d, *J*= 7.79), 7.72 (1H, d, *J*= 9.25), 9.12 (1H, bs). **^{13}C NMR** (100 MHz, $CDCl_3$) δ (ppm): 109.5, 121.4, 123.2, 123.7, 127.9, 134.0, 136.0 140.8, 162.5 **MS** (ESI positive) *m/z*: 224.0 $[M+H]^+$ ($[M+H]^+$ 223.96 required).

6-Methylquinolin-2(1H)-one 50f:

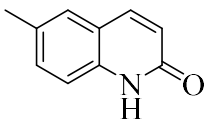

^{1}H NMR (400 MHz, $CDCl_3$) δ (ppm): 2.42 (3H,s), 6.74 (1H, d, *J*= 9.41), 7.35-7.42 (3H, m), 7.80 (1H, d, *J*= 9.40), 12.54 (1H, bs). **^{13}C NMR** (100 MHz, $CDCl_3$) δ (ppm): 21.2, 116.7, 120.6, 120.9, 127.7, 132.8, 133.1, 136.5, 141.7, 164.5 **MS** (ESI positive) *m/z*: 160.0 $[M+H]^+$ ($[M+H]^+$ 160.07 required).

General procedure for the synthesis of compounds 51a-b:

Quinolin-2(1H)-one derivatives **50a-b** (1 equiv) and Wollins' reagent (1.5 eq) in dry toluene were refluxed for 4h. Upon cooling to room temperature, water was added and extracted with ethyl acetate (20 mL x 3). The organic layer was dried over magnesium sulfate, filtered

and evaporated under reduced pressure. The residue was purified by column chromatography (hexane/ethyl acetate 70:30) to give the title compounds **51a-b**.

quinoline-2(1H)-selenone 51a:

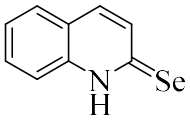

Following the general procedure, **50a** (1 equiv) and Wollins' reagent (1.5 equiv) gave **51a** as red solid (yield 68%). **^{1}H NMR** (400 MHz, $CDCl_3$) δ (ppm): 7.10 (1H, d, *J*= 10.54 Hz), 7.37-7.42 (2H, m), 7.55-7.48 (2H, m), 7.72 (1H, dd, *J*= 7.79, 0.95). **^{13}C NMR** (100 MHz, $CDCl_3$) δ (ppm): 116.9, 124.4, 125.9, 128.4, 132.0, 135.0, 135.3, 140.6 **^{77}Se NMR** (76 MHz, $CDCl_3$) δ (ppm): 469.4 **MS** (ESI positive) *m/z*: 210.0 $[M+H]^+$ ($[M+H]^+$ 209.97 required).

1-Methylquinoline-2(1H)-selenone 51b:

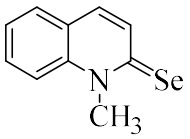

Following the general procedure, **50b** (1 equiv) and Wollins' reagent (1.5 equiv) gave **51b** as red solid (yield 98%). **^{1}H NMR** (400 MHz, $CDCl_3$) δ (ppm): 4.45 (3H, s), 7.37-7.41 (1H, m), 7.47 (1H, d, *J*= 9.02), 7.71-7.66 (3H, m) 8.02 (1H, d, *J*= 9.01). **^{13}C NMR** (100 MHz, $CDCl_3$) δ (ppm): 42.8, 116.4, 125.1, 125.9, 129.4, 130.7, 131.7, 138.1, 141.7 **^{77}Se NMR** (76 MHz, $CDCl_3$) δ (ppm): 646.7 **MS** (ESI positive) *m/z*: 224.0 $[M+H]^+$ ($[M+H]^+$ 223.99 required).

Procedure for the synthesis of 1-bromo-2-(diethoxymethyl)benzene 53:

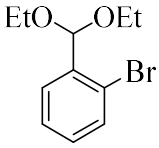

A solution of 2-bromobenzaldehyde **52** (1.0 equiv) was added to a solution of triethyl orthoformate (2 equiv) in EtOH under inert atmosphere (N_2). The solution was stirred at reflux overnight. The solution was quenched with water and extracted with ethyl acetate. The organic layer was dried over magnesium sulfate, filtered and evaporated under reduced pressure. The residue was purified by column chromatography (hexane/ethyl acetate 90:10) to give the title compound **53** as colourless oil (yield 97%). **^{1}H NMR** (400 MHz, $CDCl_3$) δ (ppm): 1.25 (6H, t, *J*= 7.06 Hz), 3.55-3.74 (4H, m), 5.66 (1H, s), 7.17 (1H, td, *J*= 1.75, 7.75), 7.32 (1H, td, *J*= 0.92, 7.56), 7.54 (1H, dd, *J*= 1.08, 7.97), 7.65 (1H, dd, *J*= 1.71, 7.75). **^{13}C NMR** (100 MHz, $CDCl_3$) δ (ppm): 15.5, 62.8, 101.7, 123.3, 127.6, 128.6, 130.2, 133.1, 138.4. **MS** (ESI positive) *m/z*: 259.1 $[M+H]^+$ ($[M+H]^+$ 259.03 required).

Procedure for the synthesis of 1,2-bis(2-(diethoxymethyl)phenyl)ditellane 54:

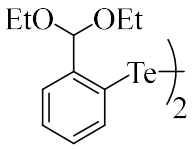

To a solution of 1-bromo-2-(diethoxymethyl)benzene **53** (1.0 equiv) in anhydrous THF (10 mL) at -78°C under nitrogen, butyl lithium (1.7M, 1.5 equiv) was added. The solution was stirred for 1 h at -78°C prior to the addition of freshly ground tellurium powder (1.0 equiv). After being stirred for 2 h at ambient temperature, the solution was quenched with a saturated ammonium chloride solution (10 mL) and extracted with ethyl acetate (20 mL x 3). The organic layer was dried over magnesium sulfate, filtered and evaporated under reduced pressure. The residue was purified by column chromatography (hexane/ethyl acetate 90:10) to give the title compound **54** as red oil (yield 90%). **^{1}H NMR** (400 MHz, $CDCl_3$) δ (ppm): 1.29 (12H, t, *J*= 7.07 Hz), 3.60-3.66 (8H, m), 5.54 (2H, s), 7.09 (2H, td, *J*= 1.47, 7.50), 7.23 (2H, td, *J*= 1.16, 7.47), 7.46 (2H, dd, *J*= 1.41, 7.61), 7.99 (2H, dd, *J*= 1.06, 7.77). **^{13}C NMR** (100 MHz, $CDCl_3$) δ (ppm): 15.7, 61.6, 103.1, 126.9, 127.5, 128.5, 129.9, 139.7, 140.7 **^{125}Te NMR** (126 MHz, $CDCl_3$) δ (ppm): 324.0 **MS** (ESI positive) *m/z*: 619.1 $[M+H]^+$ ($[M+H]^+$ 619.03 required).

Procedure for the synthesis of (2-(diethoxymethyl)phenyl)(methyl)tellane 55:

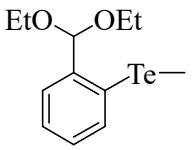

Compound **54** was dissolved in ethanol (25 mL) followed by addition of sodium borohydride (4.0 equiv) at ambient temperature under nitrogen. After being stirred for 30 min, iodomethane (2.0 equiv) was added and the solution was allowed to stir overnight. The solution was quenched with a saturated ammonium chloride solution (10 mL) and extracted with ethyl acetate (20 mL x 3), the organic layer was dried over magnesium sulfate, filtered and evaporated under reduced pressure. The residue was purified by column chromatography (hexane/ethyl acetate 90:10) to give the title compound **55** as light yellow oil (yield 80%). **^{1}H NMR** (400 MHz, $CDCl_3$) δ (ppm): 1.26 (6H, t, *J*= 7.06 Hz), 2.06 (3H, s), 3.55-3.60 (4H, m), 7.16 (1H, td, *J*= 1.66, 7.43), 7.22 (1H, td, *J*= 1.35, 7.44), 7.55 (2H, td, *J*= 1.49, 7.68). **^{13}C NMR** (100 MHz, $CDCl_3$) δ (ppm): 15.5, 15.6, 61.4, 103.2, 126.5, 127.2, 128.5, 129.2, 134.5, 141.4 **^{125}Te NMR** (126 MHz, $CDCl_3$) δ (ppm): 253.8 **MS** (ESI positive) *m/z*: 324.9 $[M+H]^+$ ($[M+H]^+$ 325.04 required).

Procedure for the synthesis of 2-(methyltellanyl)benzaldehyde 56:

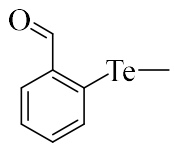

In a round-bottom flask were added (2-(diethoxymethyl)phenyl)(methyl)tellane (**55**) and concentrated HCl (0.68 mL). After being stirred for 15 min at room temperature, the solution was quenched with a saturated sodium hydrogen carbonate solution (10 mL) and extracted with diethyl ether (10 mL x 3). The organic layer was dried over magnesium sulfate, filtered and evaporated under reduced pressure. The residue was purified by column chromatography (hexane/ethyl acetate=90:10) to give the title compound **56** as a yellow oil (yield 98%). **^{1}H NMR** (400 MHz, $CDCl_3$) δ (ppm): 2.01 (3H, s), 7.37 (1H, td, *J*= 1.17, 7.33), 7.43 (1H, td, *J*= 1.71, 7.50), 7.61 (1H, d, *J*= 7.66), 7.82 (1H, dd, *J*= 1.61, 7.43), 10.16 (1H, s). **^{13}C NMR** (100 MHz, $CDCl_3$) δ (ppm): -16.0, 123.7, 125.8, 132.5, 133.9, 136.8, 137.3, 193.1 **^{125}Te NMR** (126 MHz, $CDCl_3$) δ (ppm): 417.3 **MS** (ESI positive) *m/z*: 260.0 $[M+H]^+$ ($[M+H]^+$ 250.96 required).

Procedure for the synthesis of (E)-3-(2-(methyltellanyl)phenyl)acrylic acid 57:

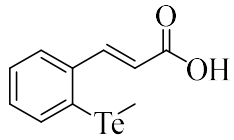

In a round-bottom flask was added 2-(methyltellanyl)benzaldehyde (**56**) (1 equiv) and malonic acid (2.3 equiv)in a solution of pyridine/piperidine (95/5). The solution was stirred at reflux overnight and after it brought at 0°C was quenched with concentrated HCl. The precipitate was collected and dried on air to give the title compound **57** as a yellow solid (yield 50%). **^{1}H NMR** (400 MHz, $CDCl_3$) δ (ppm): 2.17 (3H, s), 6.33 (1H, d, *J*= 15.69), 7.20 (1H, td, *J*= 1.41, 7.53), 7.32 (1H, td, *J*= 0.71, 7.62), 7.60 (1H, dd, *J*= 1.37, 7.82), 7.79 (1H, dd, *J*= 1.05, 7.70), 8.16 (1H, d, *J*= 15.72). **^{13}C NMR** (100 MHz, $CDCl_3$) δ (ppm): -14.8, 119.1, 119.6, 127.3, 128.6, 130.8, 138.7, 139.1, 171.8 **^{125}Te NMR** (126 MHz, $CDCl_3$) δ (ppm): 258.7 **MS** (ESI positive) *m/z*: 293.0 $[M+H]^+$ ($[M+H]^+$ 292.97 required).

Procedure for the synthesis of 2H-tellurochromen-2-one 58:

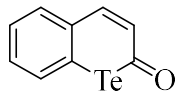

In a round-bottom flask was added (E)-3-(2-(methyltellanyl)phenyl)acrylic acid **(57)** (1 equiv) and anhydrous $ZnCl_2$ (0.1 equiv) in a solution of dichloromethyl methyl ether/ CCl_4 (33/66). The solution was stirred at room temperature overnight and the solvent was removed under reduce pressure. The crude product was

dissolved in CS_2, brought at 0°C and added $AlCl_3$ (1 equiv). After 5 min the solution was stirred at reflux for 30 minutes, quenched with HCl 3N and and extracted with diethyl ether. The organic layer was dried over magnesium sulfate, filtered and evaporated under reduced pressure. The residue was purified by column chromatography (hexane/ethyl acetate=90:10) to give the title compound **58** as a yellow solid (yield 25%). **^{1}H NMR** (400 MHz, $CDCl_3$) δ (ppm): 5.74 (1H, d, *J*= 11.60), 7.26-7.37 (2H, m), 7.69-7.72 (2H, m), 7.75-7.78 (1H, m) **^{13}C NMR** (100 MHz, $CDCl_3$) δ (ppm): 125.4, 125.7, 127.4, 130.1, 130.8, 135.5, 136.2, 145.9, 194.0 **^{125}Te NMR** (126 MHz, $CDCl_3$) δ (ppm): 859.63 (d, *J*= 19.96) **MS** (ESI positive) *m/z*: 261.0 $[M+H]^+$ ($[M+H]^+$ 260.95 required).

Carbonic anhydrase inhibition

An Applied Photophysics stopped-flow instrument has been used for assaying the CA catalyzed CO_2 hydration activity.[29] Phenol red (at a concentration of 0.2 mM) has been used as indicator, working at the absorbance maximum of 557 nm, with 20 mMHepes (pH 7.5) as buffer, and 20 mM Na_2SO_4 (for maintaining constant the ionic strength), following the initial rates of the CA-catalyzed CO_2 hydration reaction for a period of 10–100 s. The CO_2 concentrations ranged from 1.7 to 17 mM for the determination of the kinetic parameters and inhibition constants. For each inhibitor at least six traces of the initial 5–10% of the reaction have been used for determining the initial velocity. The uncatalyzed rates were determined in the same manner and subtracted from the total observed rates. Stock solutions of inhibitor (0.1 mM) were prepared in distilled-deionized water and dilutions up to 0.01 nM were done thereafter with the assay buffer. Inhibitor and enzyme solutions were preincubated together for 15 min at room temperature prior to assay, in order to allow for the formation of the E-I complex. The inhibition constants were obtained by non-linear least-squares methods using PRISM 3 and the Cheng–Prusoff equation.

Crystallization and X-ray data collection

Crystals of hCAII were obtained using the hanging drop vapor diffusion method using 24 well Linbro plate. 2 µl of 10 mg/ml solution of hCA II in Tris-HCl 20 mM pH 8.0 were mixed with 2 µl of a solution of 1.5 M sodium citrate, 0.1 M Tris pH 8.0 and were equilibrated against the same solution at 296 K. Crystals of the protein grew in one week. Afterwards hCAII crystals were soaked in 5mM inhibitor solution for 3 days. The crystals

were flash-frozen at 100K using a solution obtained by adding 15% (v/v) glycerol to the mother liquor solution as cryoprotectant. Data on crystals of the complexes were collected using synchrotron radiation at the ID23-2 beamline at ESRF (Grenoble, France) with a wavelength of 0.8731 Å and a PILATUS3 2M Dectris detector. Data were integrated and scaled using the program XDS.[22] Data processing statistics were showed in supporting information.

Structure determination

The crystal structure of hCA II (PDB accession code: 4FIK) without solvent molecules and other heteroatoms was used to obtain initial phases of the structures using Refmac5.[23] 5% of the unique reflections were selected randomly and excluded from the refinement data set for the purpose of Rfree calculations. The initial |Fo - Fc| difference electron density maps unambiguously showed the inhibitor molecules. The inhibitor was introduced in the model with 1.0 occupancy. Atomic models for inhibitors were calculated and energy minimized using the program JLigand 1.0.40.[35] Refinements proceeded using normal protocols of positional, isotropic atomic displacement parameters alternating with manual building of the models using COOT.[76] Solvent molecules were introduced automatically using the program ARP.[77] The quality of the final models were assessed with COOT and RAMPAGE.[78] Atomic coordinates were deposited in the Protein Data Bank. Graphical representations were generated with Chimera.[79]

Summary of Data Collection and Atomic Model Refinement Statistics

PDB	5ULN	5UMC	5WEX
Compound	22	14	10
Space group	$P2_1$	$P2_1$	$P2_1$
Cell dimensions			
a, b, c	42.5, 41.6, 72.2	42.5, 41.5, 72.3	42.5, 41.5, 72.4
alpha, beta, gamma	90, 104.5, 90	90, 104.4, 90	90, 104.4, 90
Resolution (Å)	41.6 - 1.35	41.5 - 2.15	41.1 – 1.26
Resolution-high (Å)	1.37 - 1.35	2.21 - 2.15	1.28 – 1.26
Rmerge	0.042 (0.284)	0.225 (0.793)	0.076 (1.175)
Rpim	0.017 (0.124)	0.112 (0.396)	0.034 (0.511)
CC ½	1.000 (0.948)	0.978 (0.755)	0.999 (0.609)
I/sigI	31.3 (6.3)	5.7 (2.0)	10.6 (2.0)
Completeness (%)	94.0 (61.5)	99.3 (92.4)	96.9 (93.4)
Redundancy	7.3 (6.1)	5.0 (4.8)	6.8 (6.0)
Refinement			
resolution (Å)	41.6 - 1.35	41.5 - 2.15	41.1 – 1.26
unique reflections	48038	12801	60631
Rwork/Rfree (%)	10.6 / 14.3	19.6 / 26.2	11.8 / 14.7
# atoms	2586	2252	2464
Protein	2230	2101	2196
metal (Zn)	1	1	1
ligand	21	22	21
water	327	95	237
B-factors (Å^2)	13.8	20.2	17.0
protein	12.9	20.4	16.4
metal (Zn)	5.7	12.3	8.2
ligand	17.1	25.4	23.2
water	27.3	20.1	29.6
r.m.s. deviations			
Bond length (Å)	0,015	0,014	0,015
Bond angle (°)	1,783	1,664	1,766

PDB	6H3Q
Compound	29c
Space group	$P2_1$
Cell dimensions	
a, b, c	42.4, 41.4, 72.1
alpha, beta, gamma	90, 104.3, 90
Resolution (Å)	41.36 - 1.31
Resolution-high (Å)	1.40 - 1.31
Rsym (%)	14.2 (100.7)
Rmeas (%)	15.7 (111.6)
CC ½	0.996 (0.503)
I/sigI	6.0 (0.95)
Completeness (%)	100.0 (99.9)
Redundancy	5.4 (5.3)
Wavelength (Å)	0.8731
Refinement	
resolution (Å)	41.36 - 1.31
unique reflections	58339 (10448)
Rwork/Rfree (%)	2824
Rfactor (%)	18.21
Rfree(%)	20.69
Ramachandran statistics (%)	
Most favored	97.3
additionally allowed	2.7
outlier regions	0.0
B-factors ($Å^2$)	17.47
ligand	27.73
water	27.74
r.m.s. deviations	
Bond length (Å)	0,0166
Bond angle (°)	1,8364

Biological Assays.

Human prostate cancer cell line PC3 and human breast cancer cell line MDA-MB-231 were obtained from American Type Culture Collection (Rockville, MD). PC3 and MDA-MB-231 were cultured in DMEM high glucose with 20% FBS in 5% CO_2 atmosphere at 37° C. Media contained 2 mM L-glutamine, 1% essential aminoacid mix, 100 IU ml^{-1} penicillin and 100 µg ml^{-1} streptomycin (Sigma, Milan, Italy). Cells were plated in 960 wells cell culture ($1 \cdot 10^4$/well) and, 24 h after, treated with the tested compounds for 48 h. Low oxygen conditions were acquired in a hypoxic workstation (Concept 400 anaerobic incubator, Ruskinn Technology Ltd., Bridgend, UK). The atmosphere in the chamber consisted of 1% O_2 (hypoxia), 5% CO_2, and residual N_2. In parallel, normoxic (21% O_2) dishes were incubated in air with 5% CO_2. Cell vitality was assessed via MTT assay. Viability is expressed as % in comparison to the control cells (arbitrarily set 100 % of viable cells). Data are presented as mean ± SEM. One-way ANOVA with a Bonferroni post-hoc test was used to compare the treated samples to the control. A p-value less than 0.05 was considered to indicate a significant difference.

References

1. Wilson W.R., Hay M.P. Targeting hypoxia in cancer therapy. *Nat Rev Cancer.* 2011, 11, 393-410.
2. Lendahl U., Lee K.L., Yang H., Poellinger L. Generating specificity and diversity in the transcriptional response to hypoxia. *Nat Rev Genet.* 2009, 10, 821-832.
3. Parks S.K., Chiche J., Pouyssegur J. pH control mechanisms of tumor survival and growth. *J Cell Physiol*. 2011, 226, 299-308.
4. Neri D., Supuran C.T. Interfering with pH regulation in tumours as a therapeutic strategy. *Nature Rev Drug Discov.* 2011, 10, 767–777.
5. Supuran C.T. Carbonic anhydrases: novel therapeutic applications for inhibitors and activators. *Nature Rev Drug Discov.* 2008, 7, 168–181.
6. Wykoff C.C., Beasley N.J., Watson P.H., Turner K.J., Pastorek J., Sibtain A., Wilson G.D., Turley H., Talks K.L., Maxwell P.H., Pugh C.W., Ratcliffe P.J., Harris A.L. Hypoxia-inducible expression of tumor-associated carbonic anhydrases. *Cancer Res.* 2000, 60, 7075-7083.
7. Robertson N., Potter C., Harris A.L. Role of carbonic anhydrase IX in human tumor cell growth, survival, and invasion. *Cancer Res.* 2004, 64, 6160-6165.
8. Lou Y., McDonald P.C., Oloumi A., Chia S., Ostlund C., Ahmadi A., Kyle A., Auf dem Keller U., Leung S., Huntsman D., Clarke B., Sutherland B.W., Waterhouse D., Bally M., Roskelley C., Overall C.M. et al. Targeting tumor hypoxia: suppression of breast tumor growth and metastasis by novel carbonic anhydrase IX inhibitors. *Cancer Res.* 2011, 71, 3364-3376.
9. Kaluz S., Kaluzova M., Liao S.Y., Lerman M., Stanbridge E.J. Transcriptional control of the tumor- and hypoxia-marker carbonic anhydrase 9: A one transcription factor (HIF-1) show? *Biochim Biophys Acta*. 2009, 1795, 162-172.
10. Alterio V., Hilvo M., Di Fiore A., Supuran C.T., Pan P., Parkkila S., Scaloni A., Pastorek J., Pastorekova S., Pedone C., Scozzafava A., Monti S.M., De Simone G. Crystal structure of the catalytic domain of the tumor-associated human carbonic anhydrase IX. *Proc Natl Acad Sci U S A.* 2009, 106, 16233-16238.
11. Wingo T., Tu C., Laipis P.J., Silverman D.N. The catalytic properties of human carbonic anhydrase IX. *Biochem Biophys Res Commun*. 2001, 288, 666-669.

12. Hilvo M., Baranauskiene L., Salzano A.M., Scaloni A., Matulis D., Innocenti A., Scozzafava A., Monti S.M., Di Fiore A., De Simone G., Lindfors M., Janis J., Valjakka J., Pastorekova S., Pastorek J., Kulomaa M.S. et al. Biochemical characterization of CA IX, one of the most active carbonic anhydrase isozymes. *J Biol Chem.* 2008, 283, 27799-27809.
13. De Simone G., Supuran C.T. Carbonic anhydrase IX: Biochemical and crystallographic characterization of a novel antitumor target. *Biochim Biophys Acta.* 2010, 1804, 404-409.
14. Innocenti A., Pastorekova S., Pastorek J., Scozzafava A., De Simone G., Supuran C.T. The proteoglycan region of the tumor-associated carbonic anhydrase isoform IX acts as anintrinsic buffer optimizing CO_2 hydration at acidic pH values characteristic of solid tumors. *Bioorg Med Chem Lett.* 2009, 19, 5825-5828.
15. Pacchiano F., Carta F., McDonald P.C., Lou Y., Vullo D., Scozzafava A., Dedhar S., Supuran C.T. Ureido-substituted benzenesulfonamides potently inhibit carbonic anhydrase IX and show antimetastatic activity in a model of breast cancer metastasis. *J Med Chem.* 2011, 54, 1896-902.
16. Cecchi A., Hulikova A., Pastorek J., Pastorekova S., Scozzafava A., Winum J.Y., Montero J.L., Supuran C.T. Carbonic anhydrase inhibitors. Design of fluorescent sulfonamides as probes of tumor-associated carbonic anhydrase IX that inhibit isozyme IX-mediated acidification of hypoxic tumors. *J. Med. Chem.* 2005, 48, 4834–4841.
17. Pastorekova S., Casini A., Scozzafava A., Vullo D., Pastorek J., Supuran C.T. Carbonic anhydrase inhibitors: The first selective, membrane-impermeant inhibitors targeting the tumor-associated isozyme IX. *Bioorg Med Chem Lett* 2004, 14, 869–873.
18. Patani A.G., LaVoie E.J. Bioisosterism: a rational approach in drug design. *Chem. Rev*., 1996, 96, 3147-3176.
19. Lima L.M., Barreiro E.J. Bioisosterism: a useful strategy for molecular modification and drug design. *Current Medicinal Chemistry*, 2005, 12, 23-49.

20. Lomelino C.L., Mahon B.P., McKenna R., Carta F., Supuran C.T. Kinetic and X-ray crystallographic investigations on carbonic anhydrase isoforms I, II, IX and XII of a thioureido analog of SLC-0111. *Bioorg. Med. Chem*. 2016, 5, 976-981.
21. https://clinicaltrials.gov/ct2/show/NCT02215850
22. Leslie A.G.W., Powell H.R., Procesing diffraction data with mosflm. In: Read RJ, Sussman JL (eds) Evolving methods for macromolecular crystallography, vol 245, NATO Science series, Springer, Dordrecht, 2007, pp. 41-51.
23. Murshudov G.N., Vagin A.A., Dodson E.J., Refinement of macromolecular structures by the maximum-likelihood method. *Acta Crystallogr D Biol Crystallogr.* 1997, 53, 240-255.
24. Chandra A.S., Kumar A.R., Sathaiah G., Luke P. V., Madabhushi S., Rao P.S. Facile N-formylation of amines using Lewis acids as novel catalysts. *Tetrahedron Lett.* 2009, 50, 7099-7101.
25. Burton D.H.R., Parekh S.I., Tajbakhsh M., Theodorakis E.A., Tse C-L. A convenient and high yielding procedure for the preparation of isoselenocyanates. Synthesis and reactivity of O-alkylselenocarbamates. *Tetrahedron*, 1994, 50, 639-654.
26. Cotarca L., Eckert H. Phosgenathion-A Handbook; Wiley-VCH: Weinheim. 2003
27. Cotarca L., Delogu P., Nardelli A., Sunji V. Bis(trichloromethyl) carbonate in organic synthesis. *Synthesis*, 1996, 5, 553-576.
28. Bolanos F.J.G., Lopez O., Ulgar V., Maya I., Fuentes J. Synthesisof O-unprotected glycosyl selenoureas. A new access to bicyclic sugar isoureas. *Tetrahedron Lett.* 2004, 45, 4081-4084.
29. Khalifah R.G. The carbon dioxide hydration activity of carbonic anhydrase. I. Stop-flow kinetic studies on the native human isoenzymes B and C. *J. Biol. Chem.* 1971, 246, 2561−2573.
30. Zade S.S., Panda S., Tripathi S.K., Singh H.-B., Wolmershäuser G. Convenient synthesis, characterization and GPx-like catalytic activity of novel ebselen derivatives. *Eur. J. Org. Chem*., 2004, 3857-3864.
31. Iwaoka M., Kumakura F. Applications of water-soluble selenides and selenoxides to protein chemistry. *Phosphorus Sulfur Silicon Relat. Elem*., 2008, 183, 1009-1017.

32. Kumakura F., Mishra B., Priyadarsini K.I., Iwaoka M.A. water-soluble cyclic selenide with enhanced glutathione peroxidase-like catalytic activities. *Eur. J. Org. Chem.* 2010, 3, 440-445.
33. Pascual P., Martinez-Lara E., Bàrcena J.A., Lòpez-Barca J., Toribio F. Direct assay of glutathione peroxidase activity using high-performance capillary electrophoresis. *J. Chromatogr*. 1992, 581, 49-56.
34. Olcott H.S., Brown W.D., Van Derveen J., Seleno methionine as an Antioxidant. *Nature*, 1961, 191, 1201.
35. Lebedev A.A., Young P., Isupov M.N., Moroz O.V., Vagin A.A., Murshudov G.N. JLigand: a graphical tool for the CCP4 template-restraint library. *Acta Crystallogr D Biol Crystallogr.* 2012, 68, 431-440.
36. Frost D.V. The Two Faces of Selenium Can Selenophobia Be Cured? *Crit. Rev. Toxicol.* 1972, 4, 467−513.
37. Ignat Grozav A.I., Gaina L., Kuete V., Silaghi-Dumitrescu L., Efferth T., Zaharia V., Microwave-assisted synthesis of new selenazole derivatives with antiproliferative activity. *Molecules*. 2013, 4, 4679-4688.
38. Zhao H.C., Shi Y.P., Liu Y.M., Li C.W., Xuan L.N., Wang P., Zhang K., Chen B.Q., Synthesis and antitumor-evaluation of 1,3-selenazole-containing 1,3,4-thiadiazole derivatives. *Bioorg Med Chem Lett.* 2013, 24, 6577-6579.
39. Angeli A., Tanini D., Capperucci A., Supuran C.T., Synthesis of novel selenides bearing benzenesulfonamide moieties as carbonic anhydrase I, II, IV, VII and IX inhibitors. *ACS Med. Chem. Lett.*, 2017, 8, 1213-1217.
40. Angeli A., Tanini D., Capperucci A., Supuran C.T., First evaluation of organotellurium derivatives as carbonic anhydrase I, II, IV, VII and IX inhibitors. *Bioorg Chem.* 2018, 76, 268-272.
41. Angeli A., Peat T.S., Bartolucci G., Nocentini A., Supuran C.T., Carta F., Intramolecular oxidative deselenization of acylselenoureas: a facile synthesis of benzoxazole amides and carbonic anhydrase inhibitors. *Org Biomol Chem.* 2016, 14, 11353-11356.
42. Di Fiore A., De Simone G., Alterio V., Riccio V., Winum J.Y., Carta F., Supuran C.T. The anticonvulsant sulfamide JNJ-26990990 and its S,S-dioxide analog

strongly inhibit carbonic anhydrases: solution and X-ray crystallographic studies. *Org Biomol Chem.* 2016, 14, 4853.

43. Klaunig J.E., Kamendulis L.M., Hocevar B.A., Oxidative stress and oxidative damage in carcinogenesis. *Toxicol. Pathol.* 2010, 38, 96–109.
44. Coussens L.M., Werb Z., Inflammation and cancer. *Nature* 2002, 420, 860–867.
45. Jacob C., Battaglia E., Burkholz T., Peng D., Bagrel D., Montenarh M. Control of oxidative posttranslational cysteine modifications: from intricate chemistry to widespread biological and medical applications. *Chem. Res. Toxicol.* 2012, 25, 588e604.
46. Doering M., Ba L.A., Lilienthal N., Nicco C., Scherer C., Abbas M., Zada A.A.P., Coriat R., Burkholz T., Wessjohann L., Diederich M., Batteux F., Herling M., Jacob C. Synthesis and selective anticancer activity of organochalcogen based redox catalysts. *J. Med. Chem*. 2010, 53, 6954-6963.
47. Ba L.A., Doring M., Jamier V., Jacob C. Tellurium: an element with great biological potency and potential. *Org. Biomol. Chem*. 2010, 8, 4203e4216.
48. Turner R.J., Weiner J.H., Taylor D.E., Tellurite-mediated thiol oxidation in Escherichia coli. *Microbiology*, 1999, 145, 2549.
49. Fleming A. On the specific antibacterial properties of penicillin and potassium tellurite. Incorporating a method of demonstrating some bacterial antagonisms *J. Pathol. Bacteriol.* 1932, 35, 831.
50. Sredni B., Caspi R.R., Klein A., Kalechman Y., Danziger Y., BenYa'akov M., Tamari T., Shalit F., Albeck M. A new immunomodulating compound (AS-101) with potential therapeutic application. *Nature*, 1987, 330, 173.
51. Montero R., Gonsebatt M.E., Gerson R., Rojas E., Herrera L.A., Ostrosky-Wegman P., AS-101: a modulator of in vitro T-cell proliferation. *Anticancer Drugs*, 1993, 3, 351.
52. Sredni B., Caspi R.R., Lustig S., Klein A., Kalechman Y., Danziger Y., Ben Ya'akov M., Tamari T., Shalit F., Albeck M. The biological activity and immunotherapeutic properties of AS-101, a synthetic organotellurium compound. *Nat Immun Cell Growth Regul*. 1988, 7, 163.

53. Cunha R.L., Gouvea I.E., Juliano L. A glimpse on biological activities of tellurium compounds. *An Acad Bras Cienc*, 2009, 81, 393.
54. Giles G.I., Giles N.M., Collins C.A., Holt K., Fry F.H., Lowden P.A.S., Gutowski N.J., Jacob C. Electrochemical, in vitro and cell culture analysis of integrated redox catalysts: implications for cancer therapy *Chem. Commun*. 2003, 16, 2030.
55. Giles G.I., Tasker K.M., Johnson R.J.K., Jacob C., Peers C., Green K.N. Electrochemistry of chalcogen compounds: prediction of antioxidant activity Chem. Commun., 2001, 23, 2490.
56. Engman L., Persson J. Improved preparation of diaryl ditellurides *J. Organomet. Chem.* 1990, 388, 71-74.
57. Tanini D., Grechi A., Dei S., Teodori E., Capperucci A. Novel functionalized organotellurides with enhanced thiol peroxidase catalytic activity *Tetrahedron*, 2017, 73, 5646.
58. Tanini D., Tiberi C., Gellini C., Salvi P.R., Capperucci A. A Straightforward Access to Stable β-Functionalized Alkyl Selenols *Adv. Synth. Catal*. 2018, DOI 10.1002/adsc.201800602.
59. Nocentini A., Ceruso M., Bua S., Lomelino C.L., Andring J.T., McKenna R., Lanzi C., Sgambellone S., Pecori R., Matucci R., Filippi L., Gratteri P., Carta F., Masini E., Selleri S., Supuran C.T. Discovery of β-Adrenergic Receptors Blocker-Carbonic Anhydrase Inhibitor Hybrids for Multitargeted Antiglaucoma Therapy. *J Med Chem.* 2018, 61, 5380-5394.
60. Dudutiene V., Zubriene A., Smirnov A., Gylyte J., Timm D., Manakova E., Gražulis S., Matulis D., 4-Substituted-2,3,5,6-tetrafluorobenzenesulfonamides as inhibitors of carbonic anhydrases I, II, VII, XII, and XIII. *Bioorg. Med. Chem*. 2013, 21, 2093.
61. Milton M.D., Khan S., Singh J.D., Khandelwa B.L. A Facile Access to Chalcogen and Dichalcogen Bearing Dialkylamines and Diols. *Tetrahedron Lett*. 2005, *46*, 755.
62. Kidane A.G., Salacinski H., Tiwari A., Bruckdorfer K.R., Seifalian A.M. Anticoagulant and Antiplatelet Agents: Their Clinical and Device Application(s) Together with Usages to Engineer Surfaces *Biomacromolecules*. 2004, 5, 798–813;

63. Appendino G., Mercalli E., Fuzzati N., Arnoldi L., Stavri M., Gibbons S., Ballero M., Maxia A. Antimycobacterial Coumarins from the Sardinian Giant Fennel (Ferula communis) *J Nat Prod.* 2004, 67, 2108–2110
64. Ma T., Liu L., Xue H., Li L., Han C., Wang L., Chen Z., Liu G. Chemical Library and Structure–Activity Relationships of 11-Demethyl-12-oxo Calanolide A Analogues as Anti-HIV-1 Agents. *J Med Chem.* 2008, 51, 1432–1446.
65. Kaur M., Kohli S., Sandhu S., Bansal Y., Bansal G. Coumarin: a promising scaffold for anticancer agents. *Anticancer Agents Med Chem.* 2015, 15, 1032-1048.
66. Lai Y., Long Y., Lei Y., Deng X., He B., Sheng M., Li M., Gu Z. A novel micelle of coumarin derivative monoend-functionalized PEG for anti-tumor drug delivery: in vitro and in vivo study. *J Drug Target.* 2012, 3, 246-254.
67. Carradori S. Selective carbonic anhydrase IX inhibitors based on coumarin scaffold as promising antimetastatic agents: WO2012070024. *Expert Opin Ther Pat.* 2013, 23, 751-756.
68. Maresca A., Temperini C., Vu H., Pham N.B., Poulsen S.A., Scozzafava A., Quinn R.J., Supuran C.T. Non-zinc mediated inhibition of carbonic anhydrases: coumarins are a new class of suicide inhibitors. *J Am Chem Soc.* 2009, 131, 3057-62.
69. Bonardi A., Falsini M., Catarzi D., Varano F., Di Cesare Mannelli L., Tenci B., Ghelardini C., Angeli A., Supuran C.T., Colotta V. Structural investigations on coumarins leading to chromeno[4,3-c]pyrazol-4-ones and pyrano[4,3-c]pyrazol-4-ones: New scaffolds for the design of the tumor-associated carbonic anhydrase isoforms IX and XII. *Eur J Med Chem.* 2018, 146, 47-59.
70. Jayachandran T., Manimaran T., Ramakrishnan V.T. Synthesis of Selenacoumarins. Indian J Chem 1984, 23B, 328-330.
71. Natarajan M., Ramakrishnan V.T. A new route for the synthesis of Coumarins, Thiacoumarins and Carbostyrils. Indian J Chem, 1984, 23B, 720-727.
72. Poon J., Yan J., Singh V.P., Gates P.J., Engman L. Alkyltelluro Substitution Improves the Radical-Trapping Capacity of Aromatic Amines. *Chem. Eur. J.* 2016, 22, 12891–12903.

73. Christiaens L., Piette J.L., Luxen A., Renson M., 2H-[1]-Benzotellurinnone-2 (telluro-1 coumarine) et Dihydro-3,4-chalcogeno-1 coumarines *J. Heterocyclic Chem.* 1984, 21, 1281.
74. De Luca L., Mancuso F., Ferro S., Buemi M.R., Angeli A., Del Prete S., Capasso C., Supuran C.T., Gitto R. Inhibitory effects and structural insights for a novel series of coumarin-based compounds that selectively target human CA IX and CA XII carbonic anhydrases. *Eur J Med Chem.* 2018, 143, 276-282.
75. Angapelly S., Sri Ramya P.V., Angeli A., Supuran C.T., Arifuddin M. Sulfocoumarin-, Coumarin-, 4-Sulfamoylphenyl-Bearing Indazole-3-carboxamide Hybrids: Synthesis and Selective Inhibition of Tumor-Associated Carbonic Anhydrase Isozymes IX and XII. *ChemMedChem.* 2017, 19, 1578-1584.
76. Emsley P., Lohkamp B., Scott W., Cowtan K., Features and development of Coot. *Acta Crystallogr D Biol Crystallogr.* 2010, 66, 486-501.
77. Lamzin V.S., Perrakis A., Wilson K.S., The ARP/wARP suite for automated construction and refinement of protein models**,** M.G. Rossmann, E. Arnold (Eds.), Int. Tables for Crystallography. Vol. F: Crystallography of Biological Macromolecules, Kluwer Academic Publishers, Dordrecht, The Netherlands (2001), pp. 720-722
78. Lovell S.C., Davis I.W., Arendall III W.B., de Bakker P.I.W., Word J.M., Prisant M.G., Richardson J.S., Richardson D.C., Structure validation by Cα geometry: ϕ,ψ and Cβ deviation, *Proteins*, 2003, 50, 437-450.
79. Pettersen E.F., Goddard T.D., Huang C.C., Couch G.S., Greenblatt D.M., Meng E.C., Ferrin T.E., UCSF Chimera-a visualization system for exploratory research and analysis, *J. Comput. Chem.*, 2004, 25, 1605-1612

Chapter 4

CAIs as possible agents against Diabetic Cerebrovascular Pathology

4.1 Introduction

Diabetes is a chronic disease and according to official reports the world population affected is expected to rise from 108 million in 1980 to 422 million in 2014.[1] Several complications of diabetes associated with hyperglycemia lead to disruption of the microvasculature of insulin-insensitive tissues in the eye, nerve, and brain.[2] These complications are mainly caused by oxidative stress and lead to pericyte loss,[3,4] disruption of the blood–brain barrier (BBB),[5,6] and cognitive decline.[7-9] The blood brain barrier (BBB) is largely composed by endothelial cells and their close proximity are the cerebral pericytes.[10] Pericyte cells are particularly susceptible to oxidative stress, which leads to cell death by apoptosis.[11] A cause of oxidative stress is the overproduction of superoxide as a byproduct during excess respiration caused by influx of glucose in insulin sensitive tissues.[2] Mitochondrial carbonic anhydrases hCA VA and VB play a central role in the metabolism of pyruvate, by sustaining the rate of respiration[12] **(Figure 1).**

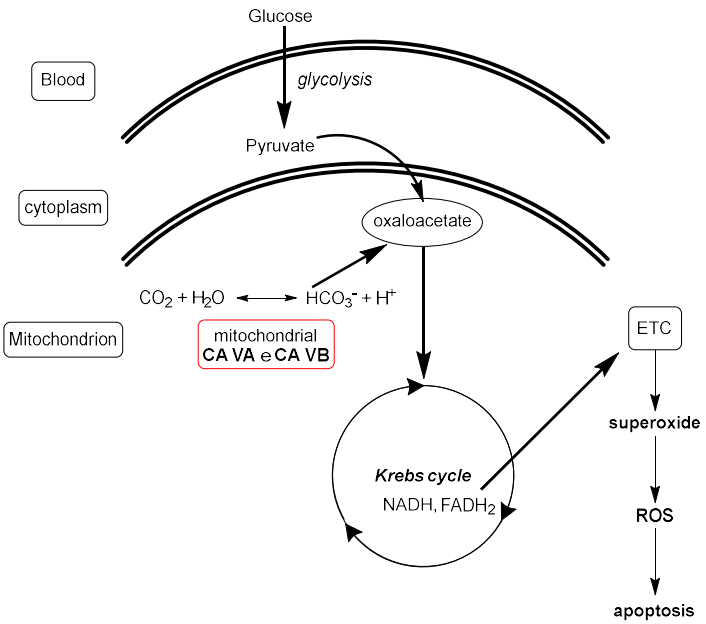

Figure 1. Mitochondrial CAs in ROS production and its role in brain pericytes apoptosis.

Pyruvate is the end-product of glucose glycolytic pathway in the cytosol. Pyruvate enters the mitochondria where it is carboxylated to oxaloacetate. In this step, the production of bicarbonate anion required for carboxylation is produced by mitochondrial hCAs through reversible reaction between water and carbon dioxide ($CO_2 + H_2O \Leftrightarrow HCO_3^- + H^+$).[17] Oxaloacetate, when entering the Krebs cycle, produces $FADH_2$ and NADH, which are carried out to the electron transfer chain (ETC) to generate ATP. O_2^- is a by-product of ETC reactions and it is the precursor of all ROS. The high activity of the Krebs cycle produces a high potential of mitochondrial membrane and this, inhibits the transport of electrons to the complex III increasing the half-life of the free radicals of the coenzyme Q, which reduces O_2 to O_2^-. Mitochondrial CA isoform VA was identify as a one of major contributor to brain diabetic disease,[13] moreover, was discover that hCAs IX and XII are recently implicated in ischemia-induced cerebrovascular pathology[14], make these enzymes attractive drug targets for obtaining agents that can interfere with these deleterious processes. This may lead to novel strategies to prevent diabetic complications in the brain and possibly in other insulin-insensitive tissues.

Sulfonamides are a widely investigated class of CAIs, and among these acetazolamide (**AAZ**) zonisamide (**ZNS**) and topiramate (**TPM**) are the best known representatives [15-17] (**Figure 2**).

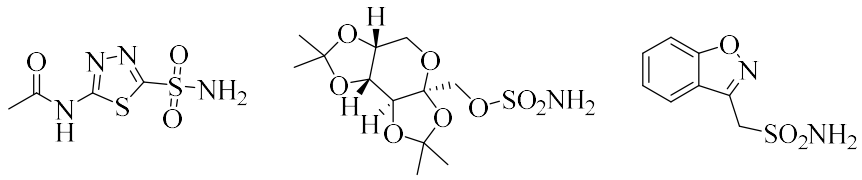

Figure 2. Structures of hCAs inhibitors: acetazolamide (**AAZ**), topiramate (**TPM**) and zonisamide (**ZNS**).

The low CA isoform selectivity as well as the ability of Topiramate to interfere with other metabolic pathways, results in serious side effects,[18-20] and in many cases it is not well tolerated by patients. Thus, it is essential to develop newer drugs having better isoform selectivity and thus fewer side effects.

4.2 Discussion

Our drug design started from the idea to combine the primary sulfonamide moiety as typical zinc binding group (ZBG) with the interesting antioxidant proprieties of organo-selenium scaffolds.[21-23] Thus, we investigated different selenides incorporating a benzenesulfonamide moiety as carbonic anhydrase inhibitors (CAI). The synthetic approach towards the synthesis of diselenide **3** is shown in **Scheme 1**. The diazonium salt of sulfanilamide was prepared by reaction of **1** with sodium nitrite in the presence of acid (Sandmeyer reaction) and used as key intermediate for the synthesis of compound **2.** Successively, the selenocyanate derivative **2** was easily converted into the diselenide **3** as reported previously by our group[24] (**Scheme 1**).

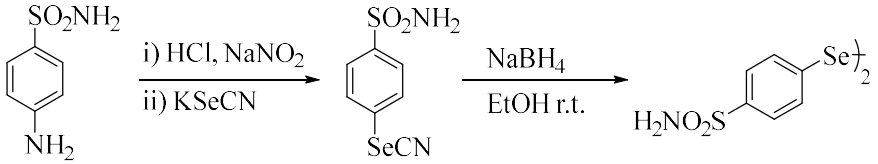

1 **2** **3**

Scheme 1. Synthesis of selenocyanate **2** and diselenide **3** bearing benzenesulfonamide moiety

Thereafter, **3** was reduced with $NaBH_4$ to the corresponding selenolate, which in turn was treated *in situ* with the appropriate halo-alkyl moieties **4a-j**, affording the selenides **5a-j** in good yield (**Table 1**).

Table 1: Synthesis of selenides bearing benzenesulfonamide moiety **5a-j**.

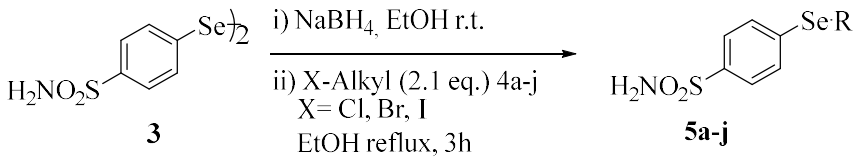

3 **5a-j**

Entry	X-Alkyl	Product
1	HO, Cl **4a**	OH, Se, H_2NO_2S **5a**
2	Br **4b**	Se, H_2NO_2S **5b**
3	ICH_3 **4c**	Se, H_2NO_2S **5c**
4	Br **4d**	Se, H_2NO_2S **5d**
5	Br **4e**	Se, H_2NO_2S **5e**
6	Br **4f**	Se, H_2NO_2S **5f**
7	Br **4g**	Se, H_2NO_2S **5g**
8	Br **4h**	Se, H_2NO_2S **5h**
9	Br **4i**	Se, H_2NO_2S **5i**
10	O, Cl **4j**	Se, O, H_2NO_2S **5j**

In order to propose an alternative way to access the target compounds, we sought to achieve selenides from the selenocyanate **2**, thus avoiding the synthesis of the diselenide **3**. We were pleased to observe that selenides **5a-j** were obtained by nucleophilic substitution with the selenolate, *in situ* generated by reducing **2**, as reported in **Scheme 2**.

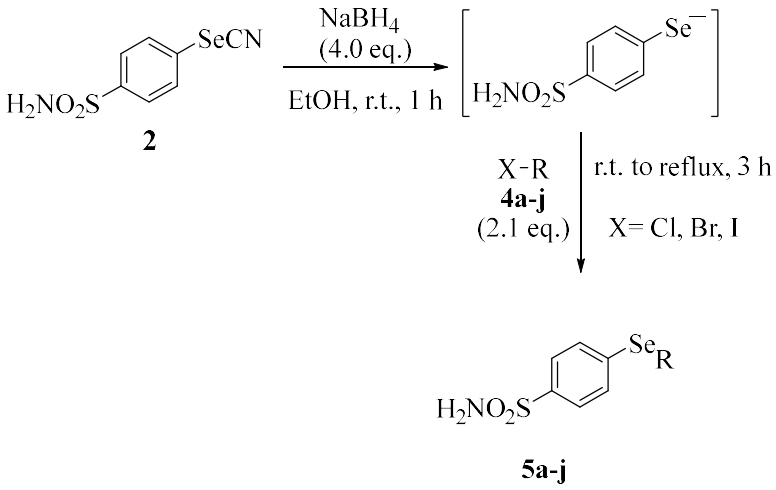

Scheme 2. Synthesis of selenides **5a-j** bearing benzenesulfonamide moiety

In order to access different benzenesulfonamide with a seleno aromatic tail (**9**), the procedure started with synthetized 4-(bromomethyl)benzenesulfonamide **7** as reported in **Scheme 3**. The compound **7** was synthesized following the method of Naganawa *et al.*[25]

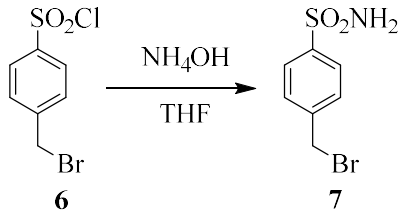

Scheme 3. Synthesis of 4-(bromomethyl)benzenesulfonamide **7**

Finally, the selenide **9** was obtained from reduction of diphenyldiselenide **8** with $NaBH_4$ and *in situ* was added sulfonamide **7** to afford in good yield the selenide **9** as outlined in **scheme 4**.

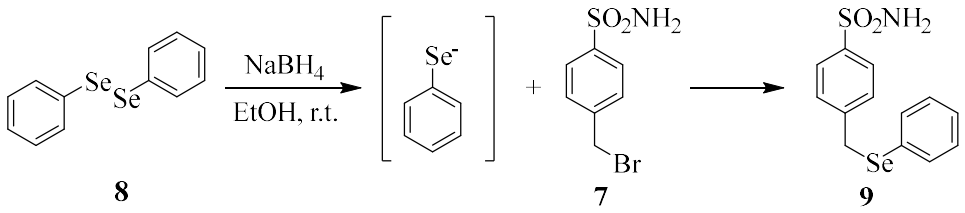

Scheme 4. Synthesis of 4-((phenylselanyl)methyl)benzenesulfonamide **9**

In this study the CA inhibition profile of compounds **2**, **3**, **5a-j** and **9** was investigated against six human isoforms such as the physiologically relevant CA I, II, VA, VB, VII and IX by means of the stopped-flow carbon dioxide hydration assay.[26] Their activities were compared to the standard CAIs acetazolamide (**AAZ**) and topiramate (**TPM**) (**Table 2**).

Table 2. Inhibition constants of hCA I, hCA II, hCA VA, hCA VB, hCA VII and hCA IX with compounds **2**, **3**, **5a-j**, **9** and **AAZ** by a stopped-flow CO_2 hydrase assay[26]

	K_i (nM)*					
Compound	hCA I	hCA II	hCA VA	hCA VB	hCA VII	hCA IX[a]
2	95.6	53.1	8.2	5.7	7.1	9.3
3	1522.7	7.9	7.3	5.7	40.5	2.7
5a	338.3	355.3	5.4	46.8	27.1	2.4
5b	256.8	9.3	5.1	36.0	0.31	8.7
5c	352.2	73.2	7.3	31.3	4.6	2.7
5d	9.7	69.9	7.1	5.7	0.28	2.4
5e	5.2	36.5	6.9	45.1	0.27	2.6
5f	7.3	9.3	5.8	22.8	0.25	2.7
5g	293.5	7.6	7.1	16.8	2.0	2.2
5h	297.1	70.8	2.9	12.3	0.38	2.6
5i	21.9	6.3	8.8	12.7	0.24	2.6
5j	261.7	41.2	4.0	5.5	0.77	12.0
9	226.1	53.0	5.4	19.1	6.6	2.7
TPM	250.0	10.0	63.0	30.0	9.0	58.0
AAZ	250.0	12.1	63.0	54.0	2.5	25.8

* Mean from three determinations by a stopped-flow, CO_2 hydrase method. Standard errors were in the range of 5–10% of the reported values.

[a] Catalytic domain

One goal of this study was to generate compounds containing organoseleno scaffolds with antioxidant properties to improve the selectivity in targeting the mitochondrial hCAs (VA and VB) when compared to the clinically used topiramate inhibitor (**TPM**). For the preliminary investigation, we tested the key intermediates **2** and **3** and we observed that the replacement of the selenocyanate group by a diselenide was well tolerated except for the hCA I (K_i 1522.7 nM for **3** against h CA I). The following structure−activity-relationship (SAR) for selenides **5a-j** and **9** were observed by analyzing CA the inhibition data in **Table 2**. The inhibition profile of hCA I was comparable to standards **AAZ** and **TPM**, except for **5d-f** and **5i**. These compounds showed an activity 10 times greater for **5i** and over 25 times greater for **5d-f**. The other dominant cytosolic isoform, hCA II, was inhibited by almost all selenides with an inhibition constant in the medium nanomolar range except for compound **5a** in high nanomolar range (K_i 6.3 to 355 nM). An interesting inhibition profile was observed for the mitochondrial isoform hCA VA. All compounds were potent inhibitors with an activity in the low nanomolar range (K_i 2.9 to 8.8 nM). On the other hand, the small and cyclic moieties found in **5c**, **5d** and **5i** led to less active inhibitors. This potency was substantially higher than for the reported standards, thus, these compounds were excellent candidates for follow-up cell-based studies. In addition, the second mitochondrial isoform hCA VB was also well inhibited by almost all selenides reported here. An interesting case was offered by compounds **5a** with **5j** with the latter being nearly 10 folds more potent. The differences in structures are represented by a hydroxyl *vs* a methoxy moiety respectively. The last cytosolic human isoform here studied, hCA VII, was also strongly inhibited by selenides **5a-j** with inhibition constants spanning from the subnanomolar (K_i 0.24 nM) to the medium nanomolar range (K_i 27.4 nM). Compound **5a**, this time, showed a potency of inhibition 35 fold less than the compound incorporating the methoxyl tail (**5j**). The transmembrane isoform hCA IX was effectively inhibited by all compounds here reported with K_is in the range of 2.2–12 nM. The SAR is almost absent in this case as all selenides showed a very comparable behavior as potent hCA IX inhibitors. In addition, hCA IX is not only implicated in ischemia-induced cerebrovascular pathology[14] but its expression is upregulated in a wide type of hypoxic tumors, thus several of these compounds may have potential as anticancer therapeutics.

The hCA II complex with compound **5e** was studied by means of X-ray experiments (**Figure 3**).[27]

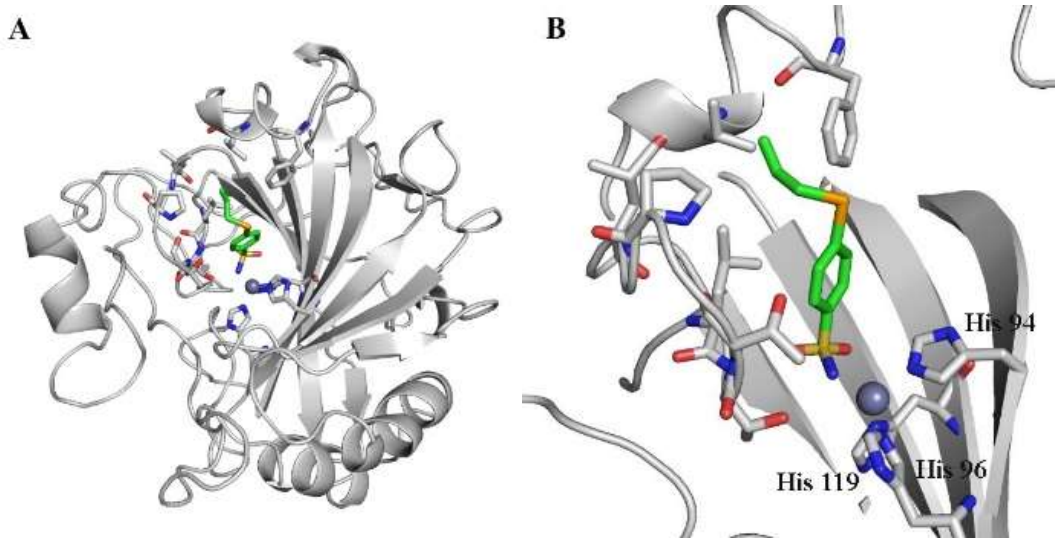

Figure 3. Whole protein hCA II with **5e** bound (**A**) and active site region of the hCA II/**5e** complex (**B**) (PDB code: 6CEH).

Active site analysis of selenide **5e** showed that the sulfonamide moiety of inhibitor was tightly coordinated to the Zn (II) ion by a binding mode to the protein similar to other CAIs containing the same ZBG.[27] Additionally, hydrophobic residues which are in relatively close proximity of the inhibitor scaffold are shown around the alkyl chain of compound **5e** (**Figure 3B**).

Some selected compounds (**3**, **5a**, **5d**, **5h** and **5j**), chosen among those possessing an interesting inhibitory profile against the mitochondrial hCA VA and VB, were tested to evaluate their effects on the viability of rat brain endothelial (RBE4) cells, cultured in oxidative stress condition in the presence of glucose oxidase (GOx). First of all, we evaluated the cytotoxicity of the tested compounds against RBE4 and the cell viability is shown in **Figure 4**.

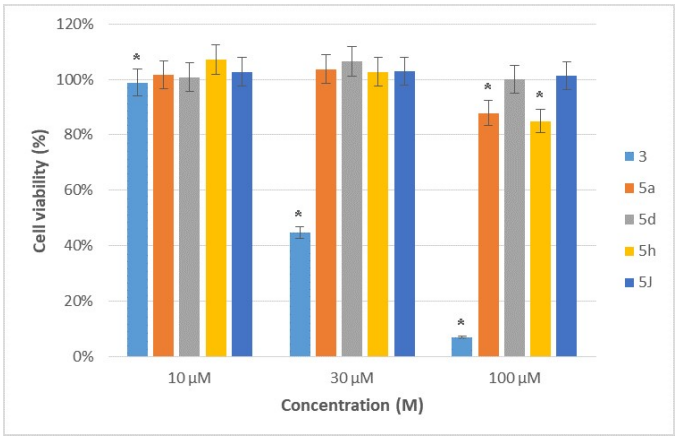

Figure 4. RBE4 cell viability ($4x10^4$ cell/well) following 24h- incubation with compounds **3**, **5a**, **5d**, **5h**, **5j** at 10, 30, 100 µM. *p<0.001 versus control

Diselenide **3** was significantly cytotoxic, inducing a mortality of about 50% at a concentration of 30 µM. All other selenides here reported proved to be safe at low concentrations. One should note that a decrease of cell viability was measured at high concentrations (100 µM), after 24h treatment with compounds **5a** and **5h**. The safe compounds **5a**, **5d**, **5h** and **5j** were evaluated as possible scavengers of oxidative stress by GOx. RBE4 cells were incubated with glucose oxidase in two concentrations (0.1 U/mL and 0.3 U/mL) and selenides. The results are shown in **Figure 5.**

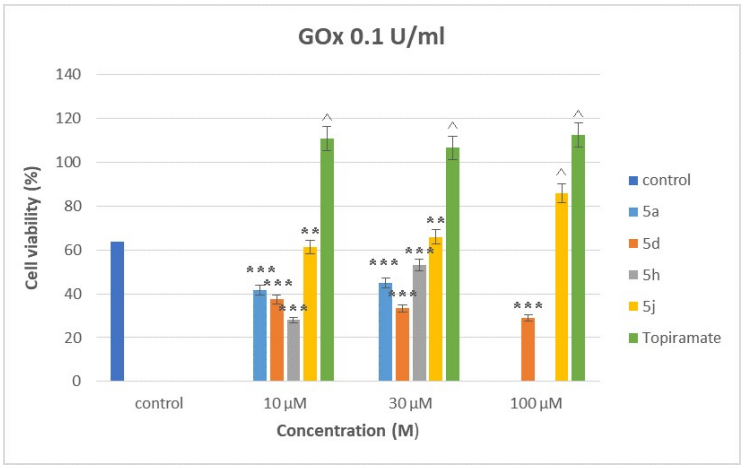

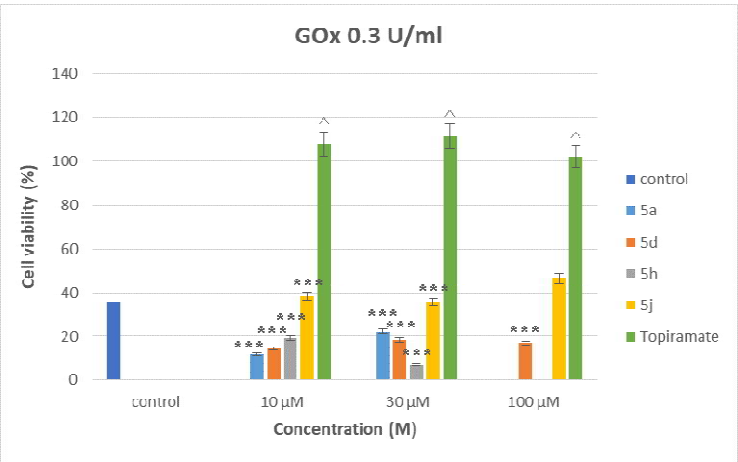

Figure 5. RBE4 cells (4x104 cell/well) were incubated 1h with GOx (0.1, 0.3 U/ml) and **5a**, **5d**, **5h**, **5j**. (10 and 30 µM, also 100 µM, when it was not cytotoxic) and the following 24h they recovered in culture medium with the compounds at the same concentrations. **p<0.01, ***p<0.001 versus control; ^p<0.05 vs GOX 0.1 U/ml

Cell viability of control decrease up to 40% with enhancement of GOx. Among the tested compounds, only the selenide **5j** showed good protection of cerebral endothelial cells from GOx damage at the higher dose (100 µM). The other selenides, did not show any significant scavenger activity in this assay conditions.

4.3 Conclusions

We synthesized, kinetically determined and studied the binding modes, by means of X-ray co-crystallographic adducts, of a novel series of selenides which behave as potent mitochondrial CA inhibitors. Compound **5j** proved to be effective as a scavenger agent on RBE4 cell line. Selective binding to mitochondrial CA is an important undertaking for targeting diabetic cerebrovascular pathology and is challenging with classical pharmacologically used sulfonamide/sulfamate CA inhibitors. The findings reported here are of substantial interest and highlight the potential of selenides bearing benzenesulfonamide groups to be exploited for the discovery of potent, mitochondrial-selective CA inhibitors.

4.4 Experimental data

General

Anhydrous solvents and all reagents were purchased from Sigma-Aldrich, Alfa Aesar and TCI. All reactions involving air- or moisture-sensitive compounds were performed under a nitrogen atmosphere using dried glassware and syringes techniques to transfer solutions. Nuclear magnetic resonance (^{1}H-NMR, ^{13}C-NMR, ^{19}F NMR, ^{77}Se-NMR) spectra were recorded using a Bruker Advance III 400 MHz spectrometer in DMSO-d_6. $(PhSe)_2$ was used as an external reference for ^{77}Se NMR (δ = 461 ppm). Chemical shifts are reported in parts per million (ppm) and the coupling constants (*J*) are expressed in Hertz (Hz). Splitting patterns are designated as follows: s, singlet; d, doublet; t, triplet; q, quadruplet; m, multiplet; brs, broad singlet; dd, double of doublets. The assignment of exchangeable protons (O*H* and N*H*) was confirmed by the addition of D_2O. Analytical thin-layer chromatography (TLC) was carried out on Merck silica gel F-254 plates. Flash chromatography purifications were performed on Merck Silica gel 60 (230-400 mesh ASTM) as the stationary phase and ethyl acetate/*n*-hexane were used as eluents. Melting points (mp) were measured in open capillary tubes with a Gallenkamp MPD350.BM3.5 apparatus and are uncorrected. The solvents used in MS measures were acetone, acetonitrile (Chromasolv grade), purchased from Sigma-Aldrich (Milan - Italy), and mQ water 18 MΩ, obtained from Millipore's Simplicity system (Milan-Italy). The mass spectra were obtained using a Varian 1200L triple quadrupole system (Palo Alto, CA, USA) equipped by Electrospray Source (ESI) operating in both positive and negative ions. Stock solutions of analytes were prepared in acetone at 1.0 mg mL^{-1} and stored at 4°C. Working solutions of each analyte were freshly prepared by diluting stock solutions in a mixture of mQ H_2O/ACN 1/1 (*v/v*) up to a concentration of 1.0 µg mL^{-1} The mass spectra of each analyte were acquired by introducing, via syringe pump at 10 µL min^{-1}, of the its working solution. Raw-data were collected andprocessed by Varian Workstation Vers. 6.8 software.

Procedure for the synthesis of compound 2:

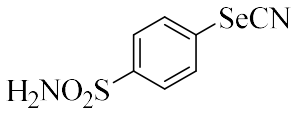

A suspension of 4-Aminonenzenesulfonamide **1** (1,72 g, 10 mmol) in H_2O (6 mL) with HCl (11 mL, 32 %) was cooled down to -5°C. Then, an aqueous solution of $NaNO_2$ (1.2 eq) was added dropwise and the mixture was kept stirring at the same temperature until a persistent pale yellow solution was formed (5–10 min). The resulting diazonium salt, kept at -5°C, was added KSeCN (1.2 eq). The reaction solution was stirred for 2 hours at the same temperature. The product was filtered off, washed with H_2O, dried under vacuo, and purified by flash column chromatography eluting with 1:1 mixture of hexane/ethyl acetate. (1.79 g, 83%). **^{1}H NMR** (400 MHz, DMSO-*d_6*) δ (ppm): 7.95 (2H, d, *J*=8.61), 7.89 (2H, d, *J*=8.68), 7.52 (2H, bs, N**H$_2$**, exchange with D2O). **^{13}C NMR** (100 MHz, DMSO-*d_6*) δ (ppm): 145.5, 134.1, 129.8, 127.9, 105.9. **^{77}Se NMR** (76 MHz, DMSO-*d_6*) δ (ppm): 340.0. MS (ESI negative) *m/z* (%): 261 $[M-H]^-$; ($[M-H]^-$ 260.93 required).

General procedure for synthesis of Compound 3:

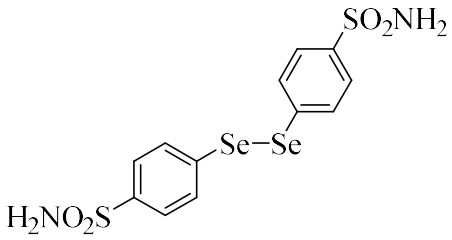

$NaBH_4$ (3 mmol) was added in small portions with caution to a solution of 4-selenocyanatobenzenesulfonamide **2** (3 mmol) in absolute ethanol (40 mL). The mixture was stirred at room temperature for 2 h. The solvents were removed under vacuum by rotary evaporation and the residue was treated with water. The mixture was extracted with ethyl acetate, dried with anhydrous Na_2SO_4, and purified by crystallization from EtOH. (529 mg, 75%). **^{1}H NMR** (400 MHz, DMSO- *d_6*) δ (ppm): 7.87 (2H, d, *J*=8.31), 7.79 (2H, d, *J*=8.36), 7.43 (2H, bs, N**H$_2$**, exchange with D_2O). **^{13}C NMR** (100 MHz, DMSO- *d_6*) δ (ppm): 144.3, 135.2, 131.5, 127.5. **^{77}Se NMR** (76 MHz, DMSO- *d_6*) δ (ppm): 446.7. MS (ESI negative) *m/z* (%):471 $[M-H]^-$; ($[M-H]^-$ 470.86 required)

General procedure for Synthesis Compounds 5a-j from diselenide 3:

$NaBH_4$ (23 mg, 0.60 mmol, 3.0 eq.) was portionwise added to a solution of 4,4'-diselanediyldibenzenesulfonamide **3** (94 mg, 0.20 mmol, 1.0 eq.) in EtOH (2 mL) at 0°C

under inert atmosphere (N_2). After 30 min, the halo-alkyl **4a-j** (0.36 mmol, 2.1 eq.) was slowly added and the reaction mixture was stirred at reflux for 3 h, until complete consumption of the starting material was observed by TLC. The reaction was quenched by addition of saturated aq. NH_4Cl (2 mL) and diluted with EtOAc (5 mL). The layers were separated and the aqueous layer was extracted with EtOAc (2 x 5 mL), dried over Na_2SO_4, filtered and concentrated under vacuum. The crude material was purified by flash chromatography to yield selenides (**5a-j**) bearing benzenesulfonamide moiety.

4-((2-hydroxyethyl)selanyl)benzenesulfonamide 5a:

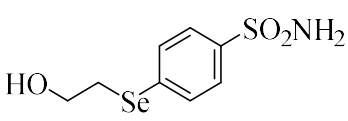

Following the general procedure, 4,4'-diselanediyldibenzenesulfonamide **3** (100 mg, 0.21 mmol) and chloroethanol **4a** (30 µl, 0.44 mmol) gave after flash chromatography (hexane/EtOAc 1:1) **5a** (80 mg, 68%). **^{1}H NMR** (400 MHz, DMSO- *d_6*) δ (ppm): 7.73 (2H, d, *J* = 8.62 Hz), 7.66 (2H, d, *J* = 8.64 Hz), 7.37 (2H, bs, N**H$_2$**, exchange with D_2O), 5.06 (1H, t, *J* = 5.5 Hz, O**H**), 3.69 (2H, dd, *J* = 6.82, 12.39 Hz), 3.16 (2H, t, *J* = 6.90 Hz). **^{13}C NMR** (100 MHz, DMSO-*d_6*) δ (ppm): 30.1, 61.4, 127.1, 131.1, 137.1, 142.6. **^{77}Se NMR** (76 MHz, DMSO-*d_6*) δ (ppm): 268.5. **MS** (ESI negative) *m/z*: 280 $[M-H]^-$; ($[M-H]^-$ 279.96 required)

4-(phenethylselanyl)benzenesulfonamide 5b:

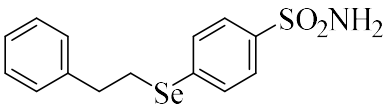

Following the general procedure, 4,4'-diselanediyldibenzenesulfonamide **3** (100 mg, 0.21 mmol) and (2-bromoethyl)benzene **4b** (60 µl, 0.44 mmol) gave after flash chromatography (hexane/EtOAc 1:1) **5b** (99 mg, 69%). **^{1}H NMR** (400 MHz, DMSO- *d_6*) δ (ppm): 7.74 (2H, d, *J* = 8.50 Hz), 7.67 (2H, d, *J* = 8.61 Hz), 7.38 (2H, bs, N**H$_2$**, exchange with D_2O), 7.36-7.26 (5H, m), 3.35 (2H, m), 3.01 (2H, t, *J* = 7.74 Hz). **^{13}C NMR** (100 MHz, DMSO-*d_6*) δ (ppm): 28.1, 36.3, 127.1, 127.3, 129.3, 131.1, 137.0, 141.4, 142,7. **MS** (ESI negative) *m/z*: 340 $[M-H]^-$; ($[M-H]^-$ 340.0 required)

4-(methylselanyl)benzenesulfonamide 5-c:

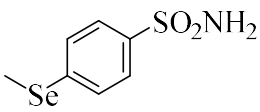

Following the general procedure, 4,4'-diselanediyldibenzenesulfonamide **3** (100 mg, 0.21 mmol) and iodomethane **4c** (27 µl, 0.44 mmol) gave after flash chromatography (hexane/EtOAc 1:1) **5c** (63 mg, 60%). **^{1}H NMR** (400 MHz, DMSO- d_6) δ (ppm): 7.73 (2H, d, J = 8.59 Hz), 7.60 (2H, d, J = 8.61 Hz), 7.36 (2H, bs, N**H$_2$**, exchange with D_2O), 2.45 (3H, s). **^{13}C NMR** (100 MHz, DMSO-d_6) δ (ppm):7.1, 127.0, 129.6, 138.5, 142.2. **MS** (ESI negative) *m/z*: 250 [M-H]$^-$; ([M-H]$^-$ 249.95 required)

4-(isopropylselanyl)benzenesulfonamide 5-d:

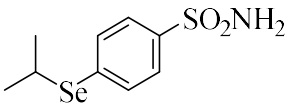

Following the general procedure, 4,4'-diselanediyldibenzenesulfonamide **3** (100 mg, 0.21 mmol) and 2-Bromopropane **4d** (41 µl, 0.44 mmol) gave after flash chromatography (hexane/EtOAc 1:1) **5d** (79 mg, 68%). **^{1}H NMR** (400 MHz, DMSO- d_6) δ (ppm): 7.76 (2H, d, J = 8.51 Hz), 7.70 (2H, d, J = 8.53 Hz), 7.40 (2H, bs, N**H$_2$**, exchange with D_2O), 3.76 (1H, m), 1.45 (6H, d, J = 6.79 Hz). **^{13}C NMR** (100 MHz, DMSO-d_6) δ (ppm):24.6, 33.9, 127.1, 133.2, 136.3, 143.2. **MS** (ESI negative) *m/z*: 278 [M-H]$^-$; ([M-H]$^-$ 277.98 required)

4-(allylselanyl)benzenesulfonamide 5-e:

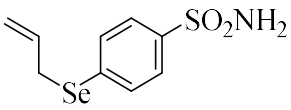

Following the general procedure, 4,4'-diselanediyldibenzenesulfonamide **3** (100 mg, 0.21 mmol) and Allyl bromide **4e** (38 µl, 0.44 mmol) gave after flash chromatography (hexane/EtOAc 1:1) **5e** (63 mg, 54%). **^{1}H NMR** (400 MHz, DMSO- d_6) δ (ppm): 7.73 (2H, d, J = 8.14 Hz), 7.66 (2H, d, J = 8.16 Hz), 7.37 (2H, bs, N**H$_2$**, exchange with D_2O), 6.0-5.9 (1H, m), 5.2 (1H, dd, J = 0.92, 16.9 Hz), 5.02 (1H, dd, J = 0.88, 9.98 Hz), 3.78 (2H, d, , J = 7.32 Hz) . **^{13}C NMR** (100 MHz, DMSO-d_6) δ (ppm): 29.7, 118.5, 127.0, 131.8, 135.0, 136.4, 143.0. **MS** (ESI negative) *m/z*: 276 [M-H]$^-$; ([M-H]$^-$ 275.97 required)

4-(prop-2-yn-1-ylselanyl)benzenesulfonamide 5-f:

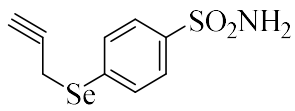

Following the general procedure, 4,4'-diselanediyldibenzenesulfonamide **3** (100 mg, 0.21 mmol) and Propargyl bromide **4f** (39 µl, 0.44 mmol) gave after flash chromatography (hexane/EtOAc 1:1) **5f** (57 mg, 50%). **^{1}H NMR** (400 MHz, DMSO- d_6) δ (ppm): 7.78 (2H, d, J = 8.59 Hz), 7.68 (2H, d, J = 8.61 Hz), 7.40 (2H, bs, N**H$_2$**, exchange with D_2O), 6.54 (1H, t, J = 6.26 Hz), 5.09 (2H, d, J = 6.26 Hz). **^{13}C NMR** (100 MHz, DMSO-d_6) δ (ppm):14.8, 76.1, 78.3, 127.3, 131.0, 136.9, 143.3. **MS** (ESI negative) *m/z*: 274 $[M-H]^-$; ($[M-H]^-$ 273.95 required)

4-(but-2-yn-1-ylselanyl)benzenesulfonamide 5g:

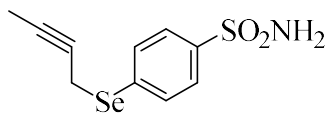

Following the general procedure, 4,4'-diselanediyldibenzenesulfonamide **3** (100 mg, 0.21 mmol) and 1-Bromo-2-butyne **4g** (39 µl, 0.44 mmol) gave after flash chromatography (hexane/EtOAc 1:1) **5g** (64 mg, 53%). **^{1}H NMR** (400 MHz, DMSO- d_6) δ (ppm): 7.76 (2H, d, J = 8.52 Hz), 7.69 (2H, d, J = 8.58 Hz), 7.39 (2H, bs, N**H$_2$**, exchange with D_2O), 3.83 (2H, dd, J = 2.56, 5.19 Hz), 1.81 (3H, t, J = 2.57 Hz). **^{13}C NMR** (100 MHz, DMSO-d_6) δ (ppm): 4.2, 12.8, 76.6, 80.5, 127.0, 131.3, 136.6, 143.0. **MS** (ESI negative) *m/z*: 288 $[M-H]^-$; ($[M-H]^-$ 287.97 required)

4-(pentylselanyl)benzenesulfonamide 5h:

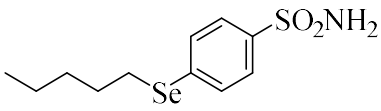

Following the general procedure, 4,4'-diselanediyldibenzenesulfonamide **3** (100 mg, 0.21 mmol) and 1-bromopentane **4h** (55 µl, 0.44 mmol) gave after flash chromatography (hexane/EtOAc 1:1) **5h** (77 mg, 60%). **^{1}H NMR** (400 MHz, DMSO- d_6) δ (ppm): 7.73 (2H, d, J = 8.59 Hz), 7.64 (2H, d, J = 8.63 Hz), 7.35 (2H, bs, N**H$_2$**, exchange with D_2O), 3.09 (2H, t, J = 7.37 Hz), 1.71 (2H, m), 1.38 (4H, m), 0.89 (3H, t, J = 7.18 Hz). **^{13}C NMR** (100 MHz, DMSO-d_6) δ (ppm):14.7, 22.4, 27.1, 29.9, 32.2, 127.1, 131.1, 137.1, 142.6. **MS** (ESI negative) *m/z*: 306 $[M-H]^-$; ($[M-H]^-$ 306.01 required)

4-(cyclohexylselanyl)benzenesulfonamide 5i:

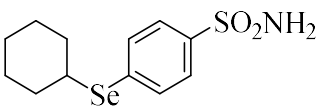

Following the general procedure, 4,4'-diselanediyldibenzenesulfonamide **3** (100 mg, 0.21 mmol) and Bromocyclohexane **4i** (54 µl, 0.44 mmol) gave after flash chromatography (hexane/EtOAc 1:1) **5i** (96 mg, 72%). **^{1}H NMR** (400 MHz, DMSO- *d_6*) δ (ppm): 7.75 (2H, d, *J* = 8.61 Hz), 7.69 (2H, d, *J* = 8.64 Hz), 7.37 (2H, bs, N**H$_2$**, exchange with D_2O), 3.60 (1H, m), 2.02 (2H, m), 1.72 (2H, m), 1.70-1.32 (6H, m). **^{13}C NMR** (100 MHz, DMSO-*d_6*) δ (ppm): 26.1, 26.9, 34.4, 43.0, 127.1, 133.2, 135.7, 143.2. **MS** (ESI negative) *m/z*: 318 $[M-H]^-$; ($[M-H]^-$ 318.01 required)

4-((2-methoxyethyl)selanyl)benzenesulfonamide 5j:

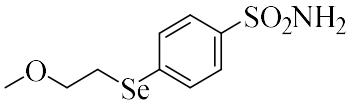

Following the general procedure, 4,4'-diselanediyldibenzenesulfonamide **3** (100 mg, 0.21 mmol) and 2-Chloroethyl methyl ether **4j** (40µl, 0.44 mmol) gave after flash chromatography (hexane/EtOAc 1:1) **5j** (108 mg, 87%). **^{1}H NMR** (400 MHz, DMSO- *d_6*) δ (ppm): 7.73 (2H, d, *J* = 8.64 Hz), 7.67 (2H, d, *J* = 8.68 Hz), 7.38 (2H, bs, N**H$_2$**, exchange with D_2O), 3.65 (2H, t, *J* = 6.64 Hz), 3.30 (3H, s), 3.26 (2H, t, *J* = 6.64 Hz). **^{13}C NMR** (100 MHz, DMSO-*d_6*) δ (ppm): 26.5, 58.7, 71.9, 127.1, 131.1, 136.9, 142.7. **MS** (ESI negative) *m/z*: 294 $[M-H]^-$; ($[M-H]^-$ 293.98 required)

General procedure for the synthesis of selenides 5a-j from selenocyanate 2:

$NaBH_4$ (30 mg, 0.80 mmol, 4.0 eq.) was portionwise added to a solution of 4-selenocyanatobenzenesulfonamide **2** (52 mg, 0.20 mmol, 1.0 eq.) in EtOH (2 mL) at room temperature under inert atmosphere (N_2). After 1 h, the halo-alkyl compounds **4a-j** (0.20 mmol, 1.0 eq.) was slowly added and the reaction mixture was stirred at reflux for 3 h, until complete consumption of the starting material was observed by TLC. The reaction was quenched by addition of saturated aq. NH_4Cl (2 mL) and diluted with EtOAc (5 mL). The layers were separated and the aqueous layer was extracted with EtOAc (2 x 5 mL), dried over Na_2SO_4, filtered and concentrated under vacuum. The crude material was purified by flash chromatography to yield selenides bearing benzenesulfonamide moiety **5a-j**.

General procedure for the synthesis of sulfonamide 7:

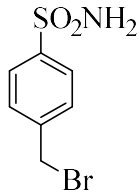

4-(bromomethyl)benzenesulfonyl chloride **6** (10 mmol) was added to a solution of THF (40 mL). 2.8 ml of ammonium hydroxide solution (30%) was added at 0° C and the mixture stirred at room temperature for 1 h. The reaction mixture was quenched with water and extracted with ethyl acetate, dried with anhydrous Na_2SO_4, and concentrated to yield **6**. (2,94 g, 95%). **^{1}H NMR** (400 MHz, DMSO-d_6) δ (ppm): 7.84 (2H, d, *J*=8.37), 7.67 (2H, d, *J*=8.39), 7.42 (2H, bs, N**H$_2$**, exchange with D_2O), 4.80 (2H, s). **^{13}C NMR** (100 MHz, DMSO- d_6) δ (ppm): 33.9, 127.0, 130.7, 142.8, 144.7.

General procedure for the synthesis of selenide 9:

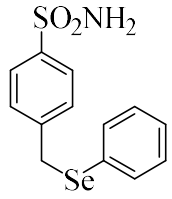

$NaBH_4$ (32 mg, 0.85 mmol, 4.0 eq.) was portionwise added to a solution of diphenyldiselenide **8** (100 mg, 0.21 mmol, 1.0 eq.) in EtOH (5 mL) at room temperature under inert atmosphere (N_2). After 30 min, sulfonamide **7** (105 mg, 0.42 mmol, 2.0 eq.) was slowly added and the reaction mixture was stirred at room temperature for 3 h, until complete consumption of the starting material was observed by TLC. The reaction was quenched by addition of saturated aq. NH_4Cl (2 mL) and diluted with EtOAc (5 mL). The layers were separated and the aqueous layer was extracted with EtOAc (2 x 5 mL), dried over Na_2SO_4, filtered and concentrated under vacuum. The crude material was purified by flash chromatography (hexane/EtOAc 1:1) to yield selenide **9**. (116 mg, 85%). **^{1}H NMR** (400 MHz, DMSO- d_6) δ (ppm): 7.72 (2H, d, *J* = 8.36 Hz), 7.651 (2H, dd, *J* = 1.72, 7.76 Hz), 7.47 (2H, d, *J* = 8.36 Hz), 7.33-7.31 (5H, m), 4.33 (2H, s). **^{13}C NMR** (100 MHz, DMSO-d_6) δ (ppm):30.6, 126.6, 128.0, 130.1, 130.7, 133.0, 143.3, 144.1. **^{77}Se NMR** (76 MHz, DMSO-d_6) δ (ppm): 373.5 **MS** (ESI negative) *m/z*: 326 $[M-H]^-$; ($[M-H]^-$ 325.98 required)

Carbonic anhydrase inhibition

An Applied Photophysics stopped-flow instrument has been used for assaying the CA catalyzed CO_2 hydration activity.[26] Phenol red (at a concentration of 0.2 mM) has been used as indicator, working at the absorbance maximum of 557 nm, with 20 mMHepes (pH 7.5) as buffer, and 20 mM Na_2SO_4 (for maintaining constant the ionic strength), following the

initial rates of the CA-catalyzed CO_2 hydration reaction for a period of 10–100 s. The CO_2 concentrations ranged from 1.7 to 17 mM for the determination of the kinetic parameters and inhibition constants. For each inhibitor at least six traces of the initial 5–10% of the reaction have been used for determining the initial velocity. The uncatalyzed rates were determined in the same manner and subtracted from the total observed rates. Stock solutions of inhibitor (0.1 mM) were prepared in distilled-deionized water and dilutions up to 0.01 nM were done thereafter with the assay buffer. Inhibitor and enzyme solutions were preincubated together for 15 min at room temperature prior to assay, in order to allow for the formation of the E-I complex. The inhibition constants were obtained by non-linear least-squares methods using PRISM 3 and the Cheng–Prusoff equation.

Protein X-ray Crystallography

The protein was concentrated to about 7 mg/mL and set up in SD2 crystallization plates (Molecular Dimensions) with the following ratio of protein plus reservoir: 200 nL + 200 nL. The plate was incubated at 8 ºC and the reservoir conditions consisted of 2.6 to 3.0 M ammonium sulfate with 0.1 M Tris buffer at pH 8.0 to pH 8.5. Dry compound was added to the crystallization drops after crystals had formed and several days before data were collected. 360 frames of one degree oscillation were obtained from the MX1 beamline of the Australian Synchrotron. The data were indexed using XDS[28] and scaled using Aimless.[29] Molecular replacement was done using Phaser[30] using 4cq0 as the initial starting model. The model was manually rebuilt using Coot[31] and refined using Refmac.[32] The compound was placed in density using the program Afitt (OpenEye Scientific Software) and further refined using Refmac.

Summary of Data Collection and Atomic Model Refinement Statistics

PDB	6CEH
Compound	5e
Space group	$P2_1$
Cell dimensions	
a, b, c	42.5, 41.5, 72.5
alpha, beta, gamma	90, 104.5, 90
Resolution (Å)	41.5 - 1.43
Resolution-high (Å)	1.46 - 1.43
Rmerge	0.092 (0.590)
Rpim	0.037 (0.240)
CC ½	0.998 (0.864)
I/sigI	17.1 (3.3)
Completeness (%)	99.3 (95.9)
Redundancy	7.1 (6.8)
Refinement	
resolution (Å)	41.5 - 1.43
unique reflections	42805
Rwork/Rfree (%)	15.2 / 20.8
# atoms	2553
Protein	2137
metal (Zn)	1
ligand	28
water	371
B-factors (Å^2)	11,0
protein	9,9
metal (Zn)	4,8
ligand	13,6
water	24,8
r.m.s. deviations	
Bond length (Å)	0,017
Bond angle (°)	1,916

Biological Assays

Cell culture and treatment

Rat brain endothelial cells RBE4 were obtained from American Type Culture Collection (Rockville, MD) and were cultured in MEM Alpha/NutriHam F-10 in 1:1 ratio (Thermo Fisher Scientific, Italy) , supplemented with 10% fetal bovine serum, 0.1% basic fibroblast growth factor, 100 IU mL^{-1} penicillin and 100 µg mL^{-1} streptomycin (Sigma, Milan, Italy) at 37°C in humidified, 5% CO_2 atmosphere. 4 x 104 cells *per* well were plated in 96-well plates and treated for cytotoxicity assay: cells were incubated with the tested compounds for 24h. The same number of cells was plated for GOx-induced oxidative stress damage: cells were co-treated with GOx 0.1 or 0.3 U/L and the non-cytotoxic compounds (0-100µM) for 1h and then were allowed to recovery in the culture medium with the compounds at the same concentration.

Cell viability assay

Cell viability was assessed using 3-(4,5-dimethylthiazol-2-yl)-2,5-diphenyltetrazolium bromide (MTT) assay. Following treatments, cells were washed and incubated with MTT solution (1 mg/ml) at 37°C for 30 minutes in humidified, 5% CO_2 atmosphere. After washing, the formazan crystals were solubilized in 200 µl DMSO and absorbance was measured at 550 nm wavelength

References

1. Mathers C.D., Loncar D. Projection of global mortality and burden of disease from 2002 to 2030. *PLoS Med*, 2006, 3, e442.
2. Balasubramanyam M., Rema M., Premanand C. Biochemical and molecular mechanisms of diabetic retinopathy. *Current Science*. 2002, 83, 1506–1514.
3. Price T.O., Eranki V., Banks W.A., Ercal N., Shah G.N. Topiramate treatment protects blood-brain barrier pericytes from hyperglycemia-induced oxidative damage in diabetic mice, *Endocrinology* 2012**,** 153, 362–372.
4. Price T.O., Farr S.A., Niehoff M.L., Ercal N., Morley J.E., Shah G.N. Protective effect of topiramate on hyperglycemia-induced cerebral oxidative stress, pericyte loss and learning behavior in diabetic mice *Int. Libr. Diabetes Metab.* 2015**,** 1, 6–12.
5. Starr J.M., Wardlaw J., Ferguson K., MacLullich A., Deary I.J., Marshall I. Increased blood-brain barrier permeability in type II diabetes demonstrated by gadolinium magnetic resonance imaging. *J. Neurol. Neurosurg. Psychiatry* 2003, 74, 70–76.
6. Woerdeman J., Van D.E., Wattjes M.P., Barkhof F., Snoek F.J., Moll A.C., Klein M., de Boer M.P., Ijzerman R.G., Serne E.H., Diamant M. Proliferative retinopathy in type 1 diabetes is associated with cerebral microbleeds, which is part of generalized microangiopathy. *Diabetes Care* 2014, 37, 1165–1168.
7. Huber J.D. Diabetes, cognitive function, and the blood-brain barrier. *Curr. Pharm. Des.* 2008**,** 14, 1594–1600.
8. Janson J., Laedtke T., Parisi J.E., O'Brien P., Petersen R.C., Butler P.C. Increased risk of type 2 diabetes in Alzheimer disease, *Diabetes* 2004**,** 53, 474–481.
9. Kalaria R.N. Neurodegenerative disease: diabetes, microvascular pathology and Alzheimer disease, *Nat. Rev. Neurol.* 2009, 5, 305–306.

10. Armulik A., Genove G., Mae M., Nisancioglu M.H., Wallgard E., Niaudet C., He L., Norlin J., Lindblom P., Strittmatter K., Johansson B.R., Betsholtz C. Pericytes regulate the blood–brain barrier, *Nature* 2010**,** 468, 557–561.

11. Shah G.N., Price T.O., Banks W.A., Morofuji Y., Kovac A., Ercal N., Sorenson C.M., Shin E.S., Sheibani N. Pharmacological inhibition of mitochondrial carbonic anhydrases protects mouse cerebral pericytes from high glucose-induced oxidative stress and apoptosis, *J. Pharmacol. Exp. Ther.* 2012 344, 637–645.

12. Price T.O., Sheibani N., Shah G.N. Regulation of high glucose-induced apoptosis of brain pericytes by mitochondrial CA VA: A specific target for prevention of diabetic cerebrovascular pathology. *Biochim Biophys Acta*. 2017, 4, 929-935.

13. Patrick P., Price T.O., Diogo A. L., Sheibani N., Banks W.A., Shah G.N. Topiramate Protects Pericytes from Glucotoxicity: Role for Mitochondrial CA VA in Cerebromicrovascular Disease in Diabetes. *J Endocrinol Diabetes*. 2015, 2, 1-7.

14. Di Cesare M.L., Micheli L., Carta F., Cozzi A., Ghelardini C., Supuran C.T. Carbonic anhydrase inhibition for the management of cerebral ischemia: in vivo evaluation of sulfonamide and coumarin inhibitors. *J. Enzyme Inhib. Med. Chem.* 2016, 31, 894–899.

15. De Simone G., Supuran C. T. Antiobesity carbonic anhydrase inhibitors. *Curr. Top. Med. Chem.* 2007, 7, 879.

16. Poulsen S.A.; Wilkinson B. L.; Innocenti A.; Vullo D.; Supuran C. T. Inhibition of human mitochondrial carbonic anhydrases VA and VB with para-(4-phenyltriazole-1-yl)-benzenesulfonamide derivatives *Bioorg. Med. Chem. Lett.* 2008, 18, 4624.

17. Supuran, C. T. Carbonic anhydrases: novel therapeutic applications for inhibitors and activators *Nature Rev. Drug Discovery* 2008, 7, 168.

18. Shah G. N., Rubbelke T. S., Hendin J., Nguyen H., Waheed A., Shoemaker J.D. Targeted mutagenesis of mitochondrial carbonic anhydrases VA and VB implicates

both enzymes in ammonia detoxification and glucose metabolism. *Proc Natl Acad Sci USA*. 2013, 110, 7423–7428.

19. Deutsch S. I., Schwartz B.L., Rosse R.B., Mastropaolo J., Marvel C.L., Drapalski A.L. Adjuvant topiramate administration: a pharmacologic strategy for addressing NMDA receptor hypofunction in schizophrenia. *Clin Neuropharmacol*. 2003; 26, 199–206.

20. Nishimori I., Vullo D., Innocenti A., Scozzafava A., Mastrolorenzo A., Supuran C. T. Carbonic anhydrase inhibitors: inhibition of the transmembrane isozyme XIV with sulfonamides. *Bioorg Med Chem Lett.* 2005, 17, 3828–3833.

21. Angeli A., Tanini D., Peat T. S., Di Cesare Mannelli L., Bartolucci G., Capperucci A., Ghelardini C., Supuran C. T., Carta F. Discovery of New Selenoureido Analogues of 4-(4-Fluorophenylureido)benzenesulfonamide as Carbonic Anhydrase Inhibitors. *ACS Med Chem Lett.* 2017, 8, 963-968.

22. Tanini D., Panzella L., Amorati R., Capperucci A., Pizzo E., Napolitano A., Menichetti S., d'Ischia M., Resveratrol-based benzoselenophenes with an enhanced antioxidant and chain breaking capacity. *Org Biomol Chem.* 2015, 13, 5757-5764.

23. Angeli A., Tanini D., Viglianisi C., Panzella L., Capperucci A., Menichetti S., Supuran C. T. Evaluation of selenide, diselenide and selenoheterocycle derivatives as carbonic anhydrase I, II, IV, VII and IX inhibitors. *Bioorg Med Chem.* 2017, 25, 2518-2523.

24. Angeli A., Tanini D., Capperucci A., Supuran C. T. Synthesis of novel selenides bearing benzenesulfonamide moieties as carbonic anhydrase I, II, IV, VII and IX inhibitors *ACS Med. Chem. Lett.*, 2017, *8*, 1213-1217.

25. Naganawa A., Matsui T., Ima M., Saito T., Murota M., Aratani Y., Kijima H., Yamamoto H., Maruyama T., Ohuchida S., Nakai H., Toda M., Further optimization of sulfonamide analogs as EP1 receptor antagonists: Synthesis and evaluation of bioisosteres for the carboxylic acid group. *Bioorg Med Chem.* 2006, 14, 7121-7137.

26. Khalifah R. G. The carbon dioxide hydration activity of carbonic anhydrase. I. Stop flow kinetic studies on the native human isoenzymes B and C. *J. Biol. Chem*. 1971, 246, 2561.

27. Alterio V.; Di Fiore A.; D'Ambrosio K.; Supuran C.T.; De Simone G. Multiple binding modes of inhibitors to carbonic anhydrases: how to design specific drugs targeting 15 different isoforms? *Chem. Rev.* 2012, 112, 4421−4468.

28. Kabsch, W. XDS. *Acta Crystallogr. Sect. D: Biol. Crystallogr.*, 2010, 66, 125-132

29. Evans P. R. An introduction to data reduction: space group determination, scaling and intensity statistics. *Acta Crystallogr. D: Biol. Crystallogr.*, 2011, 67, 282-292.

30. McCoy A.J.; Grosse Kunstleve R.W.; Adams P.D.; Winn M.D.; Storoni L.C.; Read R.J. Phaser crystallographic software. *J. Appl. Crystallogr.*, 2007, 40, 658-674.

31. Emsley P.; Lohkamp B.; Scott W.G.; Cowtan K. Features and development of Coot. *Acta Crystallogr. D: Biol. Crystallogr.* 2010, 66, 486-501.

32. Murshudov G.N.; Skubak P.; Lebedev A.A.; Pannu N.S.; Steiner R.A.; Nicholls R.A.; Winn M.D.; Long F.; Vagin A.A. REFMAC5 for the refinement of macromolecular crystal structures. *Acta Crystallogr. D Biol. Crystallogr.*, 2011, 67, 355-367.

Chapter 5

CAIs with neuropathic pain modulating effects.

5.1 Introduction

Neuropathic pain is a major public health problem that affects approximately 6% of the adult population worldwide.[1] This condition manifests specific symptoms such as spontaneous burning pain and allodynia (pain that arises due to non-noxious stimuli) due to sensory system damage or disease.[1] Such symptoms have a significant impact on a patient's quality of life and social productivity. Despite several therapeutic options currently available, the treatment or control of neuropathic pain still remains challenging since the heterogeneous etiology associated to multifactorial mechanisms underlying this disease are often concomitant.[2] Damages to the nervous tissue trigger a complex machinery pathophysiologic events. A peripheral nerve lesion may provoke aberrant regeneration of the nerve, with the neurons becoming unusually sensitive and developing an abnormal excitability called peripheral sensitization.[3,4] On the other hand, a central component of pain is developed by direct or indirect alterations. The spinothalamic tract neurons aquire an increased background activity, coupled to enlarged receptive fields and increased responses to afferent impulses, including the normally innocuous stimuli. These mechanisms together with secondary events in the central pain processing pathways contribute to the development and maintenance of a steady-state pain condition.[5] Recently, pioneering work from Kaila and Price's groups discovered the connection between Carbonic Anhydrases (CAs) modulation and neuropathic pain.[6,7] These metalloenzymes catalysed efficiently the hydration of CO_2 to bicarbonate and protons. Generation of HCO_3^- as a reaction product of CO_2 hydration is closely connected with the physiology/biochemistry of many neurotransmitters, such as γ-aminobutyric acid (GABA).[8] CA inhibition with the clinically used sulfonamide acetazolamide (**AAZ**) augments $GABA_A$ receptor-mediated analgesia via a spinal mechanism of action. *In vivo* pharmacologic and modelling studies showed that a loss function of the neuron-specific potassium-chloride (KCl) cotransporter KCC2 leads to a decrease in the efficacy of $GABA_A$-mediated spinal inhibition.[7] In order to reduced bicarbonate-dependent depolarization via GABAA receptors when the function of KCC2 is compromised, one potential strategy was inhibit CA thus mitigates the negative effects of loss of KCC2 function after nerve injury.[8] The use of CAIs in the management of neuropathic

pain[9] and cerebral ischemia[10] showed very interesting preliminary results, which might lead to new possibilities of therapeutic applications for this class of compounds.

The physical damage by chemotherapeutic drugs leads to functional impairment in neurons through oxidative stress, inflammation, apoptosis and electrophysiological disturbances. In fact, oxidative stress is identified to be responsible for the neuronal damage in different models of neuropathies such as diabetic neuropathy, acryl amide induced neuropathy and Charcot–Marie neuropathy.[11-14]

5.2 Discussion

We propose a drug design strategy based on the combination of sulfonamide moiety as a typical zinc binding group (ZBG), with the well-known antioxidant propriety of organo-selenium scaffolds.[15-17] 4,4'-Diselanediyldibenzenesulfonamide **1** was synthesized from sulfanilamide in three steps using procedures outlined in **Chapter 4**.[18] Compound **1** was then treated with $NaBH_4$ and then treated *in situ* with the appropriate halo-alkyl derivatives (**2a-f**) to afford the corresponding selenides (**3a-f**) in good yields (**Table 1**).

Table 1: Synthesis of selenides bearing benzenesulfonamide moiety **3a-f.**

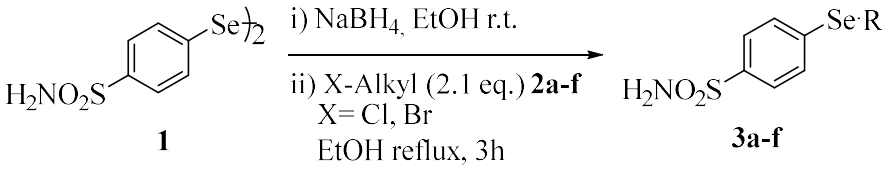

Entry	X-Alkyl	Product
1	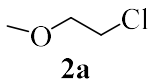 **2a**	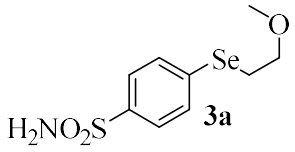 **3a**
2	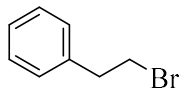 **2b**	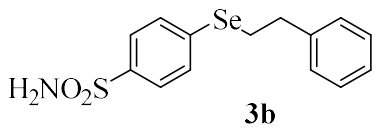 **3b**
3	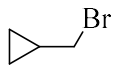 **2c**	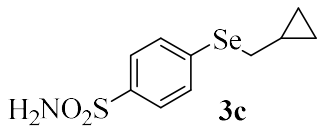 **3c**
4	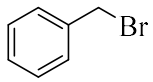 **2d**	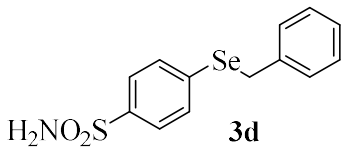 **3d**
5	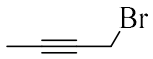 **2e**	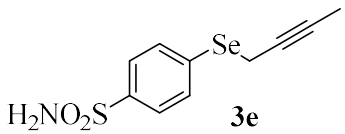 **3e**
6	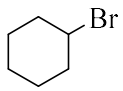 **2f**	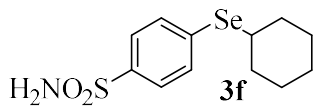 **3f**

In order to access various selenides different approaches were used. The synthesis of compounds **7a-b** was carried out according to **Scheme 1** by reduction of diselenides (**4a-b**) which was reacted with 4-(bromomethyl) benzenesulfonamide (**6**) to afford in good yields selenides **7a-b**.

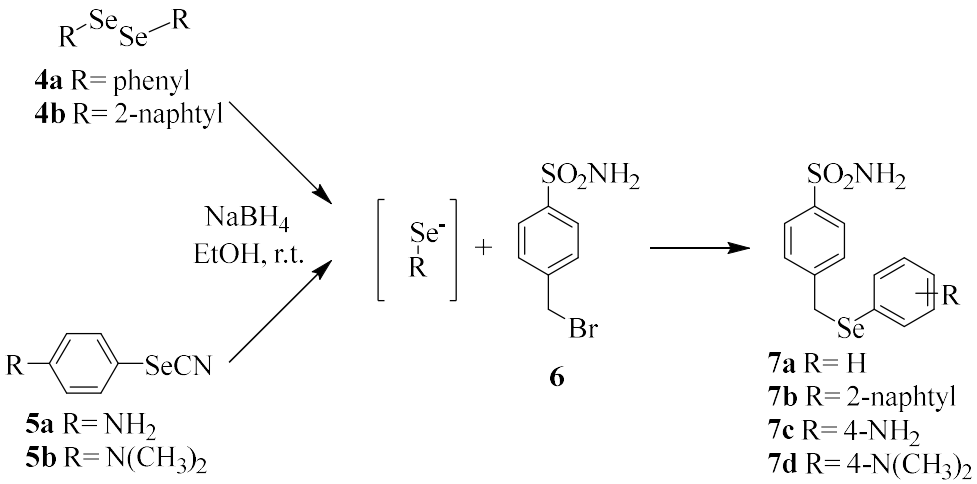

Scheme 1. Synthesis of selenides **7a-d** from different diselenides or selenocyanates

Two different amino aromatic selenocyanates (**5a-b**) proved efficient alternative to the use of diselenides for the obtainment of selenides **7c-d** as outlined in **Scheme 1.** The key intermediates selenocyanates **5a,b** were obtained according to the literature procedure [19] by addition of selenium dioxide to malononitrile in DMSO at room temperature followed by reaction with the corresponding aminoaryl derivatives. The aniline function of **7c** was then converted into two different moieties:

(i) Ureido containing compounds (**10a-c**) using the appropriate isocyanate or isothiocyanate (**8a-c**) in acetonitrile at room temperature as reported previously by our group;[20]

(ii) Amide containing derivatives (**11a-c**), obtained in excellent yield by using the appropriate acyl chloride (**9a-c**), in THF and triethylamine as reported in **Scheme 2**.

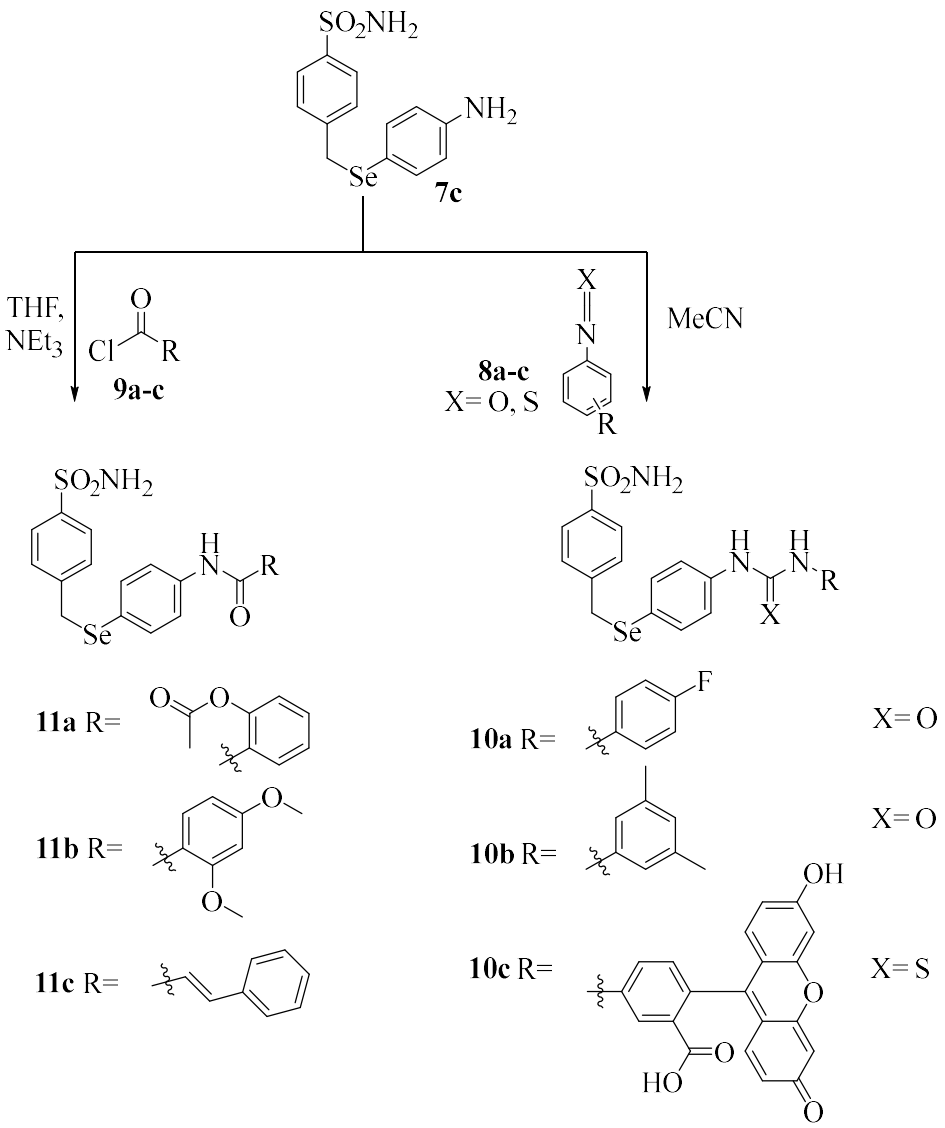

Scheme 2. Synthesis of new selenides with ureido (**10a-c**) and amido (**11a-c**) groups

Finally, the halogen pendant of 4-(bromomethyl) benzenesulfonamide **6** was used for nucleophilic displacement reactions using potassium selenocyanate to afford the 4-(selenocyanatomethyl)benzenesulfonamide **12** in good yields (**Scheme 3**).

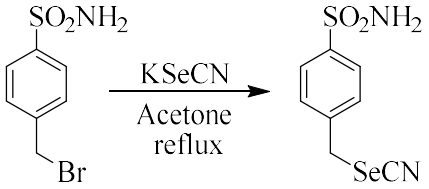

6 **12**

Scheme 3. Synthesis of 4-(selenocyanatomethyl)benzenesulfonamide **12**

All synthesized compounds **3a-f**, **7a-d**, **10a-c**, **11a-c** and **12** were tested *in vitro* for their inhibitory properties against the physiological relevant hCA isoforms (I, II, VII, and IX) by means of a stopped-flow carbon dioxide hydration assay [21] and their activities were compared to the standard carbonic anhydrase inhibitor (CAI) acetazolamide (**AAZ**) (**Table 2**).

Table 2. Inhibition constants of hCA I, hCA II, hCA VII and hCA IX with compounds **3a-f, 7a-d, 10a-c, 11a-c, 12** and **AAZ** by a stopped-flow CO_2 hydrase assay[21]

	K_i (nM)*			
Compound	hCA I	hCA II	hCA VII	hCA IX
3a	261.7	41.2	0.77	12.0
3b	256.8	9.3	0.31	8.7
3c	73.5	4.9	7.2	46.4
3d	531.2	3.9	1.8	548.6
3e	293.5	7.6	2.0	2.2
3f	21.9	6.3	0.24	2.6
7a	226.1	53.0	6.6	2.7
7b	953.7	70.8	645.0	337.4
7c	464.3	1.5	17.4	286.3
7d	841.1	46.9	311.8	450.1
10a	4767	220.5	295.6	1071
10b	926.8	6.0	86.0	1137
10c	755.4	0.94	3.8	697.4
11a	93.3	0.54	0.93	709.8
11b	5995	9.4	37.4	845.0
11c	2578	364.6	462.8	1006
12	70.2	14.0	0.97	4.0
AAZ	250	12.1	2.5	25.8

* Mean from three determinations by a stopped-flow, CO_2 hydrase method. Standard errors were in the range of 5–10% of the reported values.

The following SARs for the hCA isoforms considered are reported:

i) The ubiquitous cytosolic hCA I was weakly inhibited by all compounds except for **3f** which showed a good inhibition potency with K_i of 21.9 nM. The different tails of derivatives **3a-e** and **7a-c** did not significantly modified the activity. On the other hand, the inhibition potency decreased to the micromolar range when functionalization of compound **7c** to afford ureido (**10a-c**) and amido (**11a-c**) moieties was introduced. The only exception was represented by **11a** with K_i of 93.3 nM.

ii) The *in vitro* kinetic data showed that ureido **10c** and amido derivatives **11a** were the most potent inhibitors against the dominant cytosolic human isofom hCA II, in sub nanomolar range (K_i 0.94 and 0.54 nM respectively), followed by the compounds in series **3a-f** (K_i 3.9 to 41.2 nM). Low-medium inhibition potencies, with K_i values spanning between 220.5-364.6 nM, were obtained for compounds **10a** and **11c**.

iii) The last cytosolic human isoform studied here, hCA VII, was potently inhibited by many compounds investigated in the present article, in the sub or low-medium nanomolar range, except for derivatives **7c**, **10a** and **11c** which were active in the high nanomolar range (K_i 295.6-645.0 nM). Conversely, the different moieties of derivatives **3a-f** and **7a-c** influenced the activity, leading to a decrease of inhibition potency over 10 times for compounds **7a-c**. Further functionalization of compound **7c** to ureido (**10a-c**) and amido (**11a-c**) scaffolds determined strong change in the inhibition profiles against hCA VII, with **10c** and **11a** being highly potent.

iv) Similar to hCA I, the transmembrane tumor-associated hCA IX, was weakly inhibited by almost all compounds investigated here, which showed K_is in the high nanomolar range. Ureido and amido substituents (**10a-c** and **11a-c**), did not influence the efficacy of inhibition. On the other hand, the different moieties of selenides in the compounds series **3a-f** showed variety of inhibition profiles, thus proving to be crucial for the modulation of such hCA isoform.

Recent studies reported an enhanced expression of some cytosolic hCA isoforms (among which hCA II) in conditions connected to chronic pain, such as thrombus-induced ischemic pain,[22] or chronic musculoskeletal pain.[23] We solved the hCA II X-ray crystal structures in complex with compounds **3e** and **3f** (**Figure 1**) with the aim to obtain an insight into the ligand−protein interactions at the atomic level. As below showed the selenides bearing the sulfonamide moieties **3e-f** contain a short hydrophobic tail.

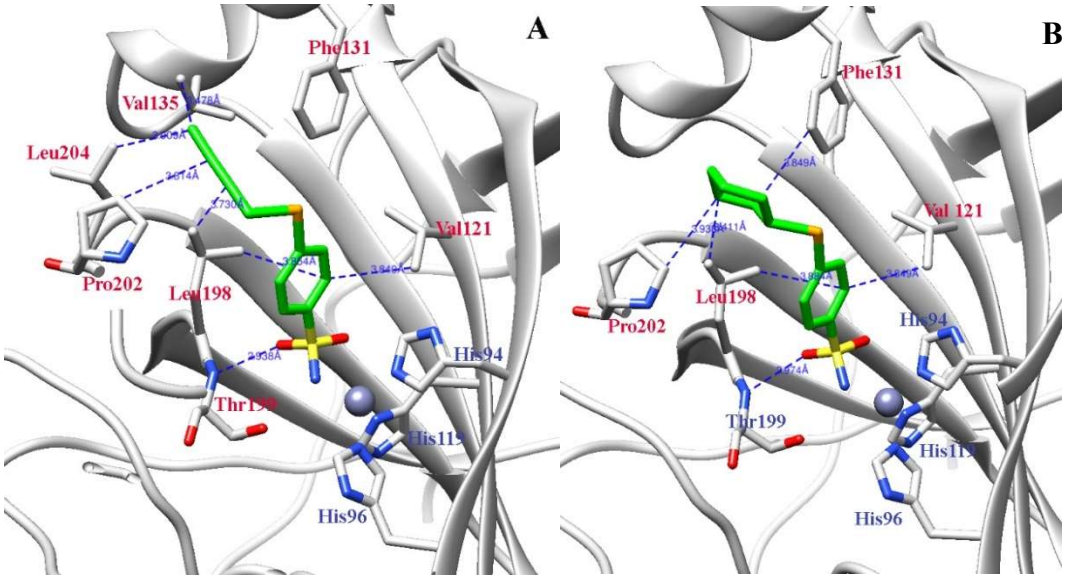

Figure 1. Inhibitors bound in the active site of hCA II. Ligands **3e** (**A**) (PDB: 6D1L) and **3f** (**B**) (PDB: 6D1M) are shown in green, the zinc ion is the gray sphere with its protein ligands (His94, 96 and 119 in blue) shown as stick model, in CPK colours. Residues involved in the binding of inhibitors are also shown and labelled in red.

In each protein–inhibitor complex the conserved zinc-bound water molecule is displaced by the inhibitors **3e** and **3f**, while additional hydrogen bond interactions with residue Thr199 further contribute to stabilize the binding (**Figure 1**). The hydrophobic tails of the inhibitors are oriented towards the hydrophobic region of the active site in a small pocket delimited by residues Val 121, Phe131, Val135, Leu198, and Pro202. We observed some different interactions in hydrophobic region between inhibitors, namely the cyclohexane tail of compound **3f** was in close proximity of Phe131, whereas the butyne moiety of **3e** showed additional hydrophobic interactions with Val135 and Leu204 residues (**Figure 1A**).

All these compounds are potent inhibitors of several physiologically relevant CA isoforms, such as hCA I, II, VII and IX., but to date there is not a precise knowledge which CA isoforms are involved in neuropathic pain responses. For this reason, we focused our attention on different cytosolic and transmembrane CAs which are commonly present in the central/peripheral nervous system such as the CA I, II, VII (the last one was predominantly expressed in the brain and being absent in most other tissues) and CA IX (transmembrane

isoform). We investigated different selenides such as **3a-b** and **7a** in comparison to acetazolamide (**AAZ**), as possible pain relievers in a mice model of neuropathic pain induced by oxaliplatin[24,25] (**Figure 2**). This platinum derivative has become a valid option as adjuvant therapy in several types of cancer.[24] However, a possible side effect is a painful neuropathy correlated with characteristic alterations of the nervous system leading to a negative influence on patients' quality of life.[24]

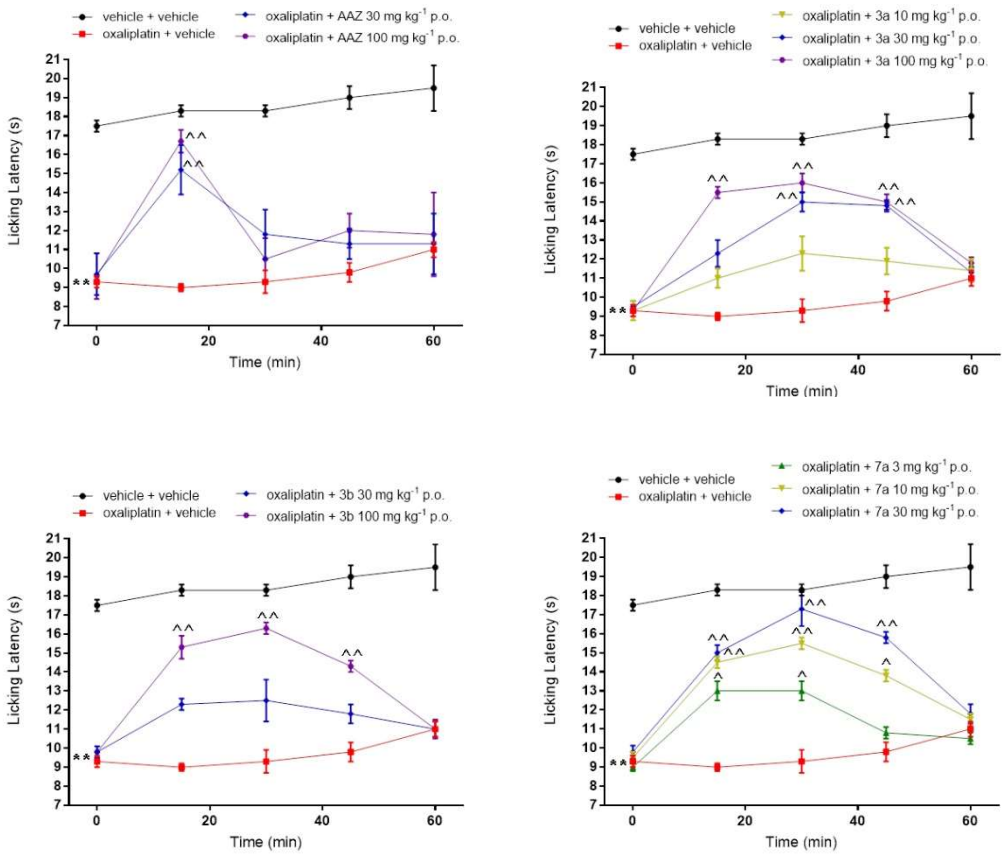

Figure 2. Effect of acute administration of carbonic anhydrase inhibitors **3a-b**, **7a** and **AAZ** on oxaliplatin induced neuropathic pain in the mouse Cold plate test. Oxaliplatin (2.4 mg kg^{-1}) was i.p. administered for 5 consecutive days every week for 2 weeks. Experiments were performed on day 14. **P<0.01 vs vehicle + vehicle treated animals; ^P<0.05 and ^^P<0.01 vs oxaliplatin + vehicle treated animals. Each value represents the mean ± S.E.M. of 10 mice performed in 2 different experimental sets.

Mice were repeatedly treated intraperitoneally with oxaliplatin (2.4 mg kg^{-1}) for 5 consecutive days every week for 2 weeks till to development of a significant painful neuropathy.[25] On day 14, a single administration of compounds **3a-b** and **7a** significantly reduced the lowering of pain threshold to cold stimuli. All selenides, here considered, relieved pain dose-dependently (3–100 mg kg^{-1} p.o.). Compounds **3a-b** showed a significant pain relief to higher dose (100 mg kg^{-1} p.o.) between 15 and 45 min after treatment. The more effective was **7a** which was able to restore the pain threshold at basal values after 30 min of administration using a dose of 30 mg kg^{-1}.

5.3 Conclusions

We reported for the first time selenides having moderate inhibition against the cytosolic isoforms hCA I and the transmembrane IX, with strong efficacy for CA II, VII. These last isoforms are present in the central/peripheral nervous system and their inhibition showed in a mice model of neuropathic pain induced by oxaliplatin efficient and long lasting pain relieving effects.

5.4 Experimental Data

Chemistry

Anhydrous solvents and all reagents were purchased from Sigma-Aldrich, Alfa Aesar and TCI. All reactions involving air- or moisture-sensitive compounds were performed under a nitrogen atmosphere using dried glassware and syringes techniques to transfer solutions. Nuclear magnetic resonance (^{1}H-NMR, ^{13}C-NMR, ^{19}F NMR, ^{77}Se-NMR) spectra were recorded using a Bruker Advance III 400 MHz spectrometer in DMSO-d_6. $(PhSe)_2$ was used as an external reference for ^{77}Se NMR (δ= 461 ppm). Chemical shifts are reported in parts per million (ppm) and the coupling constants (*J*) are expressed in Hertz (Hz). Splitting patterns are designated as follows: s, singlet; d, doublet; t, triplet; q, quadruplet; m, multiplet; brs, broad singlet; dd, double of doublets. The assignment of exchangeable protons (O*H* and N*H*) was confirmed by the addition of D_2O. Analytical thin-layer chromatography (TLC) was carried out on Merck silica gel F-254 plates. Flash chromatography purifications were

performed on Merck Silica gel 60 (230-400 mesh ASTM) as the stationary phase and ethyl acetate/*n*-hexane were used as eluents. Melting points (mp) were measured in open capillary tubes with a Gallenkamp MPD350.BM3.5 apparatus and are uncorrected. The solvents used in MS measures were acetone, acetonitrile (Chromasolv grade), purchased from Sigma-Aldrich (Milan - Italy), and mQ water 18 MΩ, obtained from Millipore's Simplicity system (Milan-Italy). The mass spectra were obtained using a Varian 1200L triple quadrupole system (Palo Alto, CA, USA) equipped by Electrospray Source (ESI) operating in both positive and negative ions. Stock solutions of analytes were prepared in acetone at 1.0 mg mL^{-1} and stored at 4°C. Working solutions of each analyte were freshly prepared by diluting stock solutions in a mixture of mQ H_2O/ACN 1/1 (*v/v*) up to a concentration of 1.0 µg mL^{-1} The mass spectra of each analyte were acquired by introducing, via syringe pump at 10 µL min^{-1}, of the its working solution. Raw-data were collected andprocessed by Varian Workstation Vers. 6.8 software.

General procedure for the synthesis of compound 3a-f:

$NaBH_4$ (23 mg, 0.60 mmol, 3.0 eq.) was portionwise added to a solution of 4,4'-diselanediyldibenzenesulfonamide **1** (94 mg, 0.20 mmol, 1.0 eq.) in EtOH (2 mL) at 0°C under inert atmosphere (N_2). After 30 min, the halo-alkyl **2a-f** (0.36 mmol, 2.1 eq.) was slowly added and the reaction mixture was stirred at reflux for 3 h, until complete consumption of the starting material was observed by TLC. The reaction was quenched by addition of saturated aq. NH_4Cl (2 mL) and diluted with EtOAc (5 mL). The layers were separated and the aqueous layer was extracted with EtOAc (2 x 5 mL), dried over Na_2SO_4, filtered and concentrated under vacuum. The crude material was purified by flash chromatography to yield selenides (**3a-f**) bearing benzenesulfonamide moiety.

4-((cyclopropylmethyl)selanyl)benzenesulfonamide 3c:

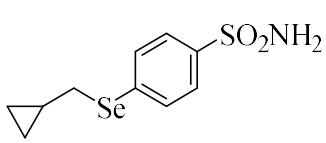

Following the general procedure, 4,4'-diselanediyldibenzenesulfonamide **1** (100 mg, 0.21 mmol) and (bromomethyl)cyclopropane **2c** (60 mg, 0.44 mmol) gave after flash chromatography (hexane/EtOAc 1:1) **3c** (91 mg, 71%). **^{1}H NMR** (400 MHz, DMSO- *d*$_6$) δ (ppm): 7.72 (2H, d, *J* = 8.61 Hz), 7.67 (2H,

d, *J* = 8.58 Hz), 7.37 (2H, bs, N**H**$_2$, exchange with D_2O), 3.08 (2H, d, *J* = 7.25 Hz), 1.14-1.07 (1H, m), 0.61-0.60 (2H, m), 0.31-0.29 (2H, m). **^{13}C NMR** (100 MHz, DMSO-d_6) δ (ppm): 142.6, 137.5, 131.3, 127.1, 32.9, 12.0, 7.7. **^{77}Se NMR** (76 MHz, DMSO-d_6) δ (ppm): 303.6. **MS** (ESI negative) *m/z*: 290.1 $[M-H]^-$

4-(benzylselanyl)benzenesulfonamide 3d:

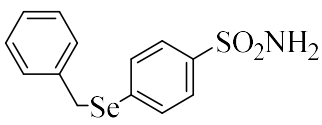

Following the general procedure, 4,4'-diselanediyldibenzenesulfonamide **1** (100 mg, 0.21 mmol) and benzyl bromide **2d** (75 mg, 0.44 mmol) gave after flash chromatography (hexane/EtOAc 1:1) **3d** (110 mg, 77%). **^{1}H NMR** (400 MHz, DMSO- d_6) δ (ppm): 7.70 (4H, apq), 7.40-7.39 (4H, m), 7.34-7.30 (2H, m), 7.26-7.23 (1H, m), 4.39 (2H, s). **^{13}C NMR** (100 MHz, DMSO-d_6) δ (ppm): 143.0, 139.0, 137.1, 131.6, 129.8, 129.3, 127.9, 127.0, 30.8. **^{77}Se NMR** (76 MHz, DMSO-d_6) δ (ppm): 367,7. **MS** (ESI negative) *m/z*: 326.1 $[M-H]^-$.

General procedure for the synthesis of selenides 7a-b:

$NaBH_4$ (0.60 mmol, 3.0 eq.) was portionwise added to a solution of diselenides **4a-b** (0.20 mmol, 1.0 eq.) in EtOH (5 mL) at room temperature under inert atmosphere (N_2). After 30 min, sulfonamide **6** (0.40 mmol, 2.0 eq.) was slowly added and the reaction mixture was stirred at room temperature for 3 h, until complete consumption of the starting material was observed by TLC. The reaction was quenched by addition of saturated aq. NH_4Cl (4 mL) and diluted with EtOAc (5 mL). The layers were separated and the aqueous layer was extracted with EtOAc (2 x 5 mL), dried over Na_2SO_4, filtered and concentrated under vacuum. The crude material was purified by flash chromatography (hexane/EtOAc 1:1) to yield selenides **7a-b**.

4-((naphthalen-2-ylselanyl)methyl)benzenesulfonamide 7b:

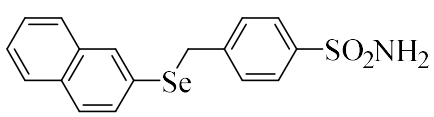

Following the general procedure, 1,2-di(naphthalen-2-yl)diselenide **4b** (83 mg, 0.20 mmol) and 4-(bromomethyl) benzenesulfonamide **6** (100 mg, 0.40 mmol) gave after flash chromatography (hexane/EtOAc 1:1) **7b** (215 mg, 70%). **^{1}H NMR** (400 MHz, DMSO- d_6) δ (ppm): 8.07 (1H, s), 7.89-7.84 (3H, m), 7.72

(2H, d, *J* = 8.41 Hz), 7.66-7.64 (2H, m), 7.56-7.51 (3H,m), 7.31 (2H, bs, N**H**$_2$, exchange with D_2O), 4.45 (2H, s). **^{13}C NMR** (100 MHz, DMSO-*d*$_6$) δ (ppm): 144.2, 143.3, 134.4, 132.6, 131.1, 130.4, 130.1, 129.3, 128.6, 128.4, 128.0, 127.6, 127.0, 126.6, 30.5. **^{77}Se NMR** (76 MHz, DMSO-*d*$_6$) δ (ppm): 375.9. **MS** (ESI negative) *m/z*: 376.1 $[M-H]^-$

General procedure for the synthesis of selenides 7c-d:

$NaBH_4$ (0.80 mmol, 4.0 eq.) was portionwise added to a solution of arylselenocyanates **5a-b** (0.20 mmol, 1.0 eq.) in EtOH (5 mL) at room temperature under inert atmosphere (N_2). After 1h, sulfonamide **6** (0.20 mmol, 1.0 eq.) was slowly added and the reaction mixture was stirred at room temperature for 3 h, until complete consumption of the starting material was observed by TLC. The reaction was quenched by addition of saturated aq. NH_4Cl (4 mL) and diluted with EtOAc (5 mL). The layers were separated and the aqueous layer was extracted with EtOAc (2 x 5 mL), dried over Na_2SO_4, filtered and concentrated under vacuum. The crude material was purified by flash chromatography (hexane/EtOAc 1:1) to yield selenides **7c-d**.

4-(((4-aminophenyl)selanyl)methyl)benzenesulfonamide 7c:

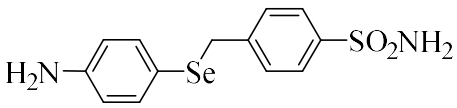

Following the general procedure, 4-selenocyanatoaniline **5a** (40 mg, 0.20 mmol) and 4-(bromomethyl) benzenesulfonamide **6** (50 mg, 0.20 mmol) gave after flash chromatography (hexane/EtOAc 1:1) **7c** (58 mg, 85%). **^{1}H NMR** (400 MHz, DMSO- *d*$_6$) δ (ppm): 7.70 (2H, d, *J* = 8.36 Hz), 7.36-7.29 (4H, m), 7.12 (2H, d, *J* = 8.51 Hz), 6.50 (2H, d, *J* = 8.53 Hz), 5,32 (2H, bs, N**H**$_2$, exchange with D_2O), 4.05 (2H, s). **^{13}C NMR** (100 MHz, DMSO-*d*$_6$) δ (ppm): 149.8, 145.0, 143.0, 136.9, 129.8, 126.4, 115.5, 113.3, 32.5. **^{77}Se NMR** (76 MHz, DMSO-*d*$_6$) δ (ppm): 370.7. **MS** (ESI negative) *m/z*: 341.2 $[M-H]^-$.

4-(((4-(dimethylamino)phenyl)selanyl)methyl)benzenesulfonamide 7d:

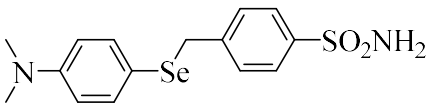

Following the general procedure, N,N-dimethyl-4-selenocyanatoaniline **5b** (45 mg, 0.20 mmol) and 4-(bromomethyl) benzenesulfonamide **6** (50 mg, 0.20 mmol) gave after flash chromatography (hexane/EtOAc 1:1) **7c** (66 mg, 90%). **^{1}H NMR**

(400 MHz, DMSO- d_6) δ (ppm): 7.70 (2H, d, J = 8.29 Hz), 7.36-7.28 (6H, m), 6.66 (2H, d, J = 8.83 Hz), 4.10 (2H, s), 2.93 (6H, s). **^{13}C NMR** (100 MHz, DMSO-d_6) δ (ppm): 151.0, 144.9, 143.0, 136.5, 129.9, 126.5, 114.2, 113.8, 40.8, 32.4. **^{77}Se NMR** (76 MHz, DMSO-d_6) δ (ppm): 365.4. **MS** (ESI positive) *m/z*: 371.2 $[M+H]^+$.

General procedure for the synthesis of selenides 10a-c:

Compound **7c** (0.20 mmol) was dissolved in acetonitrile (5 mL) and then treated with a stoichiometric amount of isocyanates **8a-b** or isothiocyanate **8c**. The mixture was stirred at room temperature until completion (TLC monitoring). The heavy precipitate formed was filtered off, washed with diethyl ether (10 mL), and dried in vacuo. The crude material was purified by flash chromatography (hexane/Acetone 1:1) to yield selenides **10a-c**.

4-(((4-(3-(4-fluorophenyl)ureido)phenyl)selanyl)methyl)benzenesulfonamide 10a:

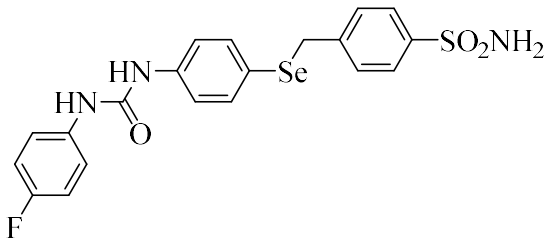

Following the general procedure, 4-(((4-aminophenyl)selanyl)methyl) benzenesulfonamide **7c** (68 mg, 0.20 mmol) and 4-Fluorophenyl isocyanate **8a** (34 mg, 0.20 mmol) gave after flash chromatography (hexane/Acetone 1:1) **10a** (76 mg, 80%). **^{1}H NMR** (400 MHz, DMSO- d_6) δ (ppm): 10.26 (2H, bs, N**H$_2$**, exchange with D_2O), 7.70 (2H, d, J = 8.37 Hz), 7.55 (2H, d, J = 8.67 Hz), 7.44-7.37 (6H, m), 7.32 (2H, bs, N**H$_2$**, exchange with D_2O), 7.19 (2H, t, J = 8.93 Hz) 4.25 (2H, s). **^{13}C NMR** (100 MHz, DMSO-d_6) δ (ppm): 170.0, 162.0 (d, J = 242.13 Hz), 144.4, 143.2, 139.5, 134.5, 132.9 (d, J = 3.15 Hz), 131.9 (d, J = 8.03 Hz), 130.0, 126.5, 123.6, 120.7, 115.9 (d, J = 21.20 Hz), 43.2. **^{19}F-NMR** (376 MHz, DMSO-d_6,) δ (ppm): -116.5. **^{77}Se NMR** (76 MHz, DMSO-d_6) δ (ppm): 373.8. **MS** (ESI negative) *m/z*: 477.2 $[M-H]^-$.

4-(((4-(3-(3,5-dimethylphenyl)ureido)phenyl)selanyl)methyl)benzenesulfonamide 10b:

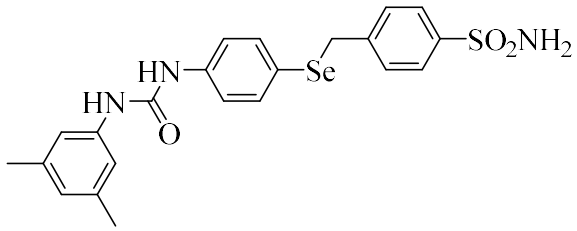

Following the general procedure, 4-(((4-aminophenyl)selanyl) methyl)benzenesulfonamide **7c** (68 mg, 0.20 mmol) and 3,5 dimethyl phenyl isocyanate **8b** (29 mg, 0.20 mmol) gave after flash chromatography (hexane/Acetone 1:1) **10b** (81 mg, 83%). **^{1}H NMR** (400 MHz, DMSO-d_6) δ (ppm): 8.78 (1H, bs, N**H$_2$**, exchange with D_2O), 8.59 (1H, bs, N**H$_2$**, exchange with D_2O), 7.72 (2H, d, J = 8.28 Hz), 7.41-7.33 (8H, m), 7.10 (2H, bs, N**H$_2$**, exchange with D_2O), 6.65 (1H, s) 4.23 (2H, s). **^{13}C NMR** (100 MHz, DMSO-d_6) δ (ppm): 153.3, 144.5, 143.2, 140.4, 140.3, 138.6, 135.0, 129.9, 126.5, 124.5, 121.5, 119.7, 116.9, 31.6, 22.0. **^{77}Se NMR** (76 MHz, DMSO-d_6) δ (ppm): 371.8. **MS** (ESI negative) *m/z*: 488.2 $[M-H]^-$.

2-(6-hydroxy-3-oxo-3H-xanthen-9-yl)-5-(3-(4-((4-sulfamoylbenzyl)selanyl)phenyl) thioureido) benzoic acid 10c:

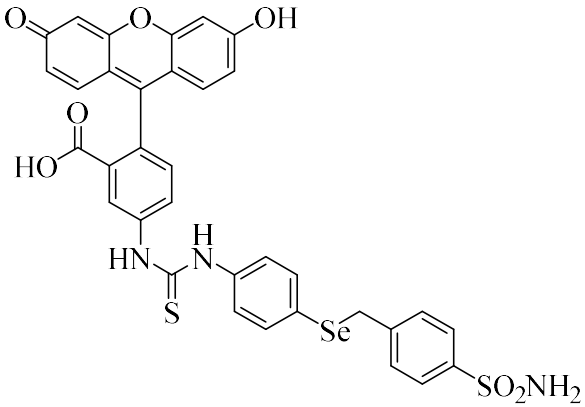

Following the general procedure, 4-(((4-aminophenyl)selanyl)methyl) benzenesulfonamide **7c** (68 mg, 0.20 mmol) and Fluorescein isothiocyanate **8c** (78 mg, 0.20 mmol) gave after flash chromatography (hexane/Acetone 1:1) **10c** (80 mg, 55%). **^{1}H NMR** (400 MHz, DMSO- d_6) δ (ppm): 10.34 (1H, bs, exchange with D_2O), 10.22-10.17 (3H, m, exchange with D_2O), 8.24 (1H, d, J = 1.49 Hz), 7.85 (2H, d, J = 8.20 Hz), 7.74 (2H, d, J = 8.25 Hz), 7.49-7.47 (5H, m), 7.34(3H, d, J = 4.63 Hz), 6.72 (2H, J = 1.93 Hz), 6.66-6.60 (4H, m), 4.33 (2H, s). **^{13}C NMR** (100 MHz, DMSO-d_6) δ (ppm): 180.5, 169.4, 160.5, 152.9, 144.3, 143.9, 143.8, 143.4, 139.4, 133.6, 130.1, 130.0, 129.9, 126.8, 126.7, 125.2, 118.6, 113.6, 110.7, 103.3,

84.0, 31.1. **^{77}Se NMR** (76 MHz, DMSO-d_6) δ (ppm): 370.1. **MS** (ESI negative) *m/z*: 730.3 [M-H]$^-$.

General procedure for the synthesis of selenides 11a-c:

Compound **7c** (0.2 mmol) was dissolved in anhydrous THF (5 mL) ,then added trimethylamine (0.24 mmol, 1.2 eq.) and a stoichiometric amount of acyl chloride **9a-c**. The mixture was stirred at room temperature until completion (TLC monitoring). The reaction was quenched by addition of saturated aq. NH_4Cl (2 mL) and diluted with EtOAc (5 mL). The layers were separated and the aqueous layer was extracted with EtOAc (2 x 5 mL), dried over Na_2SO_4, filtered and concentrated under vacuum. The crude material was purified by flash chromatography (hexane/EtOAc 1:1) to yield selenides **11a-c**.

2-((4-((4-sulfamoylbenzyl)selanyl)phenyl)carbamoyl)phenyl acetate 11a:

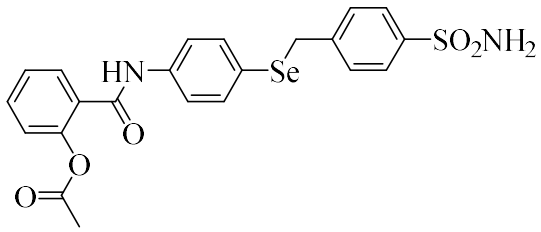

Following the general procedure, 4-(((4-aminophenyl)selanyl)methyl) benzenesulfonamide **7c** (68 mg, 0.20 mmol) and O-Acetylsalicyloyl chloride **9a** (40 mg, 0.20 mmol) gave after flash chromatography (hexane/EtOAc 1:1) **11a** (71 mg, 70%). **^{1}H NMR** (400 MHz, DMSO- d_6) δ (ppm): 10.44 (1H, bs, N**H$_2$**, exchange with D_2O), 7.85 (1H, d, *J* = 8.33 Hz), 7.74-7.64 (6H, m), 7.49-7.42 (4H, m), 7.34 (2H, d, *J* = 9.62 Hz), 7.29 (1H, dd, *J* = 8.09, 0.88 Hz), 4.29 (2H, s), 2.23 (3H, s). **^{13}C NMR** (100 MHz, DMSO-d_6) δ (ppm):169.8, 165.1, 148.9, 144.4, 143.7, 143.3, 139.4, 134,3 132.5, 130.4, 130.0, 126.8, 126.6, 124.3, 124.2, 121.4, 65.8, 21.6. **^{77}Se NMR** (76 MHz, DMSO-d_6) δ (ppm): 372.6. **MS** (ESI negative) *m/z*: 502.2 [M-H]$^-$.

2,4-dimethoxy-N-(4-((4-sulfamoylbenzyl)selanyl)phenyl)benzamide 11b:

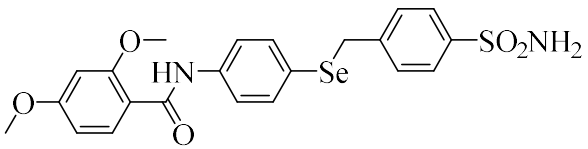

Following the general procedure, 4-(((4-aminophenyl)selanyl) methyl)benzenesulfonamide **7c** (68 mg, 0.20 mmol) and 2,4-Dimethoxybenzoyl chloride **9b** (40 mg, 0.20 mmol) gave after flash chromatography (hexane/EtOAc 1:1) **11b** (66 mg, 65%). **^{1}H NMR** (400 MHz, DMSO- d_6)

δ (ppm): 10.01 (1H, bs, N**H₂**, exchange with D_2O), 7.76 (1H, d, *J* = 8.57 Hz), 7.71 (4H, t, *J* = 8.41 Hz), 7.46 (2H, d, *J* = 8.64 Hz), 7.43 (2H, d, *J* = 8.42 Hz), 7.33 (2H, bs, N**H₂**, exchange with D_2O), 6.74, (1H, t, *J* = 2.10 Hz), 6.70 (1H, dd, *J* = 8.63, 2.29 Hz), 4.28 (2H, s), 3.98 (3H, s), 3.88 (3H, s). **^{13}C NMR** (100 MHz, DMSO-*d₆*) δ (ppm):164.6, 163.9, 159.2, 144.4, 143.2, 139.4, 134.4, 132.8, 130.0, 126.6, 123.8, 121.4, 117.0, 106.7, 99.5, 57.1, 56.5, 31.3 **^{77}Se NMR** (76 MHz, DMSO-*d₆*) δ (ppm): 373.1. **MS** (ESI negative) *m/z*: 505.2 $[M-H]^-$.

N-(4-((4-sulfamoylbenzyl)selanyl)phenyl)cinnamamide 11c:

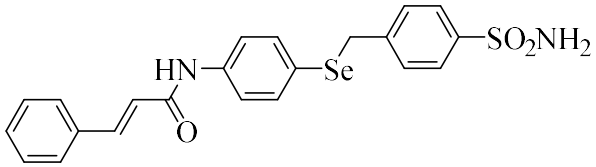

Following the general procedure, 4-(((4-aminophenyl)selanyl) methyl)benzenesulfonamide **7c** (68 mg, 0.20 mmol) and cinnamoyl chloride **9c** (40 mg, 0.20 mmol) gave after flash chromatography (hexane/EtOAc 1:1) **11c** (72 mg, 76%). **^{1}H NMR** (400 MHz, DMSO- *d₆*) δ (ppm): 10.33 (1H, bs, N**H₂**, exchange with D_2O), 7.73 (2H, d, *J* = 8.37 Hz), 7.69-7.64 (5H, m), 7.51-7.45 (5H, m), 7.43 (2H, d, *J* = 8.38 Hz), 7.34 (2H, bs, N**H₂**, exchange with D_2O), 6.86 (1H, d, *J* = 15.72 Hz), 4.28 (2H, s). **^{13}C NMR** (100 MHz, DMSO-*d₆*) δ (ppm):164.5, 144.4, 143.2, 141.3, 139.6, 135.6, 134.5, 130.8, 130.0, 129.9, 128.7, 126.6, 123.9, 123.0, 120.8, 31.3 **^{77}Se NMR** (76 MHz, DMSO-*d₆*) δ (ppm): 373.5. **MS** (ESI negative) *m/z*: 471.2 $[M-H]^-$.

General procedure for the synthesis of selenide 12:

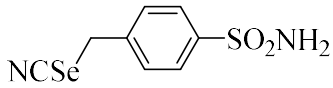

4-(bromomethyl) benzenesulfonamide **6** (125 mg, 0.5 mmol) was dissolved in acetone (10 mL) and then was added KSeCN (87 mg, 0.6 mmol, 1.2 eq.). The mixture was stirred at reflux for 4h, until completion (TLC monitoring). The reaction was quenched by addition of saturated aq. NH_4Cl (2 mL) and diluted with EtOAc (5 mL). The layers were separated and the aqueous layer was extracted with EtOAc (2 x 5 mL), dried over Na_2SO_4, filtered and concentrated under vacuum. The crude material was purified by flash chromatography (DCM/MeOH 90:10) to yield selenide **12** (70%). **^{1}H NMR** (400 MHz, DMSO- *d₆*) δ (ppm): 7.85 (2H, d, *J* = 8.39 Hz), 7.58 (2H, d, *J* = 8.41 Hz), 7.40 (2H, bs,

N**H₂**, exchange with D_2O), 4.40 (2H, s). **^{13}C NMR** (100 MHz, DMSO-d_6) δ (ppm): 144.2, 143.3, 130.2, 126.9, 105.6, 32.5 **^{77}Se NMR** (76 MHz, DMSO-d_6) δ (ppm): 327.7. **MS** (ESI negative) *m/z*: 274.0 $[M-H]^-$.

Carbonic anhydrase inhibition

An Applied Photophysics stopped-flow instrument has been used for assaying the CA catalyzed CO_2 hydration activity.[21] Phenol red (at a concentration of 0.2 mM) has been used as indicator, working at the absorbance maximum of 557 nm, with 20 mMHepes (pH 7.5) as buffer, and 20 mM Na_2SO_4 (for maintaining constant the ionic strength), following the initial rates of the CA-catalyzed CO_2 hydration reaction for a period of 10–100 s. The CO_2 concentrations ranged from 1.7 to 17 mM for the determination of the kinetic parameters and inhibition constants. For each inhibitor at least six traces of the initial 5–10% of the reaction have been used for determining the initial velocity. The uncatalyzed rates were determined in the same manner and subtracted from the total observed rates. Stock solutions of inhibitor (0.1 mM) were prepared in distilled-deionized water and dilutions up to 0.01 nM were done thereafter with the assay buffer. Inhibitor and enzyme solutions were preincubated together for 15 min at room temperature prior to assay, in order to allow for the formation of the E-I complex. The inhibition constants were obtained by non-linear least-squares methods using PRISM 3 and the Cheng–Prusoff equation.

Protein X-ray Crystallography

The protein was concentrated to about 7 mg/mL and set up in SD2 crystallization plates (Molecular Dimensions) with the following ratio of protein plus reservoir: 200 nL + 200 nL. The plate was incubated at 8 ºC and the reservoir conditions consisted of 2.6 to 3.0 M ammonium sulfate with 0.1 M Tris buffer at pH 8.0 to pH 8.5. Compounds in DMSO were added to crystallization drops after crystals had formed and several days before data were collected. 360 frames of one degree oscillation were obtained from the MX1 beamline of the Australian Synchrotron. The data were indexed using XDS[26] and scaled using Aimless.[27] Molecular replacement was done using Phaser[28] using 4cq0 as the initial starting model. The model was manually rebuilt using Coot[29] and refined using a combination of Phenix[30] and Refmac.[31] The compound was placed in density using the program Afitt (OpenEye Scientific Software) and further refined using Refmac. For structure 6D1L, two data sets from two

different crystals soaked with the same compound were merged. For structure 6D1M, a single 360 degree data set was obtained and used for the structure determination and refinement.

Summary of Data Collection and Atomic Model Refinement Statistics

PDB	6D1L	6D1M
Compound	3e	3f
Space group	$P2_1$	$P2_1$
Cell dimensions		
a, b, c	42.3, 41.3, 72.1	42.4, 41.6, 72.2
alpha, beta, gamma	90, 104.4, 90	90, 104.2, 90
Resolution (Å)	69.8 - 1.40	41.6 - 1.21
Resolution-high (Å)	1.42 - 1.40	1.23 - 1.21
Rmerge	0.177 (1.231)	0.094 (0.704)
Rpim	0.048 (0.395)	0.037 (0.290)
CC ½	0.998 (0.723)	0.999 (0.825)
I/sigI	11.8 (2.1)	15.6 (2.5)
Completeness (%)	100 (100)	97.9 (91.2)
Redundancy	14.5 (10.5)	7.2 (6.4)
Refinement		
resolution (Å)	69.8 - 1.40	41.6 - 1.21
unique reflections	45559	69692
Rwork/Rfree (%)	16.1 / 18.1	13.2 / 15.7
# atoms	2573	2669
Protein	2212	2266
metal (Zn)	1	1
ligand	30	34
water	325	363
B-factors (Å^2)	9,5	10,2
protein	8,8	9,2
metal (Zn)	3,3	4,5
ligand	11,5	9,6
water	21,0	23,9
r.m.s. deviations		
Bond length (Å)	0,009	0,009
Bond angle (°)	1,431	1,440

Biological Assays.

Oxaliplatin (2.4 mg kg^{-1}) was dissolved in 5% glucose solution and i.p. administered for 5 consecutive days every week for 2 weeks.[32] Starting from day 14, compounds and acetazolamide were suspended in CMC and p.o. administered.[33,34] Pain-related behavior (i.e. lifting and licking of the hind paw) were observed and the time (seconds) of the first sign was recorded. **$P<0.01$ vs vehicle + vehicle treated animals; ^$P<0.05$ and ^^$P<0.01$ vs oxaliplatin + vehicle treated animals. Each value represents the mean of 10 mice.

References

1. Gilron I., Watson C.P., Cahill C.M., Moulin D.E., Neuropathic pain: a practical guide for the clinician. *CMAJ,* 2006, 175, 265-275.
2. Finnerup N.B., Attal N., Haroutounian S., McNicol E., Baron R., Dworkin R.H., Gilron I., Haanpaa M., Hansson P., Jensen T.S., Kamerman P.R., Lund K., Moore A., Raja S.N., Rice A.S., Rowbotham M., Sena E., Siddall P., Smith B.H., Wallace M., Pharmacotherapy for neuropathic pain in adults: a systematic reviewand meta-analysis. *Lancet Neurol.* 2015, 14, 162–173.
3. Torrance N., Smith B.H., Bennett M.I., Lee A.J., The epidemiology of chronic pain of predominantly neuropathic origin. Results from a general population survey. *J Pain* 2006, 7, 281–289.
4. Bouhassira D., Lantéri-Minet M., Attal N., Laurent B., Touboul C., Prevalence of chronic pain with neuropathic characteristics in the general population. *Pain* 2008, 136, 380–387.
5. Wieseler-Frank J., Maier S.F., Watkins L.R., Central proinflammatory cytokines and pain enhancement. *Neuro-Signals* 2005, 14, 166–174.
6. Asiedu M., Ossipov M.H., Kaila K., Price T.J., Acetazolamide and midazolam act synergistically to inhibit neuropathic pain. *Pain* 2010, 148, 302-308.
7. Asiedu M.N., Mejia G.L., Hübner C.A., Kaila K., Price T.J., Inhibition of carbonic anhydrase augments $GABA_A$ receptor-mediated analgesia via a spinal mechanism of action. *J Pain* 2014, 15, 395-406.
8. Supuran C.T., Carbonic anhydrase inhibition and the management of neuropathic pain. *Expert Rev Neurother.* 16 2016, 16, 961-968.
9. Carta F., Di Cesare Mannelli L., Pinard M., Ghelardini C., Scozzafava A., McKenna R., Supuran C.T., A class of sulfonamide carbonic anhydrase inhibitors with neuropathic pain modulating effects. *Bioorg Med Chem*. 2015, 23, 1828-1840.
10. Di Cesare Mannelli L., Micheli L., Carta F., Cozzi A., Ghelardini C., Supuran C.T., Carbonic anhydrase inhibition for the management of cerebral ischemia: in vivo evaluation of sulfonamide and coumarin inhibitors. *J Enzyme Inhib Med Chem*. 2016, 31, 894-899.

11. Negi G., Kumar A., Joshi R.P., Sharma S.S., Oxidative stress and Nrf2 in the pathophysiology of diabetic neuropathy: old perspective with a new angle. *Biochem. Biophys. Res. Commun.* 2011, 408, 1–5.
12. Negi G., Kumar A., Sharma S.S., Melatonin modulates neuroinflammation and Oxidative stress in experimental diabetic neuropathy: effects on NF-kB and Nrf2 cascades. *J. Pineal Res.* 2011, 50, 124–131.
13. Prasad S.N., Muralidhara, Neuroprotective effect of geraniol and curcuminin an acrylamide model of neurotoxicity in Drosophila melanogaster: relevance to neuropathy, *J. Insect Physiol.* 2013, 60, 7–16.
14. Saifi G.M., Szigeti K., Snipes G.J., Garcia C.A., Lupski J.R., Molecular mechanisms, diagnosis, and rational approaches to management of and therapy for Charcot–Marie–Tooth disease and related peripheral neuropathies. *J. Investig. Med.: Off. Publ. Am. Fed. Clin. Res.* 2003, 51, 261–283.
15. Angeli A., Tanini D., Peat T.S., Di Cesare Mannelli L., Bartolucci G., Capperucci A., Ghelardini C., Supuran C.T., Carta F., Discovery of New Selenoureido Analogues of 4-(4-Fluorophenylureido)benzenesulfonamide as Carbonic Anhydrase Inhibitors. *ACS Med Chem Lett.* 2017, 8, 963-968.
16. Angeli A., Tanini D., Viglianisi C., Panzella L., Capperucci A., Menichetti S., Supuran C.T., Evaluation of selenide, diselenide and selenoheterocycle derivatives as carbonic anhydrase I, II, IV, VII and IX inhibitors. *Bioorg Med Chem.* 2017, 25, 2518-2523.
17. Yoshida S., Kumakura F., Komatsu I., Arai K., Onuma Y., Hojo H., Singh B.G., Priyadarsini K.I., Iwaoka M., Antioxidative glutathione peroxidase activity of selenoglutathione. *Angew Chem Int Ed Engl.* 2011, 50, 2125-2128.
18. Angeli A., di Cesare Mannelli L., Trallori E., Peat T.S., Ghelardini C., Carta F., Supuran C.T., Design, Synthesis, and X-ray of Selenides as New Class of Agents for Prevention of Diabetic Cerebrovascular Pathology. *ACS Med. Chem. Lett.* 2018, 9, 462–467
19. Kachanov A.V., Slabko O.Y., Baranova O.V., Shilova E.V., Kaminskii V.A., Triselenium dicyanide from malononitrile and selenium dioxide. One-pot synthesis of selenocyanates. *Tetrahedron Lett.* 2004, 45, 4461–4463

20. Pacchiano F., Carta F., McDonald P.C., Lou Y., Vullo D., Scozzafava A., Dedhar S., Supuran C.T., Ureido-substituted benzenesulfonamides potently inhibit carbonic anhydrase IX and show antimetastatic activity in a model of breast cancer metastasis. *J Med Chem.* 2011, 54, 1896-902.
21. Khalifah R.G., The carbon dioxide hydration activity of carbonic anhydrase. I. Stop flow kinetic studies on the native human isoenzymes B and C. *J. Biol. Chem*. 1971, 246, 2561.
22. Kwon S.G., Roh D.H., Yoon S.Y., Moon J.Y., Choi S.R., Choi H.S., Kang S.Y., Han H.J., Beitz A.J., Oh S.B., Lee J.H., Acid evoked thermal hyperalgesia involves peripheral P2Y1 receptor mediated TRPV1 phosphorylation in a rodent model of thrombus induced ischemic pain. *Mol. Pain,* 2014, 10, 2.
23. Olausson P., Gerdle B., Ghafouri N., Larsson B., Ghafouri B., Identification of proteins from interstitium of trapezius muscle in women with chronic myalgia using microdialysis in combination with proteomics. *PLoS One* 2012, 7, e52560.
24. Cavaletti G., Tredici G., Petruccioli M.G., Dondè E., Tredici P., Marmiroli P., Minoia C., Ronchi A., Bayssas M., Etienne G.G., Effects of different schedules of oxaliplatin treatment on the peripheral nervous system of the rat. *Eur. J. Cancer* 2001, 37, 2457-2463.
25. Di Cesare Mannelli L., Pacini A., Matera C., Zanardelli M., Mello T., De Amici M., Dallanoce C., Ghelardini C.. Involvement of α7 nAChR subtype in rat oxaliplatin-induced neuropathy: effects of selective activation. *Neuropharmacology* 2014, 79, 37-48.
26. Kabsch W., XDS. *Acta Crystallogr. Sect. D: Biol. Crystallogr*. 2010, 66, 125-132.
27. Evans P.R., An introduction to data reduction: space group determination, scaling and intensity statistics. *Acta Crystallogr. D: Biol. Crystallogr*. 2011, 67, 282-292.
28. McCoy A.J., Grosse Kunstleve R.W., Adams P.D., Winn M.D., Storoni L.C., Read R.J., Phaser crystallographic software. *J. Appl. Crystallogr*. 2007, 40,658-674.
29. Emsley P., Lohkamp B., Scott W.G., Cowtan K., Features and development of Coot. *Acta Crystallogr. D: Biol. Crystallogr*. 2010 66, 486-501.
30. Adams P.D., Afonine P.V., Bunkóczi G., Chen V.B., Davis I.W., Echols N., Headd J.J., Hung L.W., Kapral G.J., Grosse-Kunstleve R.W., McCoy A.J., Moriarty N.W.,

Oeffner R., Read R.J., Richardson D.C., Richardson J.S., Terwilliger T.C., Zwart P.H., PHENIX: a comprehensive Python—ased system for macromolecular structure solution. *Acta Cryst.* 2010, D66, 213-221

31. Murshudov G.N., Skubak P., Lebedev A.A., Pannu N.S., Steiner R.A., Nicholls R.A., Winn M.D., Long F., Vagin A.A., REFMAC5 for the refinement of macromolecular crystal structures. *Acta Crystallogr. D Biol. Crystallogr*. 2011**,** 67, 355-367.
32. Di Cesare Mannelli L., Lucarini E., Micheli L., Mosca I., Ambrosino P., Soldovieri M.V., Martelli A., Testai L., Taglialatela M., Calderone V., Ghelardini C. Effects of natural and synthetic isothiocyanate-based H_2S-releasers against chemotherapy-induced neuropathic pain: Role of Kv7 potassium channels. *Neuropharmacology.* 2017, 121, 49-59.
33. Battilocchio C., Poce G., Alfonso S., Porretta G.C., Consalvi S., Sautebin L., Pace S., Rossi A., Ghelardini C., Di Cesare Mannelli L., Schenone S., Giordani A., Di Francesco L., Patrignani P., Biava M. A class of pyrrole derivatives endowed with analgesic/anti-inflammatory activity. *Bioorg Med Chem.* 2013, 21, 3695-3701.
34. Anzini M., Valenti S.,Braile C., Cappelli A., Vomero S., Alcaro S., Ortuso F., Marinelli L., Limongelli V., Novellino E.,Betti L., Giannaccini G., Lucacchini A., Daniele S., Martini C., Ghelardini C., Di Cesare Mannelli L., Giorgi G., Mascia M.P., Biggio G. New insight into the central benzodiazepine receptor-ligand interactions: design, synthesis, biological evaluation, and molecular modeling of 3-substituted 6-phenyl-4H-imidazo[1,5-a][1,4]benzodiazepines and related compounds. *J. Med. Chem*. 2011, 54, 5694-5711.

Chapter 6

Anti-infective Carbonic Anhydrase Inhibitors

6.1 Introduction

Microorganisms existed long before human species, and as an evolutionary result we well adapted to live in an environment crowded of far more abundant living species.[1] Prokaryotes include several kind of microorganisms such as bacteria and cyanobacteria; eukaryotic microorganisms include fungi, protozoa and simple algae.[1] Most such microorganisms do not normally cause disease in humans, since a state of either commensalism or in mutualism with the host was established.[2-4] This non-harmful condition occurs when the immune system properly works, but the same organisms can cause infections when the latter fails. All microorganisms that cause diseases or illnesses to their host are defined as pathogens.[5] Microbes express their pathogenicity by means of their virulence, a term referring to the degree of pathogenicity of the microbe.[5] Hence, the determinants of virulence of a pathogen are any of its genetic, biochemical or structural features that enable it to cause a disease through its ability to enter a host, evade host defences, grow in the host environment, counteract host immune responses, assimilate iron or other nutrients from the host or sense environmental changes.[6,7] All these abilities implicate the action of numerous enzymes. The enzymes considered as virulence factors are generally active against host components and contribute to virulence by damaging host tissues.[8-10] At present, infectious diseases are the second-leading cause of death in the world and the emergence of antibiotic-resistant microorganisms is an inevitable and widespread phenomenon, inherent to most drugs.[11] Recently, Carbonic Anhydrases started to be investigated in detail in microorganisms, in the search for anti-infectives with a novel mechanism of action. It has been indeed demonstrated that in many microorganisms as pathogens, CAs are essential for their life cycle and their inhibition can lead to growth impairment and defects.[12-14]

6.2 Different seleno-scaffolds show potent inhibitory activity against carbonic anhydrases from the pathogenic bacterium *Vibrio cholerae*

During the last decades, new selenium containing scaffolds have successfully been designed and screened as antimicrobial agents.[15-17] However, until now few efforts have been made for the applications of organoselenium derivatives in enzyme inhibition studies. We reported here, the inhibition studies against two isoforms from pathogenic bacterium *Vibrio cholerae* (VchCAα and VchCAβ) with different acyl seleno ureido compounds **1-4** series, which were synthetized as previously discussed in **Chapter 2** (**Figure 1**) with the aim to detect any possible candidates for the development of new anti-infectives.

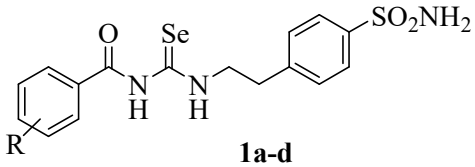

1a-d

a: R= H
b: R= 3-CH_3
c: R= 4-Ph
d: R= benzo[d][1,3]dioxole

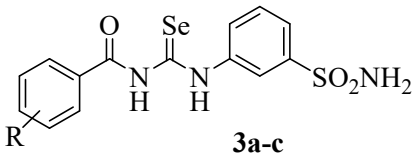

3a-c

a: R= H
b: R= 3-CH_3
c: R= 2,4 CF_3

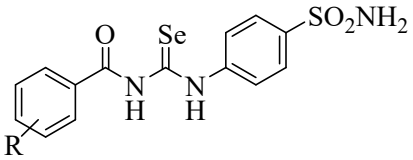

2a-e

a: R= H
b: R= benzo[d][1,3]dioxole
c: R= 3-Br, 5-OCF_3
d: R= 2-Acetate
e: R= 4-hepthyl

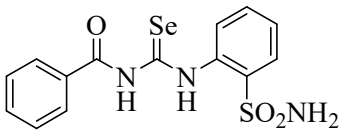

4

Figure 1: Acyl selenoureido derivatives **1-4** series

We tested *in vitro* the above compounds for their inhibitory activity against the two physiologically relevant hCA isoforms I, II (offtargets) and the bacterial enzyme VchCAα, VchCAβ by means of the stopped-flow carbon dioxide hydration assay.[18] The activities were

compared to those of the standard and clinically used CAI acetazolamide (**AAZ**) (**Table 1**). The selectivity ratios for the inhibition of the bacterial *vs* the human isoform hCA II (the physiologically dominant one) are also included in **Table 1**.

Table 1. Inhibition constants of hCA I, hCA II, VchCAα and VchCAβ with compounds **1-4** and **AAZ** by a stopped-flow CO_2 hydrase assay[18]

	K_i (nM)*				selectivity ratio[a]
Compound	hCA I	hCA II	VchCAα	VchCAβ	hCA II/ VchCAα
1a	65.6	18.7	0.67	5574	27.9
1b	514.9	21.8	0.77	5335	28.3
1c	3746	9534	0.95	5989	10035.4
1d	523.7	26.9	0.30	6777	89.7
2a	73.8	9.5	0.68	6620	14
2b	8702	402.4	0.58	5487	693.8
2c	85.7	0.7	0.88	6821	0.79
2d	85.7	9.1	0.66	5242	13.8
2e	734.2	48.9	0.30	8057	16.3
3a	521.2	247.4	0.67	8771	369.2
3b	81.6	6.6	0.36	7127	18.3
3c	9381	6072	0.74	6378	8205.8
4	61.5	66.9	8.4	4530	8
AAZ	250	12.1	6.8	451	1.8

* Mean from three determinations by a stopped-flow, CO_2 hydrase method. Standard errors were in the range of 5–10% of the reported values.

[a] Selectivity as determined by the ratio of K_i for hCA II isoform relative to VchCAα.

The following structure-activity-relationship (SAR) may be noted regarding the inhibition data in **Table 1**:

Acyl selenoureido compounds series **1-4** exhibited a highly potent inhibitory activity towards VchCAα, with inhibition constants K_is ranging in the subnanomolar range, except for derivative **4**, which was active in the low nanomolar range (overall the K_is ranged between 0.3 to 8.4 nM). These data suggest that the placement of the sulfonamide moiety in selenium-containing analogs leads to excellent inhibitory potencies against VchCAα, a kinetic result rarely observed with other CAIs of the sulfonamide type.[19,20] In fact, all these

derivatives (except **4**) were so potent CAIs that a proper SAR is difficult to draw at the moment. As mentioned above, only the *ortho*-substituted derivative **4** showed a somehow decreased activity being as active as **AAZ** (**Table 1**). The introduction of small substituents on the acyl scaffold incorporating 4-ethylamino benzensulfonamide (**1a-d**) did not influence significantly the potency for inhibition for VchCAα, although the benzodiaxole scaffold (**1d**) showed the best activity with a K_i of 0.3 nM. An interesting inhibition profile was observed for compounds **1c** and **3c**. The presence of another phenyl moiety as in **1c,** or two CF_3 groups in the acyl scaffold, as in **3c**, decreased the inhibition potency for all humans and β-CA isoforms and did not influence VchCAα kinetics. Thus, these compounds showed excellent selectivity, being over a 1000 folds more potent over the β-ones. Indeed, unlike the standard drug acetazolamide (**AAZ**) the acyl selenoureido sulfonamides reported here were generally poor inhibitors against VchCAβ, showing K_i values in the high micromolar range (K_is of 4.53-8.77 μM). Overall, all the synthesised compounds (except for **2c**) were selective inhibitors for the bacterial VchCAα isoform over the hCAs I and II and VchCA β.

In order to design new organoselenium compounds that may have anti-infective applications, we also studied the selenides **5-8** (**Figure 2**), reported above in **Chapter 4**, as inhibitors of VchCAα,β and the BpsCAβ, a β-CA from pathogenic bacteria *B. pseudomallei*.

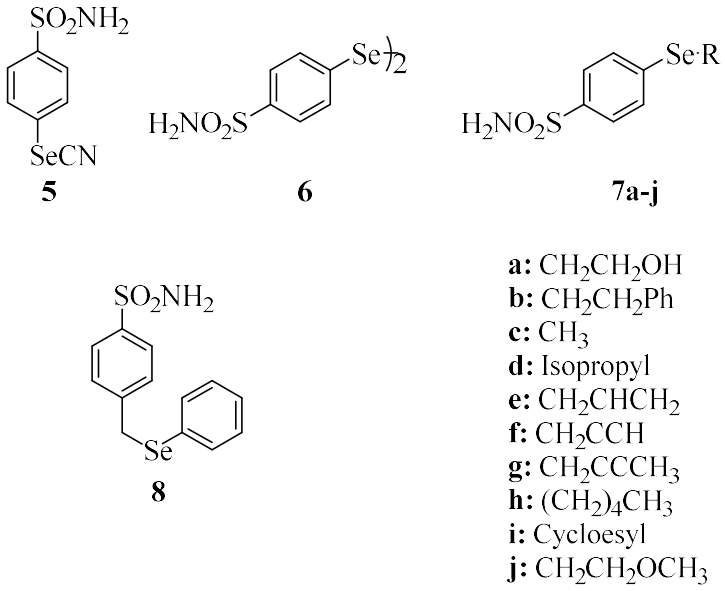

Figure 2: Acyl selenoureido derivatives **5-8**

We tested *in vitro* these compounds for their inhibitory activity against the two off-targets physiologically relevant hCA isoforms I, II and the bacterial enzymes VchCAα, VchCAβ and BpsCAβ by means of the stopped-flow carbon dioxide hydration assay.[18] These activities were compared to those of the standard and clinically used CAI acetazolamide (**AAZ**) (**Table 2**).

Table 2. Inhibition constants of hCA I, hCA II, VhCAα, VhCAβ and BpsCAβ with compounds **5-8** and **AAZ** by a stopped-flow CO_2 hydrase assay[18]

Compound	K_i (nM)*				
	hCA I	hCA II	VhCAα	VhCAβ	BpsCAβ
5	95.6	53.1	4.6	2172	75.3
6	1523	7.9	5.7	6804	83.6
7a	338.3	355.3	5.9	7598	754.2
7b	256.8	9.3	4.1	5942	845.6
7c	352.2	73.2	6.1	8727	529.8
7d	9.7	69.9	6.5	5264	51.9
7e	5.2	36.5	28.6	7853	9.1
7f	7.3	9.3	6.7	2590	21.4
7g	293.5	7.6	6.0	6901	5.4
7h	297.1	70.8	4.4	5068	823.9
7i	21.9	6.3	4.3	5897	876.9
7j	261.7	41.2	7.5	1853	866.6
8	226.1	53.0	5.4	7697	650.4
AAZ	250.0	12.1	6.8	451	745

* Mean from three determinations by a stopped-flow, CO_2 hydrase method. Standard errors were in the range of 5–10% of the reported values.

The following structure–activity relationship (SAR) can be drawn from the data of this table:

i) Selenides **5, 7a-j, 8** and diselenide **6** exhibited potent inhibitory activity towards VchCAα with inhibition constants in the low-nanomolar range, except for compound **7c**, which was active in the medium nanomolar range (overall the K_is ranged between 4.3 to 28.6 nM). Small structural differences in the tail moiety, such as the replacement of methyl (**7c**) with different methylene chains (**7a-b**, **7d-j**, **8**), did not result in particular kinetic effects, except for the selenide **7e** where efficacy decreased of about 4 times.

ii) All compounds showed poor effects on the VchCAβ with a constant of inhibition in the micromolar range (K_is ranged between 1.8 to 8.7 μM). This time, diselenide **6** was 3 fold more potent than the selenocyanate derivative **5.** Also for this isoform, small structural differences on the tail did not significantly change the inhibitory potencies.

The only exceptions were **7f** and **7j** that showed an potencies respectively almost 2 and 3 times higher.

iii) The inhibition profile of BpsCAβ differs substantially from the other β-class enzyme (VhCAβ) investigated here. An interesting inhibition profile was observed for **7e**-**g** where a rigid scaffold on the tails showed a potent activity against this isoform at low nanomolar values (K_is 5.4 and 9.1 nM for **7e** and **7g,** slightly less efficacy with K_is 21.4 nM for compound **7f**). Furthermore, selenide **5** and diselenide **6** reveal good potency of inhibition in the range of medium nanomolar (K_is 75.3 to 83.6 nM). On the other hand, scaffolds less rigid lead to drastically decrease the potency in the range of high nanomolar (K_is spanning between 529.8 to 876.9 nM).

The inhibition profiles for the two *V. cholerae* enzymes (VhCAα and β) and for selected one from *B. pseudomallei* (BpsCAβ) showed quite dissimilar also in comparison with the hCA II (**Table 3**).

Table 3. Inhibition constants of hCA I, hCA II, VhCAα, VhCAβ and BpsCAβ with compounds **5-8** and **AAZ** by a stopped-flow CO_2 hydrase assay[18]

Compound	Selectivity ratio[a]		
	hCA II/ VchCAα	hCA II/ VchCAβ	hCA II/ BpsCAβ
5	11.54	$2\ 10^{-2}$	0.7
6	1.38	$1\ 10^{-3}$	$9.4\ 10^{-2}$
7a	60.22	$4.6\ 10^{-2}$	0.47
7b	2.26	$1\ 10^{-3}$	$1\ 10^{-2}$
7c	12	$8\ 10^{-3}$	$8\ 10^{-3}$
7d	10.75	$1.3\ 10^{-2}$	1.3
7e	1.27	$4\ 10^{-3}$	4
7f	1.38	$3\ 10^{-3}$	0.43
7g	1.26	$1\ 10^{-3}$	1.4
7h	16.09	$1.3\ 10^{-2}$	$8.6\ 10^{-2}$
7i	1.46	$1\ 10^{-3}$	$7\ 10^{-3}$
7j	5.49	$2.2\ 10^{-2}$	$4.7\ 10^{-2}$
8	9.8	$7\ 10^{-3}$	$8.1\ 10^{-2}$
AAZ	1.77	$2.6\ 10^{-2}$	$1.6\ 10^{-2}$

[a] Selectivity as determined by the ratio of K_i for hCA II isoform relative to bacterial isoforms.

A relatively high number of selenides that have been investigated act as effective CAIs against the VhCAα. Among them, the compound with the ethanoyl moiety (**7a**) showed the most promising profile with a selectivity index of 60 (**Table 3**). The diselenide **6** showed quite potent inhibition but poor selectivity over the human isoforms. The selectivity ratio of BpsCAβ differs substantially from the other β-class enzyme (VhCAβ) investigated here. Only compound **7e** showed a good selective inhibition against this isoform with a 4 fold higher potency when compared to the off-target isoforms (hCA I, II) and 3 fold higher for VhCAα. Selenides **7d** and **7g**, on the other hand, exhibit slightly selectivity with 1.3 and 1.4 folds respectively.

6.3 Famotidine, an antiulcer agent, strongly inhibits *Helicobacter pylori* and human carbonic anhydrases

The third generation histamine H_2 receptor antagonists such as cimetidine, ranitidine and famotidine (**Figure 1**) are widely used for the treatment of duodenal and gastric ulcers, gastroesophageal reflux disease and pathological hyper-secretory conditions such as Zollinger-Ellison syndrome.[21-23] Famotidine incorporates a sulfamide moiety, a bioisoster of the sulfonamide group, a well-known zinc binding group present in CAIs.[24] However, the effects of famotidine on these zinc metalloenzymes was scarcely investigated up until now.[25]

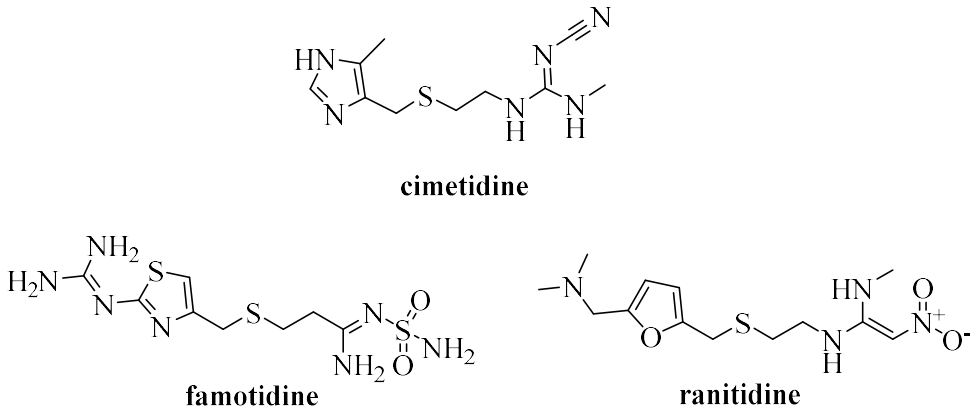

Figure 1: Third generation of H_2 antagonists in clinical use

We decided to investigate whether famotidine shows CA inhibitory effects. All catalytically active human CA isoforms (hCA I–XIV), as well as the two CAs present in the bacterial pathogen *Helicobacter pylori* (α-HpCA, β-HpCA), the etiologic agent responsible of gastric ulcers, were included in the study. Furthermore, we report the X-ray structure of famotidine in complex with hCA I and hCA II, allowing us to unravel interesting aspects related to its CA inhibition mechanism. The inhibition profiles of famotidine and acetazolamide (**AAZ**), as standard sulfonamide inhibitor against all catalytically active CA isoforms is shown in **Table 4**.

Table 4. Inhibition constants of hCA I-XIV with famotidine and acetazolamide (**AAZ**) as a standard inhibitor, by a stopped-flow CO_2 hydrase assay[18]

Enzymes	K_i nM*	
	Famotidine	AAZ
hCA I	922.4	250.0
hCA II	57.9	12.1
hCA III	>10000	>10000
hCA IV	938.8	74.0
hCA VA	1429	63.0
hCA VB	5328	54.0
hCA VI	98.2	11.0
hCA VII	3.0	2.5
hCA IX	126.3	25.8
hCA XII	45.3	5.7
hCA XIII	171.5	17.0
hCA XIV	677.2	41.0

* Mean from three determinations by a stopped-flow, CO_2 hydrase method. Standard errors were in the range of 5–10% of the reported values.

The cytosolic isoforms had a very different inhibition profile with famotidine. hCA VII was the most susceptible isoform to inhibition with this drug, with an inhibition constant K_i of 3.0 nM. On the other hand, the two widespread cytosolic isoforms hCA I and hCA II, showed a very different inhibition with this compound: hCA II was effectively inhibited (K_i 57.9 nM), whereas hCA I was more than ten times less sensitive to famotidine inhibition compared to hCA II, with a K_i of 922.4 nM. Famotidine was a moderate inhibitor of isoform hCA XIII (K_i 171.5mM) and lost any activity against hCA III with a K_i> 10 μM. The two mitochondrial isoforms (hCA VA and VB) were poorly inhibited by this sulfamide drug, in the micromolar range (K_is of 1.4 and 5.3 μM, respectively). The membrane-bound isoforms, similar to the cytosolic ones discussed above, showed a heterogeneous inhibition pattern. hCA XII, a tumor associated isoform was effectively inhibited by famotidine with a K_i of 45.3 nM. The second enzyme overexpressed in hypoxic tumors, hCA IX, was on the other hand less inhibited by famotidine, with a K_i of 126.3 nM (**Table 4**). The last two membrane-associated isoforms hCA IV and XIV, instead, were weakly inhibited by this drug, in the high nanomolar range (K_i 938.8 and 677.2 nM).

H. pylori, a Gram-negative neutralophile was shown to be the cause of chronic gastritis, peptic ulcers, and, more recently, gastric cancer, the second most common tumor in humans.[26,27] This gastric pathogen encodes for two classes of CAs, an α- and a β-one. Both enzymes are crucial for its survival in the acidic environment within the stomach, and recent studies showed that sulfonamides block the growth of the pathogen *in vitro* and *in vivo*.[28-30] Thus, in case of interference with these enzymes, famotidine might be used as a new pharmacologic tool in the management of drug-resistant *H. pylori*.[31] For this reason, we performed inhibition studies of the two bacterial CAs (**Table 5**).

Table 5. Inhibition constants of hpαCA and hpβCA with famotidine and acetazolamide (**AAZ**) as a standard inhibitor, by a stopped-flow CO_2 hydrase assay[18]

Enzymes	K_i nM*	
	Famotidine	AAZ
hpαCA	20.7	21.4
hpβCA	49.8	40.0

* Mean from three determinations by a stopped-flow, CO_2 hydrase method. Standard errors were in the range of 5–10% of the reported values.

The α-class enzyme was effective inhibited by this compound, with an inhibition constants of 20.7 nM, comparable to clinically used sulfonamide acetazolamide. On the other hand, hpβCA was less effectively inhibited by famotidine (Ki of 49.8 nM). However, also for this enzyme the activity was comparable to **AAZ**. An interesting observation was that famotidine prove to be more active against *H. pylori* enzymes compared to the two human dominant cytosolic isoforms (hCA I and hCA II), whereas **AAZ** was an effective inhibitor for both (**Table 4**). Considering the abundant localization in the gastro-intestinal tract of the cytosolic hCA I and II, as well as their crucial roles in pH regulation, we focused and obtained the high resolution X-ray crystal structures of the adducts of famotidine with these enzymes, in order to understand in detail the binding modes of the drug. Inspection of the initial $|F_o-F_c|$ electron density maps of both active sites showed well defined densities, fully compatible with the presence of famotidine and, surprisingly, revealed two possible conformations of the drug for both adducts (**Figure 2A** and **B**). Famotidine coordinates the catalytic zinc ion of the two CA isoforms by means of one nitrogen atom of the sulfamide group, displacing

the zinc bound water molecule/hydroxide ion, resulting in a tetrahedral coordination geometry of the metal ion, similarly to other sulfamide and sulfonamide compounds.[24]

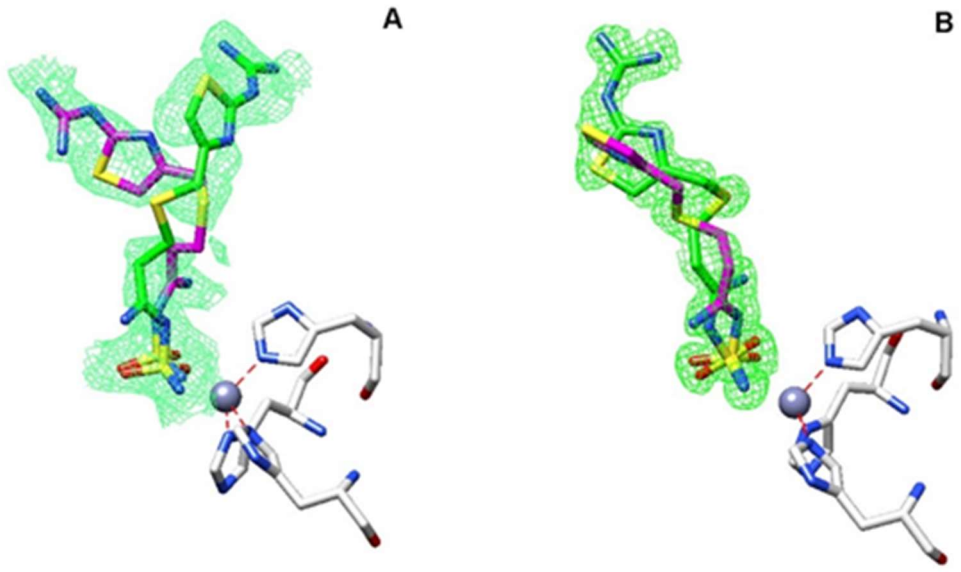

Figure 2: Active site region of hCA I/famotidine (**A**) and hCA II/famotidine (**B**) complexes. Inhibitors shown as σA-weighted $|F_o-F_c|$ density maps at 2.0 σ. The zinc ion (grey sphere) and its three His ligands are shown in CPK colour.

The hCA I/famotidine complex showed two different orientation of the inhibitor (**Figure 3**). The first one, labelled in green, exhibited different hydrogen bonds stabilizing the enzyme-inhibitor adduct, such as the ones involving the guanidine tail and Asn69 or the nitrogen atom near the sulfamide moiety and Thr199 and His200. On the other hand, hydrophobic interactions were almost non-existent in this complex. We found only one such interaction among Leu198 and the methylene chain of famotidine. The opposite orientation of the second structure (labelled in magenta), surprisingly did not show any interaction with side chains of the protein (**Figure 3**).

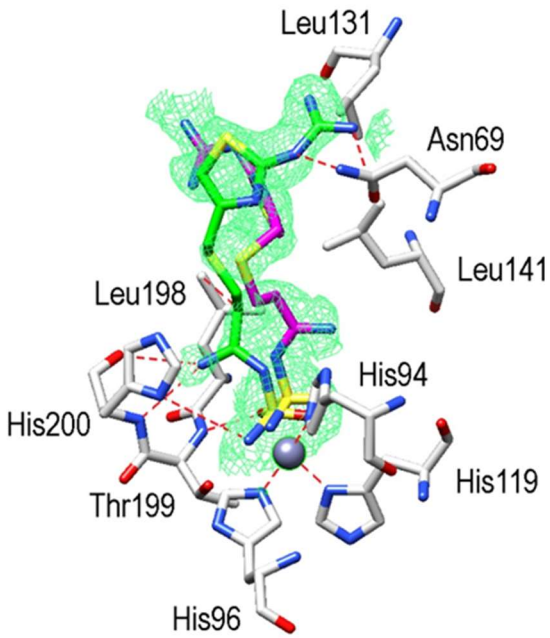

Figure 3: Active site region of hCA I/famotidine adduct. Inhibitor showed as σA-weighted $|F_o-F_c|$ density map at 2.0 σ. Hydrogen bonds, van der Waals interactions, and the active site Zn^{2+}-ion coordination are also shown

A completely different situation was observed when the hCA II active site was analyzed. Again two possible orientations of famotidine were observed, both located in the hydrophobic region delimited by a small pocket aligned by the side chains of Phe131, Leu198, and Pro201 (**Figure 4**). The thiazole ring of one famotidine orientation (labeled in green) formed strong hydrophobic interactions with these residues and a water bridge with Pro201 by means of the azomethine nitrogen atom. This portion of the molecule was oriented differently in two conformations: in one the nitrogen atom participates to several hydrogen bonds with Thr199 and Thr200. In the second one, a reverse orientation of the nitrogen was seen, with no interactions with the protein. Finally, the sulfamide oxygen is involved in a bifurcated hydrogen bond with Thr200 (**Figure 4**). Electron density was absent for the guanidine tail of the conformation labeled in magenta in **Figure 4** and was not introduced in the complex model.

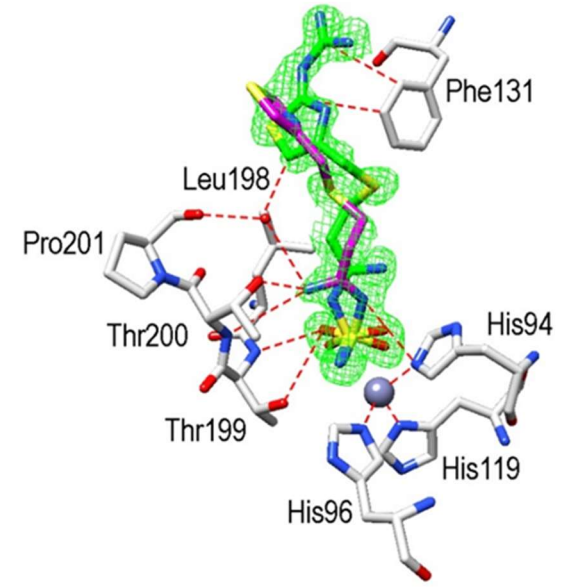

Figure 4: Active site region of hCA II/famotidine adduct. Inhibitor showed as σA-weighted $|F_o-F_c|$ density map at 2.0 σ. Hydrogen bonds, van der Waals interactions, and the active site Zn^{2+}-ion coordination are also shown.

The structural superimposition between the hCA I and hCA II complexes, is reported in **Figure 5**, and shows that, while the sulfamide moieties of famotidine are rather well superimposable, the two aliphatic tails present different orientations, and as a consequence, diverse interactions with amino acid side chains from the two active sites. Phe131 in hCA II proved to be essential to collocate famotidine within the lipophilic side of the active site cavity, which strongly correlates with the inhibition potency of this drug against hCA II. On the other hand, the presence of Leu131 in hCA I led to a loose van der Waals interaction, which did not force famotidine towards the lipophilic side of the active site, leading thus to two opposite orientations of the scaffold and few hydrophobic interactions with the active site. These characteristics reflect the loss of inhibitory potency against this isoform compared to hCA II.

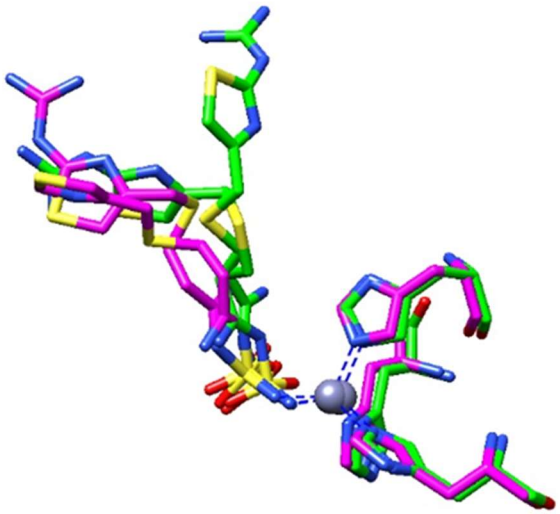

Figure 5: Structural superimposition of famotidine/hCA I and famotidine/hCA II complexes. hCA I and hCA II adducts are coloured in green and magenta, respectively.

6.4 Conclusions

We have investigated a series of selenides bearing benzenesulfonamide for their inhibition against two pathogenic bacteria from *Vibrio cholera* (VchCAα and VchCAβ) and, *Burkholderia pseudomallei* (BpsCAβ). Excellent inhibitory activity, in the nanomolar range, was observed against VchCAα whereas the β class enzyme was much less inhibited. These selenides were also VchCAα-selective inhibitors over the human off-target enzymes hCA I, II. Thus, this series of compounds might be considered important leads for obtaining more effective and selective CAIs targeting VchCAα.

Moreover, Famotidine shows particular efficacy for the cytosolic isoforms hCA II and hCA VII. Furthermore, the two class bacterial enzymes from *H. pylori* (hpαCA and hpβCA) were also highly inhibited by this drug, raising thus the possibility that the effective antiulcer effects of famotidine may be due not only to its action of H_2-receptor antagonist but also due to the inhibition of the bacterial CAs too.

6.5 Experimental Data

General

Anhydrous solvents and all reagents were purchased from Sigma-Aldrich, Alfa Aesar and TCI. The solvents used in MS measures were acetone, DMSO, acetonitrile (Chromasolv grade), purchased from Sigma-Aldrich (Milan - Italy), and mQ water 18 MΩ, obtained from Millipore's Simplicity system (Milan-Italy).

Carbonic anhydrase inhibition

An Applied Photophysics stopped-flow instrument has been used for assaying the CA catalyzed CO_2 hydration activity.[18] Phenol red (at a concentration of 0.2 mM) has been used as indicator, working at the absorbance maximum of 557 nm, with 20 mM Hepes (pH 7.5) as buffer, and 20 mM Na_2SO_4 (for maintaining constant the ionic strength), following the initial rates of the CA-catalyzed CO_2 hydration reaction for a period of 10–100 s. The CO_2 concentrations ranged from 1.7 to 17 mM for the determination of the kinetic parameters and inhibition constants. For each inhibitor at least six traces of the initial 5–10% of the reaction have been used for determining the initial velocity. The uncatalyzed rates were determined in the same manner and subtracted from the total observed rates. Stock solutions of inhibitor (0.1 mM) were prepared in distilled-deionized water and dilutions up to 0.01 nM were done thereafter with the assay buffer. Inhibitor and enzyme solutions were preincubated together for 15 min at room temperature prior to assay, in order to allow for the formation of the E-I complex. The inhibition constants were obtained by non-linear least-squares methods using PRISM 3 and the Cheng–Prusoff equation.

Crystallization and X-ray data collection

Crystals were obtained using the hanging drop vapor diffusion method using 24 well Linbro plate. 2 µl of 10 mg/ml solution of hCA I in Tris-HCl 20 mM pH 9.0 were mixed with 2 µl of a solution of 28-31% PEG4000, 0.2 M Sodium acetate, 0.1 M Tris pH 8.5-9.0 and were equilibrated against the same solution at 296 K. Crystals of the protein grew in fifteen days. Afterwards hCAI crystals were soaked in 5mM inhibitor solution for 3 days. The crystals were flash-frozen at 100K using a solution obtained by adding 15% (v/v) glycerol to the

mother liquor solution as cryoprotectant. Data on crystals of the complexes were collected using synchrotron radiation at the ID23-2 beamline at ESRF (Grenoble, France) with a wavelength of 0.873 Å and a PILATUS3 2M Dectris CCD detector. 2 µl of 0.8 mM solution of hCA II in Tris-HCl pH=8.0 were mixed with of a solution of 1.5, 1.6 and 1.7 M sodium citrate, 50 mM Tris pH 8.0 and were equilibrated against 500 µl of the same solution at 296 K. Crystals of the complexes grew in a few days. hCAII crystals were soaked in 5mM inhibitor solution for 2 days. The crystals were flash-frozen at 100K using a solution obtained by adding 25% (v/v) glycerol to the mother liquor solution as cryoprotectant. Data on crystals of the complexes were collected using synchrotron radiation at the ID-30B beamline at ESRF (Grenoble, France) with a wavelength of 0.827 Å and a PILATUS3 6M Dectris CCD detector, to a maximum resolution of 1.0. Data were integrated and scaled using the program XDS.[32]

Structure determination

The crystal structure of hCA I (PDB accession code: 1JV0) and hCA II (PDB accession code: 4FIK) without solvent molecules and other heteroatoms was used to obtain initial phases of the structures using Refmac5.[33] 5% of the unique reflections were selected randomly and excluded from the refinement data set for the purpose of Rfree calculations. The initial |Fo - Fc| difference electron density maps unambiguously showed the inhibitor molecules. Atomic models for inhibitors were calculated and energy minimized using the program JLigand 1.0.40.[34] Refinements proceeded using normal protocols of positional, isotropic atomic displacement parameters alternating with manual building of the models using COOT.[35] Solvent molecules were introduced automatically using the program ARP.[36] The quality of the final models were assessed with COOT and RAMPAGE.[37] Atomic coordinates were deposited in the Protein Data Bank (PDB accession code: 6G3Q and 6G3V). Graphical representations were generated with Chimera.[38]

Summary of Data Collection and Atomic Model Refinement Statistics

PDB	6G3Q	6G3V
Compound	Famotidine	Famotidine
Space group	$P2_1$	$P2_12_12_1$
Cell dimensions		
a, b, c	42.3, 41.4, 72.1	62.5, 71.4, 121.4
alpha, beta, gamma	90, 104.3, 90	90, 90, 90
Resolution (Å)	41.0 - 1.01	30.0 - 1.69
Resolution-high (Å)	1.08 - 1.01	1.80 - 1.69
Rsym (%)	3.8 (60.1)	6.8 (120.2)
Rmeas (%)	4.8 (76.5)	8.3 (151.7)
CC ½	0.998 (0.639)	0.997 (0.370)
I/sigI	10.80 (1.35)	8.30 (0.83)
Completeness (%)	88.6 (65.1)	93.5 (82.6)
Redundancy	2.5 (2.4)	2.75 (2.2)
Wavelength (Å)	0.827	0.873
Refinement		
resolution (Å)	30.0 - 1.01	27.0 - 1.69
unique reflections	106958	54371
Rwork/Rfree (%)	5346	2811
Rfactor (%)	12.72	21.42
Rfree(%)	15.15	26.31
Ramachandran statistics (%)		1
Most favored	96.9	97.2
additionally allowed	3.1	2.8
outlier regions	0.0	0.0
B-factors (Å^2)	18.58	30,96
ligand	19,74	31,42
water	35,53	54,66
r.m.s. deviations		
Bond length (Å)	0,009	0,0123
Bond angle (°)	1,427	2,199

References

1. Tibayrenc M., Ayala F.J. Reproductive clonality of pathogens: a perspective on pathogenic viruses, bacteria, fungi, and parasitic protozoa. *Proc Natl Acad Sci USA* 2012, 109, E3305-3313
2. Roux O., Cereghino R., Solano P.J., Dejean A. Caterpillars and fungal pathogens: two co-occurring parasites of an ant-plant mutualism. *PLoS One* 2011, 6, e20538
3. Joyce S.A., Watson R.J., Clarke D.J. The regulation of pathogenicity and mutualism in Photorhabdus. *Curr Opin Microbiol* 2006 ,9, 127-132.
4. Soto W., Punke E.B., Nishiguchi M.K. Evolutionary perspectives in a mutualism of sepiolid squid and bioluminescent bacteria: combined usage of microbial experimental evolution and temporal population genetics. *Evolution* 2012, 66, 1308-1321
5. Cardoso T., Ribeiro O., Aragao I.C., Costa-Pereira A., Sarmento A.E. Additional risk factors for infection by multidrug-resistant pathogens in healthcare-associated infection: a large cohort study. *BMC Infect Dis* 2012, 12, 375
6. Cox G.M., Mukherjee J., Cole G.T., Casadevall A., Perfect J.R. Urease as a virulence factor in experimental cryptococcosis. *Infect Immun* 2000, 68, 443-448
7. Cox G.M., McDade H.C., Chen S.C., Tucker S.C., Gottfredsson M., Wright L.C., Sorrell T.C., Leidich S.D., Casadevall A., Ghannoum M.A., Perfect J.R. Extracellular phospholipase activity is a virulence factor for Cryptococcus neoformans. *Mol Microbiol* 2001, 39, 166-175
8. Bostanci N., Belibasakis G.N. Porphyromonas gingivalis: an invasive and evasive opportunistic oral pathogen. *FEMS Microbiol Lett* 2012, 333, 1-9
9. Alp S. Putative virulence factors of Aspergillus species. *Mikrobiyol Bul* 2006, 40, 109-119
10. Schaller M., Borelli C., Korting H.C., Hube B. Hydrolytic enzymes as virulence factors of Candida albicans. *Mycoses* 2005, 48, 365-377

11. Sacarlal J., Nhacolo A.Q., Sigauque B., Nhalungo D.A., Abacassamo F., Sacoor C.N., Aide P., Machevo S., Nhampossa T., Macete E.V., Bassat Q., David C., Bardají A., Letang E., Saúte F., Aponte J.J., Thompson R., Alonso P.L. A 10 year study of the cause of death in children under 15 years in Manhica, Mozambique. *BMC Public Health* 2009, 9, 67

12. Capasso C., Supuran C.T. Anti-infective carbonic anhydrase inhibitors: a patent and literature review. *Expert Opin Ther Pat* 2013, 23, 693-704

13. Rusconi S., Scozzafava A., Mastrolorenzo A., Supuran C.T. New advances in HIV entry inhibitors development. *Curr Drug Targets Infect Disord* 2004, 4, 339-355

14. Supuran C.T. Inhibition of bacterial carbonic anhydrases and zinc proteases: from orphan targets to innovative new antibiotic drugs. *Curr Med Chem* 2012, 19, 831-844

15. Nozawa R., Yokota T., Fujimoto R., Susceptibility of methicillin-resistant Staphylococcus aureus to the selenium-containing compound 2-phenyl-1,2-benzoisoselenazol-3(2H)-one (PZ51). *Antimicrob. Agents Chemother.* 1989, 33, 1388

16. Brown G.A., Anderson K.M., Murray M., Gallagher T., Hales N.J., Preparation of Novel Selenopenams by Intramolecular Homolytic Substitution *Tetrahedron* 2000, 56, 5579.

17. Koketsu M., Ishihara H., Hatsu M., Novel compounds, 1,3-selenazine derivatives, as antibacterial agents against Escherichia coli and Staphylococcus aureus. *Res. Commun. Mol. Path. Pharmacol*. 1998, 101, 179.

18. Khalifah R.G., The carbon dioxide hydration activity of carbonic anhydrase. I. Stop flow kinetic studies on the native human isoenzymes B and C. *J. Biol. Chem*. 1971, 246, 2561.

19. Del Prete S., De Luca V., Scozzafava A., Carginale V., Supuran C.T., Capasso C. Biochemical properties of a new α-carbonic anhydrase from the human pathogenic bacterium, Vibrio cholerae.*J Enzyme Inhib Med Chem*. 2014, 29, 23-27

20. Del Prete S., Vullo D., De Luca V., Carginale V., Ferraroni M., Osman S.M., AlOthman Z., Supuran C.T., Capasso C. Sulfonamide inhibition studies of the β-carbonic anhydrase from the pathogenic bacterium Vibrio cholerae. *Bioorg Med Chem*, 2016, 24, 1115.

21. Sakurai K., Nagahara A., Inoue K., Akiyama J., Mabe K., Suzuki J., Habu Y., Araki A., Suzuki T., Satoh K., Nagami H., Harada R., Tano N., Kusaka M., Fujioka Y., Fujimura T., Shigeto N., Oumi T., Miwa J., Miwa H., Fujimoto K., Kinoshita Y., Haruma K., Efficacy of omeprazole, famotidine, mosapride and teprenone in patients with upper gastrointestinal symptoms: an omeprazole-controlled randomized study. *BMC Gastroenterol.*, 2012, 12, 42.

22. Howden C.W., Clinical pharmacology of omeprazole. *Clin. Pharmacokin.*, 1991, 20, 38.

23. Ahmadi A., Ebrahimzadeh M.A., Ahmad-Ashrafi S., Karami M., Mahdavi M.R., Saravi S.S., Hepatoprotective, antinociceptive and antioxidant activities of cimetidine, ranitidine and famotidine as histamine H2 receptor antagonists. *Fundam Clin Pharmacol.*, 2011, 25, 72

24. De Simone G., Pizika G., Monti S.M., Di Fiore A., Ivanova J., Vozny I., Trapencieris P., Zalubovskis R., Supuran C.T., Alterio V., Hydrophobic substituents of the phenylmethylsulfamide moiety can be used for the development of new selective carbonic anhydrase inhibitors. *Biomed Res Int.*, 2014, 2014, 523210

25. Demir Y., Nadaroğlu H., Demir N., Effects of omeprazole, famotidine, and ranitidine on the enzyme activities of carbonic anhydrase from bovine stomach in vitro and rat erythrocytes in vivo. *Biol Pharm Bull.*, 2004, 27, 1730.

26. Nishimori I., Minakuchi T., Kohsaki T., Onishi S., Takeuchi H., Vullo D., Scozzafava A., Supuran C.T., Carbonic anhydrase inhibitors: the beta-carbonic anhydrase from Helicobacter pylori is a new target for sulfonamide and sulfamate inhibitors. *Bioorg. Med. Chem. Lett.* 2007, 17, 3585.

27. Nishimori I., Vullo D., Minakuchi T., Morimoto K., Onishi S., Scozzafava A., Supuran C.T., Carbonic anhydrase inhibitors: DNA cloning and inhibition studies of the alpha-carbonic anhydrase from Helicobacter pylori, a new target

for developing sulfonamide and sulfamate gastric drugs. *Bioorg. Med. Chem. Lett.* 2006, 16, 2182.

28. Maresca A., Vullo D., Scozzafava A., Supuran C.T., Inhibition of the alpha- and beta-carbonic anhydrases from the gastric pathogen Helycobacter pylori with anions. *J Enzyme Inhib Med Chem.* 2013, 28, 388.
29. Capasso C., Supuran C.T., Bacterial, fungal and protozoan carbonic anhydrases as drug targets. Expert Opin Ther Targets., 2015, 19, 1689.
30. Modak J.K., Liu Y.C., Supuran C.T., Roujeinikova A., Structure-Activity Relationship for Sulfonamide Inhibition of Helicobacter pylori α-Carbonic Anhydrase. *J. Med Chem.*, 2016, 59, 11098.
31. Amin M., Iqbal M.S., Hughes R.W., Khan S.A., Reynolds P.A., Enne V.I., Sajjad-ur-Rahman, Mirza A.S., Mechanochemical synthesis and in vitro anti-Helicobacter pylori and uresase inhibitory activities of novel zinc(II)-famotidine complex. *J Enzyme Inhib Med Chem.*, 2010, 25, 383.
32. Leslie A.G.W., Powell H.R., Procesing diffraction data with mosflm. In: Read RJ, Sussman JL (eds) Evolving methods for macromolecular crystallography, vol 245, NATO Science series, Springer, Dordrecht, 2007, pp. 41-51.
33. Murshudov G.N., Vagin A.A., Dodson E.J., Refinement of macromolecular structures by the maximum-likelihood method. *Acta Crystallogr D Biol Crystallogr.* 1997, 53, 240-255.
34. Lebedev A.A., Young P., Isupov M.N., Moroz O.V., Vagin A.A., Murshudov G.N. JLigand: a graphical tool for the CCP4 template-restraint library. *Acta Crystallogr D Biol Crystallogr.* 2012, 68, 431-440.
35. Emsley P., Lohkamp B., Scott W., Cowtan K., Features and development of Coot. *Acta Crystallogr D Biol Crystallogr.* 2010, 66, 486-501.
36. Lamzin V.S., Perrakis A., Wilson K.S., The ARP/wARP suite for automated construction and refinement of protein models**,** M.G. Rossmann, E. Arnold (Eds.), Int. Tables for Crystallography. Vol. F: Crystallography of Biological Macromolecules, Kluwer Academic Publishers, Dordrecht, The Netherlands (2001), pp. 720-722

37. Lovell S.C., Davis I.W., Arendall III W.B., de Bakker P.I.W., Word J.M., Prisant M.G., Richardson J.S., Richardson D.C., Structure validation by Cα geometry: ϕ,ψ and Cβ deviation, *Proteins*, 2003, 50, 437-450.

38. Pettersen E.F., Goddard T.D., Huang C.C., Couch G.S., Greenblatt D.M., Meng E.C., Ferrin T.E., UCSF Chimera—a visualization system for exploratory research and analysis, *J. Comput. Chem.*, 2004, 25, 1605-1612

Chapter 7

New activators of human Carbonic Anhydrases

7.1 Introduction.

Carbonic Anhydrase activation properties were reported in the early 1940s by several independent groups.[1-3] As previously discussed in **Chapter 1.4** amines, such as histamine, amino acids and peptides were shown to possess such a biochemical activity.[1-3] However, the subject became highly controversial in the early 1990s, when the use of highly purified enzymes and very precise techniques became routinary.[4-6] A general mechanism of action for the Carbonic Anhydrase activators (CAAs) has been proposed based on Equation below:

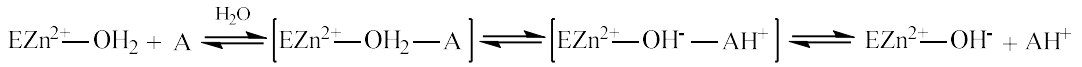

According to this model, the activator molecule participates to the rate-determining step of the catalytic cycle, the proton shuttling, acting similarly to the natural proton shuttle (i.e. His64). In such enzyme–activator complexes proposed for explaining the mechanism,[5] the proton transfer becomes intramolecular, thus being more efficient when compared to the intermolecular transfer to buffer molecules, not bound within the enzyme cavity. [4-6] Kinetic data in the presence of activators proved that the activator does not influence K_M (the affinity for the substrate) and has an effect only on k_{cat} of the enzyme-catalyzed reaction, both for the esterase (with 4-nitrophenyl acetate) and CO_2 hydration reactions.[7,8] Finally, the confirmation of CA activation mechanism arrived in 1997, by the report of the first X-ray crystal structure of an activator, histamine, bound to hCA II.[7] Although CAIs have been extensively studied, and exploited clinically for the prevention and treatment of several diseases, the field of CA activators is largely unexplored. The pharmacologic applications of the activators started to be explored in the last 15 years. Sun and Alkon reported that phenylalanine, an activator, when administered to experimental animals produces a relevant pharmacological enhancement of synaptic efficacy, spatial learning and memory, proving that this class of unexplored enzyme modulators may be used for the management of conditions in which learning and memory are impaired.[9,10] CA-deficiency and tissue engineering field[11,12] are others fields where this modulators could be used. For these reason, we continued to investigate new compounds as possible CAAs for better understand the role of different isoforms in the human body and their possible pharmacological applications.

7.2 Psychoactive substances belonging to the amphetamine class potently activate brain Carbonic Anhydrase isoforms VA, VB, VII, and XII

Psychoactive substances, such as cocaine, amphetamines, and cannabinoids, as well as new synthetic molecules belonging to a vast array of chemical families, some of which are poorly characterised from the pharmacological and toxicological viewpoints.[13-15] Our interest in this type of compounds is connected to the fact that many of the "classical" drug abuse compounds are primary, secondary, or tertiary amines incorporating the phenethylamine scaffold (such as amphetamine and methamphetamine).[13,14] This type of amines, possessing the general formula Ar-$CH_2CH(R)NHR_2$ typical of carbonic anhydrase activators (compounds **1-4** in **Figure 1**),[7,8] were never investigated as potential CAAs.

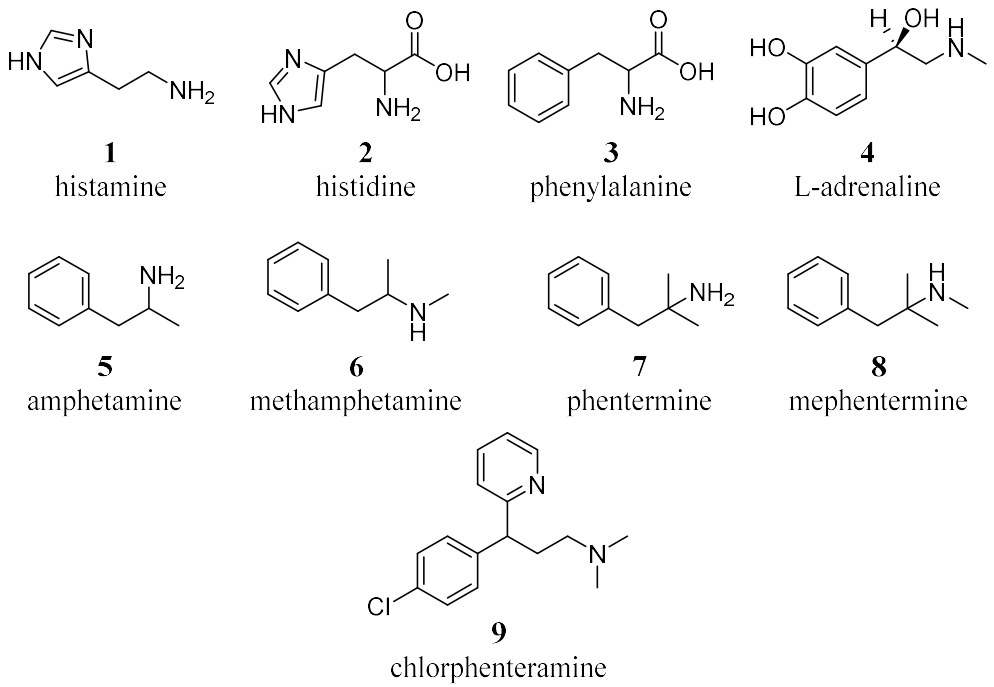

Figure 1. Structure of typical CAAs **1-4** and psychoactive substances investigated as CAAs **5-9**.

Here, we report the first study showing that amphetamine **5**, methamphetamine **6**, phentermine **7**, mephentermine **8**, and chlorphenteramine **9** (**Figure 1** entry **5-9**), potently

activate several CA isoforms, some of which are highly abundant in the brain, where they play important functions connected to cognition and memory, among others.[9,10]

Amines **5–9** are widely used psychoactive substances. They include primary amines such as amphetamine **5** and phentermine **7**, secondary ones such as methamphetamine **6** and mephentermine **8**, as well as a tertiary amine, chlorphenteramine **9**, which unlike compounds **5–8**, which possess the general formula mentioned above, typical to most CAAs **4–6**, incorporates a dimethylamino moiety linked by a three carbon atoms chain to a bulky aromatic moiety of the 4-chlorophenyl type. Furthermore, **9** also incorporates a second bulky moiety, the 2-pyridyl one, making it an interesting candidate to be tested as CAA, with structural features not encountered in other such derivatives investigated earlier. We investigated the CA activating properties of amines **5–9** against 11 catalytically active and physiologically relevant hCA isoforms, that is, the cytosolic hCA I, II, VII, and XIII, the membrane associated hCA IV, the mitochondrial hCA VA and VB, the secreted hCA VI, as well as the transmembrane isoforms hCA IX, XII, and XIV.[16-18]

The following structure–activity relationship (SAR) for the activation of these enzymes with standard CAAs **1–4** and psychotropic amines **5–9** can be drawn from data of **Tables 1** and **2**:

i) The cytosolic, widespread isoforms hCA I and II were not significantly activated by these amines up to concentrations as high as 150 μM, whereas hCA XIII, another cytosolic isoform with a more particular expression pattern (as it is widespread in many organs but with quite low expression level)[20] is moderately activated by amines **5–9**, with activation constants in the range of 24.1–79.5 μM. The best activators of hCA XIII were amphetamine **5** and methamphetamine **6**, whereas phentermine **7**, mephentermine **8**, and chlorphenteramine **9** showed a decreased potency. It is interesting to note the differences between the activating effects of amines **5–9** and the standard CAAs **1–4**: hCA I for example is effectively activated by compounds **1–4**, whereas hCA II is poorly activated by histamine **1** and L-adrenaline **4**, but highly effectively activated by amino acids such as L-His and D-Phe (**Table 1**). hCA XIII is also rather well activated by **1–3** (L-adrenaline's effects on this isoform were not investigated).

Table 1. CA activation of isoforms hCA I, II, VII, and XIII (cytosolic) and IV (membrane-associated) with compounds **1–9**, by a stopped-flow CO_2 hydrase assay.[19]

	K_a (μM)[a]				
compound	hCA I	hCA II	hCA IV	hCA VII	hCA XIII
1	2.1	125	25.3	37.5	4.7
2 (L-His)	0.03	0.90	7.3	0.92	0.13
3(L-Phe)	0.07	0.013	36.3	10.9	1.02
4	0.09	96	45	60	Nt
5	>150	>150	0.094	0.91	24.1
6	>150	>150	0.051	0.93	25.6
7	>150	>150	0.074	0.89	54.2
8	>150	>150	1.03	0.64	48.3
9	>150	>150	0.055	0.098	79.5

Nt: not tested

[a] Mean from three determinations by a stopped-flow, CO_2 hydrase method. Standard errors were in the range of 5–10% of the reported values.

ii) hCA VII, the brain-associated cytosolic CA isoform[16], known to be involved in the antiepileptic and antineuropathic pain effects of the CAIs,[16-18] was effectively activated by the psychotropic amines investigated here, with K_As ranging between 98nM and 0.93 μM. The most effective hCA VII activator was chlorphenteramine **9** whereas the remaining derivatives, possessing the phenethylamine scaffold showed rather similar, submicromolar activation constants (K_As of 0.64–0.93 μM). No major differences in the activating capacity were observed between the primary and secondary amines, or between the derivatives possessing the relatively not sterically hindered α-methyl group near the amino functionality, such as **5** and **6**, compared to the sterically hindered, structurally related amines **7** and **8** (**Table 1**). It should also be noted that except L-His, which has the same level of activity as the psychotropic amines investigated here, the other standard CAAs, such as **1**, **3**, and **4**, were quite ineffective as hCA VII activators (**Table 1**).

iii) The membrane-associated isoform hCA IV was the most sensitive one to activation by amines **5–9**, which showed K_As ranging between 51 nM and 1.03 μM. The best hCA IV activator was methamphetamine **6** and chlorphenteramine **9** (K_As of 51–55

nM), followed by phentermine **7** and amphetamine **5** (K_As of 74–94 nM). The sterically hindered (at the amino moiety) mephentermine **8** was the least effective CAA with a K_A of 1.03 μM. There is a huge difference of activity between the psychotropic amines investigated here **5–9**, which act as efficient or highly efficient hCA IV activators, and compounds **1–4**, which were quite ineffective such agents with K_As in the range of 7.3–45 μM (**Table 1**).

iv) The two mitochondrial isoforms hCA VA and VB, involved in many metabolic reactions (ureagenesis, lipogenesis, neoglucogenesis, etc.)[16-18] and also present in the brain, were also effectively activated by amines **5–9**, with K_As ranging between 0.24 and 2.56 μM (**Table 2**). The best activators against these isoforms were mephentermine **8** against hCA VB (K_A of 240 nM) and chlorphenteramine **9** against hCA VA (K_A of 310 nM), with the remaining compounds (except amphetamine **5** against hCA VB which showed a K_A of 2.56 μM) showing a rather effective, submicromolar activation profile against both isoforms and with a flat SAR (K_As ranging in a narrow interval of 0.37–0.92 μM, **Table 2**). It should be noted that apart from histamine **1**, which is an effective hCA VA activator (K_A of 10 nM), the standard CAAs **2–4** were generally less effective mitochondrial CA activators compared to the psychotropic amines **5–9** (**Table 2**).

Table 2. CA activation of isoforms hCA VA, VB (mitochondrial), VI (secreted), and IX, XII, and XIV (trans-membrane) with compounds 1–9, by a stopped-flow CO_2 hydrase assay.[19]

	K_a (μM)[a]					
Compound	hCA VA	hCA VB	hCA VI	hCA IX	hCA XII	hCA XIV
1	0.010	3.52	6.50	35.1	27.9	0.010
2 (L-His)	1.34	0.97	32.0	9.71	37.5	0.90
3 (L-Phe)	9.81	10.45	1.23	16.3	1.38	0.24
4	63	67	Nt	0.87	0.41	36.1
5	0.81	2.56	>150	>150	0.64	9.15
6	0.92	0.78	>150	>150	0.80	7.38
7	0.53	0.62	>150	34.6	3.24	12.7
8	0.37	0.24	>150	25.8	6.12	18.1
9	0.31	0.75	>150	34.1	0.97	6.81

Nt: not tested

[a] Mean from three determinations by a stopped-flow, CO_2 hydrase method. Standard errors were in the range of 5–10% of the reported values.

v) Similar to hCA I and II, the secreted isoform hCA VI was not significantly activated by amines **5–9** up until 150 μM, whereas compounds **1–3** showed a much better activating efficacy (**Table 2**).

vi) The tumor-associated, transmembrane isoform hCA IX was not significantly activated by amphetamine **5** and methamphetamine **6** (K_As >150 μM), whereas the remaining psychotropic amines **7–9** showed weak activating effects, with K_As of 25.8–34.6 μM. However, the second tumour-associated, transmembrane isoform hCA XII showed a very different activation profile with these compounds compared to hCA IX. Indeed, amphetamine **5**, methamphetamine **6**, and chlorphenteramine **9** were submicromolar activators (K_As of 0.64–0.97 μM) whereas the sterically hindered amines **7** and **8** were one order of magnitude less efficient as hCA XII activators (K_As of 3.24–6.12 μM). The primary amines **5** and **7** were in this case more effective activators compared to the corresponding secondary amines **6** and **8**. Among the standard CAAs, only L-adrenaline **4** showed the same level of activity

as amines **5** and **6**, the remaining derivatives **1–3** being generally less effective as hCA XII activators (**Table 2**).

vii) hCA XIV, another transmembrane isoform not connected with tumours, was moderately activated by amines **5–9**, which showed K_As of 6.81–18.1 μM. The best hCA XIV activator was chlorphenteramine **9** whereas the least effective one was mephentermine **8**. Some of the standard CAAs, such as histamine **1** showed much more effective, low nanomolar activating effects against this isoform.

7.3 Investigation of piperazines as human carbonic anhydrase I, II, IV and VII Activators

4-Aminoethyl-piperazine **10** (**Figure 2**), which is structurally similar to histamine **1** (**Figure 1**) has been reported for many years as an effective, low micromolar activator for several CA isoforms, but this was the only piperazine derivative until now investigated. In order to increase the structure-activity relationship (SAR) data on this class of compounds, in particular towards hCA IV and hCA VII isoforms, we evaluated the activation effects of different piperazines incorporating a variety of scaffolds **11-34**, synthesized by Romanelli's group (**Figure 2**). These particular compounds were chosen to be investigated as CAAs as they contain the endocyclic NH group able to participate in proton shuttling processes between the zinc-coordinated water from the CA active site and the external medium, in a similar manner to 4-aminoethyl-piperazine **10**, and histamine **1**, which were considered as lead compounds. Furthermore, in contrast to **10** and **1**, piperazines **11–34** do not possess the aminoethyl moiety present in the two leads, but the pK_a of the NH (or NR) groups from the heterocyclic ring is influenced by the diverse substitution patterns present in them. Indeed, both electron withdrawing as well as electron donating moieties are present in these compounds which may lead to a different basicity of the moieties able to shuttle protons between the enzyme active site and the reaction medium. The unsubstituted piperazine **35** (**Figure 2**) was also tested for comparison.

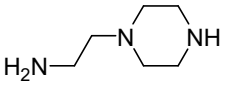

10
4-aminoethyl-piperazine

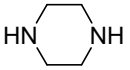

35
piperazine

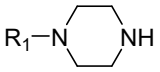

I
(**11-24**)

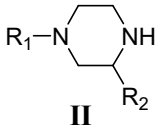

II
(**25-31**)

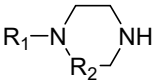

III
(**32-35**)

Compound	Structure	R_1	R_2
11	I	Phenyl	--
12	I	4-F-phenyl	--
13	I	4-Cl-phenyl	--
14	I	4-MeO-phenyl	--
15	I	4-COMe-phenyl	--
16	I	3-Cl-phenyl	--
17	I	3-MeO-phenyl	--
18	I	3-CF_3-phenyl	--
19	I	2-Pyridyl	--
20	I	Methyl	--
21	I	Benzyl	--
22	I	Acetyl	--
23	I	CH_2CH_2OH	--
24	I	2-Piperidinyl	--
25	II	H	Methyl
26	II	H	Phenyl
27	II	Benzoyl	Phenyl
28	II	H	Benzyl
29	II	Propionyl	Benzyl
30	II	Benzoyl	Benzyl
31	II	H	COOH
32	III	H	CO
33	III	H	CH_2CH_2
34	III	Benzyl	CH_2CH_2

Figure 2. Compound **10**, Piperazines **11-34** and Piperazine **35** in the CA activation study.

Activation data against four physiologically relevant hCA isoforms, hCA I, II, IV, and VII, are shown in **Table 3**. Indeed, hCA I, II, and IV are involved in a multitude of eye diseases,[17,21] and their inhibition is pharmacologically used for the treatment of glaucoma[21], edema,[22] obesity,[23] and hypoxic tumors,[24] whereas more recently, some of these isoforms were also validated as drug targets for neuropathic pain,[25] cerebral ischemia,[26] and arthritis.[27] Thus, modulators, potentially with selective action, both for inhibiting and activating these enzymes, are of great pharmacological interest. The activation of the four CA isoforms mentioned above with the piperazine derivatives **11–35** and well known activators **1** and **10** shown in **Table 3** allowed us to delineate the following structure-activity relationship (SAR):

Although unsubstituted piperazine **35** was inactive as a CAA (K_As>150 μM against all investigated enzymes), the substituted-piperazines **11–34** showed CA activating properties against hCA I (except compounds **11**, **20**, **21**, and **25**, which had K_As>150 μM) with activation constants ranging between 32.6 and 131 μM, being thus moderate – weak activators. Indeed, the leads **1** and **10** were much more potent, low micromolar activators of this isoform, with K_As of 2.1–7.4 μM (**Table 3**). The best hCA I activators in the series of investigated compounds were **14**, **29**, **31**, and **34** (K_As of 32.6–48.1 μM), and they belong to variously substituted piperazines. Small variations on the core structure of these compounds generally led to a diminution of the activity. For example, **29**, the best hCA I activator, carries a propionyl group on the piperazine ring and a benzyl moiety at 3 position. Its deacylated analog, **28**, was almost 2 times a less effective hCA I activator, with a K_A of 73.7 μM, when compared to **29**.

Table 3. CA activation of isoforms hCA I, II, IV and VII with compounds **1, 10–35**, by a stopped-flow CO_2 hydrase assay.[19]

Compound	K_A (μM)[a]			
	hCA I	hCA II	hCA IV	hCA VII
1	2.10	125.0	25.3	37.5
10	7.41	2.30	24.9	32.5
11	>150	74.9	>150	121.3
12	88.2	38.7	>150	47.8
13	104.0	110.3	>150	126.1
14	48.6	50.1	>150	80.4
15	83.7	97.9	>150	>150
16	95.2	82.7	>150	104.0
17	119.2	80.1	>150	>150
18	110.2	77.6	>150	114.5
19	131.0	75.2	>150	95.2
20	>150	78.4	>150	97.0
21	>150	85.3	>150	98.4
22	127.4	109.0	>150	96.4
23	102.1	91.6	>150	124.2
24	62.5	16.2	>150	49.2
25	>150	84.0	>150	131
26	80.3	49.7	>150	>150
27	75.2	84.5	>150	35.2
28	73.7	116	>150	17.1
29	32.6	36.1	>150	84.0
30	85.2	82.4	>150	48.5
21	47.9	46.8	>150	93.6
32	115.0	>150	>150	37.1
33	79.4	44.6	>150	98.5
34	48.1	33.2	>150	127
35	>150	>150	>150	>150

[a] Mean from three determinations by a stopped-flow, CO_2 hydrase method. Standard errors were in the range of 5–10% of the reported values.

The physiologically dominant cytosolic isoform hCA II was more sensitive to activation with piperazines **11–34** investigated here compared to hCA I (**Table 3**). Thus, only **32** was

inactive (K_A >150 μM), and the range of the activation constants for the remaining derivatives was of 16.2–116 μM. A number of compounds showed K_As in the range of 16.2–50.1 μM: for example **12**, **14**, **24**, **29**, **31**, **33** and **34**. They belong to various chemical classes and incorporated different substituents, which demonstrates that it might be possible to design much more efficient CAAs incorporating this interesting ring. However, the simple lead compound **10** was a much more potent hCA II activator compared to the other piperazines investigated here, whereas histamine **1** was a very inefficient hCA II activator with a K_A of 125 μM (**Table 3**). Amazingly, the best hCA II activator was **24**, which has two potential piperidine rings that may participate in the proton shuttling processes. Surprisingly, the membrane-bound isoform hCA IV has not activated significantly by any of the piperazines investigated here, although the leads **1** and **10** showed medium potency efficacy with K_As of 24.9–25.3 μM. The brain cytosolic isoform hCA VII was not activated by piperazines **15**, **17**, and **26** (K_A > 150 μM), whereas the remaining derivatives showed a profile of medium–weak activator, with K_As in the range of 17.1–131 μM (**Table 3**). The best hCA VII activators were **12**, **27**, **28**, **30**, and **32** (K_As in the range of 17.1–48.5 μM). For this isoform, the SAR of the couple **28**/**29** is completely different compared to what is mentioned above for the activation of hCA I. In this case, the deacetylatyed derivative **28** was 4.9 times a better hCA VII activator compared to the acetylated one **29**. Thus, small changes in the scaffold lead to a very different activation profile in this series of piperazines and their derivatives.

7.4 Five- and Six-Membered Nitrogen-Containing Compounds as Selective Carbonic Anhydrase Activators

Up to date, CA activators are chemically represented by natural endogenous compounds (histamine, catecholamines, amino acids/peptides, carnosine)[8,28-30] and some synthetic derivatives (oligopeptides, pyridinium-azoles, selective serotonin reuptake inhibitors, histidine and histamine derivatives, imidazole/ triazole/ indazole/pyrazole/oxazole/thiadiazole derivatives)[31-33] presenting common features such as:

- Steric factors leading to a proper orientation for facilitating the proton shuttle from the entrance to the active site;

- Electronic factors like pK_a values in the range 6.5–8.0 for protonatable moieties suitable to establish a network of H-bonds with water molecules or amino acid residues;
- Structural characteristics like nitrogen-containing rings or chains to provide the protonatable moiety.

On the basis of the enzyme-activator adducts and keeping in mind the central nervous system (CNS) distribution of hCA I, II, IV and VII isozymes, in collaboration with Mollica' group, we proposed novel chemotypes incorporating all the above mentioned characteristics in five- or six-membered nitrogen containing structures to elicit this peculiar biological activity and to explore the chemical space around these positions.

We selected important derivatives such as L-(+)-ergothioneine (**36**), an anti-oxidant and chelating naturally-occurring compound containing a sulfur atom in the imidazole ring of histidine, melatonin (**37**), which is a first-line defense hormone against oxidative stress in the CNS, 4-imidazole-acrylic acid (**38**) and indazole-3-carboxylic acid (**39**), both incorporating acid and basic functions, TIC HCl ((*S*)-1,2,3,4-tetrahydro-3-isoquinolinecarboxylic acid) (**40**) and spinacine ((*S*)-4,5,6,7-tetrahydro-1*H*-imidazo[4,5-c]pyridine-6-carboxylic acid) (**41**) in order to evaluate the impact of the presence/absence of an imidazole ring. Lastly we study the diketopiperazine derivatives (**42**–**44**) synthesized by Mollica' group[34] (**Figure 3**).

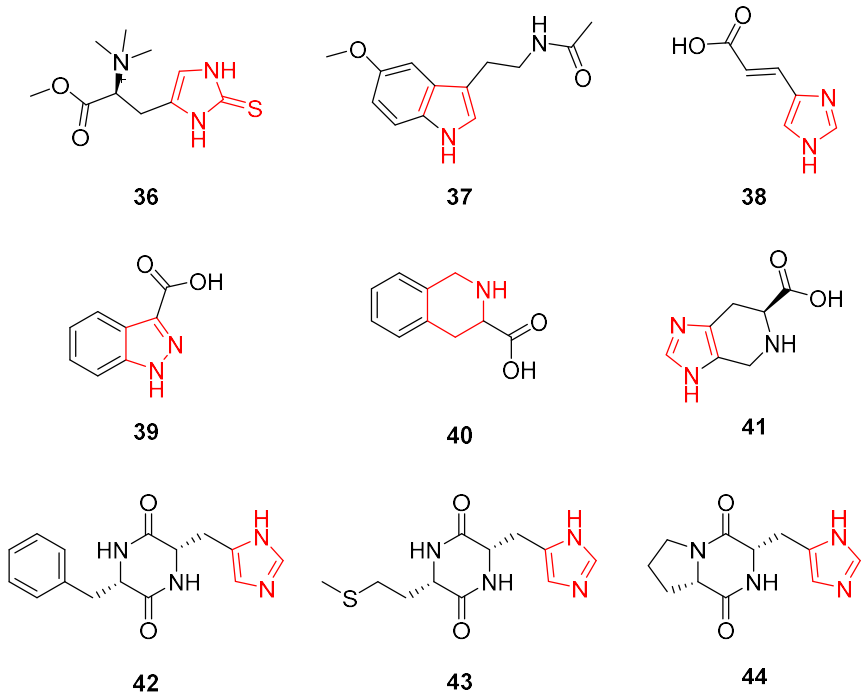

Figure 3 Chemical structures of commercial products **36-41**, and Mollica' compounds **42-44**

All compounds, except **37** (melatonin) have the possibility for accepting a proton, and can function as proton shuttles. From the data in **Table 4**, the following relationships between structure and activation profile can be concluded for this small library of nitrogen containing cyclic compounds and the first demonstrated standard activator histamine **1** (**Figure 1**):

Table4. Activation constants of hCA I, hCA II, hCA IV and hCA VII with compounds **1**, **36–44**, by a stopped-flow CO_2 hydrase assay[12]

No	compound	K_a (μM)[a]			
		hCA I	hCA II	hCA IV	hCA VII
1	histamine	2.10	125	36.9	25.3
36	L-(+)-ergothioneine	>100	>100	>100	0.82
37	melatonin	>100	>100	53.4	0.12
38	4-imidazole-acrylic acid	21.3	>100	64.7	3.46
39	indazole-3-carboxylic acid	32.4	>100	78.4	5.23
40	TIC HCl	23.1	>100	73.5	3.61
41	spinacine	7.21	>100	69.7	15.7
42	c(HisPhe)	16.3	>100	80.5	15.1
43	c(HisMet)	8.39	>100	77.0	21.6
44	c(HisPro)	7.92	>100	70.1	34.7

[a] Mean from three determinations by a stopped-flow, CO_2 hydrase method. Standard errors were in the range of 5–10% of the reported values.

i) The abundant and cytosolic hCA I isozyme was moderately activated by compounds **38**–**44** similarly to histamine (micromolar range), whereas compounds **36** and **37** did not affect its enzymatic activity up to 100 μM.

ii) As histamine **1**, all compounds reported in this work were totally inactive against hCA II isozyme, usually abundant in the choroid plexus, oligodendrocytes, astrocytes, myelinated tracts, and myelin sheets.

iii) With regards to the membrane-bound hCA IV isoform located on the luminal surface of cerebral capillaries and within the cortex, the hippocampus and thalamus, compounds **37**–**44** were poor activators (K_As 53.4–80.5 μM) such as histamine **1**. Conversely, compound **36** was totally inactive (K_A > 100 μM).

iv) The last cytosolic hCA VII isoform displayed the most promising results in terms of activation and selectivity. Derivatives **38**–**44** activated this isozyme in the micromolar range, but compounds **36** and **37** were demonstrated to be rather efficient activators with K_A values of 820 and 120 nM, respectively (best-in-class activators, more selective up to two orders of magnitude). Compound **1** showed a very selective activation of only this isoform.

7.5 Conclusions

We have investigated different series such as piperazine and cyclic derivatives as human CAAs. Moreover, psychotropic amines based on the phenethylamine scaffold, such as amphetamine, methamphetamine, phentermine, mephentermine, and the structurally diverse chlorphenteramine are investigated for their activating effects on 11 hCA isoforms. Some of these enzymes (hCA VII, VA, VB, XII) are abundant in the brain, raising the possibility that some of the cognitive effects of such psychoactive substances might be related to the activation of these enzymes. Futhermore, the activation of the brain-associated hCA VII isoform is of particular interest since is expressed at high levels in the cortex, thalamus and hippocampus. This isoform is also proved to be connected to serious central nervous system (CNS) affecting diseases such as Alzheimer or more in general neuronal degeneratios as well as epilepsy. Our experimental design let us to discover innovative lead compounds endowed with the appropriate physical-chemical characteristics such as balanced hydro/liposolubility and water solubility.

7.6 Experimental data

Carbonic Anhydrase enzyme activation assay

An Sx.18Mv-R Applied Photophysics (Oxford, UK) stopped-flow instrument has been used to assay the catalytic activity of various CA isozymes for CO_2 hydration reaction.[12] Phenol red (at a concentration of 0.2 mM) was used as indicator, working at the absorbance maximum of 557 nm, with 10 mM Hepes (pH 7.5) or TRIS (pH 8.3) as buffers, 0.1 M Na_2SO_4 (for maintaining constant ionic strength), following the CA-catalyzed CO_2 hydration reaction for a period of 10 s at 25 °C. Activity of the α-CA was measured at pH 7.5 whereas that of the β-, γ-, δ-, η-, ζ- class enzymes at pH 8.3 as it has been reported that for enzymes of this class it optimal at this pH value [1–3]. The CO_2 concentrations ranged from 1.7 to 17 mM for the determination of the kinetic parameters and activation constants. For each activator at least six traces of the initial 5–10% of the reaction have been used for determining the initial velocity. The uncatalyzed rates were determined in the same manner and subtracted from the total observed rates. Stock solutions of activators (10 mM) were prepared in distilled-deionized water and dilutions up to 1 nM were done thereafter with the

assay buffer. Activator and enzyme solutions were pre-incubated together for 15 min (standard assay at room temperature) prior to assay, in order to allow for the formation of the E–A complex. The activation constant (K_A), defined similarly with the inhibition constant K_I, can be obtained by considering the classical Michaelis–Menten equation (Eq. (**4**)), which has been fitted by non-linear least squares by using

PRISM 3:

$$V = \frac{V_{max}}{\left\{ 1 + K_M / [S] \, (1 + [A]_f / K_A) \right\}} \qquad \textbf{(4)}$$

Where $[A]_f$ is the free concentration of activator. Working at substrate concentrations considerably lower than K_M ($[S] << K_M$), and considering that $[A]_f$ can be represented in the form of the total concentration of the enzyme ($[E]_t$) and activator ($[A]_t$), the obtained competitive steady-state equation for determining the activation constant is given by Eq. (**5**):

$$V = \frac{V_0 \, K_A}{\left\{ K_A + ([A]_t - 0.5\left\{([A]_t + [E]_t + K_A) - ([A]_t + [E]_t + K_A)^2 - 4[A]_t \, [E]t)^{1/2} \right\}\right\}} \qquad \textbf{(5)}$$

Where V_0 represents the initial velocity of the enzyme-catalyzed reaction in the absence of activator. The enzymes were recombinant ones, prepared in-house as reported earlier.[50-53]

References

1. Leiner M. Das ferment kohlens¨aureanhydrase im tierk¨orper. *Naturwissenschaften* 1940, 28, 316–317.
2. Main R.E., Locke A. Activation of carbonic anhydrase by histamine. *J. Biol. Chem.* 1941, 140, LXXXI.
3. Kiese M. Die aktivierung der kohlensaureanhydrase. *Naturwissenschaften* 1941,29, 116–117.
4. Tu C.K., Silverman D.N., Forsman C., Jonsson B.H., Lindskog S. Role of histidine 64 in the catalytic mechanism of human carbonic anhydrase II studied with a site-specific mutant. *Biochemistry* 1989, 28, 7913–7918.
5. Supuran C.T. Carbonic anhydrase activators. Part 4. A general mechanism of action for activators of isozymes I, II and III. *Rev. Roum. Chim.* 1992, 37, 411–421.
6. Supuran C.T., Balaban A.T. Carbonic anhydrase activators. Part 8. pKa–activation relationship in a series of amino acid derivatives activators of isozyme II. *Rev. Roum. Chim.* 1994, 39, 107–113.
7. Briganti F., Mangani S., Orioli P., Scozzafava A., Vernaglione G., Supuran C.T. Carbonic anhydrase activators: X-ray crystallographic and spectroscopic investigations for the interaction of isozymes I and II with histamine, *Biochemistry* 1997, 36, 10384–10392
8. Briganti F., Scozzafava A., Supuran C.T. Carbonic anhydrase activators. Part 19 spectroscopic and kinetic investigations for the interaction of isozymes I and II with primary amines. *Met. Based Drugs.* 1997*,* 4, 221–227.
9. Sun M.K., Alkon D.L. Carbonic anhydrase gating of attention: memory therapy and enhancement. *Trends Pharmacol. Sci.* 2002, 23, 83–89.
10. Canto de Souza L., Provensi G., Vullo D., Carta F., Scozzafava A., Costa A., Schmidt S.D., Passani M.B., Supuran C.T., Blandina P. Carbonic anhydrase activation enhances object recognition memory in mice through phosphorylation of the extracellular signal-regulated kinase in the cortex and the hippocampus. *Neuropharmacology* 2017, 118, 148–156.

11. Wang X., Schroder H.C., Schlossmacher U., Neufurth M., Feng Q., Diehl-Seifert B., Müller W.E. Modulation of the initial mineralization process of SaOS-2 cells by carbonic anhydrase activators and polyphosphate. *Calcif. Tissue Int.* 2014, 94, 495–509.
12. Muller W.E., Schroder H.C., Schlossmacher U., Grebenjuk V.A., Ushijima H., Wang X. Induction of carbonic anhydrase in SaOS-2 cells, exposed to bicarbonate and consequences for calcium phosphate crystal formation. *Biomaterials* 2013, 34, 8671–8680.
13. European Drug report 2016: Trends and Developments. European Monitoring Centre for Drugs and drug Addicion (EMCDDA). Available from: http://www.emcdda.europa.eu/system/files/publications/2637/TDAT16001ENN.pdf.
14. Bertol E., Pascali J., Palumbo D., Catalani V., Di Milia M.G., Fioravanti A., Mari F., Vaiano F. 3-MeO-PCP intoxication in two young men: first in vivo detection in Italy. *Forensic Sci Int* 2017;274:7–12.
15. Bertol E., Vaiano F., Mari F., Bua S., Supuran C.T., Carta F. Advances in new psychoactive substances identification: the U.R.I.To.N. Consortium. *J Enzyme Inhib Med Chem* 2017, 32, 841–849.
16. Supuran C.T. Advances in structure-based drug discovery of carbonic anhydrase inhibitors. *Expert Opin Drug Discov* 2017, 12, 61–88.
17. Supuran C.T., Structure and function of carbonic anhydrases, *Biochem. J.* 2016, 473, 2023–2032.
18. Supuran C.T., Carbonic anhydrases: novel therapeutic applications for inhibitors and activators, *Nat. Rev. Drug. Discov.* 2008, 7, 168–181.
19. Khalifah R.G. The carbon dioxide hydration activity of carbonic anhydrase. I. Stop-flow kinetic studies on the native human isoenzymes B and C. *J Biol Chem.* 1971, 246, 2561-73.
20. Hilvo M., Supuran C.T., Parkkila S. Characterization and inhibition of the recently discovered carbonic anhydrase isoforms CA XIII, XIV and XV. *Curr Top Med Chem* 2007, 7, 893–899.

21. Masini E., Carta F., Scozzafava A., Supuran C.T. Antiglaucoma carbonic anhydrase inhibitors: a patent review. *Expert Opin Ther Pat* 2013, 23, 705–716.
22. Carta F., Supuran C.T. Diuretics with carbonic anhydrase inhibitory action: a patent and literature review (2005–2013). *Expert Opin Ther Pat* 2013, 23, 681–691.
23. Scozzafava A., Supuran C.T., Carta F. Antiobesity carbonic anhydrase inhibitors: a literature and patent review. *Expert Opin Ther Pat* 2013, 23, 725–35.
24. Monti S.M., Supuran C.T., De Simone G. Anticancer carbonic anhydrase inhibitors: a patent review (2008–2013). *Expert Opin Ther Pat* 2013, 23, 737–49.
25. Supuran C.T. Carbonic anhydrase inhibition and the management of neuropathic pain. *Expert Rev Neurother* 2016, 16, 961–968.
26. Di Cesare Mannelli L., Micheli L., Carta F., Cozzi A., Ghelardini C., Supuran C.T. Carbonic anhydrase inhibition for the management of cerebral ischemia: in vivo evaluation of sulfonamide and coumarin inhibitors. *J Enzyme Inhib Med Chem* 2016, 31, 894–899.
27. Margheri F., Ceruso M., Carta F., Laurenzana A., Maggi L., Lazzeri S., Simonini G., Annunziato F., Del Rosso M., Supuran C.T., Cimaz R. Overexpression of the transmembrane carbonic anhydrase isoforms IX and XII in the inflamed synovium. *J Enzyme Inhib Med Chem* 2016, 31, 60–63.
28. Vullo D., Nishimori I., Innocenti A., Scozzafava A., Supuran C.T. Carbonic anhydrase activators: An activation study of the human mitochondrial isoforms VA and VB with amino acids and amines. *Bioorg. Med. Chem. Lett.* 2007, 17, 1336–1340
29. Pastorekova S., Vullo D., Nishimori I., Scozzafava, A., Pastork J., Supuran C.T. Carbonic anhydrase activators: Activation of the human tumor-associated isozymes IX and XII with amino acids and amines. *Bioorg. Med. Chem.* 2008, 16, 3530–3536.
30. Vullo D., Nishimori I., Scozzafava A., Supuran C.T. Carbonic anhydrase activators: Activation of the human cytosolic isozyme III and membrane-

associated isoform IV with amino acids and amines. *Bioorg. Med. Chem. Lett.* 2008, 18, 4303–4307.

31. Scozzafava A., Supuran C.T. Carbonic anhydrase activators: Human isozyme II is strongly activated by oligopeptides incorporating the carboxyterminal sequence of the bicarbonate anion exchanger AE1. *Bioorg. Med. Chem. Lett.* 2002, 12, 1177–1180.
32. Ilies M., Banciu M.D., Ilies M.A., Scozzafava A., Caproiu M.T., Supuran C.T. Carbonic anhydrase activators: Design of high affinity isozymes I, II, and IV activators, incorporating tri/tetrasubstitutedpyridinium-azole moieties. *J. Med. Chem*. 2002, 45, 504–510.
33. Draghici B., Vullo D., Akocak S., Walker E.A., Supuran C.T., Ilies M.A., Ethylene bis-imidazoles are highly potent and selective activators for isozymes VA and VII of carbonic anhydrase, with a potential nootropic effect. *Chem. Commun.* 2014, 50, 5980–5983.
34. Mollica A., Macedonio G., Stefanucci A., Carradori S., Akdemir A., Angeli A., Supuran C.T. Five- and Six-Membered Nitrogen-Containing Compounds as Selective Carbonic Anhydrase Activators. *Molecules.* 2017, 22, E2178

Chapter 8

Kinetic activation study from no human CAs

8.1 Introduction

In **Chapter 6** we discussed the use of CAIs as promising tools for targeting the pathogenic bacterial and protozoal expressed CAs in order to develop new and effective anti-infective agents.[1-3] In this section we report a radical new approach in the field consisting in the activation and evaluation *in vitro* of the protozoal as well as of the bacterial CAs with the primary intent to have a better understanding of the catalytic mechanisms associated to such isoforms. Additionally, all the results obtained will be usefuls for the future technological applications in the area of CO_2 capture. Our investigations began with known CAAs on the human enzymatic isoforms such as amines, natural and non-natural amino acids of the type **1-24** reported in **Figure 1.**

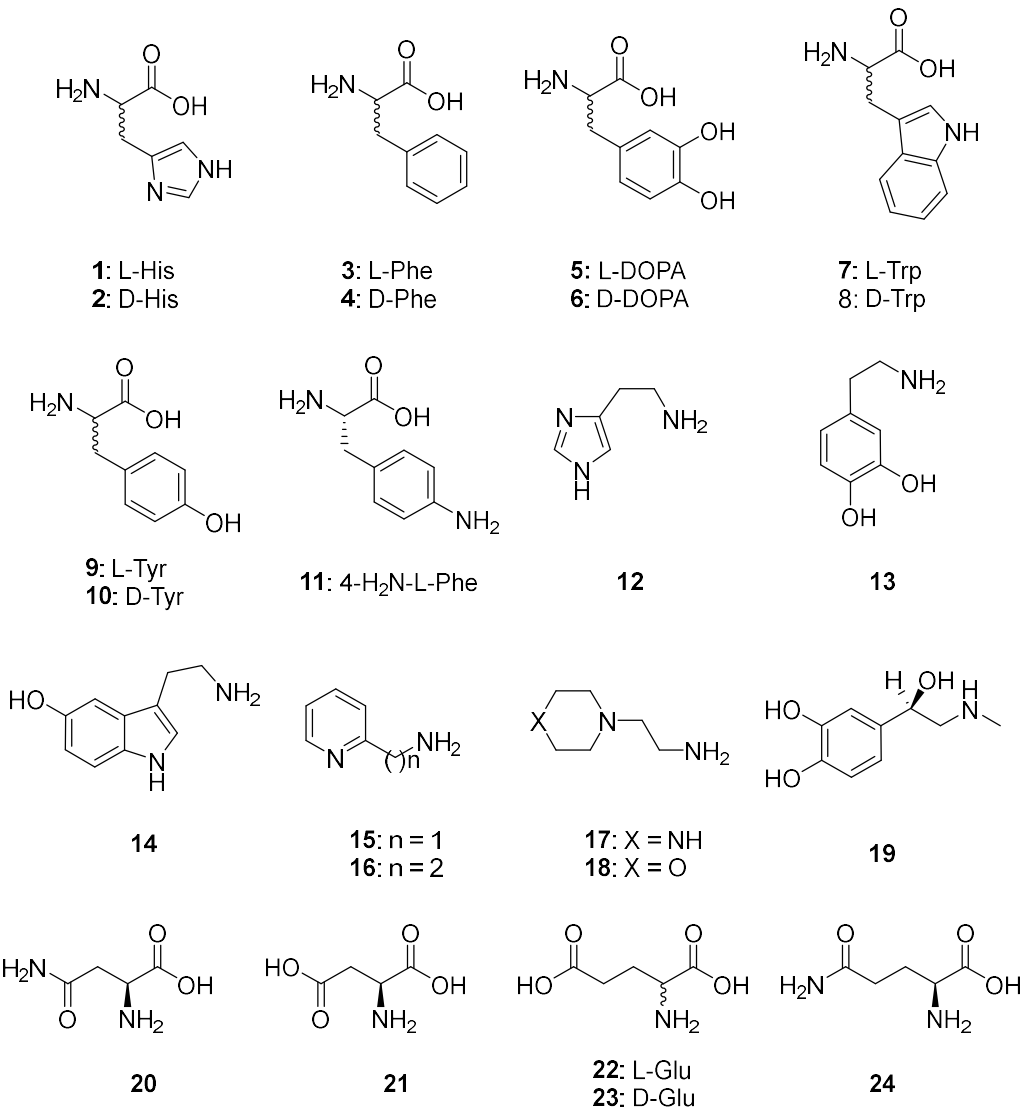

Figure 1. Amino acids and amines **1–24** investigated as CA activators (CAAs).

It must be stressed that a CAA has no influence on the K_M values, as the Michaelis–Menten constants are identical with or without activator, instead a very strong influence is observed on k_{cat}. The latest parameter is generally greatly enhanced in the presence of activators, proving that it is just the rate-determining step, that is the proton transfer between the active site and the reaction medium, to be favoured as reported in **Table A**.

Table A. Activation of human hCA I, hCA II, and the other classes of CAs studied here with L-Tyr, at 25 °C, for the CO_2 hydration reaction.[12]

Isozyme	k_{cat} (s^{-1})*	K_M (mM)*	$(k_{cat})_{L\text{-}Trp}$ (s^{-1})**	K_a (μM) L-Trp***
hCA I	2.0 x 10^5	4.0	3.4 x 10^5	44
hCA II	1.4 x 10^6	9.3	4.9 x 10^6	27
TcCAα	1.2 x 10^6	8.1	7.8 x 10^6	2.54
LdcCAβ	9.35 x 10^5	15.8	28.6 x 10^5	4.02
mtCA 3	4.3 x 10^5	10.7	13.8 x 10^5	8.98
VchCAα	8.23 x 10^5	11.7	21.9 x 10^5	8.21
VchCAβ	3.34 x 10^5	8.1	16.2 x 10^5	6.15
VchCAγ	7.39 x 10^5	11.5	25.4 x 10^5	0.12
PfaCA	3.8 x 10^5	5.2	11.2 x 10^5	1.02
TweCAδ	1.3 x 10^5	3.9	10.6 x 10^5	0.93
ZnTweCA ζ	1.4 x 10^6	8.7	6.9 x 10^6	0.98
CdTweCA ζ	1.5 x 10^6	10.7	1.5 x 10^6	>50

* Observed catalytic rate without activator. K_M values in the presence and the absence of activators were the same for the various CAs

** Observed catalytic rate in the presence of 10 μM activator.

*** The activation constant (K_A) for each enzyme was obtained by fitting the observed catalytic enhancements as a function of the activator concentration. Mean from three determinations by a stopped-flow, CO_2 hydrase method.

These data clearly showed that clear differences of activating efficacies by two amino acid antipodes against various classes of CAs are present. Such a concept paves the way to properly engineer proton transfer processes, specific for each enzymatic isoform, between the active site of the enzyme and the reaction medium.

8.2 Activation study of α-Carbonic Anhydrase from the pathogenic protozoan Trypanosoma cruzi

T. cruzi encodes for an α-class[4] CA (TcCA), which has recently been cloned, characterized and investigated for its inhibition, being shown to be a promising new target in the fight against Chagas disease, provoked after infection with this protozoan species.[3,4] In previous works, this enzyme was reported to be effectively inhibited *in vitro*,and in some cases also to interfere with the growth of some forms of the parasite *in vivo*. Such results may lead to the discovery of potential drugs devoid of the drug resistance problems currently encountered by the few clinically used compounds available the treatment of Chagas disease.[3,4] On the other hand, only few activators have been identified for protozoan CAs so far. For this reason, we investigated the activation mechanism with compounds **1-24** in order to better understand the role that this enzyme has in the life cycle of *T. cruzi*, particularly considering the fact that many of the activators identified are autacoids present in rather high concentrations in different tissues of the host mammals that are infected by these parasites. The structure-activity relationship (SAR) for the activation of TcCA with compounds **1–24** (**Figure 1**), can be delineated considering the data shown in **Table 1** with the activation data of the human isoforms hCA I and II presented for comparison.

Table1. Activation constants of hCA I, hCA II and the protozoan α-TcCA with amino acids and amines **1–24**, by a stopped-flow CO_2 hydrase assay[12]

No	Compound	K_a (μM)[a]		
		hCA I[b]	hCA II[b]	TcCA
1	L-His	0.03	10.9	11.3
2	D-His	0.09	43	7.54
3	L-Phe	0.07	0.0013	12.1
4	D-Phe	86	0.035	6.39
5	L-DOPA	3.1	11.4	0.83
6	D-DOPA	4.9	7.8	0.38
7	L-Trp	44	27	2.54
8	D-Trp	41	12	1.79
9	L-Tyr	0.02	0.011	4.92
10	D-Tyr	0.04	0.013	2.80
11	4-H2N-L-Phe	0.24	0.15	0.75
12	Histamine	2.1	125	2.73
13	Dopamine	13.5	9.20	>100
14	Serotonin	45	50	1.98
15	2-Pyridyl-methylamine	26	34	>100
16	2-(2-Aminoethyl)pyridine	13	15	>100
17	1-(2-Aminoethyl)-piperazine	7.4	2.30	>100
18	4-(2-Aminoethyl)-morpholine	0.14	0.19	6.95
19	L-Adrenaline	0.09	96	>100
20	L-Asn	11.3	>50	>100
21	L-Asp	5.20	>50	18.7
22	L-Glu	6.43	>50	>100
23	D-Glu	10.6	>50	>100
24	L-Gln	>50	>50	2.85

[a] Mean from three determinations by a stopped-flow, CO_2 hydrase method. Standard errors were in the range of 5–10% of the reported values.

[b] Human recombinant isozymes, stopped flow CO_2 hydrase assay method.[12]

The following should be noted on the data presented in **Table 1**:

i) The most effective TcCA activators were L-/D-DOPA and 4-amino-L-phenylalanine with activation constants in the range of 0.38–0.83 μM. The D-enantiomer of DOPA was more than 2 times effective as TcCA activator compared

to its L-enantiomer. In fact, among all pairs of enantiomeric amino acids investigated here, the D-enantiomer was a more effective TcCA activator compared to the corresponding L-enantiomer. This situation is very different from that observed for hCA I and II, for which many times the L-amino acids were better activators compared to their D-enatiomers (**Table 1**).

ii) Effective, low micromolar activators were also L-/D-Trp, L-/D-Tyr, L-Gln, histamine and serotonin, which showed K_As in the range of 1.79–4.92 μM. It seems that the two phenolic OH moieties from site, since DOPA was a better activator compared to Tyr (one phenolic OH moiety) which in turn was more effective than Phe, which although possessing the same scaffold as Tyr and DOPA, is lacking of OH phenolic moieties. It is also interesting to note that L-Gln is a rather effective TcCA activator whereas the structurally very similar L- (or D-Glu) are not activating at all this enzyme up to 100 μM concentration of activator in the assay system. Very small differences in the scaffold of the activator lead to very diverse effects on the enzyme, probably due to the fact that the formation of the enzyme-activator complex is very much influenced even by small perturbation in the scaffold of the compound which cannot effectively bind, probably due to steric impairment and clashes with residues crucial for the catalysis.

iii) Other compounds, among which L-/D-His, L-/D-Phe and L-Asp were less effective activators compared to the derivatives mentioned earlier, with K_As in the range of 6.39–18.7 μM (**Table 1**). Many amines, such as dopamine **13**, pyridyl-alkylamines **15** and **16**, aminoethyl-piperazine **17**, L-adrenaline **19** were devoid of activating effects on TcCA. The same behaviour was observed for L-Asn, L- and D-Glu.

8.3 Activation study of β-carbonic anhydrase from the pathogenic protozoan Leishmania donovani chagasi

Leishmaniasis is a rather diffuse sub-tropical disease provoked by protozoan belonging to *Leishmania* spp.[3,5] To date, there are limited available drugs to treat this condition, and many strains of the parasite are increasingly resistant to drug treatments. However, no *Leishmania* protozoan CA enzymes have been investigated for their activation. In this manner, we report

the first activation study of LdcCA, the β-class enzyme from the protozoan, *L. donovani chagasi*, one of the causative agents of visceral leishmaniasis.

The structure-activity-relationship (SAR) for the activation of LdcCA with compounds **1–19** (**Figure 1**), can be delineated considering the data shown in **Table 2**, where the activation data of the human isoforms hCA I and II are also presented for comparison.

Table 2. Activation constants of hCA I, hCA II and the protozoan β-LdcCA with amino acids and amines **1–19**, by a stopped-flow CO_2 hydrase assay[12]

		K_a (μM)[a]		
No	compound	hCA I[b]	hCA II[b]	LdcCA
1	L-His	0.03	10.9	8.21
2	D-His	0.09	43	4.13
3	L-Phe	0.07	0.0013	9.16
4	D-Phe	86	0.035	3.95
5	L-DOPA	3.1	11.4	1.64
6	D-DOPA	4.9	7.8	5.47
7	L-Trp	44	27	4.02
8	D-Trp	41	12	6.18
9	L-Tyr	0.02	0.011	8.05
10	D-Tyr	0.04	0.013	1.27
11	4-H2N-L-Phe	0.24	0.15	15.9
12	Histamine	2.1	125	0.74
13	Dopamine	13.5	9.20	0.81
14	Serotonin	45	50	0.62
15	2-Pyridyl-methylamine	26	34	0.23
16	2-(2-Aminoethyl)pyridine	13	15	0.012
17	1-(2-Aminoethyl)-piperazine	7.4	2.30	0.009
18	4-(2-Aminoethyl)-morpholine	0.14	0.19	0.94
19	L-Adrenaline	0.09	96	4.89

[a] Mean from three determinations by a stopped-flow, CO_2 hydrase method. Standard errors were in the range of 5–10% of the reported values.

[b] Human recombinant isozymes, stopped flow CO_2 hydrase assay method.[12]

All amino acids and amines investigated act as efficient LdcCA activators, with activation constants that range from the low nanomolar (9 nM for **17**) to the micromolar (15.9 μM for **11**). Amines are generally more effective activators compared to the amino acids, except for

L-adrenaline **19** (the only secondary amine investigated here) which has the same potency as most of the amino acids (K_A of 4.89 μM). The most effective LdcA activators were aminopyridine **16** and piperazine **17** (K_As of 9–12 nM), which incorporate a heterocyclic ring and the aminoethyl moiety (both of which can participate in proton transfer reactions between the zinc coordinated water and the external milieu).

Amines **12–15** and **18**, structurally related to the most effective activators discussed above, also show an interesting and efficient activating profile, with K_As ranging between 0.23 and 0.94 μM. Thus, the SAR here is rather well defined, with all these compounds possessing the aminoethyl- or aminomethyl tails appended to an aromatic or heterocyclic moiety. X-ray crystallography for adducts of some of these derivatives with hCA I or II showed that both these fragments of the activator are participating to the stabilization of the enzyme-activator complex, by forming hydrogen bonds and hydrophobic interaction with amino acid residues at the entrance of the active site cavity.[6,7]

The amino acids **1–10** were slightly less effective as LdcCA activators compared to the amines discussed above, with K_As ranging between 1.27 and 15.9 μM. In several cases (D-His, D-Phe, D-Tyr), the D-enantiomer was more efficient as LdcCA activator compared to the corresponding L-enantiomer, whereas for the DOPA and Trp, the L-enantiomers were the more effective activators compared to the corresponding D-amino acids (**Table 2**).

Small changes in the scaffold of the activator lead to important differences of activity: replacement of the phenolic OH from L-Tyr (**9**) by an amine moiety (as in **11**) lead to an almost 2-fold loss of activating properties. The activation of the protozoan enzyme was rather different from that of the α-class enzymes hCA I and II. For example, L-/D-Tyr were highly effective, nanomolar hCA I and II activators, whereas their effects on LdcCA are seen only at micromolar concentrations. On the contrary, amine **16** may be considered as a LdcCA-selective activator, with a K_A of 12 nM for the protozoan enzyme and of 13–15 μM for the human CAs.

8.4 Activation study of β-Carbonic Anhydrase encoded by the Rv3273 gene from the pathogenic bacterium Mycobacterium tuberculosis

Among the bacterial infections which create huge medical problems worldwide, the *Mycobacterium tuberculosis* one is among the most threatening due to a number of causes. Among these, the most important is a large number of *M. tuberculosis* strains became drug resistant or extensively drug resistant to most of almost all clinically used antiycobacterials due to no launch new drugs for the last 30 years.[8,9] In *M. tuberculosis*, three CAs belonging to the β-CA class have been discovered, encoded by the genes Rv128 (mtCA 1), Rv3588c (mtCA 2) and Rv3273 (mtCA 3)[10,11] and involved in crucial steps of the pathogen life cycle.[13,14] Considering the fact that few CA activation studies of bacterial enzymes are available, none of them for the mycobacterial enzymes and their effects were poorly studied up until now,[10,11] we evaluated the activation of mtCA 3 (encoded by the gene Rv3273) with amines and amino acid derivatives **1-19** (**Figure 1**). These compounds showed significant activating effects against mtCA 3, as observed from data of **Table 3**, in which the activation constants (K_As) against three CAs are presented (hCA I and II data are included for comparison). The following structure-activity relationship (SAR) can be evidenced from the data of **Table 3**:

Table 3. Activation constants of hCA I, hCA II and the bacterial mtCA 3 with amino acids and amines **1–19**, by a stopped-flow CO_2 hydrase assay[12]

No	compound	K_a (μM)[a]		
		hCA I[b]	hCA II[b]	mtCA3
1	L-His	0.03	10.9	18.2
2	D-His	0.09	43	32.5
3	L-Phe	0.07	0.0013	30.6
4	D-Phe	86	0.035	44.1
5	L-DOPA	3.1	11.4	30.0
6	D-DOPA	4.9	7.8	9.74
7	L-Trp	44	27	8.98
8	D-Trp	41	12	43.7
9	L-Tyr	0.02	0.011	28.9
10	D-Tyr	0.04	0.013	17.6
11	4-H2N-L-Phe	0.24	0.15	40.5
12	Histamine	2.1	125	34.2
13	Dopamine	13.5	9.20	12.1
14	Serotonin	45	50	10.3
15	2-Pyridyl-methylamine	26	34	43.3
16	2-(2-Aminoethyl)pyridine	13	15	45.9
17	1-(2-Aminoethyl)-piperazine	7.4	2.30	50.3
18	4-(2-Aminoethyl)-morpholine	0.14	0.19	52.0
19	L-Adrenaline	0.09	96	52.2

[a] Mean from three determinations by a stopped-flow, CO_2 hydrase method. Standard errors were in the range of 5–10% of the reported values.

[b] Human recombinant isozymes, stopped flow CO_2 hydrase assay method.[12]

i) The most effective mtCA 3 activators were D-DOPA, L-Trp, dopamine and serotonin, with K_As ranging between 8.98 and 12.1 μM. Thus, both amino acid and amine types of activators show efficient activating effects on mtCA 3.

ii) L-His and D-Tyr showed medium potency activating effects, with K_As in the range of 17.6–18.2 μM.

iii) The remaining derivatives showed a weaker mtCA 3 activation potency, with K_As in the range of 28.9–52.2 μM. The SAR is thus rather well defined. For example, with few exceptions the L-amino acids were more effective mtCA 3 activators

compared with the corresponding D-enantiomer. The exceptions are D-DOPA and D-Tyr which were more effective mtCA 3 activators compared with the corresponding L-enantiomer. Amines (with the exception of dopamine and serotonin) were generally less effective mtCA 3 activators compared with structurally related amino acids (compare histamine and L-/D-His; L-adrenaline and L-/D-DOPA, etc.), but the differences were not very important. In fact, no submicromolar mtCA 3 activators were detected in this study.

8.5 Activation study of α- and β-Carbonic Anhydrase from the pathogenic bacterium Vibrio cholerae

Bacteria encode for CAs belonging to three different genetic families α-, β- and γ-CAs. Recently, our groups described the biochemical properties of α-, β-, and γ-CAs from the pathogenic bacterium *Vibrio cholerae*, responsible of cholera.[15-17] These enzymes, called VchCAα/β/γ showed a significant catalytic activity for the physiologic CO_2 hydration reaction to bicarbonate and protons.[15-17] Moreover, the study of the inhibition profiles with the classical CA inhibitors (sulfonamides and anions) revealed interesting structure–activity relationship for the interaction of these enzymes with inhibitors,[15-17] but no activation studies were reported so far. Here, we present the first activation study of two such enzymes, VchCAα/β with amino acids and amines **1–19** (**Figure 1**). The following structure-activity relationship (SAR) can be evidenced from the data of **Table 4**:

Table4. Activation constants of hCA I, hCA II and the bacterial CAs VhCAα and VhCAβ with amino acids and amines **1–19**, by a stopped-flow CO_2 hydrase assay[12]

No	compound	K_a (μM)[a]			
		hCA I[b]	hCA II[b]	VhCAα	VhCAβ
1	L-His	0.03	10.9	43.2	20.3
2	D-His	0.09	43	22.7	18.0
3	L-Phe	0.07	0.0013	53.6	15.4
4	D-Phe	86	0.035	34.5	5.12
5	L-DOPA	3.1	11.4	23.1	8.36
6	D-DOPA	4.9	7.8	19.4	6.27
7	L-Trp	44	27	40.9	4.18
8	D-Trp	41	12	38.0	5.89
9	L-Tyr	0.02	0.011	8.21	6.15
10	D-Tyr	0.04	0.013	37.8	0.94
11	4-H2N-L-Phe	0.24	0.15	41.6	7.21
12	Histamine	2.1	125	9.12	9.50
13	Dopamine	13.5	9.20	35.2	1.24
14	Serotonin	45	50	11.7	1.37
15	2-Pyridyl-methylamine	26	34	68.3	0.18
16	2-(2-Aminoethyl)pyridine	13	15	71.9	1.00
17	1-(2-Aminoethyl)-piperazine	7.4	2.30	57.3	0.24
18	4-(2-Aminoethyl)-morpholine	0.14	0.19	12.0	12.8
19	L-Adrenaline	0.09	96	18.2	8.73

[a] Mean from three determinations by a stopped-flow, CO_2 hydrase method. Standard errors were in the range of 5–10% of the reported values.

[b] Human recombinant isozymes, stopped flow CO_2 hydrase assay method.[12]

i) The α-class bacterial enzyme was activated by amino acids and amines **1–19** in the micromolar range (K_As of 8.21–71.9 μM), and is thus much less sensitive to activation when compared to the human CA isoforms belonging to the same class, hCA I and II. However, a distinct SAR could be observed for these CAAs even if their potency is not very high. The most effective VchCAα activators were L-Tyr **9**, histamine **12**, serotonin **14**, and 4-aminoethylmorpholine **18**, which had K_As in the range of 8.21–12.0 μM. The remaining amines and amino acids were less effective CAAs, with K_As in the range of 19.4–71.9 μM. The stereochemistry of the amino

acid derivatives influenced the activation potency, with the D-enantiomers being generally more effective than the L-ones (for His, Phe, DOPA, and Trp), whereas the reverse situation is true for Tyr, case in which the L-enantiomer was 4.6 times more effective at activation than the D-enantiomer (**Table 4**). In some cases, the amines were more effective activators compared to the amino acids structurally related to them, e.g. histamine was more effective compared to L/D-His, whereas dopamine was less effective compared to L/D-DOPA. The least effective activators were the pyridyl-amine derivatives **15** and **16**. All these data demonstrate that relatively small differences in the scaffold of the activator induce important differences in the activation efficacy, obviously due to the fact that the structural diversity of these compounds induces diverse interactions with amino acid residues from the active site in the enzyme-activator (E-A) complex.

ii) VchCAβ was more sensitive to activation with the amines and amino acids investigated here, which showed K_As in the range of 0.18–20.3 μM (**Table 4**). The most effective activators were D-Tyr **10**, dopamine **13**, serotonin **14**, 2-pyridyl-methylamine **15**, 2-aminoethylpyridine **16**, and 2-aminoethylpiperazine **17**, which showed activation constants in the submicromolar – low micromolar range, of 0.18–1.37 μM. Apart D-Tyr, all of these most effective activators are amines. Another subset of derivatives, such as **4–9**, **11**, **12**, **18**, and **19** were slightly less effective CAAs with K_As in the range of 4.18–12.8 μM. They include both amino acid and amine derivatives. The least effective activators were L/D-His and L-Phe, with K_As in the range of 15.4–20.3 μM. Again, generally D-enantiomers of the amino acids were generally more effective activators compared to the L-enantiomers (for His, Phe, DOPA, and Tyr), whereas in the case of Trp, the L-enantiomer was a better activator compared to the D-one.

There are important differences in activation efficacy of these amino acids and amines against the two bacterial enzymes, with the β-class one being much more sensitive to activation compared to the α-class. There are also important differences of the activation profiles of these compounds for the bacterial and human CAs, which is a rather important observation as this may lead to isoform-selective activators. However, for this small panel of activators (**1-19**), the human CAs were generally much better activated compared to the

bacterial enzymes, with few exceptions, such as the activity of **13–17** for VchCAβ which was much more susceptible to be activated compared to hCA I, II, and VchCAα. This observation demonstrates that the design of bacterial CA–selective activators is feasible.

8.6 Activation study of γ-Carbonic Anhydrase from the pathogenic bacterium Vibrio cholerae

The γ-class carbonic anhydrases were discovered more than two decades ago by Ferry's group[18] and were less investigated compared to other members of this superfamily of metalloenzymes that are known to date.[19-21] γ-CAs were originally discovered in Archaea, and subsequently identified to be widely distributed in bacteria and the mitochondria of plants.[19-21] However for γ -CAs no X-ray crystal structures of enzyme activator complexes have been reported and very few X-ray crystal structures of such enzymes are available.[22] However, site directed mutagenesis and kinetic experiments suggest that at least two glutamate residues, Glu84 and Glu62 (from *Methanosarcina thermophile* γ-CA (Cam) numbering system[23]) can act as proton shuttle residues for these enzymes. Moreover, the activation of CAs from pathogenic bacteria may be relevant for understanding the factors governing virulence and colonization of the host, because pH in the tissues surrounding the pathogens likely plays a key role in such processes and many compounds that are CAAs (amines, amino acids) are abundant in such tissues. For this reason, we continued to investigate the last class of CA from pathogenic bacterium *Vibrio cholerae* (Vhcaγ) with amines and amino acids **1–19** (**Figure 1**) that possess functional groups that can participate in proton transfer processes. These compounds potently activate VchCAγ with an activation contants in the nanomolar range. For comparison K_A values for hCA I and II were also reported in **Table 5**.

Table 5. Activation constants of hCA I, hCA II and the bacterial enzyme VhCA γ with amino acids and amines **1–19**, by a stopped-flow CO_2 hydrase assay[12]

No	compound	K_a (μM)[a]		
		hCA I[b]	hCA II[b]	VhCA γ
1	L-His	0.03	10.9	1.01
2	D-His	0.09	43	14.2
3	L-Phe	0.07	0.0013	0.73
4	D-Phe	86	0.035	0.24
5	L-DOPA	3.1	11.4	0.19
6	D-DOPA	4.9	7.8	0.13
7	L-Trp	44	27	0.008
8	D-Trp	41	12	0.40
9	L-Tyr	0.02	0.011	0.12
10	D-Tyr	0.04	0.013	0.10
11	4-H2N-L-Phe	0.24	0.15	0.69
12	Histamine	2.1	125	0.31
13	Dopamine	13.5	9.20	0.45
14	Serotonin	45	50	0.17
15	2-Pyridyl-methylamine	26	34	0.14
16	2-(2-Aminoethyl)pyridine	13	15	0.26
17	1-(2-Aminoethyl)-piperazine	7.4	2.30	0.071
18	4-(2-Aminoethyl)-morpholine	0.14	0.19	0.054
19	L-Adrenaline	0.09	96	0.11

[a] Mean from three determinations by a stopped-flow, CO_2 hydrase method. Standard errors were in the range of 5–10% of the reported values.

[b] Human recombinant isozymes, stopped flow CO_2 hydrase assay method.[12]

The following structure–activity relationship (SAR) was obtained from the data of **Table 5**:

The most effective VchCAγ activators were L-Trp **7**, 1-(2-minoethyl)-piperazine **17** and 4-(2-aminoethyl)-morpholine **18** that have activation constants in the range of 8–71 nM. It can be observed that both amino acid and amine type compounds were highly effective VchCAγ activators. In fact serotonin, which is structurally related to Trp has an activity intermediate between the L- and D-Trp.

Most of the amines and amino acids **1–19** were effective, submicromolar VchCAγ activators, with K_As ranging between 0.10 and 0.73 μM. They include L-/D-Phe, L-/D-DOPA, D-Trp,

L-/D-Tyr, 4-amino-L-Phe, histamine, dopamine, serotonin, the pyridyl-alkylamines **15** and **16**, as well as L-adrenaline **19** (**Table 5**).

Except for L-Trp and D-Trp, in which the L-enantiomer was the most effective antipode, the D-enantiomer was generally potent in activating VchCAγ. X-ray crystallography on adducts of such enantiomers with hCA I and II [6,7] are in agreement with such data as L- and D-enantiomers bind differently within the active site.

Important differences in the activation profile of VchCAγ compared to the human isoforms hCA I and II were observed for amines and amino acids **1–19** (**Table 5**). For example, L-Trp is a low nanomolar VchCAγ activator, but a high micromolar activator for hCA I and II; i.e., L-Trp is highly selective for γ-CA. In contrast, L- and D-Tyr effectively activate both human and bacterial CAs, and are thus less appropriate for *in vivo* activation studies.

8.7 Activation study of η-Carbonic Anhydrase: PfaCA from from the malaria parasite Plasmodium falciparum

Malaria represents one of the most widespread infections worldwide, leading to serious morbidity and mortality.[24,25] We have reported several years ago that *Plasmodium falciparum*, the malaria parasite producing the worst type of malaria, encodes for a genetically distinct class of the metalloenzyme CA, more specifically the η-CA family (the enzyme was denominated PfaCA).[26] Unlike the remaining 6 genetic families of these enzymes (α-, β-, γ-, δ-, ζ- and θ-CAs), the zinc coordination pattern of PfaCA is unique, with the catalytically crucial zinc ion being coordinated by two His and one Gln residues.[27] In the past years, several study were performed on PfaCA with the aim to obtain new tools for the pharmacological treatment of the disease.[28,29] However, neither PfaCA nor any other η-CAs were yet investigated for their interaction with CAAs. Natural and non-natural amino acids and amines of the type **1–24** represent the most investigated simple types of CAAs, and they were evaluated for their interaction with the η-class enzyme PfaCA. The structure–activity relationship (SAR) for the activation of PfaCA with compounds **1–24**, can be delineated considering the data shown in **Table 6**, where the activation data of the human isoforms hCA I and II are also presented for comparison.

Table 6. Activation constants of hCA I, hCA II and the protozoan PfaCA with amino acids and amines **1–24**, by a stopped-flow CO_2 hydrase assay[12]

No	compound	K_a (μM)[a]		
		hCA I[b]	hCA II[b]	PfaCA
1	L-His	0.03	10.9	1.06
2	D-His	0.09	43	2.19
3	L-Phe	0.07	0.0013	0.43
4	D-Phe	86	0.035	0.75
5	L-DOPA	3.1	11.4	0.12
6	D-DOPA	4.9	7.8	0.39
7	L-Trp	44	27	5.21
8	D-Trp	41	12	8.47
9	L-Tyr	0.02	0.011	1.02
10	D-Tyr	0.04	0.013	8.55
11	4-H_2N-L-Phe	0.24	0.15	1.00
12	Histamine	2.1	125	9.86
13	Dopamine	13.5	9.20	9.97
14	Serotonin	45	50	7.18
15	2-Pyridyl-methylamine	26	34	3.69
16	2-(2-Aminoethyl)pyridine	13	15	6.75
17	1-(2-Aminoethyl)-piperazine	7.4	2.30	0.71
18	4-(2-Aminoethyl)-morpholine	0.14	0.19	5.33
19	L-Adrenaline	0.09	96	2.40
20	L-Asn	11.3	>50	4.76
21	L-Asp	5.20	>50	0.30
22	L-Glu	6.43	>50	12.9
23	D-Glu	10.6	>50	0.082
24	L-Gln	>50	>50	2.51

[a] Mean from three determinations by a stopped-flow, CO_2 hydrase method. Standard errors were in the range of 5–10% of the reported values.

[b] Human recombinant isozymes, stopped flow CO_2 hydrase assay method.[12]

Several derivatives, among which L-/D-Phe, L-/D-DOPA, 1-(2-aminoethyl)-piperazine **17**, L-Asp and D-Glu showed very effective PfaCA activating properties, with activation constants ranging between 82 nM (D-Glu) and 0.75 μM (D-Phe). All these effective, submicromolar activators belong to the amino acid class, except **17** which is the only amine.

Notable differences were observed between the enantiomers of the same amino acid, with the D-one being more effective as PfaCA activator in the case of Glu (the D-enantiomer was 157 times a more effective activator compared to the L-enantiomer), whereas for all other amino acids the L-enantiomer was a better activator compared to the corresponding D-one (**Table 6**).

Slightly less effective activators of PfaCA were L-/D-His, L-Tyr, 4-amino-L-Phe (compound **11**), 2-pyridyl-methylamine, L-adrenaline, L-Asn and L-Gln, which showed K_As in the range of 1.00-4.76 μM. It is obvious that not only the stereochemistry around the chiral center, but also other small structural changes lead to a drastic effect on the CA activating properties. For example L-Gln is 2.5 times more effective PfaCA activator compared to L-Glu; L-Asp is 15.8 times more effective activator than L-Asn; the increase of the linker between the pyridyl ring and the amino moiety from 1 to 2 CH_2 units led to a decrease of the PfaCA activating power of 1.8 times (compare the K_A of **15** and **16**, **Table 6**).

The least effective PfaCA activators were L-/D-Trp, D-Tyr, histamine, dopamine, serotonin, amine **16** discussed above, 4-(2-aminoethyl)-morpholine **18** and L-Glu. These compounds showed activation constants ranging between 5.21 and 12.9 μM. Thus, generally the amines were slightly less effective as PfaCA activators compared to structurally related amino acids. An obvious exception was L-Glu, the least effective activator detected here, which has anyhow a micromolar affinity for the enzyme.

8.8 Activation study of δ-Carbonic Anhydrase: TweCAδ from the diatom Thalassiosira weissflogii

The δ-class Carbonic Anhydrases are poorly investigated and present in several marine diatom. The diatom carbonic anhydrase shows no significant sequence similarity with other carbonic anhydrases and may represent an example of convergent evolution at the molecular level. In 2000, Morel's group discovered δ-CAs in the diatom Thalassiosira weissflogii[30] and they are responsible in part for CO_2 fixation by marine organisms.[31] Also if their roles are far from being well understood with the exception of their important role in CO_2 fixation and photosynthesis, as they provide bicarbonate or CO_2 to ribulose-1,5-bisphosphate

carboxylase/oxygenase (RUBISCO).[30-32] TweCA is an excellent catalyst for the hydration of CO_2 to bicarbonate and hydronium ions, and that its activity may be inhibited by anions and sulfonamides, as reported previously in literature.[18-20,25,33] However, no activation studies of this enzyme have been reported to date, although the CAAs are an important class of modulators for the activity of CA enzymes.[6,7] The activation profile for compounds **1-19** against TweCAδ are presented in **Table 7** and also compared with physiologically relevant isoforms hCA I and II (belonging to the α-CA family).

Table 7. Activation constants of hCA I, hCA II and the diatom TweCAδ with amino acids and amines **1–19**, by a stopped-flow CO_2 hydrase assay[12]

No	Compound	K_a (μM)[a]		
		hCA I[b]	hCA II[b]	TweCAδ
1	L-His	0.03	10.9	0.75
2	D-His	0.09	43	4.90
3	L-Phe	0.07	0.0013	2.15
4	D-Phe	86	0.035	1.96
5	L-DOPA	3.1	11.4	2.11
6	D-DOPA	4.9	7.8	6.24
7	L-Trp	44	27	0.93
8	D-Trp	41	12	0.69
9	L-Tyr	0.02	0.011	1.52
10	D-Tyr	0.04	0.013	0.051
11	4-H2N-L-Phe	0.24	0.15	18.9
12	Histamine	2.1	125	1.34
13	Dopamine	13.5	9.20	0.51
14	Serotonin	45	50	0.90
15	2-Pyridyl-methylamine	26	34	5.28
16	2-(2-Aminoethyl)pyridine	13	15	8.16
17	1-(2-Aminoethyl)-piperazine	7.4	2.30	4.37
18	4-(2-Aminoethyl)-morpholine	0.14	0.19	7.39
19	L-Adrenaline	0.09	96	2.43

[a] Mean from three determinations by a stopped-flow, CO_2 hydrase method. Standard errors were in the range of 5–10% of the reported values.

[b] Human recombinant isozymes, stopped flow CO_2 hydrase assay method.[12]

The following structure-activity relationship can be inferred for TweCAδ activation with these compounds:

i) The most effective TweCAδ activator was D-Tyr, with an activation constant of 51 nM, whereas several other amino acids and amines, such as L-His, L-Trp, D-Trp, dopamine and serotonin were submicromolar activators, with K_As ranging between 0.51 and 0.93 mM.

ii) The most ineffective activator of TweCAδ was 4-amino-L-Phe, with an activation constant of 18.9 μM.

iii) The remaining derivatives investigated were effective to moderately potent activators, with K_As ranging between 1.34 and 8.16 μM. Thus, the SAR for these compounds is rather "flat" because most were rather effective activators of this enzyme. However, the stereochemistry of the chiral centre for the amino acid derivatives seems to not be very important, since both L- (i.e. L-His, L-Trp) and D-amino acid derivatives (i.e. D-Trp, D-Tyr) showed effective TweCAδ activation (**Table 7**). Small changes in the scaffold of an activator led to important differences of activity. For example, introduction of an amino moiety at the 4 position of the phenyl ring in L-Phe (a rather effective activator) let to a massive loss of efficacy in compound **11**, which was 8.8 times less efficient activator when compared to **3**. The loss of the carboxyl moiety from L- or D-DOPA led to enhanced activating properties in dopamine **13**, compared with **5** and **6**. Another example is the nature of the moiety in **17** and **18**, with the morpholine **18** being 1.7 times a weaker activator compared to the piperazine **17**.

The activation profile of the δ-class enzyme investigated here is very different from that of the α-CAs hCA I and II. Since no crystal structure (or even modelling) of any δ-CA is available so far, it is challenging to rationalize in detail these data. In addition, the proton transfer residue(s) responsible for shuttling protons to and from the active site in this class of CAs is unknown. In conclusion, this is the first study of activation of a δ-class CA. The most effective TweCAδ activator was D-Tyr, with an activation constant of 51 nM, whereas several other amino acids and amines, such as L-His, L-Trp, D-Trp, dopamine and serotonin were submicromolar activators, with K_As ranging between 0.51 and 0.93 μM. The most

ineffective TweCAδ activator was 4-amino-L-Phe, with an activation constant of 18.9 μM. Moreover, this may lead to a more complete understanding of the role of nature amines and amino acids in the modulation of CO_2 fixation in phytoplankton.

8.9 Activation study of ζ-Carbonic Anhydrase: TweCAζ from the diatom Thalassiosira weissflogii

Morel's group discovered another genetic family of carbonic anhydrase in the diatom *Thalassiosira weissflogii*, the ζ -CAs class.[34] Together the other δ-class CA are responsible for CO_2 fixation as mentioned above. Most classes of CA use Zn(II) ion within the active site with a zinc hydroxide species acting as nucleophile,[16,18-20] but the ζ-CAs are quite particular, as it has been shown that they are cambialistic enzyme, active with both Zn(II) and Cd(II) ions within the active site. It seems that in the marine environment, due to a shortage of zinc ions availability, these enzymes are cadmium proteins, showing thus that at least for diatoms, cadmium is not a toxic metal ion.[34-36] The ζ-CA class from *T. weissflogii*, TweCAζ, can exist both with Zn(II) and Cd(II) at the active site called ZnTweCA ζ and CdTweCA ζ, respectively.[34-36] No ζ -CA activation studies are available in the literature so far. In this way, we investigated this class and showed that the zinc-containing ζ -CA is highly activated by compounds **1-24**, whereas the cadmium-containing enzyme is not affected by these modulators of activity.

Data of **Table 8** shows the Zn/CdTweCA ζ activation with amino acids and amines **1**–**24**. The activation profile with the same compounds for the widespread, physiologically relevant isoforms hCA I and II (belonging to the α-CA family) are also shown for comparison reasons.

Table 8. Activation constants of hCA I, hCA II and diatoms Zn/CdTweCAζ with amino acids and amines **1–24**, by a stopped-flow CO_2 hydrase assay[12]

No	Compound	K_a (μM)[a]			
		hCA I[b]	hCA II[b]	ZnTweCAζ	CdTweCAζ
1	L-His	0.03	10.9	0.81	>50
2	D-His	0.09	43	7.16	>50
3	L-Phe	0.07	0.0013	15.4	>50
4	D-Phe	86	0.035	9.63	>50
5	L-DOPA	3.1	11.4	3.19	>50
6	D-DOPA	4.9	7.8	2.87	>50
7	L-Trp	44	27	8.54	>50
8	D-Trp	41	12	1.79	>50
9	L-Tyr	0.02	0.011	0.98	>50
10	D-Tyr	0.04	0.013	0.62	>50
11	4-H2N-L-Phe	0.24	0.15	7.90	>50
12	Histamine	2.1	125	1.27	>50
13	Dopamine	13.5	9.20	10.1	>50
14	Serotonin	45	50	3.06	>50
15	2-Pyridyl-methylamine	26	34	0.88	>50
16	2-(2-Aminoethyl)pyridine	13	15	0.85	>50
17	1-(2-Aminoethyl)-piperazine	7.4	2.30	0.12	>50
18	4-(2-Aminoethyl)-morpholine	0.14	0.19	0.15	>50
19	L-Adrenaline	0.09	96	0.092	>50
20	L-Asn	11.3	>50	3.18	>50
21	L-Asp	5.20	>50	37.9	>50
22	L-Glu	6.43	>50	9.75	>50
23	D-Glu	10.6	>50	6.43	>50
24	L-Gln	>50	>50	8.39	>50

[a] Mean from three determinations by a stopped-flow, CO_2 hydrase method. Standard errors were in the range of 5–10% of the reported values.

[b] Human recombinant isozymes, stopped flow CO_2 hydrase assay method.[12]

The following structure-activity relationship can be inferred for Zn/CdTweCAζ activation with these compounds:

i) The cadmium-containing TweCAζ was not at all activated by amino acids and amines **1**–**24**, up to 50 μM activator concentration in the assay system (which is very high concentration), unlike ZnTweCAζ, for which the activation constants ranged between 92nM and 37.9μM (**Table 8**). This is a very unexpected and surprising finding, considering that, apart for the ionic radius, which is higher for Cd(II) compared to Zn(II), there are no significant differences of behaviour between these two[37] metal ion in metalloproteins. Thus, our finding that the Cd-CA is not activated remains unexplained for the moment. This is also the first time that a CA protein of any genetic family shows a behaviour of this type. In fact, representatives all other CA families were sensitive to activators the amine and amino acid type.[38-40]

ii) The most effective ZnTweCAζ activators belonged to the amine chemotype are L-adrenaline **19** and the heterocyclic amines **17** and **18** that showed K_As in the range of 92–150nM (**Table 8**). Thus, both compounds incorporating aminoethyl- (**17** and **18**) or methylamino-hydroxyethyl (adrenaline) show a potent activating effect, and presumably these primary/secondary amine functionalities are involved in the proton shuttling favouring catalysis.

iii) Effective ZnTweCAζ activation was also observed with L-His, L- and D-Tyr and the pyridyl-alkylamines **15** and **16**, which had K_As in the range of 0.62–0.98 μM (**Table 8**). L-/D-DOPA, D-Trp, histamine, serotonin and L-Asn were the next most efficient activators, with K_As in the range of 1.27–3.19 μM. Thus, both amines and amino acids may show this behaviour of medium potency activator against ZnTweCAζ.

iv) Weaker activation against ZnTweCAζ was observed for D-His, D-Phe, L-Trp, 4-amino-L-Phe, dopamine, L-Glu, D-Glu and L-Gln, which showed K_As in the range of 6.43–10.1 μM. Generally, the D-amino acids were more effective activators compared to the L-enantiomers, except for His, for which L-His was 8.8 times more effective CAA compared to the D-enantiomer (**Table 8**). For the two Trp enantiomers, the D-one was 4.77 times a more effective activator compared to L-Trp.

v) The least effective ZnTweCAζ activators were L-Phe (K_A of 15.4 μM) and L-Asp (K_A of 37.9 μM). It should be noted that the extra CH_2 present in L-Glu (compared to L-Asp) led to an increase of the activation efficacy of 3.88 times. When

comparing the L-Asp/L-Asn pair, the $CONH_2$ moiety of the latter derivative induced an 11.9-times increase of the activation efficacy over the dicarboxylic amino acid derivative. Thus, very small difference in the chemical structure of the activator lead to dramatic changes in the activating efficacy, which in fact has been documented for other enzyme classes with these activators.[38-40]

8.10 Activation of β- and γ-Carbonic Anhydrases from pathogenic bacteria with tripeptides

To date, the CA activation mechanism was investigated with a well know library of different simple amino acids and amines (**1-24**). In order to better understand the mechanism of activation involved in the β- and γ-Carbonic Anhydrases, we evaluated the activity of tripeptides incorporating acidic amino acid residues synthesized by Mollica' group and reported in **Table 9**.[41]

Table 9. New tripeptides.NH_2-Xaa1-Xaa2-Xaa3-NH_2 **1–6** (TFA salts).

Compounds	
25	NH_2-Tyr-Phe-Asp-NH_2
26	NH_2-His-Phe-Glu-NH_2
27	NH_2-Glu-Ile-Thr-NH_2
28	NH_2-Gln-Asp-Ser-NH_2
29	NH_2-Asn-Asp-Ser-NH_2
30	NH_2-Glu-Phe-Glu-NH_2

These compounds are investigated against several Carbonic Anhydrases from different pathogenic bacteria such as *Vibrio cholerae* (the enzymes included in the study were VchCAβ and VchCAγ), *Mycobacterium tuberculosis* (mtCA3, one of the three β-CAs) and *Burkholderia pseudomallei* (BpsCAγ).

These three pathogens produce serious diseases in humans, and understanding factors connected to their invasion, colonization and virulence, and how these factors are influenced by modulators of CA activity, may be relevant to developing new therapeutic strategies

devoid of the extensive drug resistance that has ultimately emerged for most clinically used anti-infective drugs.[42-44]

In **Table10**, the activation constants of tripeptides **25–30**, and some amino acids for four bacterial enzymes and the ubiquitous isoforms hCA I and II are shown. The six amino acids were included in this study for comparative reasons.

Table 10. Activation of hCA I, hCA II, VchCAβ, mtCA 3, VchCAγ and BpsCAγ with tripeptides **25–30** and simple amino acid derivatives, by a stopped-flow, CO_2 hydrase assay, at 25°C and pH 8.433.[12]

	K_a (μM)[a]					
Compound	hCA I[b]	hCA II[b]	VhCAβ	mtCA 3	VhCAγ	BpsCAγ
25	>50	>50	3.52±0.18	8.45±0.11	14.7±0.21	10.1±0.09
26	>50	>50	1.16±0.05	6.29±0.14	5.84±0.15	1.63±0.12
27	>50	>50	1.15±0.10	4.32±0.08	11.9±0.42	3.75±0.15
28	>50	>50	0.21±0.07	15.8±0.76	12.9±0.61	6.18±0.30
29	>50	>50	7.16±0.34	18.1±1.02	10.6±0.74	0.95±0.09
30	>50	>50	4.18±0.23	9.40±0.62	2.74±0.16	5.24±0.30
L-Asp	5.20	>50	9.87±0.41	10.1±0.84	8.95±0.46	10.7±0.85
L-Asn	11.3	>50	>50	10.0±0.71	6.37±0.29	0.98±0.08
L-Glu	6.43	>50	0.69±0.05	>50	6.48±0.50	3.25±0.17
L-Gln	>50	>50	18.1±0.94	21.6±1.1	9.21±0.82	6.15±0.30
L-His	0.03	10.9	20.3	18.2	1.01	24.7
L-Phe	0.07	0.013	15.4	30.6	0.73	1.73

[a] Mean from three determinations by a stopped-flow, CO_2 hydrase method. Standard errors were in the range of 5–10% of the reported values.

[b] Human recombinant isozymes, stopped flow CO_2 hydrase assay method.[12]

The following structure–activity relationship (SAR) can be obtained from the data in **Table 10**.

VchCAβ was effectively activated by tripeptides **25–30** with activation constants ranging between 0.21 and 7.16 μM. The most effective activator was **28** (Gln-Asp-Ser), whereas the least effective one was **29** (Asn-Asp-Ser). Thus, the extra methylene group in Gln compared

to Asn resulted in tripeptide **28** more effectively activating this enzyme by 34 times compared to **29** (**Table 10**). Other effective activators against this enzyme include tripeptides **26** and **27** that incorporate a Glu residue in the sequence. However, the tripeptide with two Glu residues (**30**) was less effective as an activator compared to **26** and **27**. It is interesting that L-Glu is a very effective VchCAβ activator (K_A of 0.69 mM), whereas L-Gln, L-His and L-Phe are much less effective activators (**Table 10**). L-Asp is moderately potent as an activator (K_A of 9.87 μM) but L-Asn is not.

The other β-CA investigated here, mtCA3, was less sensitive to these activators compared to that from *V. cholerae* enzyme; i.e. tripeptides **25–30** had K_As in the range of 4.32 to 18.1 μM for this CA. The most effective activator was **27** (Glu-Ile-Thr), whereas the least effective was **29** (Asn-Asp-Ser). Tripeptide **26** was the next most effective activator after **27**. These latter two peptides both have one Glu residue, albeit in opposed positions (amino-terminal *vs* carboxy-terminal). Considering the simple amino acid derivatives of **Table 10**, L-Glu was in this case ineffective as an activator whereas the remaining amino acids were moderately potent to weak activators (activation constants from 10.0 to 30.6 μM).

VchCAγ was activated by tripeptides **25–30** with K_As ranging between 2.74 and 14.7 μM. The most effective activator was **30**, which incorporates two Glu residues in the sequence, followed by **26**, which has one such carboxy-terminal residue. The remaining tripeptides were less effective activators, with K_As>10 μM (**Table 10**). For this isoform, the best activators were the simple aromatic amino acids L-His and L-Phe (K_As of 0.73–1.01 μM) whereas L-Asp, L-Asn, L-Glu and L-Gln showed activities in the range of 6.37–9.21 μM. Thus, the SAR is rather challenging to delineate for this enzyme and with this series of activators.

BpsCAγ was efficiently activated by tripeptides **25–30** with K_As ranging between 0.95 and 10.1 μM. The best activators were **29** and **26** (K_As of 0.95 and 1.63 μM, respectively), which do not share much in similarity except that in both sequences there is one acidic amino acid residue, Asp in **29** and Glu in **26**. The most ineffective activator was **25**, which does not incorporate such a residue. However, it is interesting to note that L-Asn with a K_A of 0.98 μM was the most effective activator among the simple amino acids considered in the study.

Indeed, this latter activation constant was one order of magnitude lower than that for L-Asp, whereas such an important difference is not seen for the L-Glu/L-Gln pair (**Table 10**).

A very interesting observation is the fact that the human isoforms hCA I and II were not at all activated by tripeptides **25–30** investigated here (K_A>50 μM), although they are highly activated by some of the amino acids, such as L-His, and L-Phe. hCA II is in fact sensitive only to these two amino acids, whereas hCA I is also activated by L-Asp, L-Asn, L-Glu (but not L-Gln) and of course, L-His and L-Phe.

8.11 Experimental data

Carbonic Anhydrase enzyme activation assay

An Sx.18Mv-R Applied Photophysics (Oxford, UK) stopped-flow instrument has been used to assay the catalytic activity of various CA isozymes for CO_2 hydration reaction.[12] Phenol red (at a concentration of 0.2 mM) was used as indicator, working at the absorbance maximum of 557 nm, with 10 mM Hepes (pH 7.5) or TRIS (pH 8.3) as buffers, 0.1 M Na_2SO_4 (for maintaining constant ionic strength), following the CA-catalyzed CO_2 hydration reaction for a period of 10 s at 25 °C. Activity of the α-CA was measured at pH 7.5 whereas that of the β-, γ-, δ-, η-, ζ- class enzymes at pH 8.3 as it has been reported that for enzymes of this class it optimal at this pH value [1–3]. The CO_2 concentrations ranged from 1.7 to 17 mM for the determination of the kinetic parameters and activation constants. For each activator at least six traces of the initial 5–10% of the reaction have been used for determining the initial velocity. The uncatalyzed rates were determined in the same manner and subtracted from the total observed rates. Stock solutions of activators (10 mM) were prepared in distilled-deionized water and dilutions up to 1 nM were done thereafter with the assay buffer. Activator and enzyme solutions were pre-incubated together for 15 min (standard assay at room temperature) prior to assay, in order to allow for the formation of the E–A complex. The activation constant (K_A), defined similarly with the inhibition constant K_I, can be obtained by considering the classical Michaelis–Menten equation (Eq. (**4**)), which has been fitted by non-linear least squares by using

PRISM 3:

$$V = \frac{V_{max}}{\left\{ 1 + K_M / [S] \, (1 + [A]_f / K_A) \right\}} \qquad \textbf{(4)}$$

Where $[A]_f$ is the free concentration of activator. Working at substrate concentrations considerably lower than K_M ($[S] << K_M$), and considering that $[A]_f$ can be represented in the form of the total concentration of the enzyme ($[E]_t$) and activator ($[A]_t$), the obtained competitive steady-state equation for determining the activation constant is given by Eq. (**5**):

$$V = \frac{V_0 \, K_A}{\left\{ K_A + ([A]_t - 0.5\left\{([A]_t + [E]_t + K_A) - ([A]_t + [E]_t + K_A)^2 - 4[A]_t \, [E]t)^{1/2} \right\}\right\}} \qquad \textbf{(5)}$$

Where V_0 represents the initial velocity of the enzyme-catalyzed reaction in the absence of activator. The enzymes were recombinant ones, prepared in-house as reported earlier.[37,50-52]

References

1. da Silva Cardoso V., Vermelho A.B., Ricci Junior E., Almeida Rodrigues I., Mazotto A.M., Supuran C.T. Antileishmanial activity of sulphonamide nanoemulsions targeting the β-carbonic anhydrase from Leishmania species. *J Enzyme Inhib Med Chem.* 2018, 33, 850-857.
2. D'Ambrosio K., Supuran C.T., De Simone G. Are Carbonic Anhydrases Suitable Targets to Fight Protozoan Parasitic Diseases? *Curr Med Chem.* 2018, DOI: 10.2174/0929867325666180326160121
3. Vermelho A.B., Capaci G.R., Rodrigues I.A., Cardoso V.S., Mazotto A.M., Supuran C.T. Carbonic anhydrases from Trypanosoma and Leishmania as anti-protozoan drug targets. *Bioorg Med Chem.* 2017, 25, 1543-1555.
4. Pan P, Vermelho AB, Capaci Rodrigues G, Scozzafava A, Tolvanen ME, Parkkila S, Capasso C, Supuran CT. Cloning, characterization, and sulfonamide and thiol inhibition studies of an α-carbonic anhydrase from Trypanosoma cruzi, the causative agent of Chagas disease. *J Med Chem.* 2013, 56, 1761-71.
5. Ponte-Sucre A., Gamarro F., Dujardin J.C., Barrett M.P., López-Vélez R., García-Hernández R., Pountain A.W., Mwenechanya R., Papadopoulou B., Drug resistance and treatment failure in leishmaniasis: a 21st century challenge, *PLoS Negl. Trop Dis*. 2017, 11, e0006052.
6. Temperini C., Scozzafava A., Vullo D., Supuran C.T. Carbonic anhydrase activators. Activation of isoforms I, II, IV, VA, VII, and XIV with L- and D-phenylalanine and crystallographic analysis of their adducts with isozyme II: stereospecific recognition within the active site of an enzyme and its consequences for the drug design, *J. Med. Chem.* 2006, 49, 3019–3027
7. Briganti F., Mangani S., Orioli P., Scozzafava A., Vernaglione G., Supuran C.T. Carbonic anhydrase activators: X-ray crystallographic and spectroscopic investigations for the interaction of isozymes I and II with histamine, *Biochemistry* 1997, 36, 10384–10392
8. Borrell S., Trauner A. Strain diversity and the evolution of antibiotic resistance. *Adv Exp Med Biol* 2017, 1019, 263–279.

9. Al-Humadi H.W., Al-Saigh R.J., Al-Humadi A.W., Addressing the challenges of tuberculosis: a brief historical account. *Front Pharmacol* 2017, 8, 689.

10. Nishimori I., Minakuchi T., Maresca A., Carta F., Scozzafava A., Supuran C.T. The β-carbonic anhydrases from Mycobacterium tuberculosis as drug targets. *Curr Pharm Des* 2010, 16, 3300–3309.

11. Nishimori I., Minakuchi T., Vullo D., Scozzafava A., Innocenti A., Supuran C.T. Carbonic anhydrase inhibitors. Cloning, characterization, and inhibition studies of a new beta-carbonic anhydrase from Mycobacterium tuberculosis. *J Med Chem* 2009, 52, 3116–3120.

12. Khalifah R.G. The carbon dioxide hydration activity of carbonic anhydrase. I. Stop-flow kinetic studies on the native human isoenzymes B and C. *J Biol Chem.* 1971, 246, 2561-73.

13. Suarez Covarrubias A., Larsson A.M., Hogbom M., Lindberg J., Bergfors T., Björkelid C., Mowbray S.L., Unge T., Jones T.A. Structure and function of carbonic anhydrases from Mycobacterium tuberculosis. *J Biol Chem* 2005, 280, 18782–18789.

14. Covarrubias A.S., Bergfors T., Jones T.A., Hogbom M. Structural mechanics of the pH-dependent activity of betacarbonic anhydrase from Mycobacterium tuberculosis. *J Biol Chem* 2006, 281, 4993–4999.

15. Del Prete S., Isik S., Vullo D., De Luca V., Carginale V., Scozzafava A., Supuran C.T., Capasso C. DNA cloning, characterization, and inhibition studies of an α-carbonic anhydrase from the pathogenic bacterium Vibrio cholerae. *J Med Chem* 2012, 55, 10742–10748.

16. Del Prete S., Vullo D., De Luca V., Carginale V., Ferraroni M., Osman SM., AlOthman Z., Supuran C.T., Capasso C. Sulfonamide inhibition studies of the β-carbonic anhydrase from the pathogenic bacterium Vibrio cholerae. *Bioorg Med Chem* 2016, 24, 1115–1120.

17. Del Prete S., Vullo D., De Luca V., Carginale V., di Fonzo P., Osman S.M., AlOthman Z., Supuran C.T., Capasso C. Anion inhibition profiles of α-, β- and γ-carbonic anhydrases from the pathogenic bacterium Vibrio cholerae. *Bioorg Med Chem* 2016, 24, 3413–3417.

18. Alber B.E., Ferry J.G. A carbonic anhydrase from the archaeon Methanosarcina thermophila, *Proc. Natl. Acad. Sci. USA* 1994, 91, 6909–6913.
19. Supuran C.T., Structure and function of carbonic anhydrases, *Biochem. J.* 2016, 473, 2023–2032.
20. Supuran C.T., Carbonic anhydrases: novel therapeutic applications for inhibitors and activators, *Nat. Rev. Drug. Discov.* 2008, 7, 168–181.
21. Capasso C., Supuran C.T., An overview of the alpha-, beta-and gamma-carbonic anhydrases from Bacteria: can bacterial carbonic anhydrases shed new light on evolution of bacteria? *J Enzyme Inhib. Med. Chem.* 2015, 30, 325–332.
22. Alber B.E., Ferry J.G., Characterization of heterologously produced carbonic anhydrase from Methanosarcina thermophila, *J. Bacteriol.* 1996, 178, 3270–3274.
23. Tripp B.C., Ferry J.G., A structure-function study of a proton transport pathway in the gamma-class carbonic anhydrase from Methanosarcina thermophila, Biochemistry 2000, 39, 9232–9240.
24. Mita T., Hombhanje F., Takahashi N., Sekihara M., Yamauchi M., Tsukahara T., Kaneko A., Endo H., Ohashi J., Rapid selection of sulphadoxine-resistant Plasmodium falciparum and its effect on within-population genetic diversity in Papua New Guinea, *Sci Rep*. 2018, 8, 5565
25. Nsanzabana C., Djalle D., Guérin P.J., Ménard D.,González I.J. Tools for surveillance of anti-malarial drug resistance: an assessment of the current landscape, *Malar. J.* 2018, 17, 75;
26. Del Prete S., De Luca V., De Simone G., Supuran C.T., Capasso C., Cloning, expression and purification of the complete domain of the η-carbonic anhydrase from Plasmodium falciparum, *J. Enzyme Inhib. Med. Chem.* 2016, 31 (sup4), 54–59.
27. De Simone G., Di Fiore A., Capasso C., Supuran C.T. The zinc coordination pattern in the η-carbonic anhydrase from Plasmodium falciparum is different from all other carbonic anhydrase genetic families, *Bioorg. Med. Chem. Lett.* 2015, 25, 1385–1389.
28. Supuran C.T., Capasso C. The η-class carbonic anhydrases as drug targets for antimalarial agents, *Expert Opin. Ther. Targets.* 2015, 19,551–563

29. Krungkrai J., Supuran C.T., The alpha-carbonic anhydrase from the malaria parasite and its inhibition, *Curr. Pharm. Des.* 2008, 14, 631–640

30. Vullo D., Del Prete S., Osman S.M., Alasmary F.A.S., AlOthman Z., Donald W.A., Capasso C., Supuran C.T. Comparison of the amine/amino acid activation profiles of the β- and γ-carbonic anhydrases from the pathogenic bacterium Burkholderia pseudomallei. *J Enzyme Inhib Med Chem* 2018, 33, 25–30.

31. Cox E.H., McLendon G.L., Morel F.M., Lane T.W., Prince R.C., Pickering I.J., George G.N. The active site structure of Thalassiosira weissflogii carbonic anhydrase 1. *Biochemistry* 2000, 39, 12128–12130.

32. McGinn P.J., Morel F.M. Expression and regulation of carbonic anhydrases in the marine diatom Thalassiosira pseudonana and in natural phytoplankton assemblages from Great Bay, New Jersey. *Physiol Plant* 2008, 133, 78–91.

33. Tachibana M., Allen A.E., Kikutani S., Endo Y., Bowler C., Matsuda Y. Localization of putative carbonic anhydrases in two marine diatoms, Phaeodactylum tricornutum and Thalassiosira pseudonana. *Photosynth Res* 2011, 109, 205–21.

34. Del Prete S., Vullo D., Scozzafava A., Capasso C., Supuran C.T. Cloning, characterization and anion inhibition study of the d-class carbonic anhydrase (TweCA) from the marine diatom Thalassiosira weissflogii. *Bioorg Med Chem* 2014, 22, 531–7.

35. Xu Y., Feng L., Jeffrey P.D., Shi Y., Morel F.M., Structure and metal exchange in the cadmium carbonic anhydrase of marine diatoms, *Nature* 2008, 452, 56–61.

36. Alterio V., Langella E., Viparelli F., Vullo D., Ascione G., Dathan N.A., Morel F.M., Supuran C.T., De Simone G., Monti S.M., Structural and inhibition insights into carbonic anhydrase CDCA1 from the marine diatom Thalassiosira weissflogii, *Biochimie* 2012, 94, 1232–1241

37. Viparelli F., Monti S.M., De Simone G., Innocenti A., Scozzafava A., Xu Y., Morel F.M., Supuran C.T., Inhibition of the R1 fragment of the cadmium-containing zeta-class carbonic anhydrase from the diatom Thalassiosira weissflogii with anions, *Bioorg. Med. Chem. Lett.* 2010, 20, 4745–4748

38. Angeli A., Vaiano F., Mari F., Bertol E., Supuran C.T., Psychoactive substances belonging to the amphetamine class potently activate brain carbonic anhydrase isoforms VA, VB, VII, and XII, *J. Enzyme Inhib. Med. Chem.* 2017, 32, 1253–1259

39. Angeli A., Kuuslahti M., Parkkila S., Supuran C.T. Activation studies with amines and amino acids of the α-carbonic anhydrase from the pathogenic protozoan Trypanosoma cruzi. *Bioorg Med Chem.* 2018, 26, 4187-4190.

40. Angeli A., Del Prete S., Alasmary F.A.S., Alqahtani L.S., AlOthman Z., Donald W.A., Capasso C., Supuran C.T. The first activation studies of the η-carbonic anhydrase from the malaria parasite Plasmodium falciparum with amines and amino acids. *Bioorg Chem.* 2018, 80, 94-98.

41. Angeli A., Donald W.A., Parkkila S., Supuran C.T. Activation studies with amines and amino acids of the β-carbonic anhydrase from the pathogenic protozoan Leishmania donovani chagasi. *Bioorg Chem.* 2018, 78, 406-410.

42. Stefanucci A., Angeli A., Dimmito MP., Luisi G., Del Prete S., Capasso C., Donald W.A., Mollica A., Supuran C.T. Activation of β- and γ-carbonic anhydrases from pathogenic bacteria with tripeptides. *J Enzyme Inhib Med Chem.* 2018, 33, 945-950.

43. Angeli A., Del Prete S., Osman S.M., Alasmary F.A.S., AlOthman Z., Donald W.A., Capasso C., Supuran C.T. Activation studies of the a- and b-carbonic anhydrases from the pathogenic bacterium Vibrio cholerae with amines and amino acids. *J Enzyme Inhib Med Chem* 2018, 33, 227–33.

44. Angeli A., Del Prete S., Donald W.A., Capasso C., Supuran C.T. The γ-carbonic anhydrase from the pathogenic bacterium Vibrio cholerae is potently activated by amines and amino acids. *Bioorg Chem* 2018, 77, 1–5.

45. Angeli A., Del Prete S., Osman S.M., Alasmary F.A.S., AlOthman Z., Donald W.A., Capasso C., Supuran C.T. Activation studies with amines and amino acids of the β-carbonic anhydrase encoded by the Rv3273 gene from the pathogenic bacterium Mycobacterium tuberculosis. *J Enzyme Inhib Med Chem* 2018, 33, 364–9.